

Electron Fluxes During Chemical Processes
in the Electronic Ground State

Inaugural-Dissertation

to obtain the academic degree

Doctor rerum naturalium (Dr. rer. nat.)

submitted to the Department of Biology, Chemistry and Pharmacy
of Freie Universität Berlin

by

Axel Schild

from Dresden

2013

This work was prepared under supervision of
Prof. Dr. Jörn Manz (Freie Universität Berlin)
and
Prof. Dr. Beate Paulus (Freie Universität Berlin)
from October 2009 until August 2013.

1. Gutachter: Prof. Dr. Jörn Manz
2. Gutachter: Prof. Dr. Beate Paulus
Disputation am 18. September 2013

The following articles were published in connection with this work:

- Hans-Christian Hege, Jörn Manz, Falko Marquardt, Beate Paulus, Axel Schild, *Electron flux during pericyclic reactions in the tunneling limit: Quantum simulation for cyclooctatetraene*, *Chemical Physics* 276 (2010), 46–55.
- Axel Schild, Deepanshu Choudhary, Vaibhav D. Sambre, Beate Paulus, *Electron Density Dynamics in the Electronic Ground State: Motion Along the Kekulé Mode of Benzene*, *The Journal of Physical Chemistry A* 116 (2012), 11355–11360.
- Axel Schild, Beate Paulus, *Multireference Calculations for Ring Inversion and Double Bond Shifting in Cyclooctatetraene*, *Journal of Computational Chemistry* 34 (2013), 1393–1397.
- Thomas Grohmann, Jörn Manz, Axel Schild, *Effects of molecular symmetry on the directions of nuclear flux densities during tunneling in double well potentials*, *Molecular Physics* 2013, doi:10.1080/00268976.2013.800599.

Summary Reaction mechanisms in chemistry are often indicated by arrows in Lewis structures. While these arrows account for changes in the electronic structure from reactant to product, they do not represent the time-dependent electron rearrangement. Such a time-dependent reaction mechanism can be obtained by calculation of an electronic flux density, but for reactions in the electronic ground state the Born-Oppenheimer separation prohibits straightforward calculation of this quantity.

In this work, the concept of the electronic flux density is reviewed and analyzed within the framework of the Born-Oppenheimer approximation. Then, time-dependent reaction mechanisms are determined for cyclic electron rearrangements by using electron fluxes into or out of suitably defined bond sectors. The investigated models, tunneling in cyclooctatetraene, motion of benzene along the Kekulé mode, proton tunneling in malonaldehyde and double proton tunneling in the formic acid dimer, yield interesting insights regarding questions like: How many electrons move from bond to bond? In which direction? Do electrons of different chemical type (like π -electrons) behave differently? It becomes apparent that already a lot can be learned from the simple model systems, but also that a lot still needs to be done until time-dependent reaction mechanisms can be routinely calculated.

Zusammenfassung Chemische Reaktionsmechanismen werden häufig mit Pfeilen in Lewisstrukturen dargestellt. Diese Pfeile repräsentieren Änderungen in der elektronischen Struktur von Reaktanden zu Produkten, aber sie geben nicht den zeitabhängigen Mechanismus wieder. Solch ein zeitlicher Reaktionsmechanismus könnte durch Berechnung der elektronischen Flussdichte erhalten werden, aber für Reaktionen im elektronischen Grundzustand verhindert die Born-Oppenheimer-Näherung eine einfache Berechnung dieser Größe.

In dieser Arbeit wird das Konzept der elektronischen Flussdichte erläutert und in Hinblick auf die Born-Oppenheimer-Näherung analysiert. Weiterhin werden zeitabhängige Reaktionsmechanismen für zyklische Elektronenumlagerungen mittels elektronischer Flüsse in oder aus geeignet definierten Bindungssektoren bestimmt. Die betrachteten Modelle, Tunneln in Cyclooctatetraen, die Bewegung von Benzol entlang der Kekulé-Mode, Protonentunneln in Malonaldehyd und Doppelprotonentunneln im Ameisensäuredimer, bringen interessante Ergebnisse zu Tage bezüglich Fragen wie: Wieviele Elektronen fließen von Bindung zu Bindung? In welche Richtung fließen die Elektronen? Verhalten sich Elektronen verschiedenen chemischen Typs (z.B. π -Elektronen im Vergleich zu anderen Valenzelektronen) unterschiedlich? Es wird deutlich, dass viel von diesen einfachen Modellsystemen gelernt werden kann, aber dass bis zur standardmäßigen Berechnung von Reaktionsmechanismen noch ein weiter Weg zurückgelegt werden muss.

Contents

1	Introduction	1
1.1	The static and the dynamic view of a chemical reaction	1
1.2	Three types of electron rearrangements	4
1.3	Simulation methods for chemical reactions	7
1.4	Current status of the dynamical view of a chemical reaction	8
1.5	Contents of this monograph	9
2	Theory	11
2.1	Abstract	11
2.2	The flux density concept	12
2.2.1	Flux densities in continuum mechanics	12
2.2.2	The continuity equation	16
2.3	The flux density in quantum mechanics	19
2.3.1	Flux density from the Schrödinger equation	19
2.3.2	Flux density via the correspondence principle	21
2.3.3	Flux density as product of a density and a velocity field	21
2.3.4	Relation to momentum and angular momentum expectation values	22
2.4	Flux densities and the Born-Oppenheimer approximation	24
2.4.1	Flux densities in the Born-Oppenheimer approximation	24
2.5	Fluxes in the Born-Oppenheimer approximation	41
3	Practice	45
3.1	Abstract	45
3.2	A brief introduction to quantum chemistry	46
3.2.1	The Hartree-Fock method	46
3.2.2	The multi-configuration self-consistent field method	48
3.2.3	Electronic basis sets	48
3.3	The static electron density in quantum chemistry	49
3.4	Time-dependent electron density and time-dependent electron numbers	51
4	Applications	57
4.1	Tunneling in cyclooctatetraene	57
4.1.1	Abstract	57
4.1.2	The model cyclooctatetraene	58
4.1.3	A theory for coherent tunneling	60
4.1.4	Fluxes during coherent tunneling	63
4.1.5	Technical details	64
4.1.6	Results	67
4.2	Dynamics along the Kekulé mode of benzene	71

4.2.1	Abstract	71
4.2.2	The Kekulé mode	72
4.2.3	A model Hamiltonian	72
4.2.4	Results	76
4.3	Proton tunneling in the formic acid dimer and in malonaldehyde	85
4.3.1	Abstract	85
4.3.2	The missing flux parameter	86
4.3.3	Average angular flux and the angular velocity operator	87
4.3.4	Model systems formic acid dimer and malonaldehyde	94
4.3.5	Results I: Fluxes from the density and the resulting mechanisms	98
4.3.6	Cluster analysis of the electron density	110
4.3.7	Results II: Cluster analysis and the resulting mechanisms	116
5	Conclusion	121
A	Notational conventions	125
B	A brief introduction to differential forms	127
C	Kinetic energy operators from symmetry-adapted curvilinear coordinates	133
C.1	The kinetic energy operator in general coordinates	135
C.2	Vibration of a diatomic molecule	136
C.3	Double bond shift of cyclobutadiene	137
C.4	The Kekulé vibrational mode of benzene	140
C.5	Double bond shift and ring inversion of cyclooctatetraene	141
D	Quantum chemistry of cyclooctatetraene	145
E	Structure of malonaldehyde and the formic acid dimer	149

List of Figures

1.1	Schematic Diels-Alder reaction (made with Inkscape [3])	2
1.2	Butadiene and ethene (made with Inkscape [3])	3
1.3	Possible mechanisms of a Diels-Alder reaction (made with Inkscape [3])	4
1.4	Potential energy surface of a diatomic (made with Inkscape [3])	5
2.1	Deformation of a volume containing particles (made with Inkscape [3])	14
2.2	Ground state potential energy surface of a diatomic (made with Inkscape [3])	32
2.3	Possible reaction mechanism for a Diels-Alder reaction (made with Inkscape [3])	41
3.1	Electron density grid for benzene (made with Inkscape [3])	52
3.2	Angular π -electron density for benzene (made with Inkscape [3] and Matlab [4])	54
3.3	Points per angle for a Cartesian grid (made with Inkscape [3] and Matlab [4])	54
4.1	Mechanisms for tunneling in cyclooctatetraene (made with Inkscape [3])	57
4.2	Ground state potential energy surface of cyclooctatetraene (made with Inkscape, Matlab [4] and Amira [196]; credit to Falko Marquardt (Zuse-Institute Berlin) for preparation of the nuclear structures)	59
4.3	Localized and delocalized nuclear wave functions of cyclooctatetraene (made with Inkscape [3]); credit to Falko Marquardt (Zuse-Institute Berlin) for preparation of the precursor of this image	61
4.4	Symmetric double-well potential, adapted from reference [149] (made with Inkscape [3])	65
4.5	Probabilities for tunneling in cyclooctatetraene (made with Inkscape [3] and Matlab [4])	67
4.6	Electron densities of cyclooctatetraene (made with Inkscape [3] and Amira [196]); credit to Falko Marquardt (Zuse Institute Berlin) for preparation of the individual density plots	68
4.7	Fluxes and electron yields for tunneling of cyclooctatetraene (made with Inkscape [3] and Matlab [4])	69
4.8	Summary of the reaction mechanism for tunneling in cyclooctatetraene (made with Inkscape [3])	70
4.9	Mechanism of motion of benzene along the Kekulé mode (made with Inkscape [3])	71
4.10	Kekulé mode of benzene (made with Inkscape [3])	73
4.11	Potential energy surface for the Kekulé mode of benzene (made with Inkscape [3], Gnuplot [2] and Matlab [4])	76
4.12	Electron density of a Kekulé structures of benzene (made with Amira [196])	77
4.13	Electron density of a Kekulé structure of benzene for different isosurface values (made with Inkscape [3] and Amira [196])	77

4.14	Nuclear density for motion of benzene along the Kekulé mode (made with Inkscape [3] and Matlab [4])	78
4.15	Bond sector for benzene (made with Inkscape [3])	79
4.16	Electron numbers in the bond sector for motion of benzene along the Kekulé mode (made with Inkscape [3] and Matlab [4])	80
4.17	Fluxes into the bond sector for motion of benzene along the Kekulé mode (made with Inkscape [3] and Matlab [4])	81
4.18	Angular electron density for motion of benzene along the Kekulé mode (made with Inkscape [3] and Matlab [4])	82
4.19	Velocity of electrons and nuclei for motion of benzene along the Kekulé mode (made with Inkscape [3] and Matlab [4])	83
4.20	Zero-flux planes for motion of benzene along the Kekulé mode and tunneling in cyclooctatetraene (made with Inkscape [3])	87
4.21	Cylinder containing the electron density (made with Inkscape [3])	89
4.22	Flux through a box (made with Inkscape [3])	90
4.23	Possible mechanisms for proton tunneling in malonaldehyde and in the formic acid dimer (made with Inkscape [3])	95
4.24	Nuclear configurations for proton tunneling of malonaldehyde and the formic acid dimer (made with Inkscape [3] and Matlab [4])	97
4.25	Orbitals for the π -electron density of the formic acid dimer (made with Inkscape [3] and Molden [5])	98
4.26	Orbitals for the π -electron density of malonaldehyde (made with Inkscape [3] and Molden [5])	98
4.27	Angular densities and fluxes for proton tunneling in the formic acid dimer (made with Inkscape [3] and Matlab [4])	100
4.28	Angular densities and fluxes for proton tunneling in malonaldehyde (made with Inkscape [3] and Matlab [4])	101
4.29	Zero-flux surfaces for zero average angular flux, for proton tunneling in the formic acid dimer (made with Inkscape [3] and Matlab [4])	104
4.30	Zero-flux surfaces for non-zero average angular flux, for proton tunneling in the formic acid dimer (made with Inkscape [3] and Matlab [4])	105
4.31	Mechanism of proton tunneling in the formic acid dimer (made with Inkscape [3])	106
4.32	Zero-flux surfaces for zero average angular flux, for proton tunneling in malonaldehyde (made with Inkscape [3] and Matlab [4])	108
4.33	Mechanism of proton tunneling in malonaldehyde (made with Inkscape [3]) .	109
4.34	Zero-flux surfaces from cluster analysis of the electron density for proton tunneling in malonaldehyde and in the formic acid dimer (made with Inkscape [3] and Matlab [4])	117
4.35	Nuclear densities and fluxes for tunneling in ammonia (made with Inkscape [3] and Matlab [4])	118
4.36	Schematic nuclear and electron density for a diatomic (made with Inkscape [3])	120
C.1	Jacobi coordinates for cyclobutadiene (made with Inkscape [3])	138
C.2	Jacobi coordinates for benzene (made with Inkscape [3])	140
C.3	Jacobi coordinates for cyclooctatetraene (made with Inkscape [3])	142
D.1	Orbital occupation in cyclooctatetraene (made with Inkscape [3])	145

Foreword and acknowledgements

The monograph at hand addresses the concept of the mechanism of a chemical reaction. This concept is one of the pillars on which the field of chemistry rests, and it is used with self-evidence to predict or rationalize the outcome of reactions. Yet, from the quantum dynamicist's point of view the theoretical foundation of this pillar is surprisingly little developed: A lot of research aims at following the motion of nuclei during chemical reactions, but little is done regarding the motion of the electrons. The situation is in sharp contrast to the typical view of chemical reactions as rearrangements of the electronic structure. Thus, a lot can still be explored in this field, and some new aspects will be discovered in this text. But before diving into the field of electron dynamics during chemical reactions, let me first make a general remark regarding the text.

Please note the following: Whenever I will speak about “the chemist” and “the chemist's view”, I am referring to my personal view of the current situation in chemistry. This view was shaped by my own experience during my chemistry studies as well as by discussion with colleagues and friends from organic and inorganic chemistry. The question of what a chemical reaction or what a chemical bond is can be answered in many different ways, and I am trying to adhere to the mainstream view. Nevertheless, I fully acknowledge that there are other views, and that the situation I will describe in the following is much simplified. Also, I will implicitly stay within the realm of organic chemistry, i.e. I will focus on hydrocarbon compounds. The periodic table is rich, and for other elements other concepts are used. Those will, however, not be discussed here.

This work would not have been possible without a number of people, and it is a pleasure to name them here and to say thank you!

First and foremost, I want to thank my supervisors Jörn Manz and Beate Paulus for their continuous support and help in a variety of ways. Both left me the freedom to work independently, but they always had an open ear for questions and problems, as well as stimulating advice.

I am grateful to Jörn Manz for his commitment, and for sharing his experience and foresight. I learned a lot from him, not only in the area of quantum dynamics, but also in areas such as teaching, scientific working, and professional interaction with students and colleagues. Also, not only working with him was a pleasure, but also taking part in the recreational activities that he initialized or co-organized.

I am grateful to Beate Paulus for her guidance and her skill to inspire successful scientific work. She managed to establish and maintain a work group such that being part of it was a joyful experience. Her organizational talent and her care for the well-being of the people working for and with her impressed me. Discussions with her on various, not necessarily work-related topics have always been a delight. Thus, I am glad that I decided to make my doctoral studies under the supervision of Jörn Manz and Beate Paulus, and that they

decided to supervise me.

Next, I thank my mother Beate Schild as well as Stefanie and Nikola Stričević for their encouragement, trust and patience, and for always providing a counterbalance and a safe haven.

There are a number of colleagues that I am grateful to for joint work or discussions related to the field of electron fluxes and electronic flux densities. I thank Gunter Hermann and Vincent Pohl for making the initially inefficient and rudimentary Magic Density Creator, the program used for handling electron densities, a flexible and fast tool that can be used for many future applications. Their independence and creativity made working with them a delight. I thank Marcus Weber for our collaboration on the cluster analysis of the electron density, which already yielded promising results, and will still be the source of a lot of interesting insights in the future. For the work on motion of benzene along the Kekulé mode, I thank Deepanshu Choudhary and Vaibhav D. Sambre, who were enthusiastic and productive during their stay as research internees. For work on the visualization of electron densities, I thank Hans-Christian Hege and Falko Marquardt as well as, again, Vincent Pohl and Gunter Hermann, and for help with the program package WavePacket I thank Burkhard Schmidt as well as Ulf Lorenz. I thank (in alphabetical order) Dirk Andrae, Matthias Berg, Timm Bredtmann, Dennis Diestler, Jhon Fredy Pérez-Torres, and Jean-Christophe Tremblay for discussions about electronic fluxes in the Born-Oppenheimer approximation. Additionally, I thank Carsten Müller and Krista Steenbergen for discussions about a number of topics, and for cheering me up significantly a number of times.

Very important for the success of this work was also the administrative and technical help. To make this very important aspect of the daily work go so smoothly, I want to thank (in alphabetical order) Julija Djordjevic, Holger Naundorf, Annerose Polinske, Boris Proppe, Robert Schüttler, and Holger Weiß.

There are a number of friends who listened patiently to my complaints if something did not quite work out as planned and who always had advice regarding work, the life and everything. In this respect, a very special thanks goes to my friend and office mate Lukas Hammerschmidt, who listened to my innumerable problems and gave either tips or the sometimes necessary distraction. Furthermore, at this place I want to thank all the other people that helped me during the different stages of my thesis in this way, and especially (in alphabetical order) Felix Ameseder, Isabel Bohrn, Jan Eichler, Loryn Fechner, Roland Frenzel, Johannes Floss, Zita Hüsges, Magdalena Kaczor, Elisavet Kanaki, Eric Lehmann, Enrique Manjavacas Arevalo, Anna Sonnenburg, and Jenny Zieschang.

Last but not least, financial support during the time of my thesis by Deutsche Forschungsgemeinschaft, project DFG Ma 515/25-1, is gratefully acknowledged.

Chapter 1

Introduction

1.1 The static and the dynamic view of a chemical reaction

In 2007, a special issue of the Journal of Computational Chemistry with the conspicuous title “90 Years of Chemical Bonding” was published [77]. Part of this issue were nine essays [19, 78, 84, 114, 132, 165, 187, 192, 213] about the chemical bond which, starting from the article “The Atom and the Molecule” from Lewis [122], discuss aspects of the idea of a chemical bond. The topics covered include theories like atoms in molecules [19], valence bond theory [213] and its relation to molecular orbital theory [132], the molecular orbital theory of Hückel [114] and the valence shell electron repulsion model [84].

Lewis introduced empirical rules which are still one of the foundations of chemistry today. In practice, chemists think in terms of bonds and electron pairs, and use the chemical structures similar to those introduced by Lewis (and thus still called Lewis structures) to derive “reaction mechanisms”. The quotes indicate that these “reaction mechanisms” have a very particular meaning different from what a layperson might expect, and this discrepancy is to be discussed below. After Lewis published his approach to chemical reactions, a number of theories were developed over the course of the years. These were influenced heavily by the development of quantum mechanics, and especially by the introduction of a versatile quantum mechanical formalism in 1926 by Schrödinger [185], which proved to be well applicable to chemistry. It was noted that an understanding of the successful empirical concepts of chemistry have to be related to quantum mechanical principles applied to a set of nuclei and electrons. An important step in this development was the publication of the first quantum mechanical description of covalent bonding in the dihydrogen molecule by Heitler and London in 1927 [99], and further steps soon followed.

Despite the knowledge that theories of chemical reactions should be based on quantum mechanics, there are a large number of empirical concepts found in chemistry which are introduced by experience rather than by derivation from first principles. Frenking and Krapp coined the term “unicorn” for these concepts, as a mythical but useful “creature which brings law and order [...] in an otherwise chaotic and disordered world” [78]. If you look at any publication in chemistry you almost certainly see some unicorns jumping around. They cause colorful rainbows which may leave the reader stunned as she tries to catch or tame the unicorn. Like Frenking and Krapp state: “Chemists had become so intimate with their unicorns [...]. This made it very difficult until today to introduce new concepts which do not agree with the unicorn world” [78].

Next to the chemical bond as a prototypical unicorn, it may even be asked to what extent

the idea of the molecule itself is a unicorn. The emergence of molecular structure from the complete molecular Hamiltonian is a difficult topic, which has already been addressed some years ago, see e.g. [49, 129, 202, 227–230]. An interesting article by Sutcliffe and Woolley [203] discusses to what extent the notion of molecular structure is influenced by time-independent calculations with clamped nuclei (see also [200, 201] for some déjà vu experience). Recently, numerical studies on three, four, and five particle systems were performed by Mátyus and coworkers [139–141] for particles with different masses, in order to see how the molecular structure emerges from the all-particle wave function.

It is, with our present mathematical understanding of quantum mechanics, impossible to solve any system which is more complex than the hydrogen atom analytically in the sense of Schrödinger’s quantum theory. Slightly larger systems may be solved to numerical accuracy, but there is no hope to obtain the complete wave function for a chemically relevant molecule. The problem of solving the quantum mechanical description of a number of interacting particles, known as the many-body problem [72, 138], has stimulated the development of a number of general approximation techniques. Studies of molecular systems inspired by the unicorns of chemistry have led to various models for chemical bonding. Based on these models, “reaction mechanisms” are used to rationalize the course of a chemical reaction. But there is one striking deficiency of the devised “reaction mechanisms”: They are a bookkeeper’s method of counting and shifting electrons, but they do usually not represent the way how electrons move during the chemical reaction. Thus, they are a static concept and do not represent the dynamic mechanism of a reaction.

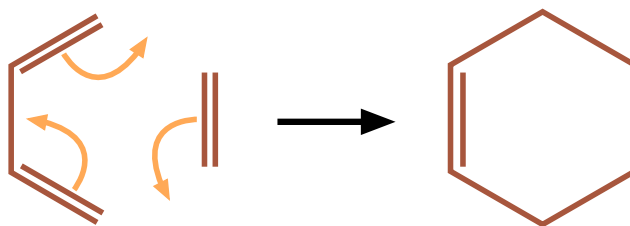


Figure 1.1: Schematic representation of a general Diels-Alder reaction using Lewis structures. Arrows indicate a possible “reaction mechanism”.

The discrepancy can best be explained by an example: Fig. 1.1 depicts the chemical reaction of ethene and butadiene to form cyclohexene. In fact, this reaction does not really happen, and this finding is often explained by invoking appropriate unicorns. Nevertheless, there are a number of reactions of molecules which are considered to proceed in the way indicated by Fig. 1.1. These reactions, known by the names of Otto Diels and Kurt Alder [65, 164], have in common that a diene (like butadiene) reacts with a so-called dienophile (like a substituted ethene) in a ring-closing reaction.

In Fig. 1.1, the molecules of the prototype reaction are represented as Lewis structures. A number of steps need to be done to arrive at this representation:

- In Schrödinger’s formulation of quantum mechanics, the molecular system is described by one complex field (the wave function) of both the electronic and nuclear coordinates. This field has to be divided approximately into two fields, one for the electrons (the electronic wave function) and one for the nuclei (the nuclear wave function). The division is accomplished by the Born-Oppenheimer approximation [36], which is discussed below extensively. Nuclei and electrons are treated completely differently in chemistry, and one has to account for that.
- The nuclei need to be localized somehow. The chemist’s molecule is a geometric structure or a three-dimensional network, for which each corner represents a specific

1.1. The static and the dynamic view of a chemical reaction

nucleus. Often, the nuclei are considered as essentially classical entities: points or very small regions with definite location and velocity in three-dimensional space. Moreover, chemists also tend to think in terms of interacting atoms. Instead of localizing only the nuclei, most electrons are also attributed to a specific nucleus, and some are considered shared between the nuclei. In calculations this thinking is reflected by the basis set used to construct the electronic wave function: This basis is generally a set of functions inspired by the eigenfunctions of the hydrogen atom and centered at the position of clamped nuclei.

- The electrons have to be divided into different groups with different chemical meaning. This chemical division also directly influences how calculations for the electronic wave function are performed: The wave function is determined in a way which is inspired by the chemical unicorns, and thus exhibits a mathematical structure that makes the partition possible. The form of the electronic wave function is thus discussed in detail in section 3.3.

What does Fig. 1.1 stand for? In Fig. 1.2, the left-hand side of Fig. 1.1 is shown in a different way, with more information. The corners in Fig. 1.1 correspond to the position of carbon nuclei (C), and there are also 10 hydrogen nuclei (H) which were not even indicated in Fig. 1.1. Note that Fig. 1.2 does not fully represent the way in which a chemist would think of this reaction: He would never imagine the hydrogen atoms in ethane and at the CH_2 groups in butadiene to be in the plane of the carbon atoms, but more or less perpendicular to this plane. Also, he would not expect the reaction itself to proceed in a plane.

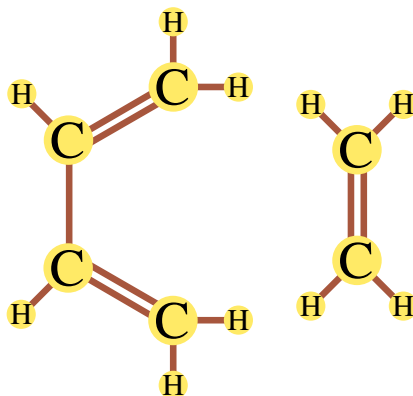


Figure 1.2: Another representation of the left-hand side of Fig. 1.1, with carbon and hydrogen atoms indicated explicitly.

Thus, in order to speak of a molecule first the nuclei have to be localized in space, e.g. by considering only the energetically most stable configuration of the nuclei (the equilibrium structure). Next, the nuclear locations are connected by lines as shown in Fig. 1.1 and Fig. 1.2, which represent the interesting parts of the electrons. The electrons are divided into two classes, core and valence electrons. Only the latter are considered to change during a chemical reaction, and only these are drawn. The former are thought of as spectators during the reaction, and may move with the nuclear position but do not change otherwise. Each line between two nuclei represents a chemical bond, which in turn is thought of as being formed by two valence electrons. In a way, there are atoms (a nucleus and, for an electronically neutral molecule, as many electrons as there would be in a free atom) which are attached to each other by sharing some electrons. There are different types of these chemical bonds: The bonds between C and H are of no interest for the reaction and are omitted in Fig. 1.1. Between the carbon nuclei there are two types of bonds: single bonds and double bonds.

These are qualitatively different and behave differently in chemical reactions: The former are so-called σ -bonds which are thought of as being along the nucleus-nucleus connection line. Of the latter, one bond is a so-called π -bond, for which the respective electron has zero probability to be found along the nucleus-nucleus connection line.

Bonds only make sense if a chemical reaction is considered. They are useful to classify and draw single molecules, but in a chemical reaction bonds are being formed or being broken, and this dynamical view is the strength of the bond concept. A chemist seeing a chemical structure does usually associate certain attributes with parts of the structure which are related to chemical reactivity in different environments. In this way, a chemical bond is an intrinsically dynamical concept.

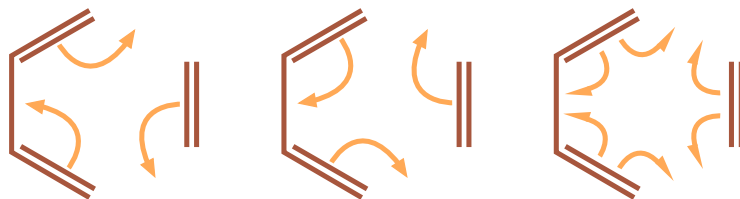


Figure 1.3: Three possible “reaction mechanisms” of the reaction of Fig. 1.1.

Fig. 1.1 shows the “reaction mechanism” in form of the arrows. These arrows indicate how the bonds have to be rearranged in order to get from the reactants (ethene and butadiene) to the product (cyclohexene). Generally, many different ways are possible to draw these arrows. There are sometimes also different arrows used with different meanings, e.g. the usual curved arrow for the shift of two electrons (a bond) and a fishhook arrow (with only half of the arrow head) for the shift of one electron only. Some possibilities for the example reaction are given in Fig. 1.3. For a throughout account on the usage of arrows in chemistry see [11]. As practical as these arrows may be, there is an important problem: The arrows represent the net change from one molecular structure to the other, but they do not represent the dynamics of the chemical reaction. That is, they do not represent how the electrons really move, and thus they do not represent the reaction mechanism (without quotation marks). This situation might be improved by finding reaction intermediates or by excluding certain mechanisms based on experience with other chemical reactions. Nevertheless, especially on the theoretical side there was little done until now to adapt a completely dynamical picture.

The special issue on chemical bonding [77] does reflect this situation very well: Although Truhlar in [213] emphasizes that chemical bonds are related to processes, this essay is the only article of the issue (with 9 essays and 28 research articles) which at least touches the topic of chemical dynamics. The well developed and well developing field of quantum chemistry is concerned with solution of the electronic structure for fixed nuclei. Statements about reaction mechanisms are often based solely on the shape of the potential energy surface, and it is customary to look at the energetically most favorable part connecting reactants and products (the minimum-energy reaction path) [220], although it is long known that this can be problematic [93].

1.2 Three types of electron rearrangements

Chemical reactions may be divided into two classes: Reactions in the electronic ground state, and reactions involving electronically excited states (called excited state reactions). It is only sensible to talk about electronic states in terms of the Born-Oppenheimer approximation which separates nuclear and electron dynamics on the basis of different time scales on which

1.2. Three types of electron rearrangements

the particles move. Fig. 1.4 shows schematically the form of possible electronic states in a diatomic. An electronic state is a function of the internuclear coordinates, and in the case of a diatomic of the internuclear distance. It constitutes a potential for the nuclear motion. In principle, for molecules other than diatomics these states may cross at conical intersections and may have complicated shapes. A ground state reaction is a reaction for which the nuclear dynamics during the whole reaction can be well described by considering only the energetically lowest electronic state. These reactions happen at energies corresponding to temperatures between zero Kelvin and ambient temperature, or are induced by moderate heating. In contrast, excited state reactions involve one or more electronically excited states at some point during the reaction. Thus, for the correct description of the nuclear dynamics several electronic states have to be taken into account. The energies needed for such reactions are usually in the range of a few electron volts, and the reaction is often induced by visible or UV light irradiation.

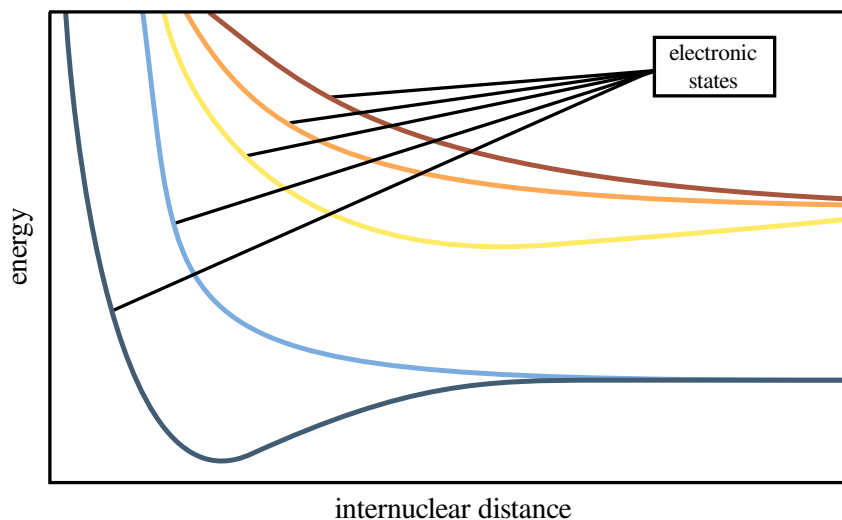


Figure 1.4: Schematic representation of the electronic states of a diatomic.

A remarkable difference between the two types of reactions is the amount of electrons flowing per time unit. For excited state dynamics, the electronic motion may happen on the time scale of attoseconds (10^{-18} s) [110]. Thus, in calculations the nuclei are often considered frozen because nuclear vibrational motion is much slower than the electronic motion in such cases. The nuclear wave function may then be approximated by only one nuclear configuration. Consequently, for a given set of nuclear positions the dynamics is described by a superposition of electronic wave functions of different electronic states. Only for longer time scales nuclear motion has to be taken into account, and then it may happen that the nuclear wave packet comes close to a conical intersection. In such cases, the electronic rearrangement happens on a similar time scale as the nuclear rearrangement, and the Born-Oppenheimer approximation is not applicable. [121, 233]. Usually, there is a strong electron flux involved in excited state reactions and the electronic structure changes qualitatively and rapidly. For example, a simulation of Ulusoy and Nest showed that the electronic character of benzene can completely vary on the attosecond time scale if appropriate electronic states are excited [214]. Another example is the laser induced ring current in magnesium porphyrin [28]: By excitation with a circularly polarized UV laser Barth, Manz, Shigeta and Yagi showed that it is possible to induce a (direct) current of 84.6×10^{-6} A, i.e. a circulation of 0.528 electrons per femtosecond. However, in the gas phase these ring currents decay quickly due to translational motion [23].

Most of practical chemistry happens in the electronic ground state, and in this work only such reactions are considered. The typical time scale of ground state reactions is that of the

nuclear motion, i.e. femtoseconds (10^{-15} s). As I personally learned, there are scientists who would say that there cannot be electron dynamics in the electronic ground state, because staying in only one electronic state means that the electronic wave functions are always stationary. However, for lots of chemical reactions the approximation that the molecules stay in the electronic ground state while the reaction takes place is appropriate for the nuclear dynamics. As discussed below, this nuclear dynamics induces a time-dependent electron density and thus an electron flux. The electron flux in this approximation is in principle an effective flux, because there are two time-scales involved: A fast electronic time scale, and a comparably slow nuclear time scale. The idea of these two time scales can be understood best in a classical picture, where there is only one definite nuclear configuration present at a certain time. Thus, either the time variable or the path of the nuclear configuration may be used to parametrize the electronic part of the problem. In this case, under the assumption that the time-dependence of the nuclear configuration is slow compared to the electronic motion, the adiabatic theorem [108] may be used. In the limit of infinitely slow change of the nuclear configuration, the electronic wave function will be restricted to only one potential energy surface for the complete motion, cf. [124]. While the quantum mechanical picture is certainly more difficult, applicability of the restriction to only one electronic state was studied in a similar spirit by the method of multiple scales in [88], see also [89]. Nevertheless, if the approximation that the reaction happens in only one electronic state is applicable, the effective electron flux should also be a very good approximation to the true electron flux, see [69].

During the effective electronic motion very few electrons actually move, as will be seen in the applications. The values of the model system benzene in section 4.2.4 shall be used for comparison. For the dynamics of Benzene along the Kekulé mode, 0.199 of the π -electrons and 0.134 of the other valence electrons move (in opposite directions). The electron density oscillates and thus gives rise to an alternating, periodic current. This is in contrast to the direct current induced in magnesium porphyrin mentioned above, where the electron dynamics is circular in one direction. The motion of Benzene along the Kekulé mode is periodic with a period of about 24 fs, and thus there is a total alternating current of about $(0.199 - 0.134)/24 = 0.0027$ electrons per femtosecond or a π -electron current of about $0.199/24 = 0.0083$ electrons per femtosecond.

There is third type of electron rearrangements which is routinely accessed experimentally, and which may be distinguish in terms of the strength of the induced electron flux. Static magnetic fields induce electronic currents in molecules. A particularly famous example is the ring current induced in benzene, which has an effect on the nuclear magnetic resonance (NMR) spectrum and is sometimes used to define the unicorn aromaticity [71, 145, 197–199]. The static magnetic field induces an electron current such that the magnetic field induced by this current compensates the effect of the external field as well as possible. In benzene and other aromatic molecules there is a static, oriented ring current which can be attributed to electrons in π -orbitals [199]. These ring currents have effects on the NMR spectrum, because the induced magnetic field amplifies or weakens the effect of the static magnetic field on the hydrogen or carbon atoms. However, the induced current is very small: In [104], Johansson, Jusélius and Sundholm give a value of about 12×10^{-9} A/T for the total current. A typical magnetic field in an NMR experiment has a strength of about 10 T and thus induces a ring current of 12×10^{-8} A, or 0.00075 electrons per femtosecond. In this context, see also the discussion in [28] on the strength of electronic ring currents in magnetic fields and in suitably chosen laser fields.

1.3 Simulation methods for chemical reactions

In order to find the mechanism of a chemical reaction, it is necessary to know both the dynamics of the nuclei and that of the electrons. In particular, it is not enough to look only at how the nuclear and the electron density change with time, i.e. to look at where the nuclei and electrons are at a certain instant of time. Information about speed and direction of the particles would be missing. For the nuclei this is usually of minor importance, because they are either treated classically and their classical velocities are known, or because the complete time-dependent wave function and thus information about the velocity of the motion is available. For the electrons, on the other hand, it is not yet possible in practice to simulate the fast dynamics together with the dynamics of the nuclei: The simulation would have to use a very small time step, and the dimensionality of the problem at hand is prohibitively large. So far, there is a complete quantum mechanical simulation of both nuclei and the electron for the dihydrogen cation [25], and there is the multi-configuration electron-nuclear dynamics method [163, 215] which was applied to diatomics like lithium hydride [97, 216].

The positions of the nuclei are thus usually known from a dynamics simulation. The arrows indicating the reaction mechanism are unknown, however, because the time-dependent electronic wave function would be necessary. Specifically, the vector field which shows the reaction mechanism is the electronic flux density (also called electronic probability current), and from this field the reaction mechanism could be directly read off. As explained in the next chapter, the flux density is a bit capricious and difficult to obtain. But before starting the exposition of the current research status in the theoretical determination of reaction mechanisms, the different ways of how dynamics in molecular systems is calculated are reviewed.

Currently, there are a number of different approaches to investigate chemical reaction dynamics, which operate on different levels of complexity and have different applicability. For large molecular systems, molecular dynamics simulations are used which solve the classical equations of motion for the nuclei using effective force fields [118]. These forces are often only working between two nuclei of the system, or even only between static fragments of the molecule. While such dynamics simulations are certainly useful to investigate complex problems as the dynamics of protein folding (see e.g. [217]), they cannot give information about the arrows or the reaction mechanism because electrons are not considered explicitly at all. However, with such techniques it is possible to identify dynamical molecular structures which are most important for the process of interest, and these can then be analyzed in detail using other methods. For smaller systems, it is possible to simulate the dynamics with *ab initio* molecular dynamics [135, 136]. In such simulations, the nuclei are still point particles, but for a given nuclear configuration the electronic problem is solved with computationally cheap quantum chemical methods like Hartree-Fock theory [204] or applied density functional theory [112]. The quantum chemistry calculation yields an electronic wave function and an electronic density. Thus, it is possible to describe chemical reactions, albeit in a comparably crude way. One may employ the method of Patchkovskii [172] to obtain an electron flux density along the classical nuclear paths. Alternatively, one may partition the density into parts which are attributed to a given atom and simply use the nuclear velocity to obtain a flux density, compare e.g. with [67]. There are several methods to partition the density sensibly. For an overview of different real space partitions of the one-electron density that could in principle be used, see [173]. To the best of my knowledge, however, there have not been any attempts to calculate electronic flux densities of an *ab initio* molecular dynamics simulation.

At the most basic level, both nuclei and electrons are described at a quantum mechanical

level. This approach may be termed quantum reaction dynamics, although there are different meanings for this term in the literature. For such a quantum mechanical simulation, there is usually no hope to describe all possible degrees of freedom: The nuclear dynamics has to be solved in many dimensions which becomes costly quickly. Additionally, quantum chemistry calculations may become the bottleneck because the nuclear wave function might explore large parts of the potential energy surface. Thus, the electronic problem has to be solved for many nuclear configurations. Especially because calculations for structures close to the transition state of a reaction are often demanding (they exhibit multireference character, see [205]), high-level quantum chemical methods may be needed for which many calculations are not feasible. One then often works with model systems in reduced dimensionality, which only include what is expected to be the relevant degrees of freedom. The approach is often applied for gas phase reactions at the ideal situation of zero temperature.

Finally, there is the possibility to treat the chemically important part by quantum dynamics, and to include effects of the molecular environment by e.g. appropriate construction of a system-bath density matrix. The dynamics of open quantum systems is a theoretical framework where such an approach is possible. For an introduction and some applications see [46, 142].

1.4 Current status of the dynamical view of a chemical reaction

Practically all dynamics simulations of molecular systems aim at a mechanistic understanding of the processes in the system. The main interest here, however, is the mechanism in terms of the electron dynamics during a chemical reaction, and there is comparably little literature about this subject in the theory of chemistry. In fact, the development and usage of the electronic flux density and electron fluxes is still only beginning, and thus it is possible to give a comprehensive overview of the field. Only studies which somehow include both nuclear and electron dynamics are presented, as only these are reaction mechanism studies in the sense of this work.

For ab initio molecular dynamics simulations, there is the possibility to calculate electron fluxes, and approximate electronic flux densities. The nuclei are treated classically, but for the electrons an electronic wave function is available. The dynamics happens usually in the electronic ground state, and in the next chapter it will be explained that it is not straightforward to obtain the electronic flux density in such a situation. There is one approach in the literature which is derived from the current density obtained from Nafie's complete adiabatic wave function [155]. While in the original formulation of Nafie the current density is calculated via electronically excited states, there is a reformulation by Patchkovskii [172], which expresses the flux density as third-order response of the ground-state electronic energy. This method was applied by Patchkovskii e.g. for an artificial model dynamics (not a dynamics simulation) of the proton transfer in 7-azaindole. Another possibility to calculate an electronic flux density in ab initio molecular dynamics is to use the empirical time shift flux introduced by Okuyama and Takatsuka [167]. Both possibilities have drawbacks that will be discussed in section 2.4.

A different approach is to describe electron dynamics by explicit inclusion of electronically excited states. Takatsuka and his group contributed a lot in this field (for an overview, see [207, 234]). Their calculations are of specific interest in this context because of several studies relating to reaction mechanisms: Using their semiclassical Ehrenfest theory, the double proton transfer reaction in the formic acid dimer [168], the gas phase and the water-

assisted proton transfer in formamide [159] as well as the excited-state proton-electron transfer of phenol with an ammonia cluster [160] could be simulated. The results from these dynamics simulations show how important it is to analyze the electron dynamics, in contrast to the traditional static view: In case of the proton transfer in the formic acid dimer it was found that the proton carries significant electron density during the transfer. Also, the compensating electron dynamics happens within the monomers, from one oxygen to the other [168]. For formamide, the simulations yield that the process is a proton transfer (in contrast to a hydrogen atom migration), and that proton motion induces an electron flux in opposite direction to the proton motion [159]. In case of the simulation of photoinduced proton-electron transfer of phenol to ammonia clusters it was found that the proton transfers without compensating electronic motion, and that the electron moves from phenol to the ammonia cluster on a different pathway [160]. Also, developments of a non-Born-Oppenheimer semiclassical wave packet theory for both electrons and nuclei seems a good candidate to investigate chemical reactions, see [206, 236]

In 2009, Barth, Hege, Ikeda, Kenfack, Koppitz, Manz, Marquardt and Paramonov solved the (non-relativistic) coupled nuclear and electron dynamics of the dihydrogen cation exactly [25] and were able to calculate not only electron fluxes but also the electronic flux density. They showed that the exact electron fluxes into or out of a region are in very good agreement with the fluxes calculated from an appropriately defined time-dependent electron density. All applications in this monograph will use these fluxes, and in the next chapter the theory of these fluxes is discussed. Subsequently, some chemical rearrangements were analyzed in terms of these fluxes: The Cope rearrangement of semibullvalene both in the tunneling regime and with energies above the reaction barrier [12, 45], vibrations in ethane, ethene and ethine contrasting the behavior of single, double and triple bonds [42], tunneling dynamics of cyclooctatetraene [98], and finally motion of benzene along the Kekulé vibrational mode [182]. The last two examples will be discussed at length in Chapter 4.

Last, there is the effort to find an approximate electronic flux density for ground state reactions. Diestler developed the coupled-channels theory for the hydrogen atom and dihydrogen cation [66], with first numerical results in [68] and further development in [69]. The road to a generalization of the theory for other molecules was started to be paved in [67].

1.5 Contents of this monograph

The direct quantum mechanical analogue of the arrows indicating reaction mechanisms is the electronic flux density. In Chapter 2 this concept is reviewed, first as general idea in continuum mechanics and then in quantum mechanics. Special emphasis is on the flux density in the Born-Oppenheimer approximation: Because the fast electronic motion is being averaged over, it is difficult to find an electronic flux density in this approximation. However, less information than the flux density provides is necessary to find the reaction mechanism: Often, it may be enough to know electron fluxes in to or out of certain volumes. These fluxes can be calculated, and they will be used to analyze model reaction mechanisms.

In Chapter 3, it will be seen how the time-dependent electron density is calculated that is needed to find the electronic fluxes. The structure of this density is important, because to make statements about chemical reaction mechanisms the electrons have to be partitioned chemically. Luckily, due to the quantum chemical methods which are used the electronic wave function readily exhibits a “chemical structure”. For example, core and valence electrons may be separated easily, and it is possible to distinguish between single and double bonds or between σ - and π -electrons.

Chapter 4 contains three applications of the electron fluxes to find details about reaction mechanisms. The examples are so-called pericyclic electron rearrangements: These are rearrangements for which the electrons are considered to flow in circles. Fig. 1.1 shows such a pericyclic mechanism. This type of reactions is particularly easy to analyze because the mechanism is effectively one dimensional, at least for one ring structure. The interesting electron dynamics can be analyzed using only one angular coordinate, and investigation of such systems yields new insights about a variety of reactions.

A first application is the tunneling dynamics in cyclooctatetraene. In this molecule, two processes happen simultaneously: inversion of the tub-shaped molecule, and shifting of the double bonds. After setting up an appropriate tunneling model, the electron flux is calculated and analyzed. The number of electrons which move effectively and the reaction mechanism will be determined. The second application is a dynamics of benzene prepared as a Kekulé structure. A nuclear quantum dynamics along the Kekulé vibrational mode is simulated and the induced electron dynamics is observed. In this model, further dynamical statements can be made regarding the way in which different chemical types of electrons move. Last, an important problem for the application of electron fluxes to yield reaction mechanisms is addressed: As the flux is defined only with respect to a closed volume, part of the information about the flux direction is not available. This information would also be needed to construct a flux density on basis of the fluxes. The consequences of the missing information, a time-dependent parameter for the fluxes, is investigated for proton tunneling in malonaldehyde and double proton tunneling in the formic acid dimer.

Chapter 2

Theory

2.1 Abstract

Models of chemical reactions mechanisms rely on assumptions of how the nuclei and electrons move during the course of a chemical reaction. In molecular quantum mechanics, the concepts which can be used to describe the movement of nuclei and electrons are probability densities and the corresponding flux (or probability current) densities: The former are scalar fields representing the probability to find the respective particles in a given volume. The latter are vector fields representing the velocity of the corresponding probability density. Hence, probability densities show where the particles are, and flux densities show what they are doing.

Probability densities are a very well known and often used quantity [191]. Most quantum chemistry programs can calculate one-electron densities, e.g. for analysis and visualization of the results. In density functional theory [112] the basic quantity is the electron density instead of the electronic wave function, and there are numerous applications in the realm of electronic structure calculations [112]. In nuclear dynamics simulations, the change of the nuclear density with time is used to illustrate the dynamics and to study and interpret the dynamical processes.

In contrast, the usage of flux densities is comparably rare in chemistry. There is a current density functional theory developed to describe the effect of magnetic fields on electronic structure [219], and there are examples of nuclear flux densities used to study nuclear dynamics, e.g. [10, 41, 143]. Flux densities were used to study laser-induced electronic ring currents in atoms [27] and molecules [28]. Also, flux densities were used for the study of vibrational transitions [155, 157, 158]. However, application of electronic flux densities for the analysis of chemical reactions are new and few, and the theory in this field is only beginning to develop. Electronic flux densities for the motion of the dihydrogen molecule cation were calculated to numerical accuracy [25] and using the scaled coupled channels theory [69]. Semi-classical Ehrenfest theory was used to determine electronic fluxes for chemical reactions [159, 160, 167, 168], also including laser fields [207] and to characterize chemical bonding [235]. There is also a model application of an electronic flux density to a molecular dynamics simulation [172]. Nevertheless, compared to the vast literature about chemical reactions these few applications are only the first shoots of the orchid of knowledge, which still has to grow and to bud. This situation is unfortunate, because chemists use models to predict reaction outcomes based on assumed motion of electrons, and more theoretical understanding to test the empirical intellectual edifice should be welcomed.

In this chapter the idea of densities and flux densities is discussed. Because the concept of a flux density is so little used in chemistry, it will be investigated in detail. First, in section

2.2, the general idea of a flux density is discussed, which can be found in any continuum mechanics. It will be seen that a density gives rise to a flux density and that the two are related by an important mathematical identity, the continuity equation. In section 2.3, the focus is on the flux density in quantum mechanics. After deriving the quantum mechanical expression for a flux density, its relation to the momentum and angular momentum expectation value will be studied.

For almost all quantum chemistry and quantum dynamics methods the Born-Oppenheimer approximation (BOA) [36] developed in 1927 is used. This approximation is an example of an adiabatic approximation, because the electrons are considered to be much faster than the nuclei. Consequently, the electrons are considered to follow the nuclei adiabatically: The nuclei are not fast enough to induce changes of the electronic structure by their motion, but only by their instantaneous position. It is important to study how this approximation influences the form of both the nuclear and the electronic flux density. In section 2.4, an expansion of the wave function in terms of the electronic eigenstates, called the Born-Oppenheimer expansion (BOE), is reviewed. Using this expansion, the BOA can easily be applied. It will be illuminating to see the mathematical structure of time-dependent electron densities and flux densities when the wave function is written as a BOE. Especially, it will be seen that restriction to only one electronic state will make nuclear and electron dynamics impossible.

This situation is of course completely unsatisfying, because for most chemical reactions of interest, and all chemical reactions discussed in this work, the approximation that the reaction happens in only one electronic state is justified. Luckily, if the BOA is invoked, the time-dependence of the electron density is regained. Notwithstanding, the corresponding electronic flux density is not as easy to obtain. Thus, section 2.4 closes with a discussion of literature-known approaches to calculate the electronic flux density in the BOA.

Finally, in section 2.5 it will be seen how the problem of the tricky electronic flux density in the BOA may be circumvented: For chemical reaction mechanisms it is in general not necessary to know how the electrons move at each point in space. Instead, it might be enough to know the flux of the electrons through observer planes. This approach will be discussed in section 2.5 in detail. All applications in chapter 4 will use only electronic fluxes, and not electronic flux densities, to analyze the dynamics of chemical model reactions.

2.2 The flux density concept

2.2.1 Flux densities in continuum mechanics

In classical particle mechanics [85, 115] the state of a system consisting of a number of point particles at time t is completely specified by the positions $\mathbf{q}(t)$ and velocities $\partial_t \mathbf{q} = \dot{\mathbf{q}}(t)$ of the constituting particles: All measurable quantities, the observables, can be calculated from \mathbf{q} and $\dot{\mathbf{q}}$. Given the dynamical equations, e.g. Newton's equations, the positions and velocities of the particles at any time can be calculated if $\mathbf{q}(t_0)$ and $\dot{\mathbf{q}}(t_0)$ are known for some time t_0 . The dynamics of the system is also easy to visualize. The time evolution of the particle positions in the three-dimensional space (3-space, for short) of the coordinates of the individual particles can be used to find out what happens in the system. Also, a vector can be attached to each position showing direction and magnitude of the instantaneous particle velocity. In this way it is straightforward to analyze the details of the system dynamics.

Although in (non-relativistic particle) quantum mechanics [146] point particles are considered, the properties of the system are not given by functions localized at points in space. Instead, the system is, at least in the formalism that will be used here, described

2.2. The flux density concept

by complex-valued functions defined over the whole configuration space (the space of the vectors \mathbf{q}). This formalism, known as Schrödinger’s wave mechanics, is the formalism which is generally used in theoretical chemistry. The system is specified by a wave function $\phi(t, \mathbf{q})$, from which all observables can be calculated. Similarly to classical particle mechanics, the wave function at some time t_0 together with the dynamical equations, e.g. the Schrödinger equation [185], completely determines the fate of the system. However, positions and velocities of the particles can only be determined by measurement, and all that is known in advance are distributions giving the probability of a certain measurement outcome.

It may nevertheless be desirable to analyze the dynamics of the system in a similar fashion as can be done in classical mechanics. The closest equivalent to the position of the particles in classical mechanics is the quantum mechanical probability density $\rho(t, \mathbf{q}) = |\phi(t, \mathbf{q})|^2$, which represents the probability of finding the particles in a volume $d\mathbf{q}$. Although ρ is a field over the whole configuration space, this function may be visualized in 3-space by integrating over all but the coordinates of one of the particles. The equivalent to the classical velocities can either be a velocity density or, more appropriately, the flux density.

On one hand, the concept of a flux density is widely used in continuum mechanics [154] as well as in scattering theory [54], and to analyze electron currents induced by stationary magnetic fields [29, 96, 195]. On the other hand, there are few recent examples showing the utility of flux densities and fluxes to analyze electron dynamics in ground and excited state chemical reactions, see [12, 25, 45, 66, 68, 98, 134, 159, 160, 167, 168, 172, 182, 207]. In this section, the idea of a flux density is introduced in a general way, applicable to any kind of continuum theory. To make the discussion more intuitive, the exposition of [17] is followed closely. The terminology is tailored to fluid dynamics, but there is no restriction imposed and the treatment can be translated to the language of quantum mechanics.

Before reading this part and the following parts of this chapter, it may be worthwhile to have a look at Appendix A to learn how the notation is designed.

As it is custom in fluid dynamics, the discussion is constrained to real 3-space throughout this section. Hence, all vectors occurring for now will be in \mathbb{R}^3 . The picture to start from is the following: Instead of looking at single particles, a continuous distribution of generalized particles is considered. This distribution will in the following be called particles, for simplicity. However, as these particles are not discrete nor countable, any quantity derived from the continuous particle distribution can only be observed if it is averaged over a region of space, which may in principle be arbitrarily small. The position \mathbf{x} of a particle at time t is determined by the dynamical equations (which will not be specified here) as well as by the position $\mathbf{y} = \mathbf{x}(0)$ of the particle at time $t = 0$,

$$\mathbf{x} = \mathbf{x}(t, \mathbf{y}). \tag{2.1}$$

The \mathbf{x} -coordinates are also called the spatial coordinates. These can be thought of as a continuous reference grid, and functions of \mathbf{x} can be thought of as describing the system by an observer fixed in space. The requirement that a particle is uniquely defined at all times is expressed by the non-vanishing determinant of the Jacobian matrix

$$J = \det \frac{\partial x_i}{\partial y_j}. \tag{2.2}$$

Because $J \neq 0$, eqn. 2.1 can be inverted,

$$\mathbf{y} = \mathbf{y}(t, \mathbf{x}). \tag{2.3}$$

The \mathbf{y} -coordinates are called the material or particle coordinates. Functions of \mathbf{y} keep track of the particles. That means, a set of numbers for \mathbf{y} can be thought of as labeling a certain particle, and in these coordinates the system is viewed by an observer following the particles. Any function $F(\mathbf{x})$ depending on the spatial coordinates can also be viewed as a function of the particle \mathbf{y} via $F(\mathbf{x}(\mathbf{y})) = \tilde{F}(\mathbf{y})$, and vice versa. Connected with these two views are two derivatives,

$$\partial_t = (\partial_t)_{\mathbf{x}}, \quad \text{the spatial (space-fixed) derivative and} \quad (2.4)$$

$$D_t = (\partial_t)_{\mathbf{y}}, \quad \text{the material (particle-fixed) derivative.} \quad (2.5)$$

The subscript of the bracket means that this variable is kept fixed when differentiating. In this section, ∂_t will from now on always mean the time derivative keeping \mathbf{x} constant.

The action of D_t on a function $F(t, \mathbf{x}(t, \mathbf{y}))$ shall now be calculated. For the derivative D_t the independent variable is \mathbf{y} , and the chain rule for derivatives is applied to F to find

$$D_t F(t, \mathbf{x}(t, \mathbf{y})) = \sum_i \frac{\partial F}{\partial x_i} D_t x_i + \partial_t F. \quad (2.6)$$

The quantity $\mathbf{x}(t, \mathbf{y})$ is the position of particle \mathbf{y} , and D_t is the time derivative keeping the particle constant. Consequently, $D_t x_i$ is the i th component of the particle velocity \mathbf{v} , and

$$D_t F(t, \mathbf{x}(t, \mathbf{y})) = (\mathbf{v} \cdot \partial_{\mathbf{x}}) F + \partial_t F. \quad (2.7)$$

Eqn. 2.7 connects the spatial and material derivative. Note that the spatial gradient is denoted by $\partial_{\mathbf{x}}$, cf. Appendix A.

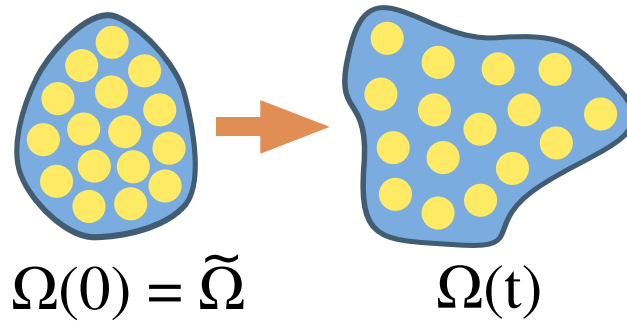


Figure 2.1: Volume Ω containing a fixed number of particles, which changes its shape during the system dynamics (left at time 0, right at time t).

Consider a volume Ω in position space (i.e., in \mathbf{x} -space) consisting of the same particles \mathbf{y} at all times, as shown schematically in Fig. 2.1. It should be kept in mind, however, that the particles are distributed continuously. Let $F(t, \mathbf{x})$ be a function defined within this volume. The main object in the following is to calculate the change in time of some $F(t, \mathbf{x})$, averaged over the well-defined particles in Ω . That is,

$$D_t \iiint_{\Omega} F(t, \mathbf{x}) d\mathbf{x} \quad (2.8)$$

is to be calculated. Note that in this section the triple integral is used explicitly to show that the integration is performed over 3-space. This is in principle also encoded in the form $d\mathbf{x}$, and later the explicit notation for multiple integrals will be dropped. If a differential form $d\mathbf{q}$ is a vector, it is understood that the integration is performed over a volume of the same dimensionality as the vector. Thus, $d\mathbf{x}$ is short for $d\mathbf{x} = dx_1 dx_2 dx_3$, cf. Appendix A.

2.2. The flux density concept

As the particle positions change, the volume $\Omega = \Omega(t)$ will in general change with time, because it consists of the same particles \mathbf{y} and the spatial region covered by these particles will vary with time. Thus, the order of integration and differentiation in eqn. 2.8 cannot be exchanged. But the transformation to particle coordinates is possible, $d\mathbf{x} = Jd\mathbf{y}$, and then the (fixed) volume of the particles $\tilde{\Omega}$ at $t = 0$ can be used instead. This yields

$$\begin{aligned} D_t \iiint_{\Omega} F(t, \mathbf{x}) d\mathbf{x} &= D_t \iiint_{\tilde{\Omega}} F(t, \mathbf{x}) J d\mathbf{y} \\ &= \iiint_{\tilde{\Omega}} (F D_t J + J D_t F) d\mathbf{y} \\ &= \iiint_{\tilde{\Omega}} (F D_t J + J((\mathbf{v} \cdot \partial_{\mathbf{x}})F + \partial_t F)) d\mathbf{y}. \end{aligned} \quad (2.9)$$

To make further progress, $D_t J$ is calculated. The calculation for three dimensions is lengthy but straightforward, and can be found in [17]. What happens can already be observed in two dimensions, for the determinant of the Jacobian matrix

$$J = \begin{vmatrix} \frac{\partial x_1}{\partial y_1} & \frac{\partial x_1}{\partial y_2} \\ \frac{\partial x_2}{\partial y_1} & \frac{\partial x_2}{\partial y_2} \end{vmatrix} = \frac{\partial x_1}{\partial y_1} \frac{\partial x_2}{\partial y_2} - \frac{\partial x_1}{\partial y_2} \frac{\partial x_2}{\partial y_1}. \quad (2.10)$$

The derivative D_t operates for fixed \mathbf{y} , thus the order of the derivatives can be changed and the particle velocities can be identified:

$$D_t \frac{\partial x_i}{\partial y_j} = \frac{\partial}{\partial y_j} (D_t x_i) = \frac{\partial v_i}{\partial y_j}. \quad (2.11)$$

Because $v_i = v_i(\mathbf{y}(\mathbf{x}))$, the chain rule is applied to find

$$D_t \frac{\partial x_i}{\partial y_j} = \sum_k \frac{\partial v_i}{\partial x_k} \frac{\partial x_k}{\partial y_j}. \quad (2.12)$$

Then, by direct calculation follows that

$$\begin{aligned} D_t J &= D_t \left(\frac{\partial x_1}{\partial y_1} \frac{\partial x_2}{\partial y_2} - \frac{\partial x_1}{\partial y_2} \frac{\partial x_2}{\partial y_1} \right) \\ &= \frac{\partial x_1}{\partial y_1} D_t \frac{\partial x_2}{\partial y_2} - \frac{\partial x_1}{\partial y_2} D_t \frac{\partial x_2}{\partial y_1} + \frac{\partial x_2}{\partial y_2} D_t \frac{\partial x_1}{\partial y_1} - \frac{\partial x_2}{\partial y_1} D_t \frac{\partial x_1}{\partial y_2} \\ &= \frac{\partial x_1}{\partial y_1} \left(\frac{\partial v_2}{\partial x_1} \frac{\partial x_1}{\partial y_2} + \frac{\partial v_2}{\partial x_2} \frac{\partial x_2}{\partial y_2} \right) - \frac{\partial x_1}{\partial y_2} \left(\frac{\partial v_2}{\partial x_1} \frac{\partial x_1}{\partial y_1} + \frac{\partial v_2}{\partial x_2} \frac{\partial x_2}{\partial y_1} \right) \\ &\quad + \frac{\partial x_2}{\partial y_2} \left(\frac{\partial v_1}{\partial x_1} \frac{\partial x_1}{\partial y_1} + \frac{\partial v_1}{\partial x_2} \frac{\partial x_2}{\partial y_1} \right) - \frac{\partial x_2}{\partial y_1} \left(\frac{\partial v_1}{\partial x_1} \frac{\partial x_1}{\partial y_2} + \frac{\partial v_1}{\partial x_2} \frac{\partial x_2}{\partial y_2} \right) \\ &= \left(\frac{\partial v_1}{\partial x_1} + \frac{\partial v_2}{\partial x_2} \right) \left(\frac{\partial x_1}{\partial y_1} \frac{\partial x_2}{\partial y_2} - \frac{\partial x_1}{\partial y_2} \frac{\partial x_2}{\partial y_1} \right) \\ &= \left(\frac{\partial v_1}{\partial x_1} + \frac{\partial v_2}{\partial x_2} \right) J \end{aligned} \quad (2.13)$$

In general, it holds that $D_t J = (\partial_{\mathbf{q}} \cdot \mathbf{v})J$ for arbitrary dimensionality of the vectors \mathbf{q} and \mathbf{v} , as can be seen from the way the calculation is performed in [17].

The calculation of D_t acting on a function $F(t, \mathbf{x})$ averaged over a volume of constant particles Ω can now be continued, using the relation $D_t J = (\partial_{\mathbf{x}} \cdot \mathbf{v})J$. From eqn. 2.9 it follows

that

$$\begin{aligned} D_t \iiint_{\Omega} F(t, \mathbf{x}) d\mathbf{x} &= \iiint_{\Omega} (F \partial_{\mathbf{x}} \cdot \mathbf{v} + (\mathbf{v} \cdot \partial_{\mathbf{x}}) F + \partial_t F) J d\mathbf{y} \\ &= \iiint_{\Omega} (\partial_t F + \partial_{\mathbf{x}} \cdot (F \mathbf{v})) d\mathbf{x}. \end{aligned} \quad (2.14)$$

The vector field $F(t, \mathbf{x})\mathbf{v}$ is the velocity field of the particles weighted by the quantity F .

Eqn. 2.14 is the topic of the next section. F is interpreted as being some kind of density: A mass density describing the distribution of mass in space, a charge density describing the distribution of charges, or a probability density describing the probability of finding some particles in space. Then $\mathbf{j} = F(t, \mathbf{x})\mathbf{v}$ is called the associated flux density, or simply the flux density. In general, \mathbf{j} is more interesting than \mathbf{v} , especially if F is a particle density: \mathbf{v} will give the velocity field independent of the amount of particles at a given place, even in regions where no particles are located at all. In contrast, \mathbf{j} represents the dynamic situation by showing how the particles are moving at a certain instant of time.

2.2.2 The continuity equation

In eqn. 2.14, the time derivative of F averaged over a volume Ω consisting of a fixed amount of particles is taken, keeping the particles themselves constant. If F is the particle density, the quantity

$$D_t \iiint_{\Omega} F(t, \mathbf{x}) d\mathbf{x} = 0 \quad (2.15)$$

for any such volume Ω means that there are no sources or drains for the particles in the system, so that particles cannot be created or destroyed. This is equivalent to stating that the density is locally conserved. In many systems, and especially for the systems of interest in the following, this is the case. Because eqn. 2.15 holds for any Ω , it follows from eqn. 2.14 that

$$\partial_t F + \partial_{\mathbf{x}} \cdot (F \mathbf{v}) = 0. \quad (2.16)$$

Eqn. 2.16 is known as the continuity equation and will be subject of this section, as it relates the density to the flux density in the most general way. For derivation of this equation very few assumptions were needed, but until now the discussion is restricted to 3-space. There is no particular reason for this restriction, and the equation shall now be formulated in a dimension independent way which is useful for quantum mechanics. It will also be investigated what can be learned about the flux density from this relation alone. In order to achieve these goals, both vector notation and differential forms are used. Note, however, that the two are equivalent, and that it is not necessary but only convenient to use the algebra of differential forms. In Appendix B there is a short summary about the aspects of differential forms used in this text.

A K -dimensional vector space with variables $\mathbf{q} = (q_1, \dots, q_K)$ and a K -form

$$\check{\rho} = \rho(t, \mathbf{q}) dq_1 \dots dq_K \quad (2.17)$$

are given. The variable t parametrizes the evolution of the system and is thus called the time. ρ should be a density, e.g. it might represent a mass density or the probability of finding a particle in a given volume Ω . Thus $\rho \geq 0$ and $\int \check{\rho}$ is finite and constant. The density ρ is conserved locally.

The latter requirement is equivalent to stating that given a volume Ω , the change of ρ in Ω with time is the flow through the bounding surface of the volume, $\partial\Omega$. Let the flow of ρ

2.2. The flux density concept

be given by the 1-form $\check{j}(t, \mathbf{q})$, the flux density. Then, the statement of local conservation is

$$\partial_t \int_{\Omega} \check{\rho} = - \int_{\partial\Omega} * \check{j}. \quad (2.18)$$

It is assumed that in the considered space Stoke's theorem eqn. B.22 holds. Application of this theorem yields

$$\partial_t \int_{\Omega} \check{\rho} = - \int_{\Omega} d * \check{j}. \quad (2.19)$$

This equation is valid for arbitrary volumes Ω , hence

$$\partial_t \check{\rho} + d * \check{j} = 0. \quad (2.20)$$

Eqn. 2.20 is the general form of the continuity equation. It should nevertheless be kept in mind that \check{j} is a product of the density ρ and a velocity field, cf. the arguments leading to eqn. 2.16.

If the 1-form $\check{j} = j_1 dq_1 + \dots + j_K dq_K$ is identified with the vector $\mathbf{j} = (j_1, \dots, j_K)$, eqn. 2.18 becomes

$$\partial_t \int_{\Omega} \rho(t, \mathbf{q}) dV = - \int_{\partial\Omega} \mathbf{j} \cdot \hat{\mathbf{n}} dA, \quad (2.21)$$

with $\hat{\mathbf{n}}$ the outward oriented unit normal to the $(K-1)$ -dimensional surface $\partial\Omega$. The notation dV and dA denote integration over the K -dimensional volume and $(K-1)$ -dimensional surface, respectively. Note that when working with differential forms the orientation is encoded in the algebra of the forms, thus such rather awkward notations are not necessary. The vector form of eqn. 2.20 is

$$\partial_t \rho(t, \mathbf{q}) + \partial_{\mathbf{q}} \cdot \mathbf{j}(t, \mathbf{q}) = 0. \quad (2.22)$$

In the context of electron densities in the Born-Oppenheimer approximation the density ρ is easily accessible. However, the corresponding flux density \check{j} is difficult to obtain. The question is: How much information can be extracted from the local conservation requirement alone, i.e. can eqn. 2.20 be solved for \check{j} (or for the functions $j_1(t, \mathbf{q}), \dots, j_K(t, \mathbf{q})$)?

The calculations in [186] for 3-space give the answer. The general solution of the continuity equation for K -dimensions, expressed in vector notation, is a sum of two components,

$$\mathbf{j}(t, \mathbf{q}) = \mathbf{j}_{\parallel}(t, \mathbf{q}) + \mathbf{j}_{\perp}(t, \mathbf{q}). \quad (2.23)$$

The first component can explicitly be given as

$$\mathbf{j}_{\parallel}(t, \mathbf{q}) = \frac{1}{A_K} \int \partial_t \rho(t, \mathbf{q}') \frac{\mathbf{q}' - \mathbf{q}}{|\mathbf{q}' - \mathbf{q}|^K} d\mathbf{q}'. \quad (2.24)$$

In eqn. 2.24, the integration over $d\mathbf{q}' = dq'_1 \dots dq'_K$ is performed over the whole space, and the constant A_K is the surface of the unit K -sphere,

$$A_K = \frac{2\pi^{K/2}}{\Gamma(K/2)}. \quad (2.25)$$

The Gamma function is defined the usual way [47], $\Gamma(x) = \int_0^{\infty} y^{x-1} \exp(-y) dy$. As will be shown below, for the component \mathbf{j}_{\parallel}

$$\partial_{\mathbf{q}} \cdot \mathbf{j}_{\parallel} = -\partial_t \rho. \quad (2.26)$$

The second component \mathbf{j}_\perp is constrained only by

$$\partial_{\mathbf{q}} \cdot \mathbf{j}_\perp(t, \mathbf{q}) = 0, \quad (2.27)$$

but is otherwise arbitrary. Thus, given only the continuity equation there is a gauge freedom for \mathbf{j} , expressed by the possibility to add any \mathbf{j}_\perp which fulfills eqn. 2.27. Below, this gauge freedom will be further investigated.

It will now be shown that the divergence of eqn. 2.24 indeed is given by eqn. 2.26, and thus that \mathbf{j}_\parallel solves the continuity equation. The argument of [186] is repeated in the following. It will first be shown that whenever $\mathbf{q} \neq \mathbf{q}'$, the divergence $\partial_{\mathbf{q}} \cdot \mathbf{j}_\parallel$ is zero. Thus, the only interesting region for the integration is where $\mathbf{q} = \mathbf{q}'$. Close to this point, the integral of eqn. 2.24 can be performed for a small ball around $\mathbf{q} = \mathbf{q}'$. Within the small ball, the smooth density ρ varies negligibly and can be taken outside the integral. Finally, explicit calculation shows that the remaining integral is just the surface of the unit K -sphere, and thus cancels with the constant $1/A_K$.

If $\mathbf{q} \neq \mathbf{q}'$, direct calculation yields

$$\begin{aligned} A_K \partial_{\mathbf{q}} \cdot \mathbf{j}_\parallel &= \partial_{\mathbf{q}} \cdot \int \partial_t \rho(t, \mathbf{q}') \frac{\mathbf{q}' - \mathbf{q}}{|\mathbf{q}' - \mathbf{q}|^K} d\mathbf{q}' \\ &= \int \partial_t \rho(t, \mathbf{q}') \left((\mathbf{q}' - \mathbf{q}) \cdot \left(\partial_{\mathbf{q}} \frac{1}{|\mathbf{q}' - \mathbf{q}|^K} \right) + \frac{1}{|\mathbf{q}' - \mathbf{q}|^K} \partial_{\mathbf{q}} \cdot (\mathbf{q}' - \mathbf{q}) \right) d\mathbf{q}' \\ &= \int \partial_t \rho(t, \mathbf{q}') \left((\mathbf{q}' - \mathbf{q}) \cdot \left(\frac{K(\mathbf{q}' - \mathbf{q})}{|\mathbf{q}' - \mathbf{q}|^{K+2}} - \frac{K}{|\mathbf{q}' - \mathbf{q}|^K} \right) \right) d\mathbf{q}' \\ &= 0. \end{aligned} \quad (2.28)$$

In the region around $\mathbf{q} = \mathbf{q}'$, the integration may be performed over a small K -dimensional ball $B_{\mathbf{q}}$ centered around \mathbf{q} . In this region, $\partial_t \rho(t, \mathbf{q})$ is a constant and can be taken out of the integral. Then

$$A_K \partial_{\mathbf{q}} \cdot \mathbf{j}_\parallel = \partial_t \rho(t, \mathbf{q}) \int_{B_{\mathbf{q}}} \partial_{\mathbf{q}} \cdot \frac{\mathbf{q}' - \mathbf{q}}{|\mathbf{q}' - \mathbf{q}|^K} d\mathbf{q}'. \quad (2.29)$$

The operator $\partial_{\mathbf{q}}$ can be replaced by $-\partial_{\mathbf{q}'}$, which does not change the result of the differentiation. Because the differentiation as well as the integral are then with respect to \mathbf{q}' , the special form of Stoke's theorem known as the divergence theorem or Gauss's theorem can be used to replace the integral over $B_{\mathbf{q}'}$ by an integral over the surface $\partial B_{\mathbf{q}}$ of the ball:

$$\begin{aligned} A_K \partial_{\mathbf{q}} \cdot \mathbf{j}_\parallel &= -\partial_t \rho(t, \mathbf{q}) \int_{B_{\mathbf{q}}} \partial_{\mathbf{q}'} \cdot \frac{\mathbf{q}' - \mathbf{q}}{|\mathbf{q}' - \mathbf{q}|^K} d\mathbf{q}' \\ &= \partial_t \rho(t, \mathbf{q}) \int_{\partial B_{\mathbf{q}}} \frac{\mathbf{q}' - \mathbf{q}}{|\mathbf{q}' - \mathbf{q}|^K} \cdot \frac{\mathbf{q}' - \mathbf{q}}{|\mathbf{q}' - \mathbf{q}|} d\mathbf{q}' \\ &= -\partial_t \rho(t, \mathbf{q}) \int_{\partial B_{\mathbf{q}}} \frac{1}{|\mathbf{q}' - \mathbf{q}|^{K-1}} d\mathbf{q}'. \end{aligned} \quad (2.30)$$

The integral in eqn. 2.30 is the surface of the unit K -sphere A_K . Thus, it follows that

$$\partial_{\mathbf{q}} \cdot \mathbf{j}_\parallel = -\partial_t \rho(t, \mathbf{q}), \quad (2.31)$$

or that eqn. 2.24 indeed solves the continuity equation. The integral of eqn. 2.30 is also performed in more detail in Appendix B.

The gauge freedom of the solution of the continuity equation for \mathbf{j} shall now be further investigated. In the language of differential forms, the solution to the continuity equation

2.3. The flux density in quantum mechanics

has the form

$$\check{j}(t, \mathbf{q}) = \check{j}_{\parallel}(t, \mathbf{q}) + \check{j}_{\perp}(t, \mathbf{q}) \quad (2.32)$$

with known \check{j}_{\parallel} , and with the arbitrary 1-form \check{j}_{\perp} satisfying

$$d * \check{j}_{\perp}(t, \mathbf{q}) = 0. \quad (2.33)$$

The decomposition eqn. 2.32 resembles the general decomposition of a vector field in a divergence-free part \mathbf{j}_{\perp} and a rotation-free part \mathbf{j}_{\parallel} (Helmholtz or Hodge decomposition, see e.g. [60]). Poincaré's lemma eqn. B.21 can be used to find that

$$* \check{j}_{\perp}(t, \mathbf{q}) = d\check{\zeta}(t, \mathbf{q}) \quad (2.34)$$

for a $(K-2)$ -form $\check{\zeta}$. Consequently, as $\check{\zeta}$ has $\binom{K}{2}$ basis vectors, the equation of continuity determines $\check{\zeta}$ only up to $\binom{K}{2}$ functions of t and \mathbf{q} , if $K > 1$.

For $K = 2$, for example, the flux density is the 1-form $\check{j} = j_1 dq_1 + j_2 dq_2$, and

$$* \check{j} = j_1 dq_2 - j_2 dq_1, \quad (2.35)$$

with

$$d * \check{j} = \left(\frac{\partial j_1}{\partial q_1} + \frac{\partial j_2}{\partial q_2} \right) dq_1 dq_2 = 0. \quad (2.36)$$

By Poincaré's lemma, there exists a 0-form $\check{\beta}(t, q_1, q_2)$ such that $d\check{\beta} = * \check{j}$. Also, for any 0-form $f(t, q_1, q_2)$,

$$d \left(\frac{\partial f}{\partial q_1} dq_1 + \frac{\partial f}{\partial q_2} dq_2 \right) = \frac{\partial^2 f}{\partial q_1 \partial q_2} dq_2 dq_1 + \frac{\partial^2 f}{\partial q_1 \partial q_2} dq_1 dq_2 = 0. \quad (2.37)$$

It follows that if the transformation $j_1 \rightarrow j_1 + \partial_{q_1} f, j_2 \rightarrow j_2 - \partial_{q_2} f$ is made in eqn. 2.35, eqn. 2.36 will be unaltered. In vector form, $\mathbf{j} = (j_1, j_2)$ is determined up to one function $f(t, q_1, q_2)$, with the unknown component of \mathbf{j} being $\mathbf{j}_{\perp} = (\partial_{q_1} f, -\partial_{q_2} f)$.

For $K = 3$, the solution to the continuity equation is specified only up to three functions of t, q_1, q_2, q_3 . Similar reasoning shows that these can be written as a 3-vector \mathbf{A} , such that $\mathbf{j}_{\perp} = \text{curl } \mathbf{A}$. Interestingly, for higher dimensions there are even more undetermined functions from eqn. 2.34 than there are elements of \mathbf{j}_{\perp} .

The one-dimensional continuity equation is special: In a one dimensional vector space $\check{\zeta}$ is a constant with respect to \mathbf{q} . Thus, the flux density $\mathbf{j} = j_1$ may be determined up to a time-dependent constant $c(t)$. For higher dimensionality, $K > 1$, as was just shown, one ($K = 2$) or at least K functions of all variables are needed to specify the complete solution.

2.3 The flux density in quantum mechanics

2.3.1 Flux density from the Schrödinger equation

Already in his seminal paper “Quantisierung als Eigenwertproblem” (quantisation as eigenvalue problem) [185] from 1926, Schrödinger gave an expression for the quantum mechanical flux density satisfying the continuity equation for the probability density. In the following, this expression is introduced in two ways: First, from the continuity equation, using Schrödinger's wave equation as the connected dynamics description. And second, as expectation value of the operator obtained from the classical expression of the flux density by the correspondence principle. Several aspects of the flux density are discussed, and another operator closely related to the flux density is related to the expectation values of linear and

angular momentum. However, the extension of the flux density to include effects of the interaction with (classical) electromagnetic fields is not discussed, as these interactions are of no concern in this work. The electromagnetic fields would modify the (conjugate) momentum operator such that a vector potential occurs in the flux density, cf. [56, 127].

Note that another interesting derivation of the form of the flux density can be found in [194]. In this article, Skála and Kapsa derive the flux density and then also the Schrödinger equation from general properties of mean values. There is also a derivation of the general flux density operator without reference to a particular representation of the wave function in [100].

The first derivation starts from the continuity equation

$$\partial_t \rho + \partial_{\mathbf{q}} \cdot \mathbf{j} = 0. \quad (2.38)$$

Here, ρ is a density and the equation is interpreted as a constraint for \mathbf{j} . The calculations are performed in the configuration space containing the vectors \mathbf{q} , where \mathbf{q} describes all possible configurations of the particles. The dynamical description of the system can be used to derive an explicit expression for \mathbf{j} , like it can be done in classical fluid dynamics [221]. In the case of quantum mechanics, the dynamics of the system is described by the Schrödinger equations

$$\begin{aligned} 0 &= \left(-\frac{\hbar^2}{2m} \partial_{\mathbf{q}}^2 + V(\mathbf{q}) - i\hbar \partial_t \right) \phi(t, \mathbf{q}) \\ 0 &= \left(-\frac{\hbar^2}{2m} \partial_{\mathbf{q}}^2 + V(\mathbf{q}) + i\hbar \partial_t \right) \phi^*(t, \mathbf{q}) \end{aligned} \quad (2.39)$$

for ϕ and its complex conjugate ϕ^* , respectively. The scalar field $V(\mathbf{q})$ is called the potential, and the constant m is the mass corresponding to the coordinate \mathbf{q} . The mass may in principle be different for each component of \mathbf{q} . This will be ignored for the moment, as different constants m_i would not yield deeper insights but only more complicated equations. Moreover, each component of \mathbf{q} may always be scaled so as to make the constants all equal, at expense of a transformation of $V(\mathbf{q})$.

The density is defined as $\rho := \phi^* \phi$. Now

$$\begin{aligned} \partial_t \rho &= \phi^* \partial_t \phi + \phi \partial_t \phi^* \\ &= -\frac{\hbar}{2im} (\phi^* \partial_{\mathbf{q}}^2 \phi - \phi \partial_{\mathbf{q}}^2 \phi^*) \\ &\stackrel{!}{=} -\partial_{\mathbf{q}} \cdot \mathbf{j} \end{aligned} \quad (2.40)$$

by the continuity equation, such that

$$\mathbf{j} = \frac{\hbar}{2im} (\phi^* \partial_{\mathbf{q}} \phi - \phi \partial_{\mathbf{q}} \phi^*) \equiv \frac{\hbar}{m} \text{Im} (\phi^* \partial_{\mathbf{q}} \phi). \quad (2.41)$$

As will be seen below, the same result is obtained by the correspondence principle, if the classical expression $\mathbf{j} = \rho \mathbf{v} = \rho \mathbf{p}/m$ is replaced by the quantum mechanical operators.

The approach based on the continuity equation has an advantage: It is apparent how the underlying dynamics equations determine the flux density directly. Hence, if a flux density is calculated using expression eqn. 2.41 and it is found that it does not satisfy the continuity equation for the given ρ , it follows that either the dynamical equations are not suited or that the flux density corresponds to another density ρ .

In [37], Boykin criticizes the approach to start from the change in time of the density, and to identify the continuity equation and the flux density. Boykin proposes to “construct

2.3. The flux density in quantum mechanics

local quantum operators $\hat{\mathbf{j}}_r$ and $\nabla \cdot \hat{\mathbf{j}}_r$, with the continuity equation following from the latter” [37]. However, this approach is conceptually even worse: The continuity equation is a mathematical requirement which follows from the properties that the probability density should have. Thus, a derivation which assumes the continuity equation in first place should be preferred.

2.3.2 Flux density via the correspondence principle

The second derivation starts with the classical flux density. Let \mathbf{q}' be the configuration of the classical particles. Consequently, the particle density is $\delta(\mathbf{q} - \mathbf{q}')$, so that any function averaged by this density can only contribute to the average at points where particles are actually located. The classical flux density is thus the particle density multiplied by the particle velocity $\partial_t \mathbf{q}$,

$$\mathbf{j}_{\text{cl}}(\mathbf{q}) = (\partial_t \mathbf{q}) \delta(\mathbf{q} - \mathbf{q}'). \quad (2.42)$$

For eqn. 2.42 to become a quantum mechanical operator, the velocity $\partial_t \mathbf{q}$ is written as momentum \mathbf{p} divided by the mass m . Thus, the momentum operator $\hat{\mathbf{p}} = -i\hbar \partial_{\mathbf{q}}$ can be used to find

$$\begin{aligned} \hat{\mathbf{j}}(\mathbf{q}) &= \frac{1}{2} \left(\frac{\hat{\mathbf{p}}}{m} \delta(\mathbf{q} - \mathbf{q}') + \delta(\mathbf{q} - \mathbf{q}') \frac{\hat{\mathbf{p}}}{m} \right) \\ &= \frac{\hbar}{2im} (\partial_{\mathbf{q}} \delta(\mathbf{q} - \mathbf{q}') + \delta(\mathbf{q} - \mathbf{q}') \partial_{\mathbf{q}}). \end{aligned} \quad (2.43)$$

A symmetrization of the operator had to be made, as $\hat{\mathbf{p}}$ and $\delta(\mathbf{q})$ do not commute and the operator would otherwise not be hermitian. The flux density can be obtained by taking the expectation value of $\hat{\mathbf{j}}$ with respect to some wave function $\phi(\mathbf{q})$,

$$\begin{aligned} \mathbf{j}(\mathbf{q}') &= \int \phi^*(\mathbf{q}) \hat{\mathbf{j}}(\mathbf{q}) \phi(\mathbf{q}) d\mathbf{q} \\ &= \frac{\hbar}{2im} \left(\int \phi^* \delta(\mathbf{q} - \mathbf{q}') \partial_{\mathbf{q}} \phi d\mathbf{q} + \int \phi^* \partial_{\mathbf{q}} (\delta(\mathbf{q} - \mathbf{q}') \phi) d\mathbf{q} \right) \\ &= \frac{\hbar}{2im} \left(\int \phi^* \delta(\mathbf{q} - \mathbf{q}') \partial_{\mathbf{q}} \phi d\mathbf{q} - \int \phi \delta(\mathbf{q} - \mathbf{q}') \partial_{\mathbf{q}} \phi^* d\mathbf{q} \right) \\ &= \frac{\hbar}{2im} (\phi^*(\mathbf{q}') \partial_{\mathbf{q}'} \phi(\mathbf{q}') - \phi(\mathbf{q}') \partial_{\mathbf{q}'} \phi^*(\mathbf{q}')). \end{aligned} \quad (2.44)$$

In the third line partial integration and the condition on ϕ that $\phi \rightarrow 0$ for $\mathbf{q} \rightarrow \pm\infty$ was used. Thus, the same expression for the flux density is obtained as from the Schrödinger equation, eqn. 2.41.

2.3.3 Flux density as product of a density and a velocity field

From eqn. 2.16 it is known that the flux density is a product of the density and a velocity field. The two derivations just presented seem to obscure this relation. It is of course always possible to factor out the density, but, after the discussion of section 2.2, this decomposition can be expected to arise naturally. This objective is readily met if a formalism well known in quantum hydrodynamics [131, 231] is followed. All that needs to be done is to consider the polar representation of the complex number $\phi(t, \mathbf{q})$,

$$\phi(t, \mathbf{q}) = A(t, \mathbf{q}) \exp\left(i \frac{S(t, \mathbf{q})}{\hbar}\right), \quad (2.45)$$

with both A, S being real. The parameter t is included to emphasize the possible time dependence. It follows that

$$\begin{aligned}\mathbf{j}(t, \mathbf{q}) &= \frac{\hbar}{2mi} \left(A e^{-iS/\hbar} \partial_{\mathbf{q}} \left(A e^{iS/\hbar} \right) - A e^{iS/\hbar} \partial_{\mathbf{q}} \left(A e^{-iS/\hbar} \right) \right) \\ &= A^2 \frac{1}{m} \partial_{\mathbf{q}} S \\ &= \rho(t, \mathbf{q}) \mathbf{v}(t, \mathbf{q})\end{aligned}\tag{2.46}$$

with $\rho = \phi^* \phi \equiv A^2$ and the velocity field $\mathbf{v} := \partial_{\mathbf{q}} S / m$. Consequently, features of the density can be found in the flux density as well, if the action S varies slow enough with position. This effect can, for example, be seen in [44], while for a tunneling dynamics \mathbf{v} is often the decisive part for the shape of \mathbf{j} , see e.g. [43, 86].

2.3.4 Relation to momentum and angular momentum expectation values

The decomposition of the flux density into a density and a velocity field motivates the following relations between the flux density and the expectation value of linear and angular momentum. By multiplying ρ with the mass m a mass density is obtained, thus the product $m\mathbf{j}$ should be a momentum density. Explicitly, by partial integration [150]

$$\int m\mathbf{j}(\mathbf{q}) d\mathbf{q} = -\frac{i\hbar}{2} \left(\int \phi^* \partial_{\mathbf{q}} \phi d\mathbf{q} - \int \phi \partial_{\mathbf{q}} \phi^* d\mathbf{q} \right)\tag{2.47}$$

$$= -i\hbar \int \phi^* \partial_{\mathbf{q}} \phi d\mathbf{q} \equiv \langle \hat{\mathbf{p}} \rangle.\tag{2.48}$$

Following [150], a new operator $\hat{\mathbf{J}}$ is introduced by the relation

$$\mathbf{j} = \phi^* \hat{\mathbf{J}} \phi.\tag{2.49}$$

This operator is defined as

$$\hat{\mathbf{J}} = \frac{\hbar}{2im} (\partial_{\mathbf{q}} - \mathfrak{G}_{\mathbf{q}}),\tag{2.50}$$

with the derivative operating to the left \mathfrak{G}_x

$$f(x) \mathfrak{G}_x g(x) := g(x) \partial_x f(x).\tag{2.51}$$

Thus, eqn. 2.48 can be written as

$$\langle m\hat{\mathbf{J}} \rangle = \langle \mathbf{p} \rangle,\tag{2.52}$$

and in this sense, the expectation value $\langle \hat{\mathbf{J}} \rangle$ is the average velocity.

Analogously, a connection between the flux density and the angular momentum can be found. For simplicity, the discussion is restricted to 3-space with coordinates \mathbf{x} , and the derivatives are abbreviated as $\partial_{x_i} = \partial_i$ and $\mathfrak{G}_{x_i} = \mathfrak{G}_i$. Then $m\mathbf{x} \times \mathbf{j}$ is an angular momentum density. Using the operator eqn. 2.50, the respective operator is

$$\hat{\boldsymbol{\lambda}} = m\hat{\mathbf{x}} \times \hat{\mathbf{J}} = -\frac{i\hbar}{2} \begin{pmatrix} x_2(\partial_3 - \mathfrak{G}_3) - x_3(\partial_2 - \mathfrak{G}_2) \\ x_3(\partial_1 - \mathfrak{G}_1) - x_1(\partial_3 - \mathfrak{G}_3) \\ x_1(\partial_2 - \mathfrak{G}_2) - x_2(\partial_1 - \mathfrak{G}_1) \end{pmatrix}.\tag{2.53}$$

The expectation value of $\hat{\boldsymbol{\lambda}}$ is found to be the same as the expectation value of the angular

2.3. The flux density in quantum mechanics

momentum: For example, for the first element of $\hat{\lambda}$,

$$\begin{aligned}\langle \hat{\lambda}_1 \rangle &= -\frac{i\hbar}{2} \left(\int \phi^* (x_2 \partial_3 - x_3 \partial_2) \phi d\mathbf{x} - \int \phi (x_2 \partial_3 - x_3 \partial_2) \phi^* d\mathbf{x} \right) \\ &= -i\hbar \int \phi^* (x_2 \partial_3 - x_3 \partial_2) \phi d\mathbf{x} \\ &\equiv \langle \hat{l}_1 \rangle.\end{aligned}\tag{2.54}$$

The operator \hat{l}_1 is first component of the angular momentum operator $\hat{\mathbf{l}}$. Thus,

$$\langle \hat{\mathbf{l}} \rangle = \langle m\hat{\mathbf{x}} \times \hat{\mathbf{v}} \rangle \equiv \int m\mathbf{x} \times \mathbf{j} d\mathbf{x}.\tag{2.55}$$

It seems like this relation is hitherto not known in the literature. However, in [134], Manz and Yamamoto established a connection between the a component of the flux density in cylindrical coordinates with the expectation value of the angular momentum along the z -axis. As the model electron dynamics examples to be discussed are cyclic rearrangements, the choice of cylindrical coordinates comes natural and thus the relation found by Manz and Yamamoto shall be discussed here further.

The cylindrical coordinates to be used are

$$\begin{aligned}x_1 &= r \cos \varphi & x_2 &= r \sin \varphi & x_3 &= z \\ r &= \sqrt{x_1^2 + x_2^2} & \varphi &= \arctan(x_2/x_1) & z &= x_3\end{aligned}\tag{2.56}$$

with volume element $d\mathbf{x} = r dr d\varphi dz$. The derivatives with respect to the coordinates transform as

$$\begin{aligned}\partial_1 &= (\partial_1 r) \partial_r + (\partial_1 \varphi) \partial_\varphi + (\partial_1 z) \partial_z = (\cos \varphi) \partial_r - \frac{\sin \varphi}{r} \partial_\varphi \\ \partial_2 &= (\partial_2 r) \partial_r + (\partial_2 \varphi) \partial_\varphi + (\partial_2 z) \partial_z = (\sin \varphi) \partial_r + \frac{\cos \varphi}{r} \partial_\varphi \\ \partial_3 &= (\partial_3 r) \partial_r + (\partial_3 \varphi) \partial_\varphi + (\partial_3 z) \partial_z = \partial_z.\end{aligned}\tag{2.57}$$

Application of these formulae to the expectation value of the z -component of the angular momentum operator yields

$$\begin{aligned}\langle \hat{l}_z \rangle &= \langle \hat{l}_3 \rangle \\ &= \frac{\hbar}{i} \int \phi^* (x_1 \partial_2 - x_2 \partial_1) \phi d\mathbf{x} \\ &= \frac{\hbar}{i} \int \phi^* \partial_\varphi \phi r dr d\varphi dz = -\frac{\hbar}{i} \int \phi \partial_\varphi \phi^* r dr d\varphi dz \\ &= \frac{\hbar}{2i} \int (\phi^* \partial_\varphi \phi - \phi \partial_\varphi \phi^*) r dr d\varphi dz.\end{aligned}\tag{2.58}$$

The gradient $\partial_{\mathbf{x}}$ in cylindrical coordinates is given by

$$\partial_{\mathbf{x}} = e_1 \partial_1 + e_2 \partial_2 + e_3 \partial_3 = e_r \partial_r + e_\varphi \frac{1}{r} \partial_\varphi + e_z \partial_z,\tag{2.59}$$

where e_1, e_2, e_3 denote the unit vectors in x_1, x_2, x_3 -directions and e_r, e_φ, e_z denote the unit vectors in r, φ, z -directions. Thus, the flux density in cylindrical coordinates is given by

$$\begin{aligned}\mathbf{j} &= \frac{\hbar}{2mi} (\phi^* \partial_{\mathbf{x}} \phi - \phi \partial_{\mathbf{x}} \phi^*) \\ &= j_r e_r + j_\varphi e_\varphi + j_z e_z\end{aligned}\tag{2.60}$$

with the components

$$\begin{aligned} j_r &= \frac{\hbar}{2mi}(\phi^* \partial_r \phi - \phi \partial_r \phi^*) \\ j_\varphi &= \frac{\hbar}{2mi} \frac{1}{r}(\phi^* \partial_\varphi \phi - \phi \partial_\varphi \phi^*) \\ j_z &= \frac{\hbar}{2mi}(\phi^* \partial_z \phi - \phi \partial_z \phi^*). \end{aligned} \quad (2.61)$$

Note the additional $1/r$ in the definition of j_φ . The expectation value of the angular momentum along z -direction is just

$$\langle \hat{l}_z \rangle = m \int j_\varphi r^2 dr d\varphi dz, \quad (2.62)$$

which is the relation found by Manz and Yamamoto in [134].

2.4 Flux densities and the Born-Oppenheimer approximation

2.4.1 Flux densities in the Born-Oppenheimer approximation

The Born-Oppenheimer approximation (BOA) [36] is the foundation of almost all quantum chemical methods for the calculation of atomic and molecular properties, see e.g. [204] or any other standard textbook on quantum chemistry. While there are different definitions of the BOA in the literature, they all encompass the idea that electrons and nuclei can be separated by a dynamical argument: Due to the much larger mass of the protons as compared to the mass of the electrons, the electrons are considered to move much faster than the nuclei. Thus, the complete problem can be adiabatically separated into an electronic and a nuclear part.

From the point of view of the fast electrons, the slow nuclei are almost frozen. In line with this picture, the electronic problem is solved separately for each nuclear configuration of interest, i.e. the stationary state of the system for fixed nuclei is determined. This procedure is what is generally understood as a quantum chemical calculation. Such a calculation yields electronic eigenfunctions and eigenvalues for a nuclear configuration. The eigenfunctions constitute in principle a complete basis for the nuclear configuration. The eigenvalues, which vary continuously with the nuclear coordinates, are called potential energy surfaces or electronic states and cause forces acting on the nuclei. In general, for a reliable representation of the dynamics of the system only few electronic states have to be taken into account. Sometimes, the BOA is defined as the case where only one electronic state needs to be taken into account to describe the process at hand. In this work, however, a more general definition is used: In the BOA, the nuclear problem is solved for each electronic state separately, and it is assumed that different electronic states do not interact. This definition includes the case where only one state needs to be considered. It also includes cases where the dynamics happens in several states, but in regions with small couplings between the states. In the jargon of reaction dynamics, it may be said that no transitions between electronic states take place.

From quantum chemical calculations it is straightforward to obtain the electron density for a given nuclear configuration and electronic state. Given the potential energy surfaces from quantum chemical calculations, the nuclear dynamics can be solved by numerically propagating nuclear wave packets on the surfaces. In turn, with this time-dependent wave packets the time-dependent electron densities can be determined, as explained below.

Consequently, there are time-dependent nuclear densities and flux densities, and time-dependent electron densities in the BOA. The electrons move effectively on the time scale of the nuclear motion. However, as explained below, it is not as straightforward to obtain electronic flux densities in the BOA. The usual definition of the flux density, eqn. 2.41, is not applicable for the electrons: It is based on the time-dependent Schrödinger equation, but in the BOA such an equation only exists for the nuclei, but not for the electrons. It would yield zero electron fluxes, as the electronic wave function is determined using a time-independent Schrödinger equation. Unfortunately, from the BOA no useful expression for the electronic flux density follows (but see [66–69, 172]), and thus it is difficult to analyze the details of the electron dynamics in the BOA. The situation is understandable in terms of the picture of the BOA: Because the electrons are so much faster than the nuclei, details of their dynamics are lost by an averaging. Only a net electronic movement survives the averaging and effort is needed to reconstruct some of the details of the dynamics.

In the following discussion, first the BOA is reviewed following, for example, [20, 51]. It is of utmost importance for the exposition of the ideas to clearly distinguish between the assumed form of the complete wave function (the Born-Oppenheimer expansion, BOE) and the approximation itself. First, expressions for the nuclear and electronic flux densities using the BOE are derived, and subsequently the BOA is applied. It will be found that without the BOA, it is not possible to have a dynamics which is only restricted to one electronic state. In the limit of the BOA such a situation is possible, and there are electronic fluxes and an electronic flux density. However, the mathematical form of the electronic flux density is not readily available. Finally, literature-known approaches to extract an electronic flux density in the BOA are discussed.

Especially in the mathematically oriented literature there is sometimes made a distinction between a stationary BOA and a dynamic BOA, see [89] and references therein. Specifically, Hagedorn and Joye state in [89] that the time-dependent BOA was developed by Fritz London in [126], and that this article is little known and little cited. However, “its ideas are the basis for almost everything that is known about molecular dynamics” [89]. A possible reason for this state of affairs might be that the article [126] is rather difficult to obtain. In this work, the mathematical formalism of the time-dependent BOA will not be discussed in detail, but the inclined reader might want to take a look at [87, 170]. There are also the works of Cederbaum [52] and Abedi, Maitra and Gross [9], which extend the idea of separating electronic and nuclear wave functions to time-dependent processes beyond the usual BOA.

The Born-Oppenheimer approximation

The aim of this section is to review a way to solve the Schrödinger equation of a molecular system consisting of a number of nuclei and electrons,

$$(H - i\hbar\partial_t)\Psi(t, \mathbf{Q}, \mathbf{q}) = 0, \quad (2.63)$$

where t is the time parameter, and where \mathbf{Q} and \mathbf{q} are the nuclear and electronic coordinates, respectively. A direct solution is computationally not viable, and thus the problem has to be approached in a way which allows to make sensible approximations. In order to simplify the equations, the coordinates \mathbf{Q} are taken to be the mass-weighted Cartesian coordinates of the nuclei, $\mathbf{Q} = (\sqrt{M_1}\mathbf{X}_1, \sqrt{M_2}\mathbf{X}_2, \dots)$. The Hamiltonian H of eqn. 2.63 is the usual molecular conservative (i.e. time-independent) Hamiltonian,

$$H = -\frac{\hbar^2}{2}\partial_{\mathbf{Q}}^2 + H_0(\mathbf{Q}) = -\frac{\hbar^2}{2}\partial_{\mathbf{Q}}^2 - \frac{\hbar^2}{2m_e}\partial_{\mathbf{q}}^2 + V(\mathbf{Q}, \mathbf{q}) \quad (2.64)$$

with the nuclear kinetic energy operator $-\frac{\hbar^2}{2}\partial_{\mathbf{Q}}^2$, the electronic kinetic energy operator $-\frac{\hbar^2}{2m_e}\partial_{\mathbf{q}}^2$ and the scalar potential $V(\mathbf{Q}, \mathbf{q})$ containing electron-electron, electron-nucleus and nucleus-nucleus Coulomb interactions. The electronic Hamiltonian $H_0(\mathbf{Q})$ consists of this potential and the electronic kinetic energy operator. Its dependence on the nuclear configuration \mathbf{Q} is emphasized, because the operator will later on be applied for fixed \mathbf{Q} . The electronic mass m_e is kept explicitly.

The BOA was introduced by Born and Oppenheimer in 1927 as expansion in terms of the ratio of electronic to nuclear mass to the power of 1/4 [36]. Born and Oppenheimer noticed that, due to the large mass difference of electronic and nuclear masses, the electrons can often be considered as moving much faster than the nuclei. Thus, it should be possible to separate the movements, solving the electronic problem for fixed nuclear coordinates, with little error in many situations. The original derivation will not be followed, but the BOA will be derived in terms of the Born-Oppenheimer expansion instead. However, this obscures to a certain extent the idea of the perturbation expansion of the wave function in terms of the mass ratio. This mass ratio will occur again in the proposed remedies known in the literature.

Eqn. 2.63 implies that a general state $|\Psi(t)\rangle$ is expressed in the basis of position eigenvectors $|\mathbf{Q}, \mathbf{q}\rangle$, such that

$$\Psi(t, \mathbf{Q}, \mathbf{q}) = \langle \mathbf{Q}, \mathbf{q} | \Psi(t) \rangle, \quad (2.65)$$

where the scalar product of the bra-ket notation $\langle \cdot \rangle$ means integration over both \mathbf{Q} and \mathbf{q} . Instead of using these position eigenvectors, the first step towards the Born-Oppenheimer approximation is to transform to a basis

$$|\mathbf{Q}, \phi_i(\mathbf{Q})\rangle = |\mathbf{Q}\rangle \otimes |\phi_i(\mathbf{Q})\rangle, \quad (2.66)$$

where the states $|\mathbf{Q}\rangle$ are the eigenvectors of the nuclear position operator, and where $|\phi_i(\mathbf{Q})\rangle$ are energy eigenstates of the Hamiltonian $H_0(\mathbf{Q})$. For a general discussion about this transformation, see [35].

To simplify the notation and to avoid ambiguity, in the following the scalar product $\langle \cdot \rangle$ is only taken with respect to \mathbf{q} , such that the bra-ket notation is only used for the eigenstates of the electronic Hamiltonian H_0 . Thus, the electronic coordinates \mathbf{q} are suppressed for the moment, but will be reintroduced later explicitly.

First, it is assumed that an orthogonal, normalized (with respect to integration over \mathbf{q}) basis of the Hilbert space of the problem is available for all nuclear configurations separately. These basis sets are obtained by solving the time-independent electronic problem for each \mathbf{Q} ,

$$\begin{aligned} (H_0(\mathbf{Q}) - E_i(\mathbf{Q}))|\phi_i(\mathbf{Q})\rangle &= 0 \\ \langle \phi_i(\mathbf{Q}) | \phi_j(\mathbf{Q}) \rangle &= \delta_{ij}. \end{aligned} \quad (2.67)$$

The ϕ_i are the eigenfunctions of H_0 and constitute a complete basis for a given nuclear configuration \mathbf{Q} . The E_i are the respective eigenvalues for the electronic state i . Thus, \mathbf{Q} is used as a fixed parameter for the electronic problem. It has to be noted that in principle the $|\phi_i(\mathbf{Q})\rangle$ are rays, i.e. they are only defined up to an arbitrary phase. The transformation $|\phi_i(\mathbf{Q})\rangle \rightarrow \exp(i\varphi_i)|\phi_i(\mathbf{Q})\rangle$ gives another valid solution of eqn. 2.67, and thus a set of φ_i needs to be chosen. This choice is called a phase convention, and the phases φ_i may depend on both t and \mathbf{Q} . Thus, it is for now assumed that the $|\phi_i(\mathbf{Q})\rangle$ are not rays but vectors with some phase convention. In practice, the $|\phi_i(\mathbf{Q})\rangle$ obtained from a quantum chemical calculation will be real functions and an additional phase will not be introduced. Note, however, that the phase convention may sometimes be important, see [20].

2.4. Flux densities and the Born-Oppenheimer approximation

Eqn. 2.63, now written as

$$(H - i\hbar\partial_t)|\Psi(t, \mathbf{Q})\rangle = 0, \quad (2.68)$$

is solved by

$$|\Psi(t, \mathbf{Q})\rangle = \sum_i \chi_i(t, \mathbf{Q})|\phi_i(\mathbf{Q})\rangle \quad (2.69)$$

where the time- and \mathbf{Q} -dependent coefficients χ_i are called the nuclear wave functions, which depend on the phase convention. Eqn. 2.69 is the Born-Oppenheimer expansion (BOE).

So far, no approximation is involved, but the wave function is represented in a particular basis. As already indicated, for molecular systems only few electronic states $E_i(\mathbf{Q})$ are usually sufficient to calculate the dynamics. For moderate temperatures, a molecule is in its electronic ground state E_0 and no other states need to be considered to describe the nuclear dynamics. However, if enough energy is acquired by the system, e.g. by UV radiation, more electronic states might be needed to describe the system. It is then said that electronic transitions took place and that some population is found in excited states. Often, the electronic states with significant population are only few and the summation over i in eqn. 2.69 can be truncated early. Nevertheless, the following calculations are performed for the exact expansion. Considering only a subset of states is straightforward.

By comparing eqn. 2.63 with

$$\langle\phi_j(\mathbf{Q})|i\hbar\partial_t|\Psi(t, \mathbf{Q})\rangle = i\hbar\partial_t\chi_j(t, \mathbf{Q}) \quad (2.70)$$

and

$$\begin{aligned} \langle\phi_j(\mathbf{Q})|H|\Psi(t, \mathbf{Q})\rangle &= \left(-\frac{\hbar^2}{2}\partial_{\mathbf{Q}}^2 + E_j(\mathbf{Q})\right)\chi_j(t, \mathbf{Q}) \\ &- \frac{\hbar^2}{2}\sum_i (2\langle\partial_{\mathbf{Q}}\chi_i(t, \mathbf{Q})|\phi_j(\mathbf{Q})\rangle\langle\partial_{\mathbf{Q}}|\phi_i(\mathbf{Q})\rangle + \chi_i(t, \mathbf{Q})\langle\phi_j(\mathbf{Q})|\partial_{\mathbf{Q}}^2|\phi_i(\mathbf{Q})\rangle), \end{aligned} \quad (2.71)$$

it follows that the BOE leads to a set of coupled time-dependent Schrödinger equations for the nuclear wave functions. In the BOA it is assumed that the terms $\langle\phi_j|\partial_{\mathbf{Q}}|\phi_i\rangle$ and $\langle\phi_j|\partial_{\mathbf{Q}}^2|\phi_i\rangle$ are small and thus can be set to zero,

$$\langle\phi_j|\partial_{\mathbf{Q}}|\phi_i\rangle = \langle\phi_j|\partial_{\mathbf{Q}}^2|\phi_i\rangle \stackrel{!}{=} 0. \quad (2.72)$$

As these terms are the only terms that couple the different electronic states, Schrödinger equations are obtained for each nuclear wave functions separately,

$$i\hbar\partial_t\chi_i(t, \mathbf{Q}) = \left(-\frac{\hbar^2}{2}\partial_{\mathbf{Q}}^2 + E_i(\mathbf{Q})\right)\chi_i(t, \mathbf{Q}). \quad (2.73)$$

Thus, in the BOA the χ_i are non-interacting wave functions.

Even if excited states are populated, it might be possible to use the BOA to propagate the nuclear wave functions independently. However, often transitions between electronic states are not negligible, especially if two electronic states are close in energy or even become degenerate (at so-called conical intersections, see [20, 121]) for some \mathbf{Q} . In such cases it is necessary to solve the coupled equations in eqn. 2.71 for the relevant subset of electronic states.

Before summarizing the results of this section for further applications, a note about the literature on the BOA shall be made: Often, the BOA is considered to be a product of an

electronic and a nuclear wave function. As Abedi, Maitra and Gross pointed out in [9], the exact wave function can always be written as such a product,

$$\Psi(t, \mathbf{Q}, \mathbf{q}) = \tilde{\chi}(t, \mathbf{Q}) \tilde{\phi}(t, \mathbf{q}, \mathbf{Q}), \quad (2.74)$$

with the nuclear wave function being

$$\tilde{\chi}(t, \mathbf{Q}) := \exp(i\tilde{\varphi}(t, \mathbf{Q})) \sqrt{\int |\Psi(t, \mathbf{Q}, \mathbf{q})|^2 d\mathbf{q}} \quad (2.75)$$

for some real $\tilde{\varphi}$, and with the electronic wave function

$$\tilde{\phi}(t, \mathbf{q}, \mathbf{Q}) := \Psi(t, \mathbf{Q}, \mathbf{q}) / \tilde{\chi}(t, \mathbf{Q}). \quad (2.76)$$

However, in contrast to the view of the BOA the electronic wave functions $\tilde{\phi}$ are in general time-dependent. Nevertheless, as shown above the assumption of a product of a time-dependent nuclear wave function and a time-independent electronic wave function is not the decisive step in the BOA, but rather the expansion in terms of electronic eigenstates as well as eqn. 2.72.

In the following sections some of the just discussed equations are needed, and these are now given in a suitable form for reference. Electronic coordinates are introduced explicitly by projecting eqn. 2.69 onto the electronic coordinates,

$$\langle \mathbf{q} | \Psi(\mathbf{Q}, t) \rangle \equiv \Psi(t, \mathbf{Q}, \mathbf{q}). \quad (2.77)$$

In this representation, the equations of interest are as follows:

- The BOE is

$$\Psi(t, \mathbf{Q}, \mathbf{q}) = \sum_i \chi_i(t, \mathbf{Q}) \phi_i(\mathbf{q}, \mathbf{Q}). \quad (2.78)$$

- The electronic wave functions are defined by the time-independent equation

$$\partial_{\mathbf{q}}^2 \phi_i(\mathbf{q}, \mathbf{Q}) = \frac{2m_e}{\hbar^2} (V - E_i(\mathbf{Q})) \phi_i(\mathbf{q}, \mathbf{Q}). \quad (2.79)$$

- The complete problem to be solved is

$$\partial_t \Psi(t, \mathbf{Q}, \mathbf{q}) = \left(-\frac{\hbar}{2i} \partial_{\mathbf{Q}}^2 - \frac{\hbar}{2im_e} \partial_{\mathbf{q}}^2 + \frac{V}{i\hbar} \right) \Psi(t, \mathbf{Q}, \mathbf{q}). \quad (2.80)$$

- In the BOE of the wave function, eqn. 2.80 becomes

$$\sum_i \phi_i(\mathbf{q}, \mathbf{Q}) \partial_t \chi_i(t, \mathbf{Q}) = \sum_i \left(-\frac{\hbar}{2i} \partial_{\mathbf{Q}}^2 - \frac{\hbar}{2im_e} \partial_{\mathbf{q}}^2 + \frac{V}{i\hbar} \right) (\chi_i(t, \mathbf{Q}) \phi_i(\mathbf{q}, \mathbf{Q})). \quad (2.81)$$

- If the BOA is invoked, eqn. 2.80 is not applicable for the dynamics anymore. Instead, the equations to be solved to determine the dynamics are

$$\partial_t \chi_i(t, \mathbf{Q}) = \left(-\frac{\hbar}{2i} \partial_{\mathbf{Q}}^2 + \frac{E_i(\mathbf{Q})}{i\hbar} \right) \chi_i(t, \mathbf{Q}). \quad (2.82)$$

In this section, care has been taken to always denote the independent variables of the functions which are of importance. In the next sections these dependencies are often

2.4. Flux densities and the Born-Oppenheimer approximation

not denoted explicitly anymore, because otherwise the equations become difficult to read. Dependencies of the functions as in eqns. 2.79-2.82 are always implied.

The electronic flux density from the time-dependent Schrödinger equation and the Born-Oppenheimer approximation

In the BOA, there is a time-dependent Schrödinger equation for the nuclei, but none for the electrons. Consequently, the usual definition of the flux density based on the time-dependent Schrödinger equation, eqn. 2.41, cannot be used for the electrons. If, for example, a wave function of the (non-degenerate) electronic ground state in the BOA is considered, it has the form

$$\Psi(t, \mathbf{Q}, \mathbf{q}) = \chi(t, \mathbf{Q})\phi(\mathbf{q}, \mathbf{Q}), \quad (2.83)$$

where $\phi = \phi_0$ is the solution of eqn. 2.79 to the smallest eigenvalue $E(\mathbf{Q}) = E_0(\mathbf{Q})$, and $\chi = \chi_0$ is the solution of eqn. 2.82. Using eqn. 2.41 with respect to the electronic coordinates gives for the electronic part of the flux density

$$\mathbf{j} = \frac{\hbar}{2im_e} |\chi|^2 (\phi^* \partial_{\mathbf{q}} \phi - \phi \partial_{\mathbf{q}} \phi^*). \quad (2.84)$$

However, because $\phi(\mathbf{q}, \mathbf{Q})$ is a solution of the time-independent Schrödinger equation, eqn. 2.79, it can always be chosen to be real. Consequently, the electronic part of the flux density is zero,

$$\mathbf{j} = 0, \quad (2.85)$$

for this definition of the flux density.

However, there is a time-dependent electron density in the BOA, and thus there has to be an electronic flux density. Below, the continuity equation and the evolution equations in case of a wave function in the BOE and in the BOA are used to try to find the correct equation for the electronic flux density in the BOA, albeit with little success. The procedure that is followed is the same as the procedure used to find the flux density for wave functions obeying the time-dependent Schrödinger equation, eqn. 2.41.

Flux densities for the Born-Oppenheimer expansion I: The complete density

Before the derivation of the different flux densities in the BOE and BOA is pursued, a short comment is in order: In principle, for N nuclei and n electrons the flux densities are vectors in \mathbb{R}^{3N} and \mathbb{R}^{3n} , respectively. These flux densities will not be all too helpful for the analysis of chemical reactions, because they are difficult to visualize. Much more useful are the reduced quantities in 3-space.

The coordinates are $\mathbf{Q} = (\tilde{\mathbf{X}}_1, \dots, \tilde{\mathbf{X}}_N)$ with $\tilde{\mathbf{X}}_i = \sqrt{M_i} \mathbf{X}_i$ and $\mathbf{q} = (\mathbf{x}_1, \dots, \mathbf{x}_n)$, and the 3-space vector fields

$$\mathbf{J}_i(t, \mathbf{X}) = \int \int \hbar \operatorname{Im} (\Psi^*(t, \mathbf{Q}, \mathbf{q}) \partial_{\tilde{\mathbf{X}}_i} \Psi(t, \mathbf{Q}, \mathbf{q})) d\mathbf{q} d\{\mathbf{Q} \setminus \tilde{\mathbf{X}}_i\} \Big|_{\tilde{\mathbf{X}}_i = \mathbf{X}} \quad (2.86)$$

$$\mathbf{j}_i(t, \mathbf{x}) = \int \int \frac{\hbar}{m_e} \operatorname{Im} (\Psi^*(t, \mathbf{Q}, \mathbf{q}) \partial_{\mathbf{x}_i} \Psi(t, \mathbf{Q}, \mathbf{q})) d\mathbf{Q} d\{\mathbf{q} \setminus \mathbf{x}_i\} \Big|_{\mathbf{x}_i = \mathbf{x}}. \quad (2.87)$$

are given. The integral over $d\{\mathbf{Q} \setminus \tilde{\mathbf{X}}_i\}$ stands for integration over all \mathbf{Q} except the coordinate

$\tilde{\mathbf{X}}_i$, which is thereafter set to \mathbf{X} . Complete flux densities can be calculated as

$$\mathbf{J}(t, \mathbf{X}) = \sum_i \mathbf{J}_i(t, \mathbf{X}) \quad (2.88)$$

$$\mathbf{j}(t, \mathbf{x}) = \sum_i \mathbf{j}_i(t, \mathbf{x}). \quad (2.89)$$

Note that the corresponding densities composed of single particle densities,

$$\rho(t, \mathbf{X}) = \sum_i \rho_i(t, \mathbf{X}) \quad (2.90)$$

$$\rho(t, \mathbf{x}) = \sum_i \rho_i(t, \mathbf{x}), \quad (2.91)$$

are normalized to the number of particles included in the sum, if Ψ is normalized to unity. Thus, the flux densities eqn. 2.88 and eqn. 2.89 are valid for this normalization.

These two flux densities are rather easy to visualize and to interpret, as they are both in \mathbb{R}^3 . For the electrons, no information is lost as all electrons are indistinguishable, and thus $\mathbf{j}_i = \mathbf{j}_j \forall i, j$. For different types of nuclei different flux densities can be defined, for each type separately. If electron and nuclear spin have to be taken into account, spin flux densities may be defined in analogy to the definition of spin densities, see e.g. [34, 179].

The expressions for the reduced quantities were given to emphasize that the discussion that follows does also apply to the reduced flux densities. However, from now on definitions of the flux densities as vectors having either the dimension of \mathbf{q} ($= 3n$) or \mathbf{Q} ($= 3N$) are used to keep the equations as simple as possible.

The nuclear and electronic flux densities are derived under the assumption that the wave function is represented as a BOE. From section 2.3.1 the expression for the quantum mechanical flux density eqn. 2.41 is known. However, it is necessary to find separate nuclear and electronic flux densities for chemical applications, and it will soon be clear that eqn. 2.41 cannot be applied directly. Instead, the procedure from section 2.3.1 is followed and the flux density is calculated via the continuity equation.

The continuity equation equates the time derivative of the density with the negative divergence of the flux density. It cannot be assumed that from the Schrödinger equation there are separate flux densities for electrons and nuclei, and this has to be investigated first. Thus, starting point for the following discussion is the time-dependence of the complete density $|\Psi|^2$. This time-dependence is determined by eqn. 2.80 as

$$\partial_t |\Psi|^2 = \Psi^* \left(-\frac{\hbar^2}{2i} \partial_{\mathbf{Q}}^2 - \frac{\hbar^2}{2im_e} \partial_{\mathbf{q}}^2 \right) \Psi - \Psi \left(-\frac{\hbar^2}{2i} \partial_{\mathbf{Q}}^2 - \frac{\hbar^2}{2im_e} \partial_{\mathbf{q}}^2 \right) \Psi^*. \quad (2.92)$$

The form of the wave function in the BOE, eqn. 2.78, is inserted to yield

$$\begin{aligned} \partial_t |\Psi|^2 &= \sum_{i,j} \phi_i \phi_j^* (\chi_j^* \partial_t \chi_i + \chi_i \partial_t \chi_j^*) \\ &= \sum_{i,j} \left[-\frac{\hbar}{2i} (\phi_j^* \chi_j^* \partial_{\mathbf{Q}}^2 (\phi_i \chi_i) - \phi_i \chi_i \partial_{\mathbf{Q}}^2 (\phi_j^* \chi_j^*)) - \frac{\hbar}{2im_e} (\chi_i \chi_j^* (\phi_j^* \partial_{\mathbf{q}}^2 \phi_i - \phi_i \partial_{\mathbf{q}}^2 \phi_j^*)) \right] \\ &= \sum_{i,j} [-\partial_{\mathbf{Q}} \cdot \mathbf{K}_{ij} - \chi_i \chi_j^* \partial_{\mathbf{q}} \cdot \mathbf{j}_{ij}]. \end{aligned} \quad (2.93)$$

In the last line, the combined electronic-nuclear flux densities

$$\mathbf{K}_{ij} = \frac{\hbar}{2i} (\phi_j^* \chi_j^* \partial_{\mathbf{Q}} (\phi_i \chi_i) - \phi_i \chi_i \partial_{\mathbf{Q}} (\phi_j^* \chi_j^*)) \quad (2.94)$$

2.4. Flux densities and the Born-Oppenheimer approximation

and the electronic flux densities

$$\mathbf{j}_{ij} = \frac{\hbar}{2im_e} (\phi_j^* \partial_{\mathbf{q}}^2 \phi_i - \phi_i \partial_{\mathbf{q}}^2 \phi_j^*) \quad (2.95)$$

are used. With eqn. 2.93 a separation of the flux density vector in two parts is achieved: an electronic flux density, which has the same number of components as there are electronic coordinates, and a mixed electronic-nuclear part, which has the same number of components as there are nuclear coordinates. Nevertheless, it is not possible to find nuclear and electronic flux densities which depend on the nuclear and electronic wave functions alone, respectively.

Eqn. 2.93 can be brought into different forms. On one hand, eqn. 2.79 can be used to find

$$\partial_t |\Psi|^2 = \sum_{i,j} \left[-\partial_{\mathbf{Q}} \cdot \mathbf{K}_{ij} + \frac{E_i - E_j}{i\hbar} \chi_i \chi_j^* \phi_i \phi_j^* \right]. \quad (2.96)$$

The electronic flux density is written here in terms of the electronic transition densities $\phi_i \phi_j^*$ and the energy difference between the states. On the other hand, $\partial_{\mathbf{Q}} \cdot \mathbf{K}_{ij}$ can be separated further, because

$$\partial_{\mathbf{Q}}^2 (\phi_i \chi_i) = \phi_i \partial_{\mathbf{Q}}^2 \chi_i + 2(\partial_{\mathbf{Q}} \phi_i)(\partial_{\mathbf{Q}} \chi_i) + \chi_i \partial_{\mathbf{Q}}^2 \phi_i. \quad (2.97)$$

It follows that

$$\begin{aligned} \partial_t |\Psi|^2 = \\ \sum_{i,j} \left[-\phi_i \phi_j^* \partial_{\mathbf{Q}} \cdot \mathbf{J}_{ij} - \chi_i \chi_j^* (m_e \partial_{\mathbf{Q}} + \partial_{\mathbf{q}}) \cdot \mathbf{j}_{ij} - \frac{\hbar}{i} ((\phi_j^* \partial_{\mathbf{Q}} \phi_i)(\chi_j^* \partial_{\mathbf{Q}} \chi_i) - (\phi_i \partial_{\mathbf{Q}} \phi_j^*)(\chi_i \partial_{\mathbf{Q}} \chi_j^*)) \right], \end{aligned} \quad (2.98)$$

where the nuclear flux densities

$$\mathbf{J}_{ij} = \frac{\hbar}{2i} (\chi_j^* \partial_{\mathbf{Q}} \chi_i - \chi_i \partial_{\mathbf{Q}} \chi_j^*) \quad (2.99)$$

are separated. However, this separation comes at the price of new nuclear-electronic terms, which are not easy to interpret.

Flux densities for the Born-Oppenheimer expansion II: The electron density

From the density $|\Psi|^2$ the time-dependent electron density

$$\rho(t, \mathbf{q}) = \int |\Psi(t, \mathbf{Q}, \mathbf{q})|^2 d\mathbf{Q} \quad (2.100)$$

is obtained, which is studied further in section 2.5. For now, note that the one-electron density

$$\tilde{\rho}(t, \mathbf{x}) = \int \rho(t, \mathbf{q}) d\{\mathbf{q} \setminus \mathbf{x}\}, \quad (2.101)$$

follows, which is a very useful quantity both for visualization purposes and for analysis of the reaction mechanism.

It is now assumed that the dynamics of the system of interest can be described by considering only one electronic state. For example, Fig. 2.2 shows the ground state potential energy surface of a diatomic. The other electronic states should be energetically far enough away from the ground state in the region of interest, so that the BOA holds between the ground and all excited states. Thus, in practice only this one electronic state should be needed to calculate the dynamics. Given a nuclear wave packet of Gaussian shape at time t_1 as shown in the figure, and given a potential that is almost harmonic, the nuclear density can be

expected to have a similar shape a short time later (t_2), at larger internuclear distance [208]. The one-electron density depends on the internuclear distance, and for a Gaussian wave packet the electron density can be approximated by the electron density for the center of the nuclear wave packet. Consequently, from eqn. 2.100 it is apparent that there is a time-dependent electron density. In the limit of a Gaussian wave packet in a harmonic oscillator, along the internuclear distance a one-electron density would be found that expands and contracts periodically.

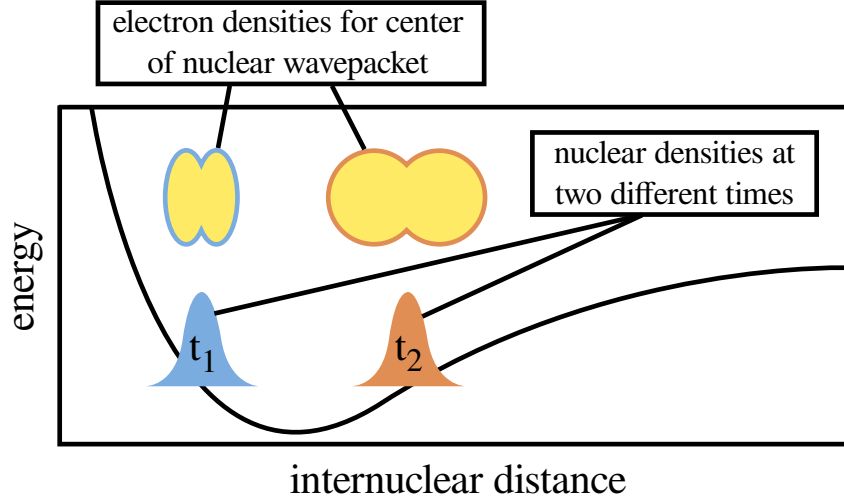


Figure 2.2: Ground state potential energy surface of a diatomic, nuclear densities at two different times t_1 and t_2 , and cut through a contour of the one-electron densities along the internuclear distance for the nuclear configurations corresponding to the center of the wave packets at the different times.

How is this picture represented in the BOE? Or, in other words, how does the time-dependence of the electron density eqn. 2.100 look if the complete wave function as BOE is used? The beauty of eqn. 2.100 is that $\partial_{\mathbf{Q}}^2$ is hermitian with respect to integration over \mathbf{Q} . Thus

$$\int \Psi^* \partial_{\mathbf{Q}}^2 \Psi d\mathbf{Q} - \int \Psi \partial_{\mathbf{Q}}^2 \Psi^* d\mathbf{Q} = 0. \quad (2.102)$$

Consequently, $\partial_{\mathbf{Q}} \cdot \mathbf{K}_{ij}$ vanishes and

$$\partial_t \rho(t, \mathbf{q}) = - \sum_{i,j} \int \chi_i \chi_j^* \partial_{\mathbf{q}} \cdot \mathbf{j}_{ij} d\mathbf{Q} = \sum_{i,j} \int \frac{E_i - E_j}{i\hbar} \chi_i \chi_j^* \phi_i \phi_j^* d\mathbf{Q}. \quad (2.103)$$

Evidently, only the electronic (transition) flux density contributes to the change in time of the density.

It is not possible to use only one electronic state in the BOE, because the coupling of the states in eqn. 2.81 introduces population in other electronic states an infinitesimal time step later. Thus, the situation described in Fig. 2.2 is not well-described in the BOE: It is not possible to confine dynamics to only one electronic state. Application of the BOA, however, changes this situation.

Flux densities in the Born-Oppenheimer approximation

In the limit of the BOA, there is an important aspect that needs to be considered: Without the BOA, the time-dependent Schrödinger equation is valid for the complete wave function (eqn. 2.80). Thus, the usual form of the quantum mechanical flux density derived from the time-dependent Schrödinger equation is valid if the complete wave function is used. In

2.4. Flux densities and the Born-Oppenheimer approximation

contrast, in the limit of the BOA there is no time-dependent Schrödinger equation for the full wave function. Instead, there are only time-dependent Schrödinger equations for the nuclear wave functions, cf. eqn. 2.82. Thus, the usual form of the quantum mechanical flux density can only be used for the nuclear wave function. Specifically, from eqn. 2.82 it follows that the time derivative of $\chi_i\chi_j^*$ is

$$\partial_t(\chi_i\chi_j^*) = -\partial_{\mathbf{Q}} \cdot \mathbf{J}_{ij} \quad (2.104)$$

in the BOA. This equation is a continuity equation for the nuclear densities only. However, as there are no electrons created or destroyed, there has to be also an independent continuity equation for the time-dependent electron density alone.

The time dependence of the total wave function in the BOA (i.e. many non-interacting nuclear wave functions) is calculated first. Thus, $\partial_t|\Psi|^2$ is determined, but using eqn. 2.82 instead of eqn. 2.80 to apply the BOA. The result is

$$\begin{aligned} \partial_t|\Psi|^2 &= \sum_{i,j} \phi_i\phi_j^*(\chi_i\partial_t\chi_j^* + \chi_j^*\partial_t\chi_i) \\ &= \sum_{i,j} \left[-\phi_i\phi_j^*\partial_{\mathbf{Q}} \cdot \mathbf{J}_{ij} + \frac{E_i - E_j}{i\hbar} \phi_i\phi_j^*\chi_i\chi_j^* \right] \end{aligned} \quad (2.105)$$

$$= \sum_{i,j} \left[-\phi_i\phi_j^*\partial_{\mathbf{Q}} \cdot \mathbf{J}_{ij} - \chi_i\chi_j^*\partial_{\mathbf{q}} \cdot \mathbf{j}_{ij} \right]. \quad (2.106)$$

A partition of the complete flux density into a nuclear and an electronic part is readily achieved. Although the single nuclear wave functions are not coupled, there are transition flux densities \mathbf{J}_{ij} and \mathbf{j}_{ij} for $i \neq j$. These flux densities occur because the total density is not the sum of individual densities of the electronic states, but the absolute square of the sum of the wave functions.

At first sight, these transition flux densities seem strange, because in the BOA independent nuclear dynamics on the states takes place. The the sum of the nuclear densities on each state should add up to the total nuclear density, and fluxes should only happen in the states, but not between the states.

As soon as the BOE is used, the total nuclear density is the sum of the individual nuclear densities by virtue of the orthonormality of the electronic states with respect to integration over \mathbf{q} :

$$\begin{aligned} \varrho(t, \mathbf{Q}) &= \int |\Psi|^2 d\mathbf{q} \\ &= \int \sum_{i,j} \phi_i\phi_j^*\chi_i\chi_j^* d\mathbf{q} \\ &= \sum_i |\chi_i|^2. \end{aligned} \quad (2.107)$$

This results holds with and without the BOA, but in the BOA also the nuclear flux densities are a sum of the individual flux densities. From eqn. 2.105 follows that

$$\begin{aligned} \partial_t\varrho(t, \mathbf{Q}) &= \int \partial_t|\Psi|^2 d\mathbf{q} \\ &= \sum_{i,j} \int \left[-\phi_i\phi_j^*\partial_{\mathbf{Q}} \cdot \mathbf{J}_{ij} + \frac{E_i - E_j}{i\hbar} \phi_i\phi_j^*\chi_i\chi_j^* \right] d\mathbf{q} \end{aligned} \quad (2.108)$$

$$= -\sum_i \partial_{\mathbf{Q}} \cdot \mathbf{J}_{ii} = \sum_i \partial_t|\chi_i|^2. \quad (2.109)$$

By eqn. 2.104, this relation is valid for each state i separately,

$$-\partial_{\mathbf{Q}} \cdot \mathbf{J}_{ii} = \partial_t |\chi_i|^2, \quad (2.110)$$

so that there is no interaction of the nuclear wave packets on different electronic states. The result is completely in line with the picture of the decoupled time evolution of the nuclear wave packets.

For the time-dependent electron density ρ of eqn. 2.100, the BOA yields

$$\begin{aligned} \partial_t \rho &= \sum_{i,j} \int [-\phi_i \phi_j^* \partial_{\mathbf{Q}} \cdot \mathbf{J}_{ij} - \chi_i \chi_j^* \partial_{\mathbf{q}} \cdot \mathbf{j}_{ij}] d\mathbf{Q} \\ &= \sum_{i,j} \int [\partial_{\mathbf{Q}}(\phi_i \phi_j^*) \cdot \mathbf{J}_{ij} - \chi_i \chi_j^* \partial_{\mathbf{q}} \cdot \mathbf{j}_{ij}] d\mathbf{Q}. \end{aligned} \quad (2.111)$$

How is the situation of Fig. 2.2 described now? That is, what happens if only one state is taken into account for the nuclear dynamics?

Only the state k is kept, with $\phi = \phi_k$, $\chi = \chi_k$, $E = E_k$ and $\mathbf{J} = \mathbf{J}_{kk}$. In accord with the discussion of Fig. 2.2, the time-dependent electron density is

$$\partial_t \rho = \int |\phi|^2 \partial_t |\chi|^2 d\mathbf{Q} = - \int |\phi|^2 \partial_{\mathbf{Q}} \cdot \mathbf{J} d\mathbf{Q}. \quad (2.112)$$

It follows that in the limit of the BOA there is a well-defined time-dependent electron density. Consequently, there are electronic fluxes and thus there also has to be an electronic flux density.

Despite the time-dependence of ρ which follows from eqn. 2.112, it is not straightforward to find an expression for the electronic flux density in this case: The right-hand side of eqn. 2.112 cannot be written as the divergence with respect to \mathbf{q} of some vector field $\mathbf{j}(t, \mathbf{q})$ in a unique way. Due to this problem, a few approaches to extract an electronic flux density in the BOA were developed. These are discussed below, and their advantages and disadvantages are shown.

Finally, there is the possibility to not neglect all of the terms $\langle \phi_j | \partial_{\mathbf{Q}} | \phi_i \rangle$ and $\langle \phi_j | \partial_{\mathbf{Q}}^2 | \phi_i \rangle$ of eqn. 2.71 as is done in the BOA, but only those coupling different electronic states. For the nuclear wave functions, the Schrödinger equations would then be

$$\partial_t \chi_i = \left(-\frac{\hbar}{2i} \partial_{\mathbf{Q}}^2 - \frac{2\langle \phi_i | \partial_{\mathbf{Q}} | \phi_i \rangle}{i\hbar} \partial_{\mathbf{Q}} + \frac{E_i - \langle \phi_i | \partial_{\mathbf{Q}}^2 | \phi_i \rangle}{i\hbar} \right) \chi_i \quad (2.113)$$

$$\partial_t \chi_i^* = \left(\frac{\hbar}{2i} \partial_{\mathbf{Q}}^2 + \frac{2\langle \phi_i | \partial_{\mathbf{Q}} | \phi_i \rangle^*}{i\hbar} \partial_{\mathbf{Q}} - \frac{E_i - \langle \phi_i | \partial_{\mathbf{Q}}^2 | \phi_i \rangle^*}{i\hbar} \right) \chi_i^*. \quad (2.114)$$

In this case, the time-dependence of the complete wave function is determined by

$$\begin{aligned} \partial_t |\Psi|^2 &= \sum_{i,j} \left[-\phi_i \phi_j^* \partial_{\mathbf{Q}} \cdot \mathbf{J}_{ij} - \frac{2}{i\hbar} \phi_i \phi_j^* (\langle \phi_i | \partial_{\mathbf{Q}} | \phi_i \rangle \chi_j^* \partial_{\mathbf{Q}} \chi_i - \langle \phi_j | \partial_{\mathbf{Q}} | \phi_j \rangle^* \chi_i \partial_{\mathbf{Q}} \chi_j^*) \right] \\ &+ \sum_{i,j} \left[\frac{E_i - \langle \phi_i | \partial_{\mathbf{Q}}^2 | \phi_i \rangle - E_j + \langle \phi_j | \partial_{\mathbf{Q}}^2 | \phi_j \rangle^*}{i\hbar} \phi_i \phi_j^* \chi_i \chi_j^* \right]. \end{aligned} \quad (2.115)$$

The discussion is again restricted to only one electronic state. To calculate the time-dependent one-electron density, an integration is performed over \mathbf{Q} . The quantities $\langle \phi_i | \partial_{\mathbf{Q}} | \phi_i \rangle$ and $\langle \phi_i | \partial_{\mathbf{Q}}^2 | \phi_i \rangle$ are anti-hermitian and hermitian with respect to integration over \mathbf{Q} , hence it

2.4. Flux densities and the Born-Oppenheimer approximation

follows that

$$\partial_t \rho = - \int |\phi|^2 \left(\partial_{\mathbf{Q}} \cdot \mathbf{J} + \frac{\partial_{\mathbf{Q}} \langle \phi | \phi \rangle}{\hbar^2} \cdot \mathbf{J} \right) d\mathbf{Q} \quad (2.116)$$

$$= - \int |\phi|^2 \partial_{\mathbf{Q}} \cdot \mathbf{J} d\mathbf{Q} \quad (2.117)$$

(note that $\langle \phi | \phi \rangle = 1$ for all \mathbf{Q}). This is the same result as eqn. 2.112. Consequently, the diagonal Born-Oppenheimer corrections for the nuclear wavefunction do not contribute to the time-dependence of the electronic density.

The exact electronic flux density

Before reviewing calculations of electronic flux densities in the BOA, it should be remarked again that there is one calculation of the electronic flux density during nuclear motion without the BOA. Barth, Hege, Ikeda, Kenfack, Koppitz, Manz, Marquardt and Paramonov calculated the electronic flux density for a quantum dynamics simulation of the dihydrogen cation [25], and Diestler, Kenfack, Manz, Paulus, Jhon Fredy Pérez-Torres and Vincent Pohl improved this calculation significantly [69]. Results of both simulations are in good agreement with the scaled coupled-channels flux density [69], see below.

Laser induced electronic ring currents

Laser induced electronic flux densities in the BOA were studied by Barth and Manz for atoms [27], and by Barth, Manz, Shigeta and Yagi for magnesium porphyrin [28]. The electron dynamics is induced by excitation of degenerate atomic or molecular orbitals with circularly polarized light and it was found that strong currents and magnetic fields can be produced. However, in both cases the nuclei were kept frozen.

Okuyama's and Takatsuka's time-shift flux density

Okuyama and Takatsuka note in [167] the deficiency of the BOA to produce a non-zero electronic flux density for the quantum mechanical definition of the electronic flux density. However, in their semiclassical Ehrenfest approach to electron dynamics they are able to calculate electronic flux densities directly. They proposed to use a time shift flux density in the BOA, which when tested against the definition of the flux density seemed to give qualitatively good results. This quantity is discussed now.

Consider the time shift flux density

$$\mathbf{j}(t, \Delta t) = \frac{\hbar}{2im} (\phi^*(t - \Delta t/2) \partial_{\mathbf{q}} \phi(t + \Delta t/2) - \phi(t + \Delta t/2) \partial_{\mathbf{q}} \phi^*(t - \Delta t/2)) \quad (2.118)$$

with some unspecified time difference Δt . Given a Schrödinger equation

$$\left(i\hbar \partial_t + \frac{\hbar^2}{2m} \partial_{\mathbf{q}}^2 - V(\mathbf{q}) \right) \phi = (i\hbar \partial_t - H) \phi = 0 \quad (2.119)$$

and the equation of continuity, $\partial_t \rho + \partial_{\mathbf{q}} \cdot \mathbf{j} = 0$, the time shift flux density corresponds to a density $\rho = \phi^*(t - \Delta t/2) \phi(t + \Delta t/2)$, i.e. the overlap between the time-shifted wave functions. Thus, for a given volume, \mathbf{j} gives the change of overlap between the time-shifted functions. As Okuyama and Takatsuka explained in [167], \mathbf{j} can be interpreted as deformation direction of the wave function, and it is always imaginary in case the shifted wave functions are both real.

The time shift flux density is interesting. The complex conjugate of eqn. 2.119 for time-independent H is

$$\begin{aligned} 0 &= (i\hbar\partial_t + H)\phi^*(t) \\ &= (i\hbar\partial_t + H)\phi(-t), \end{aligned} \quad (2.120)$$

and taking the complex conjugate of this equations yields

$$0 = (i\hbar\partial_t - H)\phi^*(-t). \quad (2.121)$$

By applying the Schrödinger equations eqn. 2.119 and eqn. 2.121 repeatedly in the Taylor series expansion of $\phi(t + \Delta t/2)$ and $\phi^*(t - \Delta t/2)$ around t it is found that

$$\phi(t + \Delta t/2) = U\phi(t) \quad (2.122)$$

$$\phi^*(t - \Delta t/2) = U\phi(t)^* \quad (2.123)$$

with the same time-evolution operator for both quantities,

$$U(\Delta t) = 1 + \frac{H}{i\hbar} \frac{\Delta t}{2} - \frac{H^2}{\hbar^2} \left(\frac{\Delta t}{2}\right)^2 + \dots = \exp\left(\frac{\Delta t H}{2i\hbar}\right). \quad (2.124)$$

Consequently, $\phi(t_0 + \Delta t) = \phi^*(t_0 - \Delta t)$ if $\phi(t_0)$ is real, reflecting the fact that the evolution of an initially real ϕ forward in time equals the evolution of ϕ^* backward in time [146]. Thus, the time-shift flux density for a real wave function $\phi(t)$ is zero if this wave function is the solution of the Schrödinger equation. Note also that if there is a point in time t_0 when the wave function is real, $\phi(t_0) = \phi^*(t_0)$, then due to the Schrödinger equation the wave function will be complex an infinitesimal time step dt later.

The wave function that Okuyama and Takatsuka study is not a solution of the time-dependent Schrödinger equation. Instead, the nuclear motion is determined semiclassically and the electronic wave function is the stationary wave function of the respective nuclear configuration.

The time shift flux of Okuyama and Takatsuka might be an interesting quantity to calculate, and it can in principle be used in the BOA. However, it might be difficult to interpret because of the just mentioned puzzling relation with respect to the correct wave function and because of the undetermined parameter Δt . Also, so far it was only used for processes that involved diabatic transitions between electronic states, and was never applied nor tested for chemical reactions in the electronic ground state.

Diestler's coupled-channels flux density

A promising approach for extracting a flux density completely within the framework of the BOA was proposed by Diestler [66], with numerical results [68] and solution of the dihydrogen cation [69]. In [66], Diestler derives a flux density based on a suitable coordinate transformation of electronic and nuclear coordinates. The transformation is done in such a way that the ratio of electronic and nuclear masses occurs, and that terms proportional to this ratio can be dropped. Diestler derives the expressions first for the hydrogen atom and compares these to the exact solution. The treatment is then extended to the dihydrogen cation. The basic ideas of Diestler's approach shall now be reviewed.

Starting point is the flux density operator $\hat{\mathbf{j}}$ defined in eqn. 2.43, in 3-space written as

$$\hat{\mathbf{j}} = \frac{\hbar}{2im} (\partial_{\mathbf{x}}\delta(\mathbf{x} - \mathbf{x}') + \delta(\mathbf{x} - \mathbf{x}')\partial_{\mathbf{x}}). \quad (2.125)$$

2.4. Flux densities and the Born-Oppenheimer approximation

The expectation value of this operator with respect to a wave function $\Psi(t, \mathbf{Q}, \mathbf{x})$ depending on the coordinates of one electron \mathbf{x} and on the coordinates of all nuclei \mathbf{Q} may be evaluated. This procedure is similar to eqn. 2.44, but with an extra integration over \mathbf{Q} . However, in [66] the final integrations are not performed, but:

$$\mathbf{j}(t, \mathbf{x}') = \iint \delta(\mathbf{x}' - \mathbf{x})(\Psi^* \partial_{\mathbf{x}} \Psi - \Psi \partial_{\mathbf{x}} \Psi^*) d\mathbf{Q} d\mathbf{x} \quad (2.126)$$

is kept. Note that \mathbf{x}' is used for the spacial coordinates and \mathbf{x} for the position of the electrons, but these will finally be identified. The BOA and the form of the wave function

$$\Psi(t, \mathbf{x}, \mathbf{Q}) = \chi(t, \mathbf{Q}) \phi(\mathbf{x}, \mathbf{Q}) \quad (2.127)$$

is assumed, as well as that ϕ is real. Thus, this wave function will give zero flux density in eqn. 2.126.

By analyzing the exact solution of the hydrogen atom (with $\mathbf{Q} = \mathbf{X}$, as there is only one nucleus), Diestler found that a switch from \mathbf{x}, \mathbf{X} to coordinates

$$\mathbf{y} = \mathbf{x} - \mathbf{X} \quad (2.128)$$

$$\mathbf{Y} = \epsilon \mathbf{x} + \frac{M_{\text{P}}}{M} \mathbf{X} \quad (2.129)$$

is helpful. Here, $M = M_{\text{P}} + m_e$ is the mass of the system, i.e. the sum of the proton (M_{P}) and electron mass (m_e), and $\epsilon = \frac{m_e}{M}$. For the hydrogen atom only the distance from the one proton matters for ϕ , so that $\phi(x, \mathbf{Q}) = \tilde{\phi}(\mathbf{y})$. The mass ratio ϵ is small. After performing the transformation and neglecting terms which are smaller than or of order ϵ , it is found from eqn. 2.126 that

$$\begin{aligned} \mathbf{j}(t, \mathbf{x}') &= \frac{\hbar}{m_e} \iint \delta(\mathbf{x}' - \mathbf{Y} - \mathbf{y}) |\chi(t, \mathbf{Y})|^2 \text{Im} \left[\tilde{\phi}^*(\mathbf{y}) \partial_{\mathbf{y}} \tilde{\phi}(\mathbf{y}) \right] d\mathbf{Y} d\mathbf{y} \\ &\quad + \frac{\hbar}{M_{\text{P}}} \iint \delta(\mathbf{x}' - \mathbf{Y} - \mathbf{y}) |\tilde{\phi}(\mathbf{y})|^2 \text{Im} [\chi^*(t, \mathbf{Y}) \partial_{\mathbf{Y}} \chi(t, \mathbf{Y})] d\mathbf{Y} d\mathbf{y} \\ &= \int |\phi(\mathbf{x}' - \mathbf{Y})|^2 \mathbf{J}(t, \mathbf{Y}) d\mathbf{Y} \end{aligned} \quad (2.130)$$

with the proton flux density \mathbf{J} defined analogously to the electronic flux density. For $\epsilon \approx 0$ and $\frac{M_{\text{P}}}{M} \approx 1$, it follows that $\mathbf{Y} \approx \mathbf{X}$, and that the electron is simply dragged along by the proton. This is of course expected on physical grounds and compares well with the exact treatment of the problem [66]. Diestler extends the procedure from the hydrogen atom to the dihydrogen cation. The 3-space position vectors of the two protons are denoted by \mathbf{X}_1 and \mathbf{X}_2 , respectively, and the total mass of the system is $M = 2M_{\text{P}} + m_e$. Two sets of coordinates are introduced: The ‘‘channel 2’’ Jacobi coordinates

$$\begin{aligned} \mathbf{y}_2 &= \mathbf{x} - \mathbf{X}_2 \\ \mathbf{Y}_2 &= \frac{M_{\text{P}} \mathbf{X}_2 + m_e \mathbf{x}}{M_{\text{P}} + m_e} - \mathbf{X}_1 \approx \mathbf{X}_2 - \mathbf{X}_1 \\ \mathbf{Z} &= \frac{M_{\text{P}} (\mathbf{X}_1 + \mathbf{X}_2) + m_e \mathbf{x}}{M} \end{aligned} \quad (2.131)$$

and the “channel 1” Jacobi coordinates

$$\begin{aligned} \mathbf{y}_1 &= \mathbf{x} - \mathbf{X}_1 \\ \mathbf{Y}_1 &= \frac{M_P \mathbf{X}_1 + m_e \mathbf{x}}{M_P + m_e} - \mathbf{X}_2 \approx \mathbf{X}_1 - \mathbf{X}_2 \\ \mathbf{Z} &= \frac{M_P (\mathbf{X}_1 + \mathbf{X}_2) + m_e \mathbf{x}}{M}. \end{aligned} \quad (2.132)$$

The center of mass of the complete system is \mathbf{Z} . The picture is inspired by scattering theory: In each of the two channels, the coordinates \mathbf{Y}_i are the distances between an effective particle, consisting of a proton together with an electron, and the other proton. An important step in the following is the approximate identification of the center of mass of the effective particle with the position of the proton, as indicated in the equations for \mathbf{Y}_i . This is justified by the smallness of the electron mass compared to the proton mass.

Next, it is assumed that the Born-Oppenheimer electronic wave function can be separated into two parts, each belonging to either \mathbf{X}_1 or \mathbf{X}_2 ,

$$\phi(\mathbf{x}, \mathbf{X}_1 - \mathbf{X}_2) = \phi_1(\mathbf{y}_1, \mathbf{Y}_1) + \phi_2(\mathbf{y}_2, \mathbf{Y}_2), \quad (2.133)$$

where the two parts are expressed in terms of the respective channel coordinates. Note that the fact that ϕ only depends on the relative distance of the two protons but not on the position of the center of mass is already included in this formulas. The decomposition of the electronic wave function into two parts carries over to the electronic fluxes so that contributions are obtained from each of the two channels.

Diestler always derives the approximate electronic flux density relative to a certain reference point. For example, he defines the classical electronic flux relative to the position of the electron with respect to one of the protons, e.g. the proton at \mathbf{X}_1 , to obtain

$$\mathbf{j}_1(t, x') = \delta(\mathbf{x}' - \mathbf{y}_2) \partial_t \mathbf{y}_1, \quad (2.134)$$

or with respect to the nuclear center of mass $\mathbf{X}_{\text{cm}} = \frac{\mathbf{X}_1 + \mathbf{X}_2}{2}$,

$$\mathbf{j}_{\text{cm}}(t, x') = \delta(\mathbf{x}' - (\mathbf{x} - \mathbf{X}_{\text{cm}})) \partial_t (\mathbf{x} - \mathbf{X}_{\text{cm}}). \quad (2.135)$$

The final expression for the electronic flux densities of the two channels depends on the chosen reference point. Before it is possible to obtain the expectation values of the operators corresponding to eqn. 2.134 and eqn. 2.135, respectively, it is necessary to drop terms of the order $\frac{m_e}{M_P}$. For example, the fact that $\mathbf{Y}_1, \mathbf{Y}_2$ are approximately equal to the inter-proton distance is used; in other words, in the “collision” of the proton with the atom, the center of mass of the atom is approximated by the center of mass of its nucleus.

Diestler’s electronic flux density has the advantage that it only needs the ground state electronic wave function. Also, the extension and calculations of the dihydrogen cation in [69] show that the exact electronic flux density and the electronic flux density obtained from this ansatz are in very good agreement. However, the artificial (albeit for H_2^+ seemingly unimportant) dependence on a reference might be a problem. Also, it is not yet known how the expression of the electron density corresponding to the coupled-channels electron flux density via the continuity equation looks like.

The extension of Diestler’s flux to molecules other than diatomics and inclusion of more than one electron are interesting problems that will hopefully be tackled in the future. First steps towards the generalization to more than two nuclei were already taken in [67].

Nafie's complete adiabatic flux density

In 1983, Nafie [155] proposed the “complete adiabatic” (CA) wave function: In the adiabatic approximation, the ground state wave function $\Psi(t, \mathbf{Q}, \mathbf{q})$ is a product of the ground state electronic wave function $\phi_0(\mathbf{q}, \mathbf{Q})$ and the ground state nuclear wave function $\chi(t, \mathbf{Q})$. Nafie searched for a similar product form,

$$\Psi(t, \mathbf{Q}, \mathbf{q}) = \phi_0^{\text{CA}}(\mathbf{q}, \mathbf{Q})\chi(t, \mathbf{Q}), \quad (2.136)$$

with the same χ but with ϕ_0^{CA} containing as much information as possible, including also contributions from electronically excited states. A possible derivation of ϕ_0^{CA} is reviewed in the following.

The Hamiltonian for the problem at hand is again eqn. 2.64,

$$H = \frac{\mathbf{P}^2}{2} + H_0(\mathbf{Q}) = -\frac{\hbar^2}{2}\partial_{\mathbf{Q}}^2 + H_0(\mathbf{Q}), \quad (2.137)$$

with the nuclear momentum \mathbf{P} and the electronic Hamiltonian H_0 . Note that mass scaled nuclear coordinates \mathbf{Q} are used.

The eigenfunctions of H_0 are given by

$$(H_0 - E_k(\mathbf{Q}))\phi_k = 0. \quad (2.138)$$

Operation of the complete Hamiltonian H on the product $\phi_0^{\text{CA}}\chi$ yields

$$H(\phi_0^{\text{CA}}\chi) = \phi_0^{\text{CA}}(T_{\text{nu}} + E_0)\chi - \hbar^2 \left((\partial_{\mathbf{Q}}\chi) \cdot (\partial_{\mathbf{Q}}\phi_0) + \frac{1}{2}\chi\partial_{\mathbf{Q}}^2\phi_0 \right). \quad (2.139)$$

If only the first term is kept for the determination of the dynamics, the situation would be equivalent to the BOA: The nuclear wave function χ is time-dependent, and thus the electronic wave function would not contribute to the dynamics (it factors to both sides of the time-dependent Schrödinger equation). However, instead of neglecting the second term of eqn. 2.139, this term is treated as perturbation.

The electronic wave functions ϕ_k^{CA} are defined to be eigenfunctions of the complete Hamiltonian for fixed nuclear positions and momenta,

$$(H - E_k^{\text{CA}}(\mathbf{Q}, \mathbf{P}))\phi_k^{\text{CA}}(\mathbf{q}, \mathbf{Q}, \mathbf{P}) = 0. \quad (2.140)$$

Note the additional appearance of the (classical) nuclear momentum as dependent variable for ϕ_k^{CA} . However, in the end the momentum operator $\mathbf{P} = -i\hbar\partial_{\mathbf{Q}}$ will be used, and the ϕ_k^{CA} themselves will become operators.

The functions ϕ_k are used as basis, and ϕ_0^{CA} is to first order in the perturbation $T = \frac{\mathbf{P}^2}{M}$ given by

$$\phi_0^{\text{CA}} = \phi_0 + \sum_{k>0} \frac{\phi_k}{E_0 - E_k} \left\langle \phi_k \left| \frac{\mathbf{P}^2}{2} \right| \phi_0 \right\rangle. \quad (2.141)$$

Note that, again, the bra-ket notation $\langle \cdot |$ indicates integration over the electronic coordinates \mathbf{q} only. The complete wave function eqn. 2.136 is a product of the nuclear wave function χ and ϕ_0^{CA} . In order to find the quantum mechanical expression for ϕ_0^{CA} , the nuclear momentum

operator has to be used, and this operator also acts on χ . Thus,

$$\begin{aligned}\phi_0^{\text{CA}}\chi &= \phi_0\chi + \frac{\hbar^2}{2} \sum_{k>0} \frac{\phi_k}{E_k - E_0} (\langle\phi_k|\partial_{\mathbf{Q}}^2|\phi_0\rangle\chi + 2\langle\phi_k|\partial_{\mathbf{Q}}\phi_0\rangle \cdot \partial_{\mathbf{Q}}\chi + \langle\phi_k|\phi_0\rangle\partial_{\mathbf{Q}}^2\chi) \\ &= \left(\phi_0 + \frac{\hbar^2}{2} \sum_{k>0} \phi_k \frac{\langle\phi_k|\partial_{\mathbf{Q}}^2|\phi_0\rangle + 2\langle\phi_k|\partial_{\mathbf{Q}}\phi_0\rangle \cdot \partial_{\mathbf{Q}}}{E_k - E_0} \right) \chi\end{aligned}\quad (2.142)$$

or

$$\phi_0^{\text{CA}} = \phi_0 + \frac{\hbar^2}{2} \sum_{k>0} \phi_k \frac{\langle\phi_k|\partial_{\mathbf{Q}}^2|\phi_0\rangle + 2\langle\phi_k|\partial_{\mathbf{Q}}\phi_0\rangle \cdot \partial_{\mathbf{Q}}}{E_k - E_0}.\quad (2.143)$$

There are two ways how ϕ_0^{CA} can be used: If the classical nuclear momentum is used in eqn. 2.141, this function is a number. It can be used as an improved electronic wave function in a molecular dynamics simulation in which the nuclei are treated classically. If the quantum mechanical nuclear momentum is used, ϕ_0^{CA} is the operator of eqn. 2.143. In both cases, calculation of the function is difficult because excited electronic states are needed.

Nafie calls ϕ_0^{CA} the “complete adiabatic wave function” because ϕ_0^{CA} “contains the entire factorable part of the molecular wave function” [155]. As was just seen, this view is peculiar because of the operator nature of ϕ_0^{CA} . Also, “adiabatic” may refer to the property that information from only one electronic state is needed, which is in conflict with the occurrence of excited states due to the perturbation expansion.

It is straightforward to calculate an electronic flux density for the wave function eqn. 2.136 as follows:

$$\begin{aligned}\mathbf{j}(t, \mathbf{q}, \mathbf{Q}) &= \frac{\hbar}{2im_e} (\Psi^* \partial_{\mathbf{q}} \Psi - \Psi \partial_{\mathbf{q}} \Psi^*) \\ &= \frac{\hbar}{2im_e} ((\phi_0^{\text{CA}}\chi)^* \partial_{\mathbf{q}}(\phi_0^{\text{CA}}\chi) - (\phi_0^{\text{CA}}\chi) \partial_{\mathbf{q}}(\phi_0^{\text{CA}}\chi)^*).\end{aligned}\quad (2.144)$$

To simplify the following equations, abbreviations for the matrix elements

$$a_{k0}(\mathbf{Q}) := \langle\phi_k|\partial_{\mathbf{Q}}\phi_0\rangle\quad (2.145)$$

and

$$2b_{k0}(\mathbf{Q}) := \langle\phi_k|\partial_{\mathbf{Q}}^2\phi_0\rangle\quad (2.146)$$

are useful. With these definitions, the full wave function eqn. 2.142 and its gradient with respect to the electronic coordinates can be written as

$$\begin{aligned}\Psi &= \chi\phi_0 + \hbar^2 \sum_{k>0} \frac{1}{E_k - E_0} (a_{k0}\partial_{\mathbf{Q}}\chi + b_{k0}\chi)\phi_k, \\ \partial_{\mathbf{q}}\Psi &= \chi\partial_{\mathbf{q}}\phi_0 + \hbar^2 \sum_{k>0} \frac{1}{E_k - E_0} (a_{k0}\partial_{\mathbf{Q}}\chi + b_{k0}\chi)\partial_{\mathbf{q}}\phi_k\end{aligned}\quad (2.147)$$

and the electronic flux density becomes

$$\begin{aligned}\mathbf{j}(t, \mathbf{q}, \mathbf{Q}) &\approx \frac{\hbar}{2im_e} (\phi_0^* \partial_{\mathbf{q}} \phi_0 - \phi_0 \partial_{\mathbf{q}} \phi_0^*) |\chi|^2 \\ &+ \frac{\hbar}{2im_e} \hbar^2 \sum_{k>0} \frac{1}{E_k - E_0} ([a_{k0}^* \chi \partial_{\mathbf{Q}} \chi^* + b_{k0}^* |\chi|^2] [\phi_k^* \partial_{\mathbf{q}} \phi_0 - \phi_0 \partial_{\mathbf{q}} \phi_k^*]) \\ &+ \frac{\hbar}{2im_e} \hbar^2 \sum_{k>0} \frac{1}{E_k - E_0} ([a_{k0} \chi^* \partial_{\mathbf{Q}} \chi + b_{k0} |\chi|^2] [\phi_0^* \partial_{\mathbf{q}} \phi_k - \phi_k \partial_{\mathbf{q}} \phi_0^*])\end{aligned}\quad (2.148)$$

Terms quadratic in the first-order perturbation correction are neglected.

2.5. Fluxes in the Born-Oppenheimer approximation

It is handy to define the (transition) flux densities

$$\mathbf{j}_{kl} := \frac{\hbar}{2im_e} (\phi_l^* \partial_{\mathbf{q}} \phi_k - \phi_k \partial_{\mathbf{q}} \phi_l^*) = \mathbf{j}_{lk}^* \quad (2.149)$$

and the nuclear density $\varrho := |\chi|^2$. Then, eqn. 2.148 becomes

$$\begin{aligned} \mathbf{j}(t, \mathbf{q}, \mathbf{Q}) &\approx \rho \mathbf{j}_{00} + \hbar^2 \sum_{k>0} \frac{1}{E_k - E_0} ([a_{k0}^* \chi \partial_{\mathbf{Q}} \chi^* + b_{k0}^* |\chi|^2] \mathbf{j}_{k0} + [a_{k0} \chi^* \partial_{\mathbf{Q}} \chi + b_{k0} |\chi|^2] \mathbf{j}_{k0}) \\ &= \rho \mathbf{j}_{00} + 2 \sum_{k>0} \frac{\hbar^2}{E_k - E_0} \operatorname{Re} ([a_{k0} \chi^* \partial_{\mathbf{Q}} \chi + b_{k0} \rho] \mathbf{j}_{k0}) \\ &= \rho \mathbf{j}_{00} + 2 \sum_{k>0} \frac{\hbar^2}{E_k - E_0} \operatorname{Re} ([\langle \phi_k | \partial_{\mathbf{Q}} \phi_0 \rangle \chi^* \partial_{\mathbf{Q}} \chi + \langle \phi_k | \partial_{\mathbf{Q}}^2 \phi_0 \rangle \rho] \mathbf{j}_{k0}) \end{aligned} \quad (2.150)$$

In general, the basis functions ϕ_k are real or can be chosen to be real (in case of degenerate eigenvalues). If the ϕ_k are assumed to be real, the transition flux densities \mathbf{j}_{k0} are completely imaginary and the flux density \mathbf{j}_{00} is zero. Moreover, $\langle \phi_k | \partial_{\mathbf{Q}}^2 \phi_0 \rangle$ is real and ρ is always real. Thus, $\operatorname{Re}(\langle \phi_k | \partial_{\mathbf{Q}}^2 \phi_0 \rangle \rho \mathbf{j}_{k0}) = 0$ in this case and eqn. 2.150 simplifies to

$$\mathbf{j}(t, \mathbf{q}, \mathbf{Q}) \approx \sum_{k>0} \hbar^2 \frac{\langle \phi_k | \partial_{\mathbf{Q}} \phi_0 \rangle}{E_k - E_0} \cdot (\chi^* \partial_{\mathbf{Q}} \chi + \chi \partial_{\mathbf{Q}} \chi^*) \mathbf{j}_{0k}. \quad (2.151)$$

The complete adiabatic wave function formalism was first developed by Nafie [155] (but see also [158]) and later used in the theory of vibrational circular dichroism [156]. It was also used with special emphasis on the transition current densities for vibronic and vibrational transitions in molecules [75, 76, 157]. In 2012, Patchkovskii derived the complete adiabatic wave function and eqn. 2.151 in a different manner than presented here, with a similar form of eqn. 2.150 [172]. Additionally, he proposed to calculate \mathbf{j} via double perturbation theory as third-order response of the ground state energy (for comparison, see [18, 102]). However, Patchkovskii’s calculation method is so far restricted to molecular dynamics simulations, i.e. for (semi-)classical treatment of the nuclei.

2.5 Fluxes in the Born-Oppenheimer approximation

Goal of this work is to improve the understanding of chemical reaction mechanisms, and especially of the arrows drawn typically in Lewis structures to indicate the course of a reaction in the electronic ground state. Applications will be focused on pericyclic reactions like the reaction shown in Fig. 2.3, known from the introduction. In this figure, the Diels-Alder reaction of butadiene with ethene is represented by Lewis structures. Arrows indicate the rearrangement of the electron pairs from product to reactant. This “reaction mechanism” should in general not be understood as the time-dependent course of the reaction, but only as effective changes from the static structures of the reactants to those of the products.

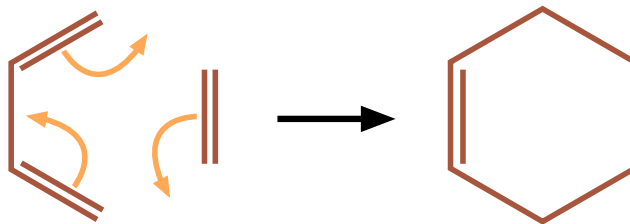


Figure 2.3: Lewis structures and reaction mechanism (arrows) for the schematic Diels-Alder reaction of ethane and butadiene to cyclohexene.

The quest is, however, to give these arrows a time-dependent meaning, so that the quotation marks from “reaction mechanism” may be removed. Analysis of the time-dependent flux density is surely the best method to achieve this goal. However, it is preferable to work in the framework of the BOA, because almost all quantum-chemical methods rely on this simplification. As seen in the previous part, especially for a quantum mechanical description of both the nuclei and the electrons the electronic flux density is difficult or impossible to obtain. Luckily, the time-dependent electron density is immediately available, and thus it is desirable to work with this quantity. The question is: Does the electron density contain enough information to solve the quest?

The flux density provides a lot of information about the motion of the particles. If a chemical reaction is considered, the arrows drawn indicate the qualitative change of the electron bonds or the electronic structure. Thus, they provide much less information than could be obtained from the complete flux density, which gives velocity vectors at each point in space. To give the arrows in Lewis structures time-dependent quantitative meaning, what is needed is the net flow of the electrons with time out of, or into specified regions of space. This flow can (almost completely) be determined by an electron density alone, if this density mirrors the effective dynamics of the electrons.

If such a time-dependent electron density is used, two points have to be taken care of: Sensible assumptions about what the Lewis structures mean have to be made, and the regions of space for which the flow is calculated have to be defined. These regions should represent the chemical bonds. Hence, it is necessary to include the quantum chemical methods in the discussion of the electron density to be able to sensibly divide the density into the different “types” of electrons and bonds (like σ -bonds or π -electrons) a chemist likes to think of.

An appropriate time-dependent electron density can be defined according to [25] as (cf. eqn. 2.101)

$$\rho(t, \mathbf{x}) := \int \rho^{\text{QC}}(\mathbf{x}, \mathbf{Q}) |\chi(t, \mathbf{Q})|^2 d\mathbf{Q}. \quad (2.152)$$

The density ρ^{QC} is a time-independent one-electron density. In practice, this density will be obtained from a quantum chemical calculation for a fixed nuclear configuration \mathbf{Q} , and calculations have to be performed for all necessary \mathbf{Q} . In section 3.3 there are more information on how these densities are obtained.

The time-dependence is introduced via the nuclear wave function χ , which is the solution of the time-dependent Schrödinger equation in the BOA for the potential of the respective electronic state. In this work, only ground-state chemical reactions are considered. Note also that the quantity ρ can be viewed as the expectation value of the operator ρ^{QC} with respect to the nuclear coordinates.

The procedure in [25] will now be followed: The time-dependent one-electron density is used to calculate fluxes into or out of observer volumes which should correspond to certain bonds in the Lewis structures. From eqn. 2.21 it is known that the electron flux $F(t, \Omega)$ out of an observer volume Ω is given by

$$F(t, \Omega) = \partial_t \int_{\Omega} \rho(t, \mathbf{x}) d\mathbf{x}. \quad (2.153)$$

Equally useful is the time-integrated electronic flux, the so-called electronic yield

$$\begin{aligned} Y(t, \Omega) &= \int_0^t F(t', \Omega) dt' \\ &= \int_{\Omega} (\rho(t, \mathbf{x}) d\mathbf{x} - \rho(0, \mathbf{x})) d\mathbf{x}. \end{aligned} \quad (2.154)$$

This yield represents the difference of the number of electrons in the sector Ω at time t with respect to the reference number at time 0. Closely related to the electron yield is the time-dependent electron number $N(t, \Omega)$, which is just the number of electrons in the sector Ω . Both quantities differ just in a time-independent constant. Conceptually, the electron number, electron flux and electron yield may be ordered as $N(t, \Omega) \rightarrow F(t, \Omega) \rightarrow Y(t, \Omega)$. The arrows indicate that the quantity at the arrow head follows from the other quantity. In section 4.1, the model system cyclooctatetraene will be discussed in terms of electronic fluxes and yields. Thereafter, in section 4.2, the model system benzene will be discussed in terms of electron numbers and fluxes. It shall be left to the reader to decide which approach is better suited.

In [25], F and Y were tested against the corresponding fluxes and yields for the full non-Born-Oppenheimer solution of the dihydrogen cation. It was shown that the fluxes in the BOA and the exact results are in very good agreement. In general, it may be expected that this is the case whenever the BOA is applicable to the dynamics of the system.

All applications presented here will be studies on cyclic electron rearrangements, i.e. pericyclic reactions in simple ring-shaped molecules. Consequently, it will be of interest in which direction the electrons flow along an angular coordinate φ as well as how many electrons actually flow. To this end, cylindrical coordinates r, φ, z are used and the volume is partitioned into sectors along the angular coordinate. The sectors represent a given carbon-carbon bond in the Lewis structure. The electron density in this sectors is summed up, so that electron numbers are obtained for the sectors. Hence, in practice only one-dimensional electronic fluxes are of interest. In the paragraph after eqn. 2.34 it was noted already that the one-dimensional continuity equation determines the flux density up to a time-dependent parameter. This parameter will not play a role in the applications of Section 4.1 and 4.2 due to the symmetry of the processes discussed there, but it will be important for the examples discussed in Section 4.3.

Chapter 3

Practice

3.1 Abstract

In the previous chapter, while discussing the flux densities efforts were made to stay within the realm of the Born-Oppenheimer approximation. The main reason for this confinement is the enormous intellectual edifice known as electronic structure methods. During the last century, methods for the solution of the electronic problem, i.e. the solution of the time-independent Schrödinger Equation for clamped nuclei, were developed to the point where energies and properties could be calculated to chemical accuracy: Exact enough to compare different, but maybe very similar molecular structures. For information about the history of quantum chemistry and for some recent developments in this field, see e.g. the Quantum Chemistry 2012 issue of Chemical Reviews [177, 178].

In this chapter, first the basic concepts of quantum chemistry are reviewed. After introduction of the Hartree-Fock method and its practical application, the multi-configuration self-consistent field method is discussed, as well as the closely connected complete active space self-consistent field method. Subsequently, details about the form of the electronic wave function are presented.

Next to the potential energy needed for the motion of the nuclei, the electron density is the main ingredient needed below to investigate the chemical model reactions. It is vital to know how the density is obtained and what its mathematical structure looks like. Thus, the chapter continues with a discussion on how the electron density is constructed in practice from the results of a quantum chemical calculation. Finally, problems and solutions for the usage of the electron density to calculate electronic fluxes is discussed.

Information about the general quantum chemical topics discussed in the following sections can be found in [111, 180, 204, 223], or in any introductory quantum chemistry text. Note that the following discussion is based on molecular orbital theory, where the wave function is a product of molecular orbitals, that are themselves linear combinations of atomic orbitals. There is also valence bond theory [188], where the wave function is a linear combination of valence bond orbitals, which themselves are products of atomic orbitals. The latter method is much less used but gained importance recently as generalized valence bond theory, or for analysis of a molecular orbital quantum chemical calculation.

3.2 A brief introduction to quantum chemistry

The object of a quantum chemical calculation is to solve the time-independent electronic Schrödinger equation

$$H_0(\mathbf{Q})\phi_i(\mathbf{q}, \mathbf{Q}) = \left(\frac{-\hbar^2}{2m_e} \partial_{\mathbf{q}}^2 + V(\mathbf{Q}, \mathbf{q}) \right) \phi_i(\mathbf{q}, \mathbf{Q}) = E_i(\mathbf{Q})\phi_i(\mathbf{q}, \mathbf{Q}). \quad (3.1)$$

The eigenfunctions ϕ_i and eigenvalues E_i are to be determined for a given nuclear structure \mathbf{Q} , and V is the molecular potential for this structure including nucleus-nucleus, nucleus-electron and electron-electron Coulomb interaction. In the following, only the ground state electronic wave function with $\phi := \phi_0$, $E := E_0$ is considered. Because all calculations need to be done for fixed \mathbf{Q} , the dependence on this parameter is dropped in the notation. Electron spin is not included explicitly, because there is no spin-dependent term in the Hamiltonian. In principle, a spin function needs to be included, which is separable due to the structure of H_0 . In practice, two electrons can be assigned to one of the spacial orbitals described below, for the two different possible spin states.

3.2.1 The Hartree-Fock method

The first step for the solution of the electronic problem with fixed nuclei is usually a Hartree Fock (HF) calculation. The following procedure is applied:

- Ansatz for the electronic wave function with n electrons is an anti-symmetric product of single electron functions, called the molecular orbitals (MO) or simply the orbitals,

$$\phi_{\text{HF}}(\mathbf{q}) = \hat{A} \prod_i^n \phi_i^{\text{MO}}(\mathbf{x}_i), \quad (3.2)$$

where \hat{A} is the anti-symmetrization operator. This wave function can be written as the so-called Slater determinant

$$\phi_{\text{HF}} = \frac{1}{\sqrt{n!}} \det(\phi_i^{\text{MO}}(\mathbf{x}_j)), \quad (3.3)$$

where the factor $\frac{1}{\sqrt{n!}}$ ensures normalization of the wave function. The anti-symmetry of the wave function with respect to the interchange of two electronic coordinates has to be included explicitly, as the determining equations do not enforce this symmetry.

- A solution to the molecular Hamiltonian with fixed nuclei is sought in the form of eqn. 3.2 by minimization of the energy. If the Hamiltonian for a nuclear structure \mathbf{Q} is $H_0(\mathbf{Q})$,

$$\min E_0(\mathbf{Q}) = \min \langle \phi_{\text{HF}} | H_0 | \phi_{\text{HF}} \rangle \quad (3.4)$$

is sought. Again, the scalar product $\langle \cdot \rangle$ is taken with respect to the electronic coordinates, and \mathbf{Q} is a parameter. The search space is the space of all possible molecular orbitals ϕ_i^{MO} , but with the orthogonality constraint $\langle \phi_i^{\text{MO}} | \phi_j^{\text{MO}} \rangle = \delta_{ij}$. Application of a variational procedure yields the eigenvalue equation

$$F(j)\phi_i^{\text{MO}}(\mathbf{x}_j) = \epsilon_i \phi_i^{\text{MO}}(\mathbf{x}_j) \quad (3.5)$$

3.2. A brief introduction to quantum chemistry

with the Fock operator

$$F(j) = \frac{-\hbar^2}{2m_e} \partial_{\mathbf{x}_j}^2 + U^{\text{HF}}(\mathbf{x}_j) - \sum_i^N \frac{Z_i}{|\mathbf{x}_j - \mathbf{X}_i|}. \quad (3.6)$$

This operator is composed of the electronic kinetic energy, the Hartree-Fock potential and the Coulomb interaction of the electron with all nuclei. The Hartree-Fock potential is given by

$$\begin{aligned} U^{\text{HF}}(\mathbf{x}_1) &= \sum_{i \neq j} \int \frac{|\phi_j^{\text{MO}}(\mathbf{x}_2)|^2}{|\mathbf{x}_1 - \mathbf{x}_2|} d\mathbf{x}_2 \phi_i^{\text{MO}}(\mathbf{x}_1) && \text{(Coulomb term)} \\ &+ \sum_{i \neq j} \int \frac{\phi_j^{\text{MO}}(\mathbf{x}_2)^* \phi_i^{\text{MO}}(\mathbf{x}_2)}{|\mathbf{x}_1 - \mathbf{x}_2|} d\mathbf{x}_2 \phi_j^{\text{MO}}(\mathbf{x}_1) && \text{(exchange term)}. \end{aligned} \quad (3.7)$$

Consequently, it depends itself on the molecular orbitals, and eqn. 3.6 has to be solved for ϵ_i and ϕ_i^{MO} in a self-consistent way. The Hartree-Fock potential is also a one-particle potential. Thus, the Hartree-Fock method may be viewed as the best possible solution of the electronic problem, if the electron-electron interaction is replaced by an effective single-electron potential.

- The MOs are parametrized and an initial guess for the parameters is made. From this guess, the energy and parameters are optimized using a variational principle and a set of U_i is obtained. This is called the HF method. From the set of independent potentials, new MOs can be calculated. The procedure is repeated until convergence. Because of the repetition until the solutions do not change within a certain error, the method is also called self-consistent field method.
- To be able to solve the HF equations in practice, the MOs are assumed to be linear combinations of atomic orbitals. These atomic orbitals are inspired by the solution of the time-independent Schrödinger equation for the hydrogen atom. They are the basis sets, to be discussed below. The coefficients of the linear combination are optimized during the self-consistent calculation, and the system of equations to be solved is called the Roothaan-Hall equations.

After a HF calculation, optimized MOs ϕ_i^{MO} and eigenvalues ϵ_i are obtained. The solution of eqn. 3.1 is the anti-symmetric product of the ϕ_i^{MO} with the smallest eigenvalues. If there are n electrons with n being even, the first $n/2$ MOs are included (occupied) and two electrons are assigned to each MO (one electron for each of the two possible electron spin directions). If n is odd, there is one electron occupying the MO number $(n + 1)/2$.

In principle, for a complete electronic basis the possible products of the solutions to the HF equations span the whole electronic space. Thus, a correction to the HF solution can be obtained by considering more than just one anti-symmetric product of the MOs. Electrons are assigned to some ϕ_i^{MO} with higher eigenvalues ϵ_i . A given assignment is called a configuration, and a product which is not the HF ground state product is called an excited configuration. Such calculations are thus termed configuration interaction calculations (CI). The possible products of HF MOs are used as basis functions and a new solution is sought as linear combination of the configurations. Specifically, the new ansatz for the electronic wave function is

$$\phi_{\text{CI}} = \phi_{\text{HF}} + \sum_i^a c_i^a \phi_i^a + \sum_{i,j}^{a,b} c_{ij}^{ab} \phi_{ij}^{ab} + \dots, \quad (3.8)$$

with ϕ_i^a, ϕ_{ij}^{ab} etc. being other anti-symmetric products of the MOs than ϕ_{HF} . The subscripts denote MOs that do not occur in the product anymore, while the superscripts denote MOs that are included instead. The coefficients of the configurations, c_i^a, c_{ij}^{ab} , are optimized. In practice, the basis is neither complete nor are all possible excited configurations considered. A typical example is the configuration interaction singles and doubles (CISD) method, for which all singly and doubly excited configurations are taken into account.

3.2.2 The multi-configuration self-consistent field method

The minimum of a region of the potential energy surface which corresponds to a certain chemical structure is called the equilibrium structure. This nuclear structure is often well approximated by a single Slater determinant. During a reaction, it happens that the order of the MO eigenvalues changes, or that two MO eigenvalues become equal (degenerate). If the degenerate MOs are those corresponding to the highest eigenvalue of the occupied MOs and those to the lowest eigenvalue of the unoccupied MOs, it is not sensible to use only one Slater determinant. Such so-called multireference cases occur often at transition states, i.e. at the nuclear structure corresponding to the maximum of the path of minimal energy connecting reactants and product. An example for a multireference case is the transition state of the double bond shift in cyclooctatetraene, discussed in section 4.1.

The method of choice in such situations is the multi-configuration self-consistent field (MCSCF) method. In an MCSCF calculation the wave function is a linear combination of different configurations,

$$\phi_{\text{MCSCF}} = \sum_I c_I \phi_I, \quad (3.9)$$

where the (multi-)index I denotes the set of configurations. The expansion coefficients c_I are similar to the expansion coefficients $c_i^a, c_{ij}^{ab}, \dots$ of eqn. 3.8 for a CI calculation. Both denote the coefficients for a superposition of selected configurations, and both are optimized during the calculation. While for the CI calculation the coefficients are constructed systematically by excited configurations, the choice of the configurations I for an MCSCF calculation is guided by intuition or testing. However, in contrast to a CI calculation, for an MCSCF calculation not only the expansion coefficients c_I are optimized, but also the coefficients e_{ij} (introduced below) from which the ϕ_i^{MO} are constructed.

If the number of included configurations is restricted (the active space), the calculation is also called a complete active space self-consistent field (CASSCF) calculation. Within the active space, all possible excitations are calculated, and thus the configuration interaction calculation in this subspace is complete.

The MOs included in the active space are treated differently from the other MOs. It may be necessary to improve the results further by inclusion of excitations from some or all (valence) MOs, in order to achieve a balanced description of the system. Thus, subsequently a configuration interaction calculation may be performed (multireference configuration interaction, MRCI). Recent developments in the field of multireference methods can be found in [205].

3.2.3 Electronic basis sets

The basis sets which are used to build the ϕ_i^{MO} are linear combinations of atomic orbitals. For these atomic orbitals (AO) there are two common choices: Slater-type orbitals (STOs) and Gaussian-type orbitals (GTOs). While interest in STOs (or rather Slater-type geminals) is revived due to their superior performance in R12/F12-methods [211], GTOs are still mainly used. In the following, only GTOs are considered, because all calculations presented in the

3.3. The static electron density in quantum chemistry

next chapter are performed using those functions. However, the general statements hold for STOs, too. More about basis functions and their use in quantum chemistry can be found in [103] or in the documentation of quantum chemistry program packages, like Molpro [225].

The components of the basis set, the AOs ϕ_j^{AO} , are functions centered at a given nucleus. They are itself composed of several functions, and their functional form is inspired by the analytically known non-relativistic quantum mechanical solution of the hydrogen atom. It is common to use the functions expressed in either a spherical or a Cartesian coordinate system. In the former, the basis functions are products of a radial part and the spherical harmonics. Thus, for a given angular momentum quantum number to be included there is one s-type AO and there are 3 p-type, 5 d-type and 7 f-type AOs, etc.

In the latter, the AOs are built as

$$\phi_j^{\text{AO}}(\mathbf{x}) = \sum_k x_1^{a_k} x_2^{b_k} x_3^{c_k} \exp(-d_k(x_1^2 + x_2^2 + x_3^2)) \quad (3.10)$$

where the exponents $a_k, b_k, c_k \geq 0$ are chosen according to the angular quantum number the respective ϕ_j^{AO} should represent. The possible ranges of the exponents are determined by

$$\begin{aligned} a_k + b_k + c_k &= 0 && \text{for s-type functions,} \\ a_k + b_k + c_k &= 1 && \text{for p-type functions,} \\ a_k + b_k + c_k &= 2 && \text{for d-type functions,} \end{aligned} \quad (3.11)$$

etc. Thus, there is 1 s-type function, and there are 3 p-type, 6 d-type, 10 f-type, etc. functions. Compared to the basis set in spherical coordinates there is a redundancy starting with d-type basis functions. If this basis sets were used in the calculation, it would effectively result in further s-type basis functions (see [103] for an explanation). Although typically (e.g. in Molpro) by default the basis set in spherical coordinates is used for the calculations, the output is often given in the basis set in Cartesian coordinates. Note that for the exponents a_k, b_k, c_k, d_k , the index j was not given explicitly. These exponents are usually the same for a given type of nucleus, but differ from nucleus to nucleus and should thus in principle also carry the index j . The MOs ϕ_i^{MO} are linear combinations of the AOs,

$$\phi_i^{\text{MO}}(\mathbf{x}) = \sum_j e_{ij} \phi_j^{\text{AO}}(\mathbf{x} - \mathbf{X}_j). \quad (3.12)$$

Here, \mathbf{X}_j are the Cartesian coordinates of the respective nucleus around which the functions are centered.

While the coefficients a_k, b_k, c_k and the exponents d_k are fixed, the coefficients e_{ij} are varied in the determination of the MOs in a HF or a CASSCF calculation.

3.3 The static electron density in quantum chemistry

A one-electron density can be calculated from the complete electronic wave function as

$$\rho(\mathbf{x}) = \int \phi(\mathbf{q}) \phi(\mathbf{q})^* d\mathbf{x}_2 \dots d\mathbf{x}_n \Big|_{\mathbf{x}_1=\mathbf{x}}. \quad (3.13)$$

The selection of the coordinates \mathbf{x}_1 of the first electron is arbitrary. However, as the electrons are indistinguishable, the result will be the same independent of the chosen electron. This property is ensured by the anti-symmetry of the electronic wave function.

A nice way to calculate the density from the electron orbitals is given by the transformation

to natural orbitals. These were introduced by Löwdin [128] and have desirable properties for quantum chemistry calculations [61]. However, the reason they are discussed here is because of their advantages in terms of the chemical interpretation of orbitals, and because of the simple structure of the electron density in terms of natural orbitals.

In order to define natural orbitals, first the density matrix $\tilde{\rho}(\mathbf{x}_1, \mathbf{x}_2)$ is introduced. It is given in terms of the MOs as

$$\tilde{\rho}(\mathbf{x}_1, \mathbf{x}_2) = \sum_{i,j} f_{ij} \phi_i(\mathbf{x}_1) \phi_j^*(\mathbf{x}_2). \quad (3.14)$$

The matrix of the coefficients f_{ij} are the density matrix in the basis of the MOs. From the density matrix the one-electron density is obtained as

$$\rho(\mathbf{x}) = \tilde{\rho}(\mathbf{x}, \mathbf{x}). \quad (3.15)$$

For a single determinant wave function eqn. 3.2, for example,

$$\begin{aligned} \rho_{\text{HF}}(\mathbf{x}) &= \frac{1}{n!} \int \det(\phi_i^{\text{MO}}(\mathbf{x}_j)) \det((\phi_i^{\text{MO}}(\mathbf{x}_j))^*) d\mathbf{x}_2 \dots d\mathbf{x}_n \Big|_{\mathbf{x}_1=\mathbf{x}} \\ &= \frac{1}{n!} \int \det \left(\sum_k \phi_k^{\text{MO}}(\mathbf{x}_k) (\phi_k^{\text{MO}}(\mathbf{x}_j))^* \right) d\mathbf{x}_2 \dots d\mathbf{x}_n \Big|_{\mathbf{x}_1=\mathbf{x}} \\ &= \frac{1}{n} \sum_i \phi_i^{\text{MO}}(\mathbf{x}) (\phi_i^{\text{MO}}(\mathbf{x}))^* \end{aligned} \quad (3.16)$$

by orthonormality of the MOs. Note that $\rho_{\text{HF}}(\mathbf{x})$ in this case is normalized to 1, but more common is the normalization to the number of particles,

$$\int \rho(\mathbf{x}) d\mathbf{x} = n, \quad (3.17)$$

which for the HF wave function gives

$$\rho_{\text{HF}}(\mathbf{x}) = \sum_i \phi_i^{\text{MO}}(\mathbf{x}) (\phi_i^{\text{MO}}(\mathbf{x}))^*. \quad (3.18)$$

The HF density eqn. 3.18 is special, because the matrix f_{ij} in eqn. 3.14 is diagonal. Consequently, the numbers f_{ii} are one if the orbital is included in the Slater determinant, or zero if it is not. If the electronic wave function is a superposition of several Slater determinants, like in the case of a CI calculation, f_{ij} is not diagonal anymore and the interpretation of the diagonal entries is lost. However, f_{ij} may be diagonalized. This results in the diagonal matrix g_{ij} and transformed orbitals ϕ_i^{NO} , such that

$$\rho(\mathbf{x}) = \sum_i g_{ii} \phi_i^{\text{NO}}(\mathbf{x}) (\phi_i^{\text{NO}}(\mathbf{x}))^*. \quad (3.19)$$

The orbitals ϕ_i^{NO} are called natural orbitals and the numbers g_{ii} are called occupation numbers. Note that the occupation numbers may be any number between 0 and 1, and the sum in eqn. 3.19 in general includes all orbitals, not only the orbitals that were occupied after a HF calculation.

If the electron density shall be used for analysis of chemical reactions, it is desirable to have an electron density for each of the different types of electrons (e.g. core electrons, valence electrons, or π -electrons). For this partitioning it is helpful if the density matrix is diagonal, as otherwise mixed orbital contributions occur. Thus, natural orbitals are a

sensible choice for calculations of the different densities. But there is an ambiguity: Because in principle all natural orbitals have a non-zero occupation number, it may be difficult to assign the orbitals to one of the chosen densities.

This problem does not occur if only a HF calculation is performed, but it does luckily also not occur in a severe way for a CASSCF calculation. In the latter, only excitations within the active space are considered. Thus, natural orbitals will have an occupation number of 0 or 1 for the inactive space, and only within the active space fractional occupation numbers occur. Also, the active space is usually selected on basis of chemical reasoning, and these electrons should usually be treated together anyway. Examples will be seen below, where the active space was chosen to include all π -orbitals of carbon-carbon bonds in cyclooctatetraene and benzene. Consequently, using all active space orbitals to define a partitioned electron density is a sound choice.

Note that the electron density is a rather robust quantity. Although the energy and equilibrium structure of a molecule may change drastically if corrections to the HF method are included, it was found that the HF one-electron density (for the corrected structure) is in very good agreement with the density obtained from the corrected wave function.

3.4 Time-dependent electron density and time-dependent electron numbers

In the following, a one-electron density obtained from a quantum chemical calculation performed at a nuclear configuration \mathbf{Q} is denoted by $\rho_{\text{QC}}(\mathbf{x}, \mathbf{Q})$. The time-dependent one-electron density in the Born-Oppenheimer approximation, for a ground state reaction with nuclear wave function $\chi(t, \mathbf{Q})$, is defined as

$$\rho(t, \mathbf{x}) = \int \rho_{\text{QC}}(\mathbf{x}, \mathbf{Q}) |\chi(t, \mathbf{Q})|^2 d\mathbf{Q} \quad (3.20)$$

From the quantum chemical calculations for a set of values \mathbf{Q} , the potential $V(\mathbf{Q})$ and the density $\rho_{\text{QC}}(\mathbf{x}, \mathbf{Q})$ are obtained. The potential is needed for the quantum dynamics simulation which calculates χ .

Quantum chemical calculations may be computationally expensive. For the determination of the time-dependent electron density, this gives rise to two issues:

- The nuclear quantum dynamics simulation is performed for a model with reduced degrees of freedom \mathbf{Q} . Because the potential $V(\mathbf{Q})$ is a continuous function, in general only few points \mathbf{Q}_i are needed for the nuclear dynamics. If necessary, further points may be interpolated. However, the electron density $\rho_{\text{QC}}(\mathbf{x}, \mathbf{Q}_i)$ is only given at these points, and depending on the form of χ more points might be necessary to obtain a reliable time-dependent electron density, especially for multi-dimensional simulations.
- Quantum chemistry programs normally give ρ_{QC} on a user-defined grid, and thus $\rho(t, \mathbf{x})$ is necessarily given on the same grid. For integration of the density in a sector many points might be necessary, and to check the convergence more than one grid size needs to be stored. This storage demands quickly become too costly to be handled.

Consequently, it is desirable not to rely on the quantum chemistry program to calculate the one-electron densities, but rather to have a tool which can built or integrate the electron densities from the basis set coefficients. A set of Python [6] functions, the Magic Density Creator, was written to satisfy this need. This tool was subsequently further developed by Gunter Hermann and Vincent Pohl (Freie Universität Berlin).

The first issue, the interpolation of the densities, is still work in progress. All applications presented later are effectively only one-dimensional, and thus the interpolation problem does not occur. Consequently, this issue will not be further discussed here.

However, integration of the electron density in bonding sectors (sectors representing a given chemical bond) have to be performed. All bonding sectors for the pericyclic reactions to be discussed are “cake slices” as shown in Fig. 3.1. In this figure, a nuclear configuration of benzene is indicated schematically, as well as the integration sector and the rectangular grid. The integration sector Ω is defined such that its boundaries are perpendicular to the molecular plane, pass through adjacent carbon atoms and cross at the nuclear center of mass. For further analysis, the cylindrical coordinates r, φ, z are introduced as

$$\begin{aligned}x_1 &= r \cos \varphi \\x_2 &= r \sin \varphi \\x_3 &= z\end{aligned}\tag{3.21}$$

with $z = 0$ defined as the plane containing all nuclei.

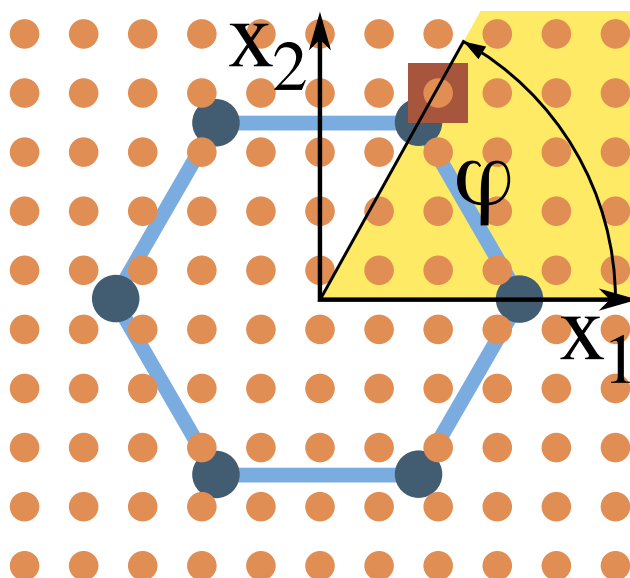


Figure 3.1: Representation of the equilibrium nuclear configuration of benzene (light blue lines: bonds; dark blue dots: carbon atoms) with integration sector (yellow) indicated. Light brown dots represent the grid on which the electron density is given, and the dark brown square represents the volume the respective point represents.

The one-electron densities may be calculated on a grid in cylindrical coordinates. However, for consistent representation of the density the number of points along the angular coordinate φ has to increase with the value of the radial coordinate r , and a regular grid might be more desirable. Thus, for all calculations a Cartesian grid along \mathbf{x} is used. Such a grid is shown in Fig. 3.1, and there are two issues which make integration on such a grid problematic:

1. Points close to the boundary of the bond sector may be counted as inside or outside of the sector, but the volume they represent may be cut by the sector. In Fig. 3.1, such a situation is shown with the dark brown square. The value of the electron density near the nuclei is large, and the integration error due to this effect is significant. For a bond sector this problem always occurs, because the sector boundaries pass right through the center of one of the carbon atoms.
2. For a small sector with opening angle $d\varphi$, the number of points included in this sector

3.4. Time-dependent electron density and time-dependent electron numbers

changes drastically along φ , as exemplified below.

Suitably chosen grids can solve the first issue in some cases, and in the cases discussed in the following. If the boundary passes through a nucleus, it is enough to distribute the grid symmetrical around the nucleus. For arbitrary nuclear configurations, an equidistant grid may be symmetric around two of the nuclei, but in general not more. In the cases discussed below, it is enough to center the grid around the two carbon nuclei at the boundaries to obtain converged results. This is, however, only possible because the hydrogen atoms (two of which are at the or close to the sector boundaries) have comparably little electron density. Thus, the only general satisfying solution would be to use symmetry-adapted grids or more sophisticated integration methods.

The second issue is best illustrated with an example. In the following, the calculations for benzene in section 4.2 will serve as this example. There, a time-dependent one-dimensional electron density

$$n(t, \varphi) = \int_{-\pi/6}^{\pi/6} |\chi(t, \Theta)|^2 \int_0^\infty \int_{-\infty}^\infty \rho_{\text{QC}}(\mathbf{x}, \Theta) r dz dr d\Theta \quad (3.22)$$

is used to analyze the electron dynamics. Note that \mathbf{x} is given in Cartesian coordinates. The angle Θ represents an effective nuclear coordinate, and is defined in section 4.2.2 (but of not much interest for the present discussion). The $n(t, \varphi)$ is obtained as follows:

- First the number of electrons in a sector $\varphi \in [0, \tilde{\varphi}]$,

$$N(\tilde{\varphi}, \Theta) = \int_0^{\tilde{\varphi}} \int_0^\infty \int_{-\infty}^\infty \rho_{\text{QC}}(\mathbf{x}, \Theta) r dz dr d\varphi \quad (3.23)$$

was calculated numerically on some grid in $\tilde{\varphi}$, Θ and \mathbf{x} . Ignoring the grid for \mathbf{x} for the moment, the number of electrons N was calculated for selected configurations Θ_j , and integrated up to selected angles $\tilde{\varphi}_i$. Consequently, for each nuclear structure Θ_j and each upper bound $\tilde{\varphi}_i$ of the angular integration over the electron density, there is an electron number

$$N_{ij} = \int_0^{\tilde{\varphi}_i} \int_0^\infty \int_{-\infty}^\infty \rho_{\text{QC}}(\mathbf{x}, \Theta_j) r dz dr d\varphi. \quad (3.24)$$

- The ratio of number of electrons up to an angle $\tilde{\varphi}_i$ with the size of the angular space $\tilde{\varphi}_i$, that is $N_{ij}/\tilde{\varphi}_i$, is an approximation to the number of electrons for a given Θ_j in the sector from $\tilde{\varphi}_i - \Delta\tilde{\varphi}/2$ to $\tilde{\varphi}_i + \Delta\tilde{\varphi}/2$. The spacing $\Delta\tilde{\varphi}$ is the (equidistant) spacing of the electronic angular variable $\tilde{\varphi}$. Thus, the density of electrons at some angle $\tilde{\varphi}$ for the nuclear structure Θ_j is

$$\int_0^\infty \int_{-\infty}^\infty \rho_{\text{QC}}(r, \tilde{\varphi}, z, \Theta_j) r dz dr \approx \frac{N_{ij}}{\tilde{\varphi}_i}. \quad (3.25)$$

- To obtain the discrete analog of $n(t, \varphi)$, these numbers have to be weighted by the probability to find the nuclear structure Θ_j . Using eqn. 3.25, the discrete analogue of eqn. 3.22 is

$$n(t, \varphi_i) =: n_i(t) = \sum_j \frac{N_{ij}}{\varphi_i} |\chi(t, \Theta_j)|^2 \Delta\Theta_j. \quad (3.26)$$

The electron numbers N_{ij} were computed on a different grid for each Θ_j , chosen such that the grid \mathbf{x} of $\rho_{\text{QC}}(\mathbf{x}, \Theta_j)$ is symmetric around one (and by symmetry automatically around a second) carbon atom. For the grid Cartesian coordinates $\mathbf{x} = (x_1, x_2, x_3)$ were used. The x_3 -range was fixed to $x_3^{\text{min}} = 0$, $x_3^{\text{max}} = 8 a_0$, while the x_1 - and x_2 -range was

varied within the approximate intervals $x_1^{\min} \in [-8, -10] a_0$, $x_1^{\max} \in [8, 10] a_0$ and $x_2^{\min} \approx 0$, $x_2^{\max} \in [10, 8] a_0$. The number of points in the x_1 -, x_2 - and x_3 -range was 600, 275 and 275, respectively. Thus, for each Θ_j the density was calculated in 45.375.00 grid points. The deviation of the total number of electrons $\int \rho_{QC}(\mathbf{x}, \Theta_j) d\mathbf{x}$ from the number of electrons in benzene (42 electrons, of which 30 are valence electrons, and six of these are π -electrons) is less than 0.0003 electrons.

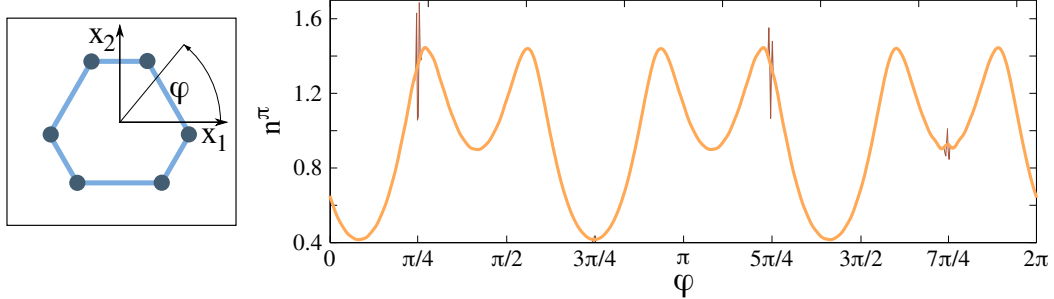


Figure 3.2: The one-dimensional π -electron density $n(0, \varphi)$ for the simulation of benzene, described in section 4.2.4. The molecule has a nuclear structure like in shown to the left. Orange line is a fit of the data using a Fourier series, while dark brown line (mostly covered by the orange line) are the original data obtained from numerical integration.

Figure 3.2 shows $n(t, \phi)$ for $t = 0$, and for the π -electrons only. Due to the large number of points and the suitably chosen grid there is little problem at the positions of the carbon atoms (the maxima of the underlying smooth function). However, figure 3.2 shows that close to $\varphi = \pi/4$ and $5\pi/4$ there is a problem in the integration. While the original data (dark brown) is mostly beneath the smoothed function, at this values the data is discontinuous. Close inspection reveals that similar, but smaller deviations can be found at $\varphi = 3\pi/4$ and $7\pi/4$.

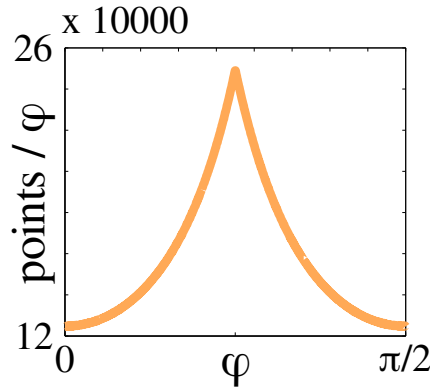


Figure 3.3: Distribution of points per angle φ for a two-dimensional rectangular grid with 500×500 points in the positive quadrant (i.e. the integral of this curve gives 250.000 points).

This behavior can be rationalized by taking into account the number of points which belong to a sector $\varphi \in [0, \tilde{\varphi}]$. For example, in two dimensions the number of points up to angle $\tilde{\varphi}$ can be estimated as

$$NPts(\tilde{\varphi}) = \text{Floor} \left(\frac{(x_1^{\max})^2 \tan(\tilde{\varphi})/2}{\Delta x_1 \Delta x_2} \right) \quad (3.27)$$

for $\tilde{\varphi} \leq \pi/4$ and

$$NPts(\tilde{\varphi}) = \text{Floor} \left(\frac{x_1^{\max} x_2^{\max} - (x_2^{\max})^2 / \tan(\tilde{\varphi})/2}{\Delta x_1 \Delta x_2} \right) \quad (3.28)$$

3.4. Time-dependent electron density and time-dependent electron numbers

for $\pi/4 \leq \phi \leq \pi/2$. The function $\text{Floor}(x)$ returns the closest integer smaller than x . Fig. 3.3 shows the change of the number of points with the angle, $\partial_\varphi N Pts(\varphi)$, for a grid with 500 points in both positive x_1 - and x_2 -direction (i.e. 250.000 points in the quadrant). This function is periodic with period $\pi/2$. From the figure can be seen that there is a rise of the number of points per angle up to $\varphi = \pi/4$, where the function has a cusp, and drops thereafter. Thus, the integration can be expected to become instable close to this cusp, as the number of points in this region of φ strongly depends on the value of φ .

This problem is illustrated in the calculated data of Fig. 3.2. The discontinuities are expected to be the stronger the larger the difference between neighboring discrete values φ_i is. Hence, at $\varphi = \pi/4$ and $5\pi/4$ there are strong discontinuities because the slope of the curve is strong, while at $\varphi = 3\pi/4$ and $7\pi/4$ there are small discontinuities as the curve has local minima there.

One remedy for this type of integration problems in the angular coordinate is to approximate the function by a Fourier series. This can be done as the function is periodic in φ , and because most of the points have a very good accuracy. The advantage of approximation by a Fourier series is that this will approximate the function in the mean [62], and hence deviations of the function in small regions will not affect the fit. As is the case in this example, most points are of high quality and consequently the fit will yield a reliable result. Also, the result is an analytical function, which can be handled easily. Figure 3.2 shows such a fit of the points of figure 3.2 with a Fourier series of 70th order (orange line), obtained using the Matlab [4] toolbox “Simple real Fourier series approximation” [210].

Another remedy, used for malonaldehyde and the formic acid dimer in chapter 4.3, is an angular average: The numerical instabilities occur at certain angles φ in the electronic coordinate space. Consequently, if the whole molecule is rotated by an angle ξ relative to the space-fixed electronic coordinate system, the instabilities will be at the same angles φ , but the graph of the one-dimensional electron density will be slightly shifted. By shifting the one-dimensional electron density n by ξ , but in opposite direction to the rotation of the molecule, the original electron density and the electron density obtained with the rotated molecule should have the same graph. However, the region of numerical instability is effectively shifted by the angle ξ . By performing the calculation of n for several different ξ and averaging the results, the quality of the angular electron density n may be improved significantly.

For malonaldehyde and the formic acid dimer, it was necessary to make this angular average with 20 calculations in the range $\xi \in [0, \pi]$, and to fit the resulting one-dimensional density to a Fourier series in order to obtain converged values for the fluxes.

Chapter 4

Applications

4.1 Tunneling in cyclooctatetraene

4.1.1 Abstract

The first pericyclic model reaction to be investigated is the double bond shift in cyclooctatetraene, in the tunneling limit. The reaction is shown schematically in Fig. 4.1. In the figure, a top view of the molecule represented by the Lewis structures of the reactant (R) and the product (P) configuration is depicted. Reactants and products have the same molecular shape, but different orientation relative to a space-fixed coordinate system. They may be distinguished by partial deuteration. The figure contains arrows indicating the possible mechanisms that lead from R to P. It will be investigated what the arrows might represent in a time-dependent picture using electronic fluxes.

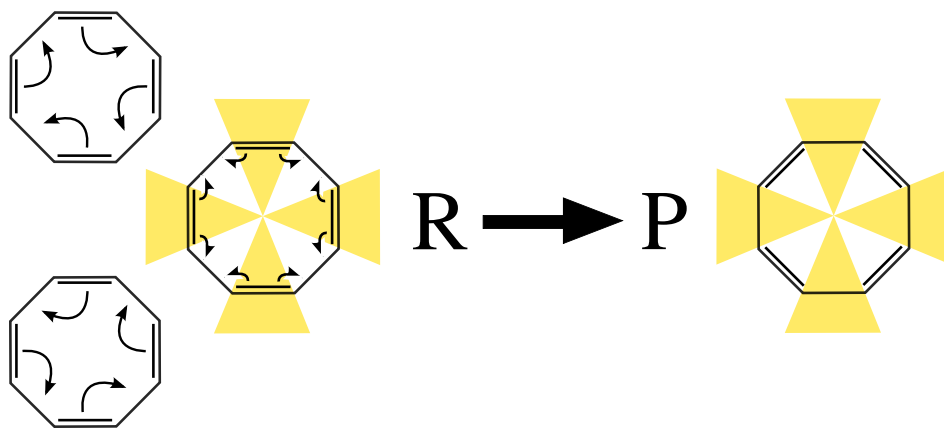


Figure 4.1: Lewis structures of the double bond shift in cyclooctatetraene from the reactant (R) to the product (P) structure. The arrows in the R structures indicate the possible mechanisms for electron rearrangement. Four colored triangles represent the sectors attributed to carbon-carbon bonds. A border of one of the triangles starts in the nuclear center of mass, passes through the respective carbon atom and continues to infinity. The sector itself continues to infinity above and below the paper plane. Note that cyclooctatetraene is not planar, and this is only a top view of the system.

Fig. 4.1 shows four equivalent sectors, which are attributed to the corresponding carbon-carbon bonds. Initially, configuration R with carbon-carbon double bonds in the sectors is assumed. After the rearrangement, the sectors will contain carbon-carbon single bonds. The flux of electrons into or out of this sector represents the net electronic motion during the reaction and can be used to interpret and quantify the arrows. It is especially interesting

to partition the electron density chemically into pericyclic and other valence electrons, as well as in core electrons, and to investigate how the different types of electrons behave. It will be apparent that the pericyclic and the valence electrons move effectively into opposite directions, with the pericyclic electrons following the central mechanism of Fig. 4.1. Moreover, it will be shown that in total only very few electrons move during the reaction, in contrast to the four times two electrons shifting as suggested by the Lewis structures.

4.1.2 The model cyclooctatetraene

Cyclooctatetraene with its eight π -like electrons is the prototypical anti-aromatic molecule [188]. It has a tub-shaped equilibrium structure with D_{2d} point group symmetry, depicted schematically in Fig. 4.2. In the following, this molecule is used as a model system to investigate the electronic motion indicated in Fig. 4.1, i.e., the interconversion of single and double bonds in the Lewis structures. Specifically, the goal is to answer the questions: Which of the mechanisms of Fig. 4.1 is correct? How much electrons flow? How do the different chemical types of electrons (core, π -like/pericyclic and the other valence electrons) behave?

For the reaction shown in Fig. 4.1 to happen, the nuclear configuration should best be close to planar. Experimentally, it is possible to prepare the cyclooctatetraene anion, which is planar and has D_{4h} point group symmetry [148]. Thus, if the anion is photoionized, the molecule is prepared with a nuclear structure which corresponds to the left-hand side of Fig. 4.1. The photoionization experiment of Wenthold et. al. [224], e.g. shows that the corresponding mode is indeed active for some time before the molecule starts to distort back to the equilibrium configuration. These findings are supported by calculations of the ground state energy surface close to the respective D_{4h} structure: Towards the D_{2d} minima, the potential surface close to the D_{4h} ring inversion transition state (which is close to the nuclear structure of the anion) is very shallow. For more information about the quantum chemical calculations, see appendix D and [183].

Instead of simulating the dynamics after photoionization of its anion, tunneling dynamics of cyclooctatetraene in the limit of zero temperature will be addressed. The advantage of the tunneling model developed in the next section is that the results are mostly analytical, and that it can already answer very well the questions posed above. The disadvantage is that the kind of nuclear tunneling which will be considered happens on a time scale that is far too long to be observed experimentally. However, the procedure can be applied to other systems with observable proton tunneling as well, see [45].

First, the shape of the ground state potential energy surface of cyclooctatetraene needs to be discussed. Only the qualitative features of the potential will be presented here. Appendix D and [183] contain details of the quantum chemical calculations, and especially of the determination of reliable barrier heights for the tunneling processes.

Fig. 4.2 shows the qualitative features of the ground state potential energy surface of cyclooctatetraene that are of interest for the discussion. The potential is a symmetric quadruple minimum potential which supports four equivalent equilibrium structures of D_{2d} nuclear point group symmetry. The two structures R1, R2 contribute both to the R-configuration of Fig. 4.1, while the two structures P1, P2 contribute to the P-configuration. The structures R1 and R2 as well as the structures P1 and P2 are connected by a ring inversion coordinate, while transition from an R to a P structure happens, for energies close to the barrier, along a double bond shift coordinate.

However, the dynamics in the tunneling regime will be subject of this part, for energies sufficiently far below the barriers of ring inversion or double bond shift. The coherent tunneling is described by the lowest four vibrational eigenstates of the potential, which are

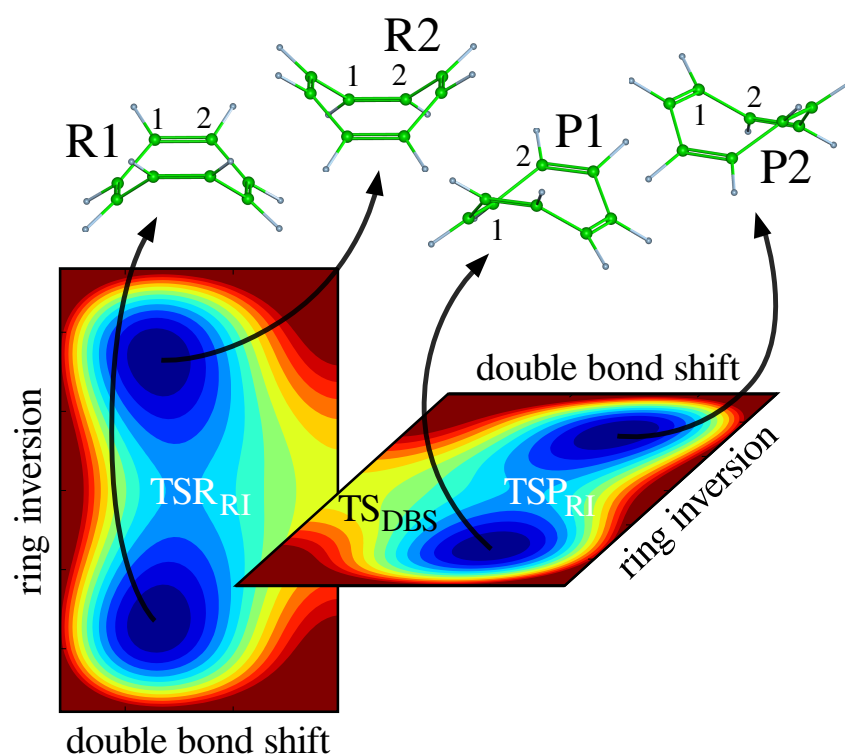


Figure 4.2: Schematic representation of the ground state potential energy surface of cyclooctatetraene along the coordinates of interest. The four equivalent minima correspond to the structures R1, R2, P1 and P2 with D_{2d} point group symmetry, respectively. The pairs R1, R2 and P1, P2 are each connected by a ring inversion coordinate with transition states $TS_{R_{RI}}$ and $TS_{P_{RI}}$ of point group symmetry D_{4h} , respectively. For the double bond shift coordinate, the transition state TS_{DBS} has D_{8h} point group symmetry. There are two valley ridge inflection points between TS_{DBS} and $TS_{R_{RI}}/TS_{P_{RI}}$ (not shown).

delocalized over the four minima. Because of the large energy gap between the ground and first excited state (ca. 386 kJ/mol [80]), it can be expected that the nuclear wave functions are well described within the Born-Oppenheimer approximation.

4.1.3 A theory for coherent tunneling

For cyclooctatetraene, tunneling happens in a quadruple well potential, thus a tunneling theory analogous to that of a double well potential (e.g. that of the ammonia inversion, cf. [55]) shall be developed. Note that there is also a discussion about tunneling in a quadruple minimum potential in [39]. To develop the tunneling theory for the quadruple well potential, first the theory for the potential $V(\mathbf{Q})$ being a symmetric double well is reviewed. Only one reactant R and product P will be needed, which may be distinguished e.g. by spatial symmetry breaking due to isotopic substitution. The situation of tunneling in a double well will again be encountered in section 4.3.4, where the tunneling dynamics of the formic acid dimer and malonaldehyde will be described by the same model.

Given is a symmetric double well potential $V(\mathbf{Q})$. The lowest two nuclear eigenfunctions χ_+ and χ_- of the potential V shall constitute a tunneling doublet with eigenvalues E_+ and E_- . That means, the two states are almost degenerate bound states with different symmetry. The function χ_+ shall be gerade, while χ_- denotes the ungerade eigenfunction with respect to the symmetry of the potential. The localized reactant (χ_R) and product (χ_P) wave functions are thus

$$\begin{aligned}\chi_R(\mathbf{Q}) &= \frac{1}{\sqrt{2}}(\chi_+(\mathbf{Q}) + \chi_-(\mathbf{Q})) \\ \chi_P(\mathbf{Q}) &= \frac{1}{\sqrt{2}}(\chi_+(\mathbf{Q}) - \chi_-(\mathbf{Q}))\end{aligned}\quad (4.1)$$

with the same mean energy

$$\bar{E} = \frac{1}{2}(E_+ + E_-) \quad (4.2)$$

and with tunneling splitting

$$\Delta E = E_- - E_+. \quad (4.3)$$

Consequently, the time-dependent wave functions are

$$\begin{aligned}\chi_R(t, \mathbf{Q}) &= \frac{1}{\sqrt{2}}(\chi_+(\mathbf{Q})e^{-iE_+t/\hbar} + \chi_-(\mathbf{Q})e^{-iE_-t/\hbar}) \\ \chi_P(t, \mathbf{Q}) &= \frac{1}{\sqrt{2}}(\chi_+(\mathbf{Q})e^{-iE_+t/\hbar} - \chi_-(\mathbf{Q})e^{-iE_-t/\hbar})\end{aligned}\quad (4.4)$$

and the probability of finding configuration R at time t , given configuration R at time 0, is

$$P_R(t) = |\langle \chi_R(0) | \chi_R(t) \rangle|^2 = \cos^2(\Delta Et / (2\hbar)). \quad (4.5)$$

Accordingly, starting with R at time 0, configuration P is observed at time t with probability

$$P_P(t) = |\langle \chi_R(0) | \chi_P(t) \rangle|^2 = \sin^2(\Delta Et / (2\hbar)). \quad (4.6)$$

These probabilities oscillate with the tunneling time $\tau = \hbar / (2\pi\Delta E)$.

The time-dependent one-electron density in the Born-Oppenheimer approximation needs to be determined, which can in principle be calculated from the one-electron densities $\rho_{QC}(\mathbf{x}, \mathbf{Q})$ for each nuclear configuration \mathbf{Q} as

$$\rho(t, \mathbf{x}) = \iint \rho_{QC}(\mathbf{x}, \mathbf{Q}) |\chi_R(t, \mathbf{Q})|^2 d\mathbf{Q}, \quad (4.7)$$

4.1. Tunneling in cyclooctatetraene

cf. section 2.5. However, calculation of the nuclear wave function χ shall be avoided. Thus, instead of using eqn. 4.7, the time-dependent electron density is approximated by a sum of the one-electron density at the reactant configuration, ρ_R , and that of the product configuration, ρ_P , using the probabilities of finding the respective nuclear configuration. Specifically,

$$\rho(t, \mathbf{x}) \approx \rho_R(\mathbf{x})P_R(t) + \rho_P(\mathbf{x})P_P(t). \quad (4.8)$$

The subscript QC for the static densities ρ_R and ρ_P is dropped, but these are the one-electron densities obtained from a quantum chemical calculation at the respective nuclear configuration.

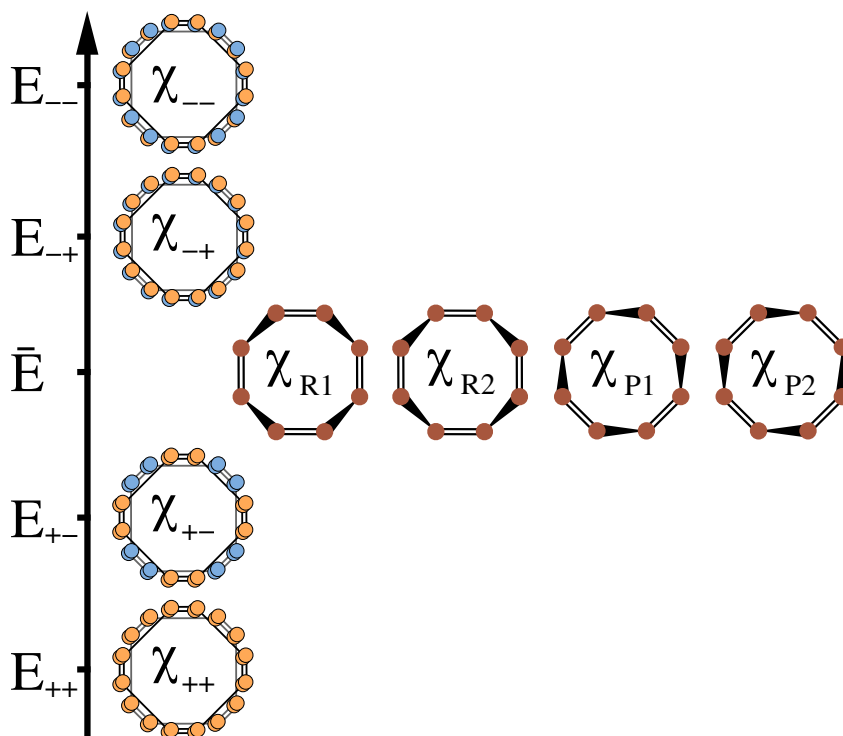


Figure 4.3: Schematic representation of the delocalized nuclear wave functions $\chi_{++}, \chi_{+-}, \chi_{-+}, \chi_{--}$ (the eigenstates of the potential) and the localized nuclear wave functions $\chi_{R1}, \chi_{R2}, \chi_{P1}, \chi_{P2}$. Each dot represents a local maximum in the nuclear density. For the delocalized wave functions, the signs of the wave function are indicated by the orange and blue color of the dots. Each of these plots consists of 16 dots in one plane and 16 dots in a plane below. Single and double bonds are only used as guides for the structures. For the localized wave functions, the dots at the broad end of the triangles are in one plane, while those at the narrow end are in a plane beneath.

For cyclooctatetraene the situation is analogous, but four minima have to be taken into account and two different tunneling processes (ring inversion and double bond shifting). One of the minima is chosen as reactant configuration R1, and the other minimum, which is obtained via ring inversion, is R2. The other two minima connected to these via double bond shift are the product structures P1 and P2, respectively. There is a tunneling quartet given by the lowest four nuclear eigenfunctions χ_{++} and $\chi_{+-}, \chi_{-+}, \chi_{--}$, with eigenvalues $E_{++} < E_{+-} < E_{-+} < E_{--}$. The first subscript indicates gerade (+) or ungerade (-) symmetry with respect to ring inversion, and the second subscript indicates that symmetry

with respect to double bond shifting. The localized nuclear states are given by

$$\begin{aligned}
\chi_{R1}(\mathbf{Q}) &= \frac{1}{2}(\chi_{++}(\mathbf{Q}) + \chi_{+-}(\mathbf{Q}) + \chi_{-+}(\mathbf{Q}) + \chi_{--}(\mathbf{Q})) \\
\chi_{R2}(\mathbf{Q}) &= \frac{1}{2}(\chi_{++}(\mathbf{Q}) + \chi_{+-}(\mathbf{Q}) - \chi_{-+}(\mathbf{Q}) - \chi_{--}(\mathbf{Q})) \\
\chi_{P1}(\mathbf{Q}) &= \frac{1}{2}(\chi_{++}(\mathbf{Q}) - \chi_{+-}(\mathbf{Q}) - \chi_{-+}(\mathbf{Q}) + \chi_{--}(\mathbf{Q})) \\
\chi_{P2}(\mathbf{Q}) &= \frac{1}{2}(\chi_{++}(\mathbf{Q}) - \chi_{+-}(\mathbf{Q}) + \chi_{-+}(\mathbf{Q}) - \chi_{--}(\mathbf{Q}))
\end{aligned} \tag{4.9}$$

with mean energy

$$\bar{E} = \frac{1}{4}(E_{++} + E_{+-} + E_{-+} + E_{--}). \tag{4.10}$$

There is a tunneling splitting ΔE_{DBS} and tunneling time τ_{DBS} for double bond shifting given by

$$\Delta E_{\text{DBS}} = E_{+-} - E_{++} \approx E_{--} - E_{-+} = \hbar/(2\pi\tau_{\text{DBS}}), \tag{4.11}$$

and another tunneling splitting ΔE_{RI} and tunneling time τ_{RI} for ring inversion, given by

$$\Delta E_{\text{RI}} = E_{-+} - E_{++} \approx E_{--} - E_{+-} = \hbar/(2\pi\tau_{\text{RI}}). \tag{4.12}$$

The small difference in the splitting of the first two and the second two states is neglected. From the relation

$$\Delta V_{\text{DBS}} > \Delta V_{\text{RI}} \tag{4.13}$$

between the barriers for the respective processes, it is inferred that

$$\begin{aligned}
\Delta E_{\text{DBS}} &\gg \Delta E_{\text{RI}} \\
\tau_{\text{DBS}} &\ll \tau_{\text{RI}}.
\end{aligned} \tag{4.14}$$

Following the same procedure as for the double well potential, the probabilities for finding configuration R1 or R2, P1, P2 at time t , given there was configuration R₁ at time 0, are

$$\begin{aligned}
P_{R1}(t) &= |\langle \chi_{R1}(0) | \chi_{R1}(t) \rangle|^2 = \cos^2(2\Delta E_{\text{DBS}}t/\hbar) \cos^2(\Delta E_{\text{RI}}t/(2\hbar)) \\
P_{R2}(t) &= |\langle \chi_{R1}(0) | \chi_{R2}(t) \rangle|^2 = \cos^2(2\Delta E_{\text{DBS}}t/\hbar) \sin^2(\Delta E_{\text{RI}}t/(2\hbar)) \\
P_{P1}(t) &= |\langle \chi_{R1}(0) | \chi_{P1}(t) \rangle|^2 = \sin^2(2\Delta E_{\text{DBS}}t/\hbar) \cos^2(\Delta E_{\text{RI}}t/(2\hbar)) \\
P_{P2}(t) &= |\langle \chi_{R1}(0) | \chi_{P2}(t) \rangle|^2 = \sin^2(2\Delta E_{\text{DBS}}t/\hbar) \sin^2(\Delta E_{\text{RI}}t/(2\hbar)),
\end{aligned} \tag{4.15}$$

respectively. The probability of finding any of the two reactant or product configurations is

$$\begin{aligned}
P_{\text{R}}(t) &= P_{R1}(t) + P_{R2}(t) = \cos^2(\Delta E_{\text{DBS}}t/(2\hbar)) \\
P_{\text{P}}(t) &= P_{P1}(t) + P_{P2}(t) = \sin^2(\Delta E_{\text{DBS}}t/(2\hbar)).
\end{aligned} \tag{4.16}$$

Note that the sums of these probabilities add up to one, i.e. one of the configurations will definitively be found during a measurement. The average probability of finding any of the four equivalent structures is 1/4.

The time-dependent one-electron density is again assumed to be well-described by a superposition of the individual one-electron densities of the localized nuclear configurations, weighted by the probability of finding these configurations, i.e.

$$\rho(t, \mathbf{x}) \approx \rho_{R1}(\mathbf{x})P_{R1}(t) + \rho_{R2}(\mathbf{x})P_{R2}(t) + \rho_{P1}(\mathbf{x})P_{P1}(t) + \rho_{P2}(\mathbf{x})P_{P2}(t). \tag{4.17}$$

4.1. Tunneling in cyclooctatetraene

Again, the one-electron densities ρ_{R1} and ρ_{R2} , ρ_{P1} , ρ_{P2} are related by symmetry transformations and may be obtained from quantum chemical calculations for the respective nuclear configurations.

4.1.4 Fluxes during coherent tunneling

The electronic flux

$$F(t, \Omega) = \partial_t \int_{\Omega} \rho(t, \mathbf{x}) d\mathbf{x} \quad (4.18)$$

is the electron flow through the boundary of an observer volume Ω . The observer volumes for the investigation of the reaction are shown in Fig. 4.1. They shall represent a carbon-carbon bond, and are defined as follows: One D_{2d} equilibrium structure is considered, and the plane containing the centers of all carbon-carbon single bonds is the x_1, x_2 -plane for the rectangular coordinates $\mathbf{x} = (x_1, x_2, x_3)$. The origin \mathbf{x} is set to be the center of mass of the nuclei (and also of the whole molecule, due to symmetry). Then the sector boundaries of the bond sectors originate in $(0, 0, x_3)$, pass through the x_1, x_2 -coordinates of one of the carbon atoms and continue to infinity, for all values of x_3 . These ‘‘cake slices’’ are called bond sectors, as they contain essentially one carbon-carbon bond (initially a double bond).

Using eqn. 4.17, the flux can be partitioned into a reactant and a product contribution,

$$F(t, \Omega) = F_R(t, \Omega) + F_P(t, \Omega). \quad (4.19)$$

As Fig. 4.1 shows, the bond to be monitored is a double bond for the reactants. Thus, the observer volume is the bond sector $\Omega = \Omega_{DB}$ containing the double bond. The corresponding flux for this volume is

$$\begin{aligned} F_{DB,R}(t) &= \partial_t \left(P_{R1}(t) \int_{\Omega_{DB}} \rho_{R1}(\mathbf{x}) d\mathbf{x} + P_{R2}(t) \int_{\Omega_{DB}} \rho_{R2}(\mathbf{x}) d\mathbf{x} \right) \\ &= \partial_t (P_{R1}(t) N_{DB,R1} + P_{R2}(t) N_{DB,R2}). \end{aligned} \quad (4.20)$$

The $N_{DB,R1}, N_{DB,R2}$ are the numbers of electrons in the bond sector if the nuclear configuration is R1 or R2, respectively. However, because ring inversion between R1 and R2 does not change the number of electrons in the bond sector, $N_{DB,R1} = N_{DB,R2} =: N_{DB,R}$, and hence

$$\begin{aligned} F_{DB,R}(t) &= N_{DB,R} \partial_t P_R(t) \\ &= -\frac{N_{DB,R}}{2} (\Delta E_{DBS}/\hbar) \sin(\Delta E_{DBS} t/\hbar). \end{aligned} \quad (4.21)$$

Following the definition of the sectors as in Fig. 4.1, there will be single bond in the observer volume of the product. Thus, the bond sector for the product is $\Omega = \Omega_{SB}$, and the respective flux is

$$\begin{aligned} F_{SB,P}(t) &= N_{SB,P} \partial_t P_P(t) \\ &= \frac{N_{SB,P}}{2} (\Delta E_{DBS}/\hbar) \sin(\Delta E_{DBS} t/\hbar) \end{aligned} \quad (4.22)$$

with the number of electrons in this sector,

$$N_{SB,P} = \int_{\Omega_{SB}} \rho_{P1}(\mathbf{x}) d\mathbf{x} = \int_{\Omega_{SB}} \rho_{P2}(\mathbf{x}) d\mathbf{x}. \quad (4.23)$$

To obtain the total flux, according to eqn. 4.19 the two contributions eqn. 4.21 and eqn. 4.22

need to be added. Thus,

$$F(t, \Omega) = \frac{N_{\text{SB,P}} - N_{\text{DB,P}}}{2} \Delta E_{\text{DBS}} / \hbar \sin(\Delta E_{\text{DBS}} t / \hbar). \quad (4.24)$$

The electron yield is obtained by summation of the fluxes up to time t ,

$$Y(t, \Omega) = \int_0^t F(t', \Omega) dt' = \frac{N_{\text{SB,P}} - N_{\text{DB,P}}}{2} (1 - \cos(\Delta E_{\text{DBS}} t / \hbar)). \quad (4.25)$$

After half of the tunnel time of the double bond shift, the yield is

$$Y(\tau_{\text{DBS}}/2, \Omega) = N_{\text{SB,P}} - N_{\text{DB,P}}. \quad (4.26)$$

This result is easily understood: At time $\tau_{\text{DBS}}/2$, the initial R-configurations changes to P-configurations. Thus, the number of electrons to move until then into or out of the bonding sector has to equal the difference of the number of electrons in the initial and final bond sector, $N_{\text{SB,P}} - N_{\text{DB,P}}$. Note that ring inversions do not play a role in the expressions for the fluxes and yields from R to P, and back. However, these processes are of importance if the population of a specific reactant or product R1 or R2, P1, P2, is observed.

4.1.5 Technical details

The one-electron densities are obtained using the program package Molpro [225]. A CASSCF(8,8) calculation with an active space of eight π -like electrons in eight π -like orbitals was performed. For this calculations, cc-pVTZ basis set [70] was used, and the reference nuclear structure was optimized using an MRCI calculation with Davidson correction [116]. However, for the electron densities the CASSCF wave function calculated at the optimized nuclear structure is used because then the density can be partitioned further, cf. section 3.3. With the optimized structure parameters the opening angle of a single bond sector is 0.753, and the opening angle of a double bond sector is 0.818. Consequently, the volume of a single bond sector is 0.920 times the volume of a double bond sector. This seems counterintuitive, as it might be expected that the single bond sector is larger than the double bond sector, because the single bond length is larger (by a factor of 1.103) than the double bond length. However, cyclooctatetraene is not planar: The double bond is perpendicular to the x_3 -direction and thus to the sector boundaries, whereas the single bond is not. Thus, if a top view of the system is drawn, the single bonds would look shorter than the double bonds.

Natural orbitals are used to partition the density into three groups: There are eight carbon 1s core orbitals (“core”), eight carbon π -like orbitals (pericyclic orbitals, “peri”) and 16 other valence orbitals (“oval”), which include the carbon-carbon single bonds and the hydrogen-carbon bonds. Thus, the total density is

$$\rho_{\text{R1}}(\mathbf{x}) = \rho_{\text{R1}}^{\text{core}}(\mathbf{x}) + \rho_{\text{R1}}^{\text{oval}}(\mathbf{x}) + \rho_{\text{R1}}^{\text{peri}}(\mathbf{x}). \quad (4.27)$$

The fluxes due to the pericyclic density are expected to reproduce the shift of the double bonds in the Lewis structures. For the calculation of the electron densities, a standard Cartesian grid of $440 \times 440 \times 440$ points with grid spacing of 2.6 pm was used. The decomposition of the electron densities carries over to the electron numbers, and consequently to the fluxes and yields.

The tunneling splittings for cyclooctatetraene are very small and thus difficult to obtain numerically. However, they can be estimated using the semi-classical tunneling theory of Miller [149] for double well potentials. Fig. 4.4 shows a sketch of a symmetric one-

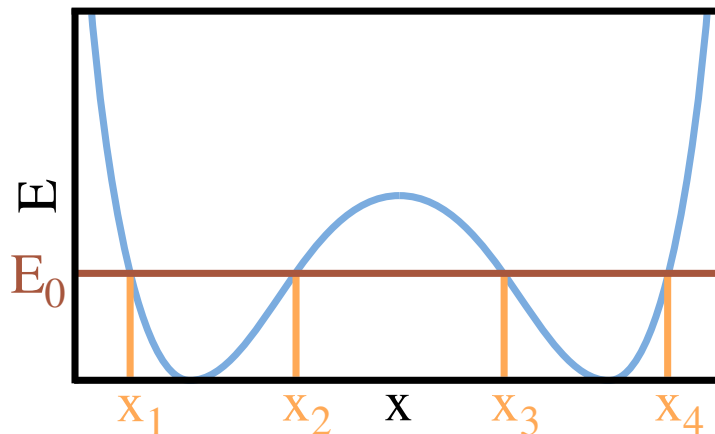


Figure 4.4: A generic one-dimensional double well potential $V(x)$ as model for tunneling. The energy E_0 is the approximate energy of the first two eigenstates. These two states are almost degenerate, and the tunnel splitting is the difference in energy between the two states, centered around E_0 . x_1, x_2, x_3 and x_4 are the positions along the reaction coordinate x where $V(x) = E_0$.

dimensional double well potential $V(x)$. The energy E_0 corresponds to the unsplit eigenvalue, and $V(x_1) = V(x_2) = V(x_3) = V(x_4) = E_0$. The equation for the tunnel splitting ΔE is eqn. 17 of [149],

$$\Delta E = \frac{\exp(-\theta)}{\pi n'(E_0)}, \quad (4.28)$$

with

$$\theta = \int_{x_2}^{x_3} \sqrt{2\mu(V(x) - E_0)} dx. \quad (4.29)$$

The parameter μ is the mass of the (effective) particle. As $E_0 - V(x)$ is the kinetic energy of the particle, $\sqrt{2\mu(V(x) - E_0)}$ for $V(x) > E_0$ is the imaginary momentum of a particle passing from x_2 to x_3 . Hence, eqn. 4.29 is the imaginary action integral for this motion. The number $n'(E_0)$ is the first derivative of the integer n with respect to the energy, evaluated at E_0 , where n is determined by the action from x_1 to x_2 ,

$$\left(n + \frac{1}{2}\right) \pi = \int_{x_1}^{x_2} \sqrt{2\mu(E_0 - V(x))} dx. \quad (4.30)$$

For the tunnel splittings of ring inversion and double bond shift in cyclooctatetraene, the tunneling potential is estimated by the forth-order polynomial function

$$V(x) = ax^4 - bx^2 \quad (4.31)$$

for $a, b > 0$. The reduced mass to be used is $\mu = 2(m_C + m_H)$ in both cases, as there are four CH-fragments moving against four CH-fragments. The distance traveled along the coordinate x from the D_{2d} equilibrium structure to the D_{4h} transition state for ring inversion is approximated as follows: The position of the carbon and hydrogen atoms is interpolated linearly between the two structures along spherical coordinates. Then, for each configuration, the position of the center of mass of the CH-group is calculated. This distance, $0.94 a_0$, is taken as good approximation for the distance along x . For the distance from the D_{2d} equilibrium structure to the D_{8h} transition state for double bond shift, the same value is used: The distance traveled by the center of mass of the CH-groups would be a little bit smaller than for ring inversion. However, there is a valley ridge inflection point (bifurcation) along the intrinsic reaction coordinate [50]: Starting from the D_{8h} double bond shift transition

state, the structure of the molecule initially distorts towards the D_{4h} ring inversion transition state until the bifurcation point, see Fig. 4.2. Consequently, the distance for double bond shift is a bit larger than that for ring inversion. However, in total the difference between the D_{4h} ring inversion transition state and the D_{8h} double bond shift transition state is very small, and thus this effect is neglected.

With these values and with the barrier heights the parameters for eqn. 4.31 can be determined unambiguously. The stationary Schrödinger equation for this potentials is solved by approximating the second derivative in the kinetic energy operator as (cf. [90])

$$\partial_x^2 f(x) \approx \frac{f(x + \epsilon) - 2f(x) + f(x - \epsilon)}{\epsilon^2} + \mathcal{O}(\epsilon^2), \quad (4.32)$$

and by diagonalizing the resulting kinetic and potential energy matrices using GNU Octave [1]. This gives the unsplit eigenvalue E_0 . Subsequently, the derivative of n with respect to E_0 , $n'(E_0)$, is calculated approximately by using eqn. 4.30 with E_0 , and with the slightly shifted value $E_0 + \epsilon$, as

$$n'(E_0) \approx \frac{n(E_0 + \epsilon) - n(E_0)}{\epsilon}. \quad (4.33)$$

The determination of the barrier heights is explained in appendix D. If the values of [80], $\delta E_{\text{RI}} = 12.4$ kcal/mol and $\delta E_{\text{DBS}} = 13.2$ kcal/mol, were used, the ratio of the tunneling times would be

$$\frac{\tau_{\text{DBS}}}{\tau_{\text{RI}}} = 5.3 \quad (4.34)$$

with tunneling times $\tau_{\text{DBS}} = 7.0 \times 10^8$ s and $\tau_{\text{RI}} = 1.3 \times 10^8$ s. However, more accurate values were calculated for the barrier heights than those previously known in the literature. With these values, $\delta E_{\text{RI}} = 10.5$ kcal/mol and $\delta E_{\text{DBS}} = 17.19$ kcal/mol, the ratio of the tunneling times is

$$\frac{\tau_{\text{DBS}}}{\tau_{\text{RI}}} = 8.1 \times 10^5 \quad (4.35)$$

with $\tau_{\text{DBS}} = 1.6 \times 10^{12}$ s and $\tau_{\text{RI}} = 1.9 \times 10^6$ s. Consequently, nuclear tunneling in cyclooctatetraene for temperatures close to zero Kelvin is experimentally not observable. Also, the tunneling time for ring inversion is orders of magnitude smaller than that for double bond shifting (20 days vs. 52000 years).

It should be noted that the values for the tunneling times depend strongly on the chosen distance that needs to be traveled: In [98], $1.7 a_0$ were used (in contrast to the $2 \times 0.94 a_0$ used here), and it was found with $\delta E_{\text{DBS}} = 13.2$ kcal/mol a tunneling time for double bond shift of $\tau_{\text{DBS}} = 1.9 \times 10^6$ s. On one hand, for accurate tunneling times more sophisticated methods need to be used, see e.g. [58, 222]. On the other hand, the ratio of the two tunneling times shows only little changes, because the effective distances traveled in both processes are very similar. Nevertheless, the conclusion that this kind of tunneling cannot be observed experimentally remains unchallenged.

Tunneling processes in chemistry are common, although often neglected [123]. In the case of cyclooctatetraene, tunneling of the lowest quadruplet cannot be observed, but it may be possible to observe tunneling of higher quadruplets. Also, the insights presented in the next section are similar for other systems. For illustrative purposes, the ratio of tunneling times of eqn. 4.34 is adapted. It should be kept in mind, though, that tunneling due to ring inversion should be much faster than tunneling due to double bond shifting.

4.1.6 Results

From the three possible mechanisms shown in Fig. 4.1 only the central mechanism is possible: The electron rearrangement happens in the electronic ground state, and thus the electronic angular momentum expectation value is zero (see [134]). Consequently, the electrons have to move in equal amounts through the two boundary surfaces of the bond sector. In this way the effective number of electrons moving during the reaction can be easily determined. Note also that there are eight half planes with zero net flux. The union of these planes corresponds to the two times two mirror planes in the D_{4h} symmetry perpendicular to the molecular plane. The other two mechanisms of Fig. 4.1 are possible in excited electronic states, see e.g. [26, 28, 106, 107].

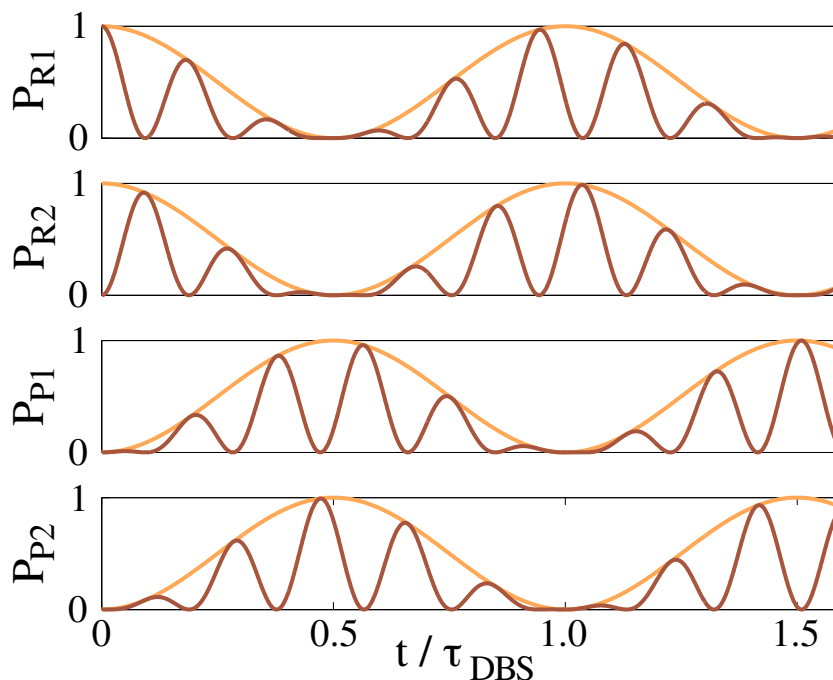


Figure 4.5: Brown, fast oscillating curve: Probabilities P_{R1} and P_{R2} , P_{P1} , P_{P2} that the reactants R1, R2 or products P1, P2 (both converted into each other via ring inversion) are observed given the initial state is R1. Orange, slow oscillating envelope: Corresponding probabilities P_R , P_P to observe reactants or products of double bond shift, independent of ring inversion. This picture is for ratio of the tunneling times $\tau_{DBS}/\tau_{RI} = 5.3$. Actually, the ratio is in the order of 10^6 , as explained in the text. The correct oscillation due to ring inversion is much faster than that of double bond shift and could not be resolved in the figure.

As a first step, the probabilities of finding the different configurations with the ratio of the tunneling times eqn. 4.34 shall be analyzed. In Fig. 4.5, both the results of eqn. 4.15 and eqn. 4.16 are shown. The probabilities P_R and P_P to find the reactants and products show oscillations which correspond to the interconversion of the reactant to product and back, $R \rightarrow P \rightarrow R \rightarrow \dots$. The probabilities to find the individual configurations, P_{R1} , P_{R2} , P_{P1} , P_{P2} , have the same amplitude envelope but a faster oscillation period. This represents the ring inversion process of both the reactants and products, i.e. $R1 \rightarrow R2 \rightarrow R1 \rightarrow \dots$ and $P1 \rightarrow P2 \rightarrow P1 \rightarrow \dots$, respectively. For the correct ratio of tunneling times, eqn. 4.35, the oscillation due to ring inversion would be so fast compared to double bond shifting that the whole double bond shift envelope would essentially be filled.

Next to the time-dependent probabilities of finding a particular nuclear configuration, the second ingredient for the recipe to determine the reaction mechanism is the one-electron

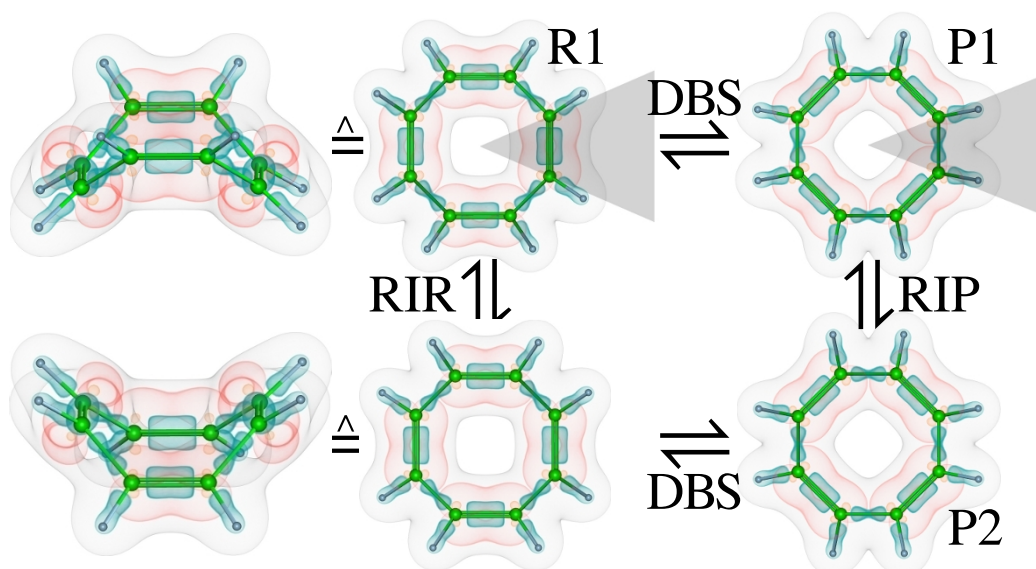


Figure 4.6: Isosurface plots of the electron densities of the pericyclic orbitals (orange/red, with isosurface values $0.04/0.4 a_0^{-3}$), all valence orbitals (blue/green, with isosurface values $0.27/0.53 a_0^{-3}$) and all electrons (gray, with isosurface value $0.05 a_0^{-3}$). In green, the nuclear configuration is also drawn for the reactants R1 and R2 (perspective and top view) interconverted via ring inversion RIR and the products P1 and P2 (only top view) interconverted via ring inversion RIP. Rearrangement from reactant to product takes place via double bond shift. The bond sectors are indicated for R1 and P1.

density of the four configurations. These are depicted in Fig. 4.6 as transparent isosurface plots for the different configurations. Each of those pictures shows an isosurface of all electrons, one of the valence electrons and one of the pericyclic electrons. On the left side of the figure, the reactants R1 and R2 are shown both as perspective side view and as top view. In the side view, the effect of ring inversion can clearly be seen. The densities for the top views look the same, which is in accord with the notion that for double bond shift the two reactant Lewis structures do not differ. Thus, the bond sectors are equal, and consequently also the electron numbers in this sector. The right side of Fig. 4.6 shows the top view of the product structures P1 and P2. They also look the same, and their bond sector as well as their electron number in the bond sector are the same.

It is interesting to look closely at the electron density isosurfaces. Clearly, there is more electron density between carbon nuclei if there is a double bond in between them than if there is a single bond. The pericyclic orbitals have both significant values at the carbon atoms and between the carbon atoms connected by a double bond. Note also that the hydrogens of a CH-group are not at the boundary of the bond sector, but that they are mostly within the sector belonging to a single bond. Thus, when the density changes from R to P, the electron density around these hydrogens will move inside the observer volume. This should be observable in the electronic flux of the valence electrons. Note that it is not straightforward to separate a CH-bond density from the other-valence density, because the molecular orbitals cannot be easily separated.

Neutral cyclooctatetraene has 56 electrons in total, 16 of which occupy the eight carbon 1s core orbitals. Thus, there are 40 valence electrons, of which eight are the pericyclic (π -like) electrons and 32 are other valence electrons. It holds for the electron numbers in the bond

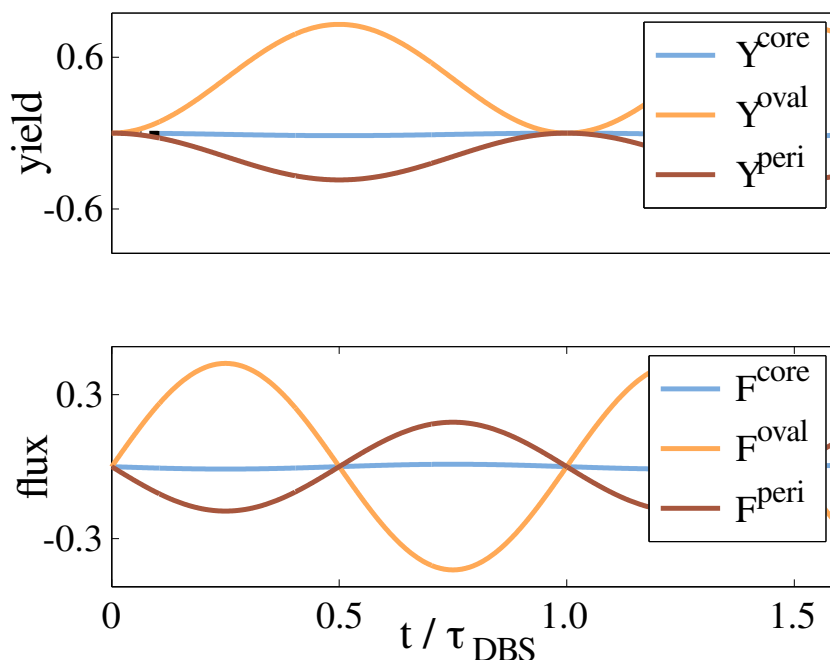


Figure 4.7: Electronic fluxes and yields for double bond shift during tunneling in cyclooctatetraene for core electrons (“core”), pericyclic electrons (“peri”) and all valence electrons except the pericyclic electrons (“oval”).

sectors that

$$\begin{aligned} 4(N_{\text{DB,R}} + N_{\text{SB,P}}) &= 56 \\ 4(N_{\text{DB,R}}^{\text{core}} + N_{\text{SB,P}}^{\text{core}}) &= 16 \\ 4(N_{\text{DB,R}}^{\text{oval}} + N_{\text{SB,P}}^{\text{oval}}) &= 32 \\ 4(N_{\text{DB,R}}^{\text{peri}} + N_{\text{SB,P}}^{\text{peri}}) &= 8. \end{aligned}$$

Integration of the density in the sectors gives

$$\begin{aligned} N_{\text{DB,R}} - N_{\text{SB,P}} &= 2N_{\text{DB,R}} - 56/4 = -0.47 \\ N_{\text{DB,R}}^{\text{core}} - N_{\text{SB,P}}^{\text{core}} &= 2N_{\text{DB,R}}^{\text{core}} - 16/4 = 0.02 \\ N_{\text{DB,R}}^{\text{oval}} - N_{\text{SB,P}}^{\text{oval}} &= 2N_{\text{DB,R}}^{\text{oval}} - 32/4 = -0.86 \\ N_{\text{DB,R}}^{\text{peri}} - N_{\text{SB,P}}^{\text{peri}} &= 2N_{\text{DB,R}}^{\text{peri}} - 8/4 = 0.37 \end{aligned}$$

From these numbers the electronic yields and fluxes may be calculated.

Fig. 4.7 shows the fluxes and yields for double bond shift of cyclooctatetraene. After half the tunneling time, $\tau_{\text{DBS}}/2$, there is net yield of -0.37 pericyclic electrons in the observer volume of Fig. 4.6, i.e. there are 0.37 pericyclic electrons less in the volume. This is qualitatively in accord with the picture of the reaction in terms of the Lewis structures, because initially the volume contains a double bond, and finally it contains a single bond. Thus, there are electrons moving out of the observer volume. As the mechanism is known by symmetry, it can be concluded that there are $0.37/2$ pericyclic electrons to be assigned to one of the fishhook arrows for the central mechanism shown in Fig. 4.1. This is in contrast to what the Lewis structures suggest: Instead of a total pericyclic movement of 4×2 electrons, only $4 \times 0.37 = 1.48$ electrons move. The reason for this small number is the delocalized nature of the density. As can be seen in Fig. 4.6, there is significant pericyclic density also in the sectors belonging to single bonds.

The flux of the core electrons is negligible, as these are well localized at the carbon atoms and have an almost spherical shape, which distorts little during the rearrangement. Interestingly, the other valence electrons move into the opposite direction than the pericyclic electrons. After $\tau_{\text{DBS}}/2$, 0.86 other valence electrons have flown into the sector which morphed from a double bond to a single bond. Thus, in total 0.47 electrons moved into the sector, which seems to contradict the mechanistic view of the reaction so far.

This behavior of the other valence electrons can partly be explained by the fact that density which may be assigned to the CH-bond is in the observer volume of the products, but not in the observer volume of the reactants, cf. Fig. 4.6. But this is not the only effect, as will be seen in the example of benzene in the next section: The other valence electrons of the carbon-carbon bonds move indeed into opposite direction to those of the pericyclic electrons. This effect is an interplay of the nuclear dynamics, which induces the electron motion, and quantum chemistry, which partitions the electrons into classes depending on the current nuclear configuration. In the example of the dynamics of benzene in chapter 4.2 this is further discussed.

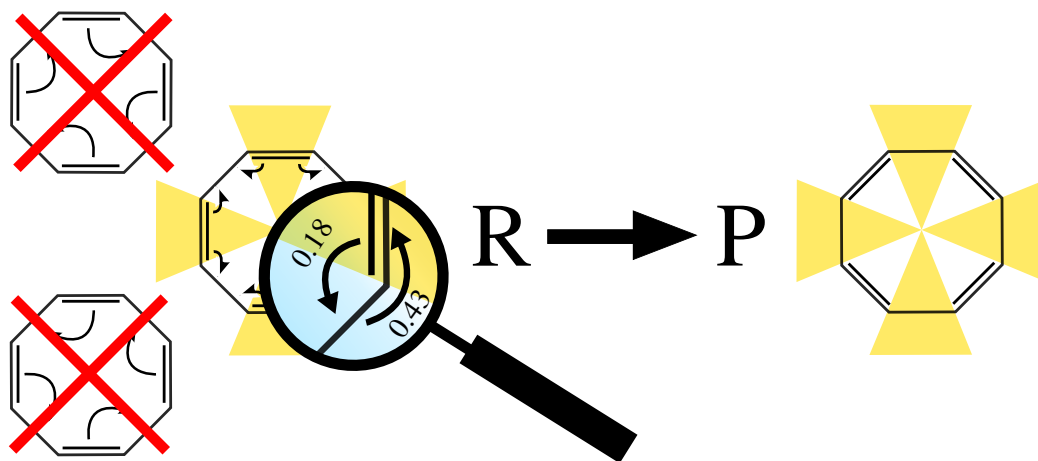


Figure 4.8: Mechanism for the double bond shift of cyclooctatetraene: Two possible mechanisms are ruled out by symmetry and zero angular momentum constraint of the electronic ground state. For the allowed mechanism, 0.37π electrons flow out of the bond sector, while 0.86 other valence electrons flow into the bond sector. The figure shows the flow through one of the boundaries of the sector. Note that the flow into the bond sector is not only due to the carbon-carbon bonds but also due to the carbon-hydrogen bond.

Fig. 4.8 shows a summary of the results of the example of tunneling in cyclooctatetraene, with respect to the questions posed in the introduction. Firstly, unidirectional reaction mechanisms may be ruled out by the zero angular momentum constraint in the electronic ground state. Secondly, it was found that only few electrons flow effectively, in contrast to the number of electrons shifting as suggested by the Lewis structures. Thirdly, it was found that the pericyclic electrons move as indicated by the reaction mechanism, but the other valence electrons move into opposite direction.

4.2 Dynamics along the Kekulé mode of benzene

4.2.1 Abstract

The second pericyclic model reaction to be investigated is a certain dynamics of the benzene molecule, shown schematically in Fig. 4.9. An initial nuclear configuration is prepared which resembles a Kekulé structure of benzene, i.e. a structure with alternating single and double bonds. This structure is a non-equilibrium structure and thus there will be a time-dependent nuclear and electronic density. The dynamics is expected to be initially as shown in Fig. 4.9, i.e. one Kekulé structure will be converted to the other, and vice versa. This dynamics is to be monitored and mechanistic details of the reaction mechanism are to be investigated.

Specifically, the motion of benzene along the Kekulé vibrational mode (the mode that interconverts the two Kekulé structures) will be simulated using a quantum dynamics simulation. Thus, first a model of reduced dimensionality needs to be set up, which can describe this dynamics appropriately. The model yields a one-dimensional effective Hamiltonian that describes the process. With this Hamiltonian, the time-dependent Schrödinger equation for an initial state like the one shown in Fig. 4.9 can be solved and the time-dependent electron density can be obtained.

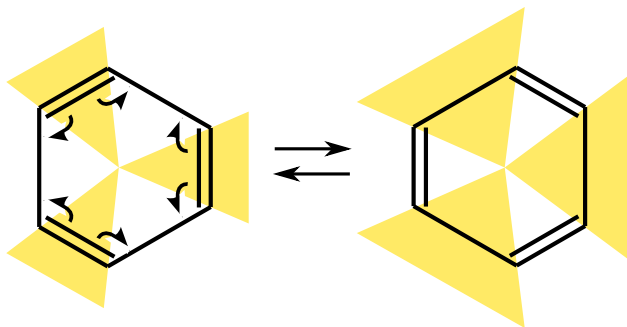


Figure 4.9: Lewis structures of the dynamics of benzene along the Kekulé mode. The arrows indicate the mechanism for electron rearrangement during the dynamics. Three colored triangles represent the sectors attributed to carbon-carbon bonds, defined analogously to the bond sectors used for cyclooctatetraene in section 4.1.1.

In Fig. 4.9, observer volumes are shown which indicate the bond sectors that are to be monitored. However, because there is a nuclear wave packet, the time-dependent electron density is a superposition of electron densities for different nuclear configurations. For each nuclear configuration the bond sector is different, and consequently the total bond sector can be thought of as being fuzzy (i.e. it has no sharp boundaries). Note that in Fig. 4.9 only one reaction mechanism is shown: Again, as for cyclooctatetraene, other possible (uni-directional) reaction mechanisms are ruled out from the beginning by the constraint of zero electronic angular momentum in the electronic ground state.

Like for cyclooctatetraene in the previous section, the electron densities will be divided into π - and other valence electrons in order to compare with the mechanism in terms of Lewis structures. Because of the simplicity of the model new insights can be obtained. The issue of different direction of the flux due to the pericyclic and the other valence electrons can be illuminated further. It is possible to make dynamical statements, and it will be seen that the electrons move effectively with different speed. The π -electrons are faster than the sector boundary, while the other valence electrons are slower. Consequently, the net flux into or out of the observer volume can be interpreted in terms of these dynamical phenomena.

4.2.2 The Kekulé mode

In contrast to cyclooctatetraene as anti-aromatic system, benzene is the prototypical aromatic molecule. Thus, instead of a low symmetry equilibrium structure with localized alternating single and double bonds, in the equilibrium structure of benzene the carbon (and the hydrogen) nuclei constitute a regular hexagon. Nevertheless, a process similar to the double bond shift in cyclooctatetraene is to be investigated, which will be initialized by a non-equilibrium initial condition. In contrast to the tunneling model in the previous section there is thus dynamics with an energy which is significantly above the ground state energy.

Fig. 4.9 shows the process to be studied in terms of Lewis structures. Benzene is to be prepared in a situation describable by a Kekulé structure, that is, with alternating single and double carbon-carbon bonds. There are two conceptually different ways of realizing this Kekulé structure of benzene: On one hand, a Kekulé structure may be prepared by a superposition of sensibly chosen electronic states, such that the electronic structure resembles the electronic structure indicated by the Lewis structures. Ulusoy and Nest describe such a possibility in [214], for a case where the nuclei can be considered to stay at the equilibrium configuration (at least for a short time). On the other hand, benzene may be forced into a Kekulé structure by the position of the nuclei. Specifically, a non-equilibrium nuclear wave packet may be prepared along the Kekulé vibrational mode, realizing the indicated single and double bonds via the distance of the carbon atoms from each other. As shown below, indeed for such a nuclear configuration the π -orbitals will show a depletion if the carbon atoms are farther away from each other and an accumulation if the carbon atoms come closer together. It is this dynamics that will be the topic of the current chapter, as electron dynamics induced by nuclear dynamics in the electronic ground state. However, later the model will also be compared with the excited state dynamics as simulated by Ulusoy and Nest.

Before even starting to model the system, one peculiarity of the quantum description of the process shall be brought to attention: Initially, the dynamics of the nuclear wave packet along the Kekulé mode will represent the interconversion from one of the two possible Kekulé structures with point group symmetry D_{3h} to the other Kekulé structure via a configuration with equal bond lengths of D_{6h} symmetry. However, the nuclear dynamics is described quantum mechanically and the nuclear potential along the considered mode is not exactly harmonic, as shown below. The D_{3h} symmetry elements will always stay intact, as each possible nuclear configuration along the coordinate has this symmetry elements. But the nuclear wave function of the molecule will never have D_{6h} symmetry, because the nuclear wave function will never be symmetric with respect to the equilibrium configuration (the position expectation value, though, will at some time have D_{6h} symmetry again). The more the nuclear density differs in shape from a Gaussian, the less will the Lewis structures be an appropriate representation of the process. Especially for longer time scales, the dynamics will become more complicated and more difficult to analyze in terms of these simple pictures. It would also be not adequate to use a one-dimensional model anymore, because other vibrational modes would start to become important.

4.2.3 A model Hamiltonian

At first, a model Hamiltonian needs to be set up which can be used with the time-dependent Schrödinger equation for the propagation of the nuclear wave packet. The distortion of one Kekulé structure into the other needs to be described and an appropriate coordinate is needed. A suitable choice is the angle Θ shown in Fig. 4.10. This angle represents the displacement of all carbon atoms from their equilibrium position ($\Theta = 0$, brown structure), and it shall be counted positive in the indicated direction. For later convenience, the absolute value

4.2. Dynamics along the Kekulé mode of benzene

of Θ is defined to be twice the displacement of one of the carbon atoms from equilibrium, indicated as the yellow area in the figure. There is another such angle for the hydrogen atoms. However, in the model to be used the angle Θ for the carbon nuclei and that for the hydrogen nuclei will be set equal, such that the origin, each carbon nucleus and its corresponding hydrogen nucleus are on a straight line.

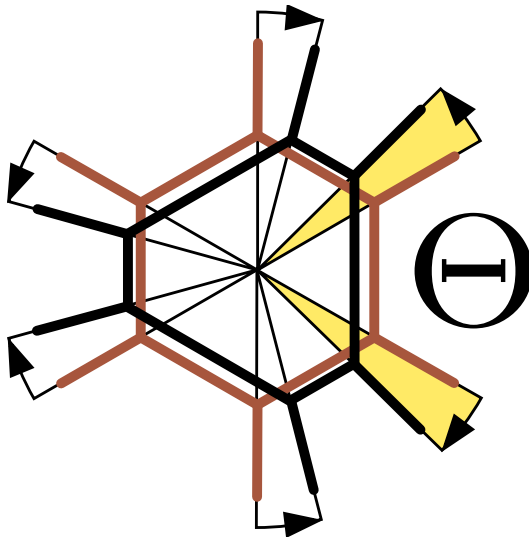


Figure 4.10: Angle Θ parameterizing the Kekulé mode. A change in Θ corresponds to the indicated collective motion of the carbon and hydrogen atoms relative to their equilibrium position (brown structure, $\Theta = 0$). Θ is positive if the motion is directed as indicated, and negative if the motion is in opposite direction relative to the equilibrium structure. The value of Θ corresponds to twice the displacement of one CH-group (indicated by the yellow areas), and $\Theta \in (-\pi/3, \pi/3)$.

The model Hamiltonian is derived as follows: First, the potential is expanded to second order in the displacement of the nuclei along Θ . This expansion automatically incorporates the symmetry implied by motion along the Kekulé mode. Subsequently, the potential matrix will be diagonalized, which will keep the kinetic energy matrix also diagonal. This method resembles vibrational normal mode analysis, with the difference that the resulting coordinate is not rectilinear (as normal modes generally are) but curvilinear (an angle). While this approach is straightforward, extension of the model to include further degrees of freedom is rather difficult due to the intuitive, but unsystematic nature of the approach. Additionally, the other modes which are neglected are unknown.

Thus, in Appendix C another method is presented which can be used to obtain curvilinear coordinates tailored to constrained, highly symmetric molecular systems, like benzene or also cyclooctatetraene. The route followed in Appendix C is to explicitly set up Jacobian coordinates, express them in terms of spherical coordinates and combine the angles and distances in a symmetry-adapted way. The kinetic energy operator of this section is also derived in Appendix C, and possible extensions of the model are immediately apparent.

In the model at hand, the carbon nuclei are constrained to move along a circle with fixed radius around the nuclear center of mass. The displacement of the carbon atoms from their equilibrium position at the corners of a regular hexagon is measured by an angle Θ_i for carbon i , with $\Theta_i = 0$ being the equilibrium position. All Θ_i are counted positive in the same direction, say, counter-clockwise. The hydrogen atoms are constrained to another circle with larger (fixed) radius and the hydrogens have the same Θ_i as the corresponding carbon nucleus they are attached to. Thus, it is assumed that the light hydrogens adopt to the motion of the heavy carbon nuclei quickly and that vibrations of the carbon-hydrogen bonds

are fast.

The displacements of the CH-groups from their equilibrium positions Θ_i for group i can be written as a vector $\Theta = (\Theta_1, \dots, \Theta_6)$. Expansion of V at the minimum to second order in the angles yields

$$\begin{aligned} V(\Theta) &= \frac{k}{2} ((\Theta_2 - \Theta_1)^2 + (\Theta_3 - \Theta_2)^2 + (\Theta_4 - \Theta_3)^2 \\ &\quad + (\Theta_5 - \Theta_4)^2 + (\Theta_6 - \Theta_5)^2 + (\Theta_1 - \Theta_6)^2) \\ &= \frac{k}{2} \Theta M \Theta^T \end{aligned} \quad (4.36)$$

with the matrix M defined as

$$M = \begin{pmatrix} 2 & -1 & 0 & 0 & 0 & -1 \\ -1 & 2 & -1 & 0 & 0 & 0 \\ 0 & -1 & 2 & -1 & 0 & 0 \\ 0 & 0 & -1 & 2 & -1 & 0 \\ 0 & 0 & 0 & -1 & 2 & -1 \\ -1 & 0 & 0 & 0 & -1 & 2 \end{pmatrix} \quad (4.37)$$

and with Θ^T denoting the transpose of the row vector Θ , i.e., the respective column vector. The constant k is the same for all angles due to the symmetry along the mode. The next step is to make the similarity transformation

$$\Theta M \Theta^T = \Theta K^T K M K^T K \Theta^T = \Theta K^T \Lambda K \Theta^T = \tilde{\Theta} \Lambda \tilde{\Theta}^T, \quad (4.38)$$

where $\Lambda = \text{diag}(0, 1, 1, 3, 3, 4)$ is the diagonal matrix of the eigenvalues of M , and where the rows of the matrix K are the eigenvectors of M to the respective eigenvalues. Thus $K K^T = K^T K = 1$. For the two doubly-degenerate eigenvalues there is some freedom in choosing the independent eigenvectors. The choice taken here is

$$K = \begin{pmatrix} a & a & a & a & a & a \\ b & -b & -c & -b & b & c \\ 1/2 & 1/2 & 0 & -1/2 & -1/2 & 0 \\ -1/2 & 1/2 & 0 & -1/2 & 1/2 & 0 \\ -b & -b & c & -b & -b & c \\ -a & a & -a & a & -a & a \end{pmatrix} \quad (4.39)$$

with $a = 1/\sqrt{6}$, $b = 1/(2\sqrt{3})$ and $c = 1/\sqrt{3}$. For the symmetry implied by the Kekulé mode, the absolute value of all the Θ_i is the same, but the signs differ. Specifically, $\Theta_1 = \Theta_3 = \Theta_5 = -\Theta_2 = -\Theta_4 = -\Theta_6 =: \Theta/2$. Using this symmetry, the new angles $\tilde{\Theta}$ become

$$\tilde{\Theta} = \Theta K^T = (0, 0, 0, 0, 0, \sqrt{3/2}\Theta). \quad (4.40)$$

The potential V takes the form

$$V = 6 \frac{k}{2} \Theta^2. \quad (4.41)$$

Consequently, for the Kekulé mode the potential is six times a harmonic oscillator potential with force constant k .

The new coordinates $\tilde{\Theta}$ diagonalize the potential energy and they also keep the kinetic

4.2. Dynamics along the Kekulé mode of benzene

energy diagonal. The expression for the kinetic energy operator in the old coordinates,

$$T = -\frac{\hbar^2}{2m_{\text{CH}}r_{\text{CH}}^2} \sum_i \partial_{\Theta_i}^2, \quad (4.42)$$

needs to be transformed to the new coordinates $\tilde{\Theta}_k$. Here, m_{CH} denotes the mass of a CH-group, and r_{CH} is the distance from the origin to the center of mass of the CH-group. Application of the chain rule for the derivative yields (see [100])

$$\begin{aligned} T &= -\frac{\hbar^2}{2m_{\text{CH}}r_{\text{CH}}^2} \sum_i \partial_{\Theta_i}^2 \\ &= -\frac{\hbar^2}{2m_{\text{CH}}r_{\text{CH}}^2} \sum_{i,k,l} \left(\frac{\partial \tilde{\Theta}_k}{\partial \Theta_i} \frac{\partial}{\partial \tilde{\Theta}_k} \right) \left(\frac{\partial \tilde{\Theta}_l}{\partial \Theta_i} \frac{\partial}{\partial \tilde{\Theta}_l} \right) \\ &= -\frac{\hbar^2}{2m_{\text{CH}}r_{\text{CH}}^2} \sum_{i,k,l} K_{ik} \frac{\partial}{\partial \tilde{\Theta}_k} K_{il} \frac{\partial}{\partial \tilde{\Theta}_l} \\ &= -\frac{\hbar^2}{2m_{\text{CH}}r_{\text{CH}}^2} \sum_{k,l} \left(\sum_i K_{ik} K_{il} \right) \frac{\partial}{\partial \tilde{\Theta}_k} \frac{\partial}{\partial \tilde{\Theta}_l} \\ &= -\frac{\hbar^2}{2m_{\text{CH}}r_{\text{CH}}^2} \sum_{k,l} \delta_{kl} \frac{\partial}{\partial \tilde{\Theta}_k} \frac{\partial}{\partial \tilde{\Theta}_l} \\ &= -\frac{\hbar^2}{2m_{\text{CH}}r_{\text{CH}}^2} \sum_k \frac{\partial^2}{\partial \tilde{\Theta}_k^2}. \end{aligned} \quad (4.43)$$

For the symmetry constraints of the Kekulé mode, the kinetic energy operator simplifies to

$$T = -\frac{\hbar^2}{2\mu r_{\text{CH}}^2} \frac{\partial^2}{\partial \Theta^2} \quad (4.44)$$

with $\mu = 3m_{\text{CH}}/2$, the reduced mass of three times two masses moving against each other. The model Hamiltonian for the Kekulé mode thus reads

$$H = -\frac{\hbar^2}{2\mu r_{\text{CH}}^2} \frac{\partial^2}{\partial \Theta^2} + \frac{k}{2} 6\Theta^2. \quad (4.45)$$

In the following, however, instead of the harmonic potential the potential V obtained by quantum chemical calculations will be used. Note that this approach is essentially the same as followed by normal mode analysis, although it was chosen to work with angles instead of rectilinear coordinates. Thus, the definition of the Kekulé mode here is the same as the Kekulé normal mode for small displacements. Also, if the model is treated as being only one-dimensional, coupling to other modes is assumed to be unimportant and is thus neglected.

For the potential V along Θ complete-active space self-consistent field calculations with six electrons in six π -orbitals (CASSCF(6,6)) were performed using the program package MOLPRO [225], with a cc-pVTZ basis set [70]. Although $V(\Theta)$ is also well described with single-reference methods like CCSD(T) [91], using CASSCF(6,6) makes the partition of the electron densities in core, π - and other valence electron densities possible, as explained in section 3.2. Fig. 4.11 shows a comparison of the CASSCF(6,6) result, the CCSD(T) potential and a harmonic fit around the minimum of the CASSCF(6,6) curve. The density of the initial nuclear wave packet is also shown, which is centered around $\Theta = -5^\circ$. During the nuclear dynamics, the density of the wave packet will be negligible for $|\Theta| > 10^\circ$. Thus, Fig. 4.11 shows that the potentials do not differ much in the region the wave packet explores, but for values of $|\Theta| \approx 10^\circ$ there is already a notable deviation of the quantum chemical

potential from the harmonic fit. The effect of the anharmonicity of the potential will become apparent in the nuclear wave packet dynamics, c.f. Fig. 4.14. The harmonic fit corresponds to a vibrational period of 25.5 fs, which compares reasonably well with the vibrational period of the corresponding normal mode, ca. 28 fs (obtained with a CASSCF(6,6)/cc-pVTZ calculation).

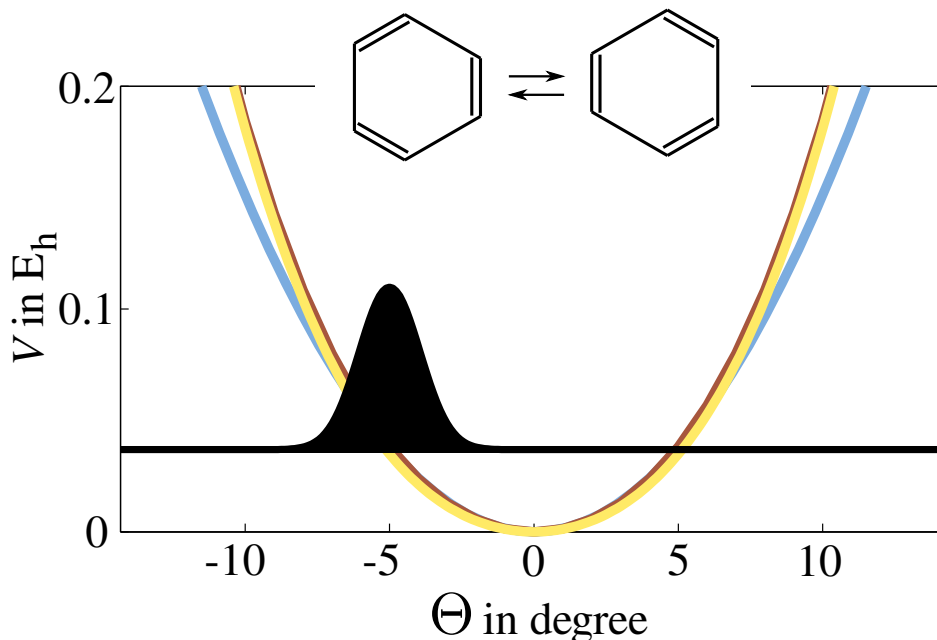


Figure 4.11: CASSCF(6,6) (yellow) and CCSD(T) (brown) potential energy surface V along the Kekulé mode defined in the text, for a cc-pVTZ basis set, and harmonic fit of V around the minimum (blue). The black curve shows the initial wave packet, shifted on the energy scale to its initial total (= potential) energy expectation value. Lewis structures denote schematically the nuclear configurations belonging to $\Theta = \pm 5^\circ$, respectively.

The time-independent and time-dependent solutions of the Schrödinger equation with the one-dimensional model Hamiltonian were calculated numerically with the Matlab [4] program package WavePacket [184]. For determination of the ground state of $V(\Theta)$, the Fourier grid Hamiltonian method was used, while the propagation was performed with the split-operator method, both as implemented in WavePacket.

4.2.4 Results

In the following, first the time-independent one-electron densities along the Kekulé mode are investigated. Thereafter, the nuclear wave packet dynamics is analyzed. From these two ingredients, the time-dependent one-electron density is constructed. Finally, the electron rearrangement is discussed using the number of electrons in the bond sector, the electronic fluxes and a reduced one-dimensional electron density along an angular coordinate.

As initial nuclear wave packet $\chi(0, \Theta)$ a shifted ground-state wave function was chosen. Due to the almost harmonic nature close to the minimum the ground-state wave function of the potential $V(\Theta)$ has the shape of a Gaussian. This function is shifted such that its center (as well as its initial position expectation value) is located at $\Theta = -5^\circ$. The initial nuclear density $|\chi(0, \Theta)|^2$ is shown in Fig. 4.11. At the equilibrium structure, benzene has a carbon-carbon bond length of 139.5 pm. At $\Theta = -5^\circ$, the carbon-carbon bonds have bond lengths of 128.9 pm and 150.0 pm, respectively.

Like in the case of cyclooctatetraene, the total electron density is partitioned into core, pericyclic and other valence electrons. Because the pericyclic electrons are the π -electrons,

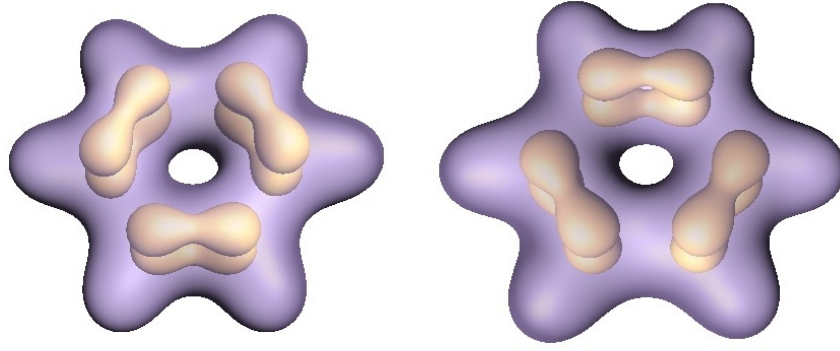


Figure 4.12: Perspective view on the one-electron densities belonging to $\Theta = -5^\circ$ and 5° . Violet transparent surface is an isosurface for the valence electron density $\rho_{\text{QC}}^{\text{val}}$, while the light orange surface is an isosurface for the π -electron density ρ_{QC}^π (both with an isosurface value of 0.05 a_0^{-3}).

instead of the label “pericyclic” the superscript π is used. For the static one-electron densities obtained from a quantum chemical calculation at the nuclear configuration Θ

$$\rho_{\text{QC}}(\mathbf{x}, \Theta) = \rho_{\text{QC}}^{\text{core}}(\mathbf{x}, \Theta) + \rho_{\text{QC}}^\pi(\mathbf{x}, \Theta) + \rho_{\text{QC}}^{\text{oval}}(\mathbf{x}, \Theta). \quad (4.46)$$

The valence electron density is thus

$$\rho_{\text{QC}}^{\text{val}}(\mathbf{x}, \Theta) = \rho_{\text{QC}}^\pi(\mathbf{x}, \Theta) + \rho_{\text{QC}}^{\text{oval}}(\mathbf{x}, \Theta). \quad (4.47)$$

There are 42 electrons in total, of which 12 are core electrons (the carbon 1s electrons), 6 are π electrons and 24 are other valence electrons.

In Fig. 4.12 isosurfaces of the π - and valence electron densities, ρ_{QC}^π and $\rho_{\text{QC}}^{\text{val}}$, are shown for $\Theta = \pm 5^\circ$, i.e. for the nuclear structure representing the center of the initial nuclear wave packet and for the corresponding symmetry-equivalent structure. As can be seen from the figure, the respective Lewis structures for these configurations are indeed the Kekulé structures with alternating single and double bonds. There is a build-up of π -electron density between every second carbon-carbon bond. As shown below, the amount of π -electrons in the region between two carbon atoms is, however, only about 0.2 electrons larger for a double bond sector compared to a single bond sector. This is understandable, as on one hand there is significant electron density distributed symmetrically around the carbon nuclei, and on the other hand the electron density is also rather delocalized.

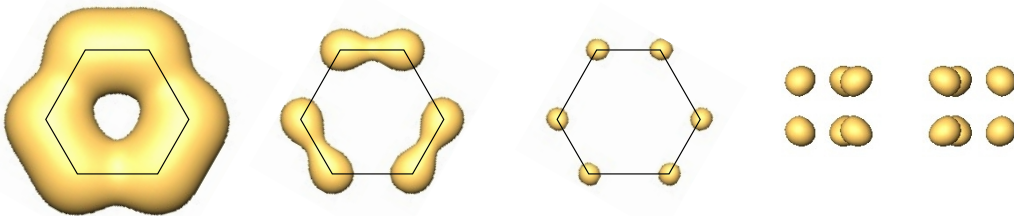


Figure 4.13: For left to right: Top views of the π -electron density ρ_{QC}^π at $\Theta = 5^\circ$ for isosurface values 0.01 , 0.05 and 0.10 a_0^{-3} , and side view for the isosurface value 0.10 a_0^{-3} . In the top views, the nuclear configuration is indicated by hexagons.

Both effects are illustrated in Fig. 4.13. In the figure, top views on the π -electron density are shown for different isosurface values together with the position of the nuclei. Also, a side

view is shown for the largest isosurface value. As can be seen from the top views, for small isosurface values it becomes apparent that the density is distributed around the whole ring. For large isosurface values, it can be seen that there is significant electron density localized close to the nuclear positions. This density seems to be distributed almost spherically around the carbon nuclei. However, the side view shows that there are two such balls for each carbon nucleus, one above the nuclear position and one below. The fact that significant π -electron density is localized close to the nuclei will also be seen later, when an integrated one-electron density is used along φ for the electronic coordinates expressed in cylindrical coordinates, $\mathbf{x} = r, \varphi, z$.

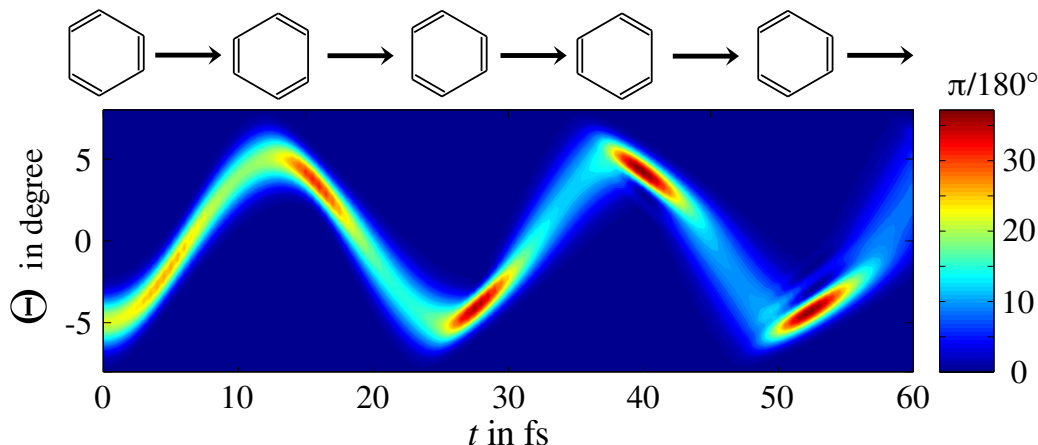


Figure 4.14: Time evolution of the nuclear density $|\chi(t, \Theta)|^2$.

The time evolution of the nuclear density $|\chi|^2$ for the first 60 fs is depicted in Fig. 4.14. If the potential was perfectly harmonic, a wave packet with initially Gaussian shape would stay Gaussian, and the expectation value $\langle \chi(t) | \Theta | \chi(t) \rangle$ would follow the trajectory of a classical particle in the same harmonic potential [208]. The initial wave packet is almost of Gaussian shape, and the potential is also similar to a harmonic potential, cf. Fig. 4.11. From Fig. 4.14 can be seen that during the considered time interval the shape of the wave packet does not distort much from the initial Gaussian shape, and that the expectation value of Θ oscillates back and forth between the two values $\Theta = -5^\circ$ and $\Theta = +5^\circ$, with a period of about 24 fs. Nevertheless, effects of the anharmonicity of the potential are apparent in the density. For example, a Gaussian density in a harmonic potential with initially zero momentum expectation value would have its maximal amplitude either at the turning points or at the center of reflection of the potential, or it would keep its shape. In the first case, the width of the Gaussian is larger than the lowest eigenstate of the potential, while in the second case it is smaller. The third case happens whenever the Gaussian has the same parameters as the lowest eigenstate. As can be seen from Fig. 4.14, the density of the shifted ground state of the wave packet has its maximal amplitude 2-3 fs after the beginning of the propagation. Also, the approximate symmetry of the wave packet with respect to $\Theta = 0$ is little pronounced. For longer propagation times, stronger shape changes away from the Gaussian shape happen, as can be seen already at about 50 fs, where additional structure appears in the density. However, for longer times coupling to other vibrational degrees of freedom would become increasingly important, and the one-dimensional model would be inappropriate. For the considered time interval, Kekulé structures can still represent the nuclear configurations at the turning points of the nuclear wave packet. These structures are shown at the top of Fig. 4.14. Thus, the dynamics up to about 60 fs indeed represents interconversion of the Kekulé structures.

The time-dependent one-electron density is obtained as

$$\rho(t, \mathbf{x}) = \int |\chi(t, \Theta)|^2 \rho_{\text{qc}}(\mathbf{x}, \Theta) d\Theta. \quad (4.48)$$

Via eqn. 4.46 and eqn. 4.47, this density is also composed of densities for core, π -, and other valence electrons as

$$\rho(t, \mathbf{x}) = \rho^{\text{core}}(t, \mathbf{x}) + \rho^{\text{val}}(t, \mathbf{x}) = \rho^{\text{core}}(t, \mathbf{x}) + \rho^{\pi}(t, \mathbf{x}) + \rho^{\text{oval}}(t, \mathbf{x}). \quad (4.49)$$

For analysis of the electron density it is suitable to use cylindrical coordinates $\mathbf{x} = (r, \varphi, z)$. The definition of the angular coordinate $\varphi \in (-\pi, \pi]$ is shown in Fig. 4.15.

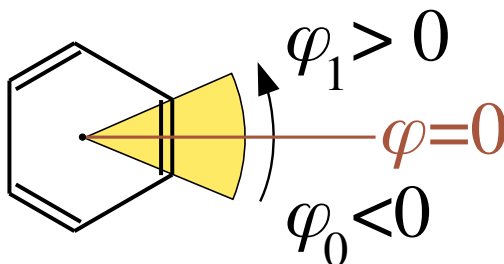


Figure 4.15: Definition of the angle φ and the bond sector (yellow), extending from φ_0 to φ_1 . As shown in brown, $\varphi = 0$ corresponds to one of the mirror planes of the molecule.

For the analysis of the electron dynamics two routes will be followed: the complete time evolution along the angle φ will be investigated, and the space \mathbf{x} will be partitioned into bond sectors for which electronic fluxes can be calculated. As the interesting part of the dynamics, i.e. the part that determines the reaction mechanism, is along the angular coordinate φ , the one-electron density is integrated over r and z . The time-independent electron number in a sector from φ_0 to φ_1 , for a given nuclear configuration Θ , is given by

$$\tilde{N}(\varphi_1, \varphi_0, \Theta) = \int_{\varphi_0}^{\varphi_1} \int_0^{\infty} \int_{-\infty}^{\infty} r \rho_{\text{QC}}(r, \varphi, z, \Theta) dz dr d\varphi. \quad (4.50)$$

A bond sector is a sector which starts at the angle φ_0 being the angle belonging to one carbon atom and ends at the angle φ_1 belonging to the adjacent carbon atom. Such a bond sector is shown in Fig. 4.15, and it is called a static bond sector.

The static bond sector is defined for a given nuclear configuration Θ , because the opening angle between two adjacent carbon atoms changes with Θ , cf. Fig. 4.10. The sector boundaries are thus functions of Θ , i.e. $\varphi_0 = \varphi_0(\Theta)$ and $\varphi_1 = \varphi_1(\Theta)$, if φ_0 and φ_1 are the boundaries of the static bond sectors. The time-dependent electron density eqn. 4.48 is a superposition of the static electron densities for all possible configurations Θ weighted by the probability of finding the respective configuration $|\chi(t, \Theta)|^2$. For the time-dependent electron density a (dynamic, time-dependent) bond sector is thus also the superposition of all possible static bond sectors, weighted by the probability of finding the respective nuclear configuration. Thus, a time-dependent electron number for such a bond sector can be defined as (see also [12])

$$N(t) = \int_{-\pi/3}^{\pi/3} |\chi(t, \Theta)|^2 \tilde{N}(\varphi_1(\Theta), \varphi_0(\Theta), \Theta) d\Theta. \quad (4.51)$$

The functions $\varphi_1(\Theta)$ and $\varphi_0(\Theta)$ are defined such that $\tilde{N}(\varphi_1(\Theta), \varphi_0(\Theta), \Theta)$ is the number of electrons in the static bond sector for the given nuclear configuration Θ . One may also think of $N(t)$ as being obtained from a sector defined for the time-dependent electron density, but with

smooth boundaries determined by the nuclear density. Of course, due to the decomposition of the electron densities in core and valence (i.e. π - and other valence) electrons, there are separate time-independent electron numbers \tilde{N}^{core} and $\tilde{N}^{\text{val}} = \tilde{N}^{\pi} + \tilde{N}^{\text{oval}}$, and thus also separate time-dependent electron numbers N^{core} and $N^{\text{val}} = N^{\pi} + N^{\text{oval}}$.

Because the electronic rearrangement is cyclic, it is reasonable to define a reduced time-dependent one-electron density along the angle φ only. This density, $n(t, \varphi)$, can be obtained either from the time-dependent electron numbers \tilde{N} or from the static electron densities as

$$\begin{aligned} n(t, \varphi) &= \int_{-\pi/3}^{\pi/3} |\chi(t, \Theta)|^2 \left. \frac{\partial \tilde{N}(\tilde{\varphi}, \varphi, \Theta)}{\partial \tilde{\varphi}} \right|_{\tilde{\varphi}=\varphi} d\Theta \\ &= \int_{-\pi/3}^{\pi/3} |\chi(t, \Theta)|^2 \int_0^{\infty} \int_{-\infty}^{\infty} \rho_{\text{QC}}(r, \varphi, z, \Theta) r dz dr d\Theta. \end{aligned} \quad (4.52)$$

Again, due to the decomposition of the electron densities there exists different reduced electron densities for the different types of electrons, i.e. n^{core} and $n^{\text{val}} = n^{\pi} + n^{\text{oval}}$. Note that the time-dependent electron numbers N cannot be obtained from the reduced densities n , because the integral over Θ is already performed in eqn. 4.52, but the angles φ were kept independent from Θ .

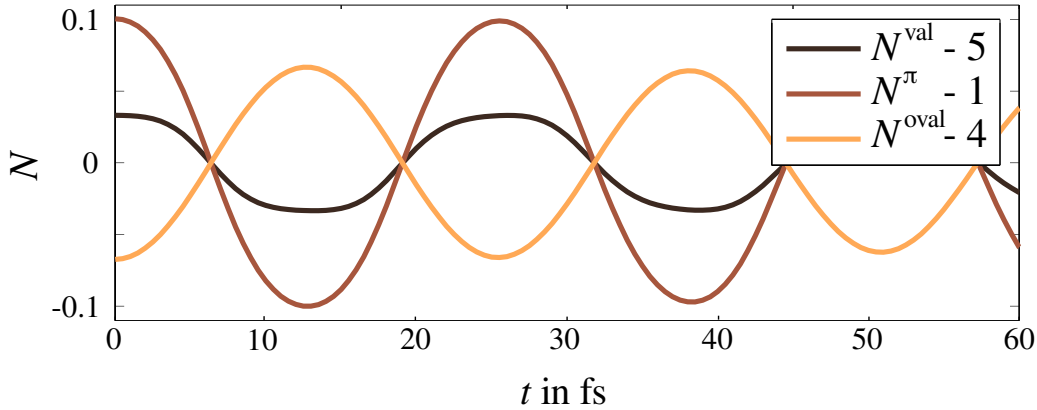


Figure 4.16: Deviation of the time-dependent electron numbers $N(t)$ in the bond sector for valence, π and other valence electrons, relative to their values at equilibrium.

At the equilibrium configuration $\Theta = 0$ of benzene, the electron density $\rho_{\text{QC}}(\mathbf{x}, 0)$ in the bond sector amounts to seven electrons in total. Two of those electrons are core electrons, while one of those electrons is a π electron. This statement is also true for the electron density $\rho(\mathbf{x}, t)$ corresponding to the ground-state nuclear wave function, because the nuclear density has mirror symmetry with respect to $\Theta = 0$. Consequently, at equilibrium there is $N^{\text{val}} = 5$, $N^{\text{oval}} = 4$ and $N^{\pi} = 1$.

Fig. 4.16 shows the calculated time-dependent electron numbers N^{val} , N^{oval} and N^{π} of the bond sector for the nuclear dynamics of Fig. 4.14. The electron numbers oscillate around their equilibrium values. Core electrons are not shown, as these do not move with respect to the sector boundaries but follow the motions of the carbon atoms closely, and thus $N^{\text{core}} = 2$ all the time during the propagation. From the graph of N^{val} the behavior anticipated from the description of the process in terms of Lewis structures can be found: Initially, the bond sector contains a double bond, hence electrons leave the sector until the nuclear wave packet reaches its turning point, at $t \approx 12$ fs. Then electron density returns back inside the bond sector, until it reaches its initial value of 0.033. Thus, in total $4 \times (2 \times 0.033) = 0.264$ valence electrons move within the first 12 fs for the three equivalent bond sectors.

However, during the first half of a period of oscillation 0.199 π electrons move out of the

double bond sector into the nascent double bond sectors. Thus, the other valence electrons have to compensate, moving effectively into the direction opposite to those of the π -electrons. The effect is apparent from figure 4.16, where it can be seen that the other valence electrons move into the section of the nascent single bonds. As discussed before, similar effects are found for cyclooctatetraene and also for semibullvalene, see [12], but were in both cases originally attributed to hydrogen atoms moving into the nascent single bond sectors. However, as already indicated in the discussion of cyclooctatetraene, this is not the only effect. In the benzene model, the hydrogen atoms are constrained to the sector boundaries, and thus they do not move into or out of the bond sector during the time evolution.

It shall be remarked that the oscillations of N^{val} and N^{π} , N^{oval} closely follow the oscillations of the nuclear wave packet, cf. Fig. 4.14. However, effects of the anharmonicity of the potential are negligible for the electron numbers, at least within the considered time interval.

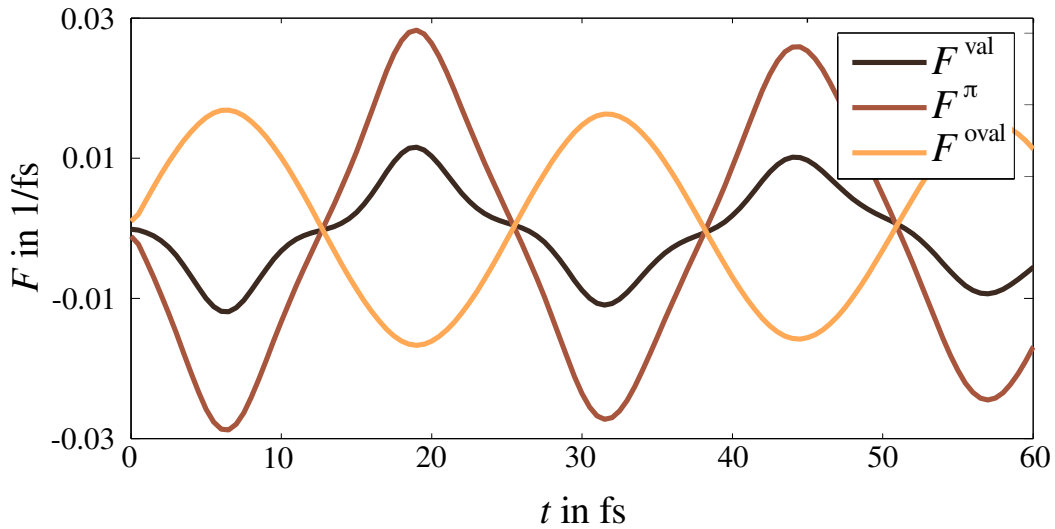


Figure 4.17: Electronic fluxes $F(t)$ into or out of the bond sector for valence, π and other valence electrons.

Electronic fluxes may be calculated from the time-dependent electron numbers. While both quantities have in principle the same information content, the fluxes show more details about the electronic motion. Specifically, the fluxes into or out of the bond sector are calculated as

$$F(t) = \partial_t N(t). \quad (4.53)$$

These are shown in Fig. 4.17. Interestingly, the π -electrons behave differently than the other valence electrons: While for the π electrons there is an approximately linear increase of the absolute value of the flux up to the maximum, a sharp peak and then linear decrease of the absolute value of the fluxes again, for the other valence electrons the change in slope is smoother. Thus, for the other valence electrons, the curvature close to the maximum is not as strong. This behavior is also visible in the fluxes of all valence electrons. Initially, there is not much flux as the contributions of π and other valence electrons approximately cancel each other. However, the π electron flux eventually dominates and the slope of the flux changes strongly. Note also that the electronic fluxes show a small but notable decrease in amplitude during the time evolution due to the anharmonicity of the potential and the corresponding dispersion of the nuclear wave packet.

Another tool to monitor the progress of the electron rearrangement is the reduced electron density $n(t, \varphi)$ along φ . This function is shown for the π - and the other valence electrons in

Fig. 4.18, where both $n^\pi(t, \varphi)$ and $n^{\text{oval}}(t, \varphi)$ are plotted. The functions n are periodic in φ with a period of $2\pi/3$, and only one period is depicted. The motion of the nuclear wave packet can also be found in Fig. 4.18, if the maximum of the densities close to $\varphi = 0, \pm\pi/3$ is followed. It is possible to identify the change in the electronic coordinates φ with the angle Θ describing the nuclear configuration. For this purpose, φ has to be identified with 2Θ , because a change in Θ changes the opening angle of the sector by displacing the two C-H groups at the boundaries by the same amount, in opposite directions. Detailed inspection shows that the maxima of $|\chi(t, \Theta)|^2$ and $n(t, \varphi)$ are very similar. This is reasonable, as most of the electron density is localized close to the position of the nuclei, and the maximum of $|\chi(t, \Theta)|^2$ corresponds almost to the expectation value of the nuclear wave packet along Θ .

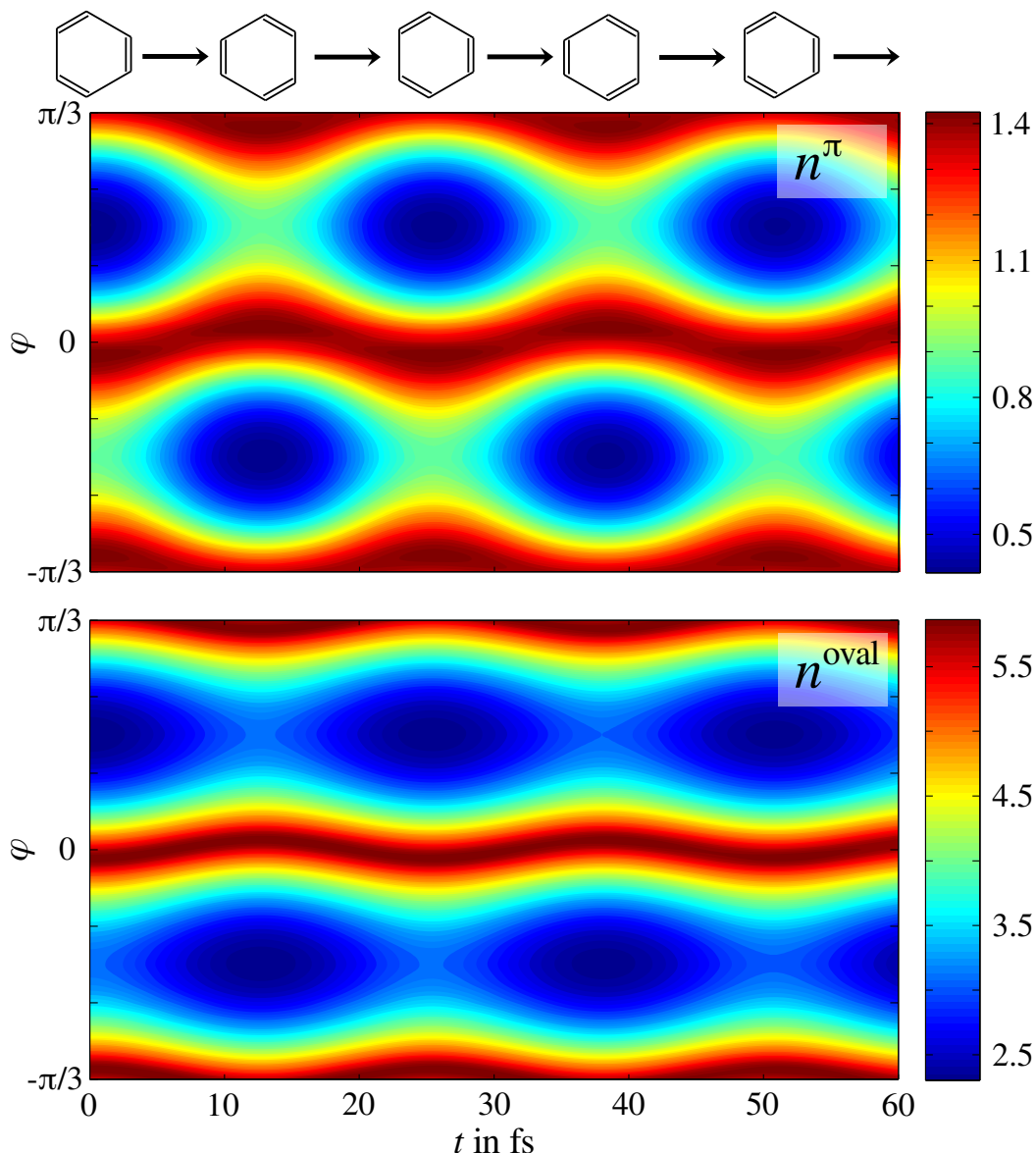


Figure 4.18: Contour plots of the reduced electron density $n(t, \varphi)$ for π -electrons (top panel) and for the other valence electrons (bottom panel), for the first 60 fs of the propagation along the Kekulé mode. Above the graphs, Lewis structures representing the nuclear configuration at the respective times are drawn, cf. Fig. 4.14. The functions n^π and n^{oval} are periodic along φ with a period of $2\pi/3$, and only one period is shown.

In Fig. 4.18, the location of the single and double bonds can easily be identified. Initially, there is significant electron density around $\varphi = \pi/6$ but little at $\varphi = -\pi/6$. After ca. 12 fs, the situation is reversed. Details about the direction of the electronic motion are not directly

4.2. Dynamics along the Kekulé mode of benzene

apparent from the plot. However, because the D_{3h} symmetry is kept during the process, and because of the the constraint of zero angular momentum in the electronic ground state, the electronic motion has to be symmetric with respect to the angle defining the center of the carbon-carbon bonds. Consequently, the electron density being initially in the region around $\varphi = \pi/6$ has to move symmetrically towards smaller and larger values of φ , whereas the region around $\varphi = -\pi/6$ gains electrons symmetrically from smaller and larger φ values.

In contrast to the time evolution of $N^{\text{val}}(t)$, $N^{\text{ova}}(t)$ and $N^\pi(t)$, all one-dimensional electron densities n^{val} , n^{ova} , and n^π show the same qualitative behavior, and thus all electrons move in the same direction. This is understandable, because the motion is induced by the nuclei: As long as the nuclear wave packet moves completely into one direction, the electron densities cannot move in the opposite direction, at least in the Born-Oppenheimer approximation. At first sight, this seems to be in contradiction to the fact that the time-dependent electron numbers N^π and N^{ova} move into opposite directions. However, taking the two results together, it must be concluded that the π -electrons move faster into or out of the bond region than the other valence electrons. Moreover, the π -electrons should move faster than the average boundaries of the bond sector, while the other valence electrons should move slower.

This conclusion can be quantified by calculating the corresponding velocities of the motions. The bond sector is determined by the nuclear wave packet χ , and the average velocity of the sector boundaries of a bond sector is thus given by the average velocity of the expectation value of χ along Θ . Specifically, the average velocity of one of the two sector boundaries

$$v_{\text{nuc}}(t) = \frac{1}{2} \partial_t \int_{-\pi/6}^{\pi/6} \Theta |\chi(t, \Theta)|^2 d\Theta, \quad (4.54)$$

where the factor $1/2$ is due to the fact that a change in Θ moves the two sector boundaries by an equal amount into opposite directions. For the electrons, average velocities can be defined by taking the expectation value of the electron densities $n(t, \varphi)$ along φ in some part of the total angular space. A suitable definition is

$$v(t) = \partial_t \left(\frac{\int_{-\pi/6}^{\pi/6} \varphi n(t, \varphi) d\varphi}{\int_{-\pi/6}^{\pi/6} n(t, \varphi) d\varphi} \right), \quad (4.55)$$

which results in velocities v^π , v^{oval} , etc. for the different electron densities. The integration boundaries $\pm\pi/6$ are defined such that the velocity represents the time derivative of the average value of φ with respect to n for the region of one CH-group. This is the group at the sector boundary that is to be monitored. The denominator is needed for normalization, as the densities n are normalized to the number of electrons of the respective type and the velocities would otherwise not be comparable.

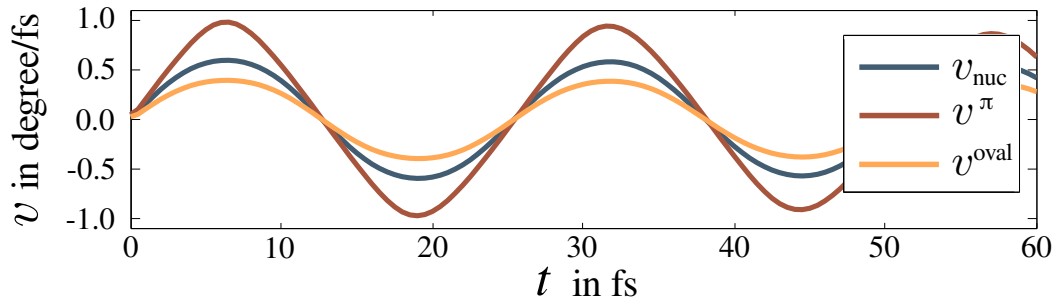


Figure 4.19: Velocity of the expectation value of the sector boundary v_{nuc} , average velocity of the π -electrons v_π , and average velocity of the other valence electrons v_{oval} .

In Fig. 4.19 the velocities are shown. In line with the results presented above, the π electrons are faster than the sector boundary, and the other valence electrons are slower. The maximum velocity for the π electrons is $0.98^\circ/\text{fs}$, as compared to the maximum velocity of the sector boundary of $0.58^\circ/\text{fs}$ and that of the other valence electrons, $0.39^\circ/\text{fs}$.

The underlying dynamics is the same for all the different types of electrons, i.e. the dynamics of the nuclei. Consequently, the different behavior of the π - and the other valence electrons is due to the way how the electronic problem is solved. As the static structure of the electron density changes from one nuclear configuration to the other, the same nuclear dynamics yields different electron dynamics for the different types of electrons.

Finally, the ground state electron dynamics study presented in this section shall be compared with a similar electron dynamics describing the interconversion of the Kekulé structures of benzene by means of a superposition of excited states. This interesting electron dynamics study was performed by Ulusoy and Nest [214]: They used optimal control theory to prepare superpositions of the S_0 and S_1 as well as of the S_0 and S_2 electronic state of benzene. The former is a state of alternating bond order of the carbon-carbon bonds, while the latter is a state of alternating Mulliken charges at the carbon atoms. Ulusoy and Nest used time-dependent configuration interaction theory to monitor the time evolution of the electronic states for fixed nuclear positions. They found that the resulting electronic superposition states oscillate on an attosecond time scale between the symmetry equivalent structures.

The process studied by Ulusoy and Nest is rather different from what is studied in this work: Due to the superposition of electronic states the electrons move rapidly, while here the electronic motion induced by the nuclear motion is studied, which is thus much slower. The S_0 - S_1 superposition is a realization of one Kekulé structure of benzene for the nuclei fixed at equilibrium position. This is in contrast to the dynamics performed here, where the nuclei are allowed to move. Direct comparison of the two scenarios would be very interesting: One would need the time-dependent one-electron density of the S_0 - S_1 superposition. The construction of this density yields further problems, which are beyond the scope of this work but may be studied in the future.

4.3 Proton tunneling in the formic acid dimer and in malonaldehyde

4.3.1 Abstract

In the examples discussed so far, the mechanism of the electron rearrangement was determined by the symmetry of the process and the requirement of zero expectation value of the electronic angular momentum. Knowledge of the qualitative mechanism made quantitative analysis in terms of the electronic fluxes possible: The amount of moving electrons as well as their speed could be determined for different electron densities, and it could be distinguished how π - and the other valence electrons move during the process.

For a general cyclic electron rearrangement the reaction mechanism is not known by symmetry and needs first to be determined. The electron flux representing the reaction mechanism may be determined from the time-dependent electron density. However, already for the one-dimensional problem of determining the angular fluxes of the cyclic reaction there is a problem: Fluxes into or out of a volume are easily calculated, but fluxes through a surface at some angle are only known up to a parameter $c(t)$. This parameter is the same for all angles, but it may change with time. Without further information $c(t)$ is undetermined, but its value is important for the reaction mechanism.

In principle, changing the value of $c(t)$ can completely alter the reaction mechanism from mainly clockwise to mainly counter-clockwise, with all possibilities in between. In practice, its influence depends on the shape of the angular flux. The purpose of this chapter is to investigate the unknown parameter formally, and to test the dependence of the reaction mechanism on the value of $c(t)$ in two model systems.

The value of the unknown flux parameter $c(t)$ is equivalent to the average angular flux at time t . Thus, using the connection of the flux density and the angular momentum operator, a new operator is found whose expectation value provides the average angular flux. This operator is the quantum mechanical analogue of the angular velocity. The time dependence of the expectation value of the angular velocity operator is studied using Ehrenfest's theorem, in order to investigate the time-dependence of $c(t)$. It is found that the value of $c(t)$ for cyclic reactions cannot be inferred from linear or angular momentum conservation, and that the average angular flux and thus $c(t)$ has no simple time-evolution. Its time-dependence is determined by the details of the angular and radial flux densities.

Two model systems are used to study the effect of the unknown flux parameter on reaction mechanisms of pericyclic reactions: Coherent proton tunneling in malonaldehyde and coherent double proton tunneling in the formic acid dimer. First, the fluxes are determined via the continuity equation, but the systems is constrained to zero average angular flux at all times. In this case the flux is fixed, and especially the angles where the flux is zero are known. From these, the reaction mechanism can be read off, and the number electrons moving from the region of one bond to the region of another can directly be calculated. Then, the influence of a time-dependent average angular flux is investigated qualitatively by focusing on the location of the zero-flux planes. Finally, the assumption that the electron flux is determined by how much the density changes locally from point to point is made, and zero-flux surfaces are calculated for this case.

It is found that already a lot about the reaction mechanism can be learned without the knowledge of $c(t)$. Specifically, it is found that the reaction mechanism for proton tunneling in malonaldehyde is similar to the previous examples of cyclooctatetraene and benzene, while the mechanism of double proton transfer in the formic acid dimer is surprising, as the net flux does not follow any of the typically attributed mechanisms.

The assumption that the flux can be obtained from the local change of density turns out to be equivalent to zero average angular flux, if the electron density exhibits a behavior that is similar to classical particle dynamics. It thus gives sensible results for regions of the heavy nuclei, but fails to describe proton tunneling appropriately.

After explanation of the problem in section 4.3.2, the average angular flux is discussed in section 4.3.3. Details about the model systems formic acid dimer and malonaldehyde are given in section 4.3.4. Thereafter, in section 4.3.5 the electron fluxes are analyzed, and the dependence of the reaction mechanism on the time-dependence of the average angular flux is investigated. Section 4.3.6 contains details about how zero-flux planes can be determined from the assumption that the flux is determined from the local change in electron density, and in section 4.3.7 the mechanisms resulting from these assumptions are compared with the results from section 4.3.5.

4.3.2 The missing flux parameter

As shown in the previous examples, in pericyclic reactions it may be possible to decide for a reaction mechanisms by analyzing the dynamics of a one-dimensional time-dependent electron density $n(t, \varphi)$ along an angular coordinate φ . This density may be obtained from the one-electron density $\rho(t, \mathbf{x})$, with cylindrical coordinates $\mathbf{x} = (r, \varphi, z)$, as

$$n(t, \varphi) = \iint \rho(t, \mathbf{x}) r dr dz. \quad (4.56)$$

Being a proper density, the angular electron density is locally conserved, and the corresponding continuity equation

$$\partial_t n(t, \varphi) + \partial_\varphi j(t, \varphi) = 0 \quad (4.57)$$

may be solved for the flux density j ,

$$j(t, \varphi) = - \int_{\varphi_0}^{\varphi} \partial_t n(t, \varphi') d\varphi' + j(t, \varphi_0), \quad (4.58)$$

where $j(t, \varphi_0)$ is the flux density at φ_0 , the (possibly time-dependent) start of the integration. Thus, the angular flux density and thus the reaction mechanism is determined by the electron density n , if j is known along a curve $\varphi_0(t)$.

If j was sought for a Cartesian coordinate, e.g. $j(t, x)$, it would always be possible to determine j unambiguously, because the density and thus the flux density decay to zero for $|x| \rightarrow \infty$. It would be enough to start the integration at values $x = x_0$ small enough to be sure that $j(t, x_0) = 0$. However, the flux density depends on the angle φ , and no points φ_0 exist where $j(t, \varphi_0)$ is known already. In particular, it is not known where $j(t, \varphi) = 0$, and thus where the flux changes direction. This piece of information is of course very relevant for the reaction mechanism.

In the following, the start of the integration φ_0 will be fixed fixed by some condition, and the missing integration constant of eqn. 4.58 is the time-dependent, but angle-independent parameter

$$c(t) = j(t, \varphi_0). \quad (4.59)$$

This parameter is called the flux parameter, and it is an important entity in this chapter.

For the example reactions of the molecules of the previous sections, cyclooctatetraene and benzene, an unknown time-dependent parameter does not occur. The considered reactions happen in the electronic ground state and under assumption of zero electronic angular momentum. Consequently, as explained below there is no unidirectional flux possible, and

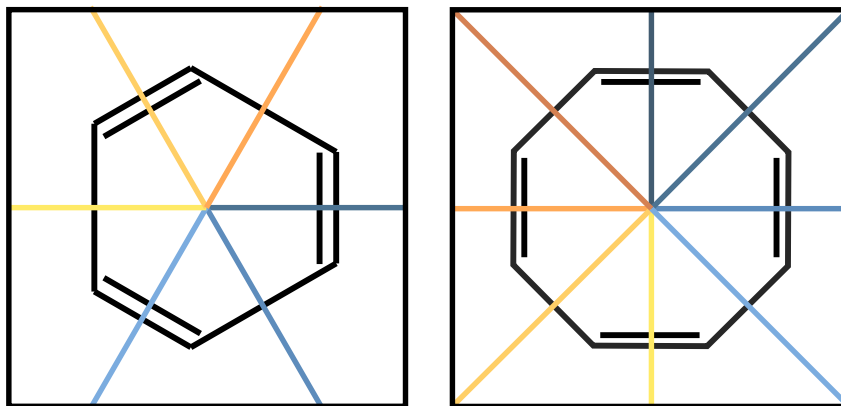


Figure 4.20: Planes of zero net electron flux with respect to the processes described in the previous examples for benzene and cyclooctatetraene. Each of those half planes continues to infinity above and below the paper plane.

the symmetry of the molecules forces the net fluxes through some planes at some angles φ to be zero. Because this symmetry does not break during the process, these planes do not change with time and the parameter c may be easily determined. Fig. 4.20 shows these zero-flux planes for the two molecules.

In general, however, such symmetries do not need to exist, and thus it may be asked if there are other ways to determine the complete angular flux density. If appropriately defined by a suitable choice of the start of integration in eqn. 4.58, a flux parameter of zero, $c(t) = 0$, may mean that there is zero average angular flux (called G in the following), and the value of $c(t)$ can be related to the average angular flux. It is tempting to look for a connection between the average angular flux and the expectation value of the angular momentum operator \hat{l}_z around the z -axis perpendicular to the molecular plane. These two quantities are related but they are not the same, and instead the average angular momentum represents the expectation value of a new operator, the angular velocity operator $\hat{\omega}_z$. In the next section, the relation between G , $\langle \hat{l}_z \rangle$ and $\langle \hat{\omega}_z \rangle$ is explored, and the time-dependence of $\langle \hat{\omega}_z \rangle$ is studied in order to learn something about the time-dependence of the flux parameter $c(t)$.

It will be found that there is no simple time-dependence of $\langle \hat{\omega}_z \rangle$, and hence also not for $c(t)$. The problem will be discussed further in section 4.3.5, where the reference case $c(t) = 0$ will be defined such that $c(t)$ represents the average angular flux. There, it will be argued that due to the connection between the average angular flux and the expectation value of the angular momentum, and due to the shape of the electron density and its known behavior, $c(t)$ can be expected to be approximately zero for all times.

4.3.3 Average angular flux and the angular velocity operator

As known from section 2.3.4, there is a relationship between the flux density operator and the expectation value of the angular momentum operator. It might be tempting to try to find the missing flux parameter $c(t) = j(t, \varphi_0)$ of eqn. 4.58 by comparison of the expectation value of the angular momentum with the average angular flux. Below, it is shown that this comparison has only limited value, and the average angular flux is thus further analyzed.

In section 2.3.4, a general connection between the integral of the flux density operator and the expectation value of the angular momentum operator $\hat{\mathbf{l}}$ was derived. The relation, in 3-space, is

$$\langle \hat{\mathbf{l}} \rangle = \int m \mathbf{x} \times \mathbf{j} d\mathbf{x}. \quad (4.60)$$

Using cylindrical coordinates $x_1 = r \cos \varphi$, $x_2 = r \sin \varphi$, $x_3 = z$, and with $\mathbf{j} = j_r e_r + j_\varphi e_\varphi + j_z e_z$ the relation

$$\langle \hat{l}_z \rangle = m \int j_\varphi r^2 dr d\varphi dz \quad (4.61)$$

was deduced for the expectation value of the angular momentum operator in z -direction. Note that the φ -component of the gradient and thus also of the flux density has an additional factor $1/r$,

$$j_\varphi = \frac{\hbar}{2mi} \frac{1}{r} (\phi^* \partial_\varphi \phi - \phi \partial_\varphi \phi^*), \quad (4.62)$$

as in contrast e.g. to the r -component

$$j_r = \frac{\hbar}{2mi} (\phi^* \partial_r \phi - \phi \partial_r \phi^*). \quad (4.63)$$

Eqn. 4.61 was already obtained by Manz and Yamamoto in [134]. The significance of this equation stems from the following property: Due to the decoupling of electronic and nuclear momenta in the Born-Oppenheimer approximation, the expectation value of the electronic angular momentum alone (as well as the expectation value of the nuclear angular momentum) is conserved. This expectation value is zero for a reaction in a non-degenerate electronic ground state. Consequently, when reading the above equations as equations for the electrons, setting $\langle \hat{l}_z \rangle$ to zero tells something about the flux along φ . Because the interest here is in the mechanism of pericyclic reactions along the angle φ only, the constraint of zero electronic angular momentum tells something about the desired reaction mechanism. Can the unknown parameter for the solution of the continuity equation be determined from the requirement of zero electronic angular momentum?

In [134], Manz and Yamamoto show that zero expectation value of the electronic angular momentum does not help directly. With the additional assumption that $\int j_\varphi dz$ is not changing sign along r , eqn. 4.61 can only become zero when there is a change of sign of $\int j_\varphi r^2 dz dr$ along φ . In consequence, as r is always positive and real, the fluxes through a half plane at an angle φ given by $\int j_\varphi dz dr$ (see below) must change sign somewhere along φ . Manz and Yamamoto conclude that in order to fulfill the constraint of zero electronic angular momentum the reaction must not be unidirectional. However, it may be enough to have an arbitrary small flux opposite to the main flux direction in order to make eqn. 4.61 zero, although the corresponding flux density is rather difficult to envision, cf. section 4.3.5. Thus, albeit important in principle, in practice the selection rule found in [134] has only limited value.

In the following, the idea of [134] to investigate fluxes through half planes at an angle φ in terms of the flux density in cylindrical coordinates will be extended. These fluxes are exactly the fluxes investigated so far, and these are the fluxes that can be obtained from the density alone, up to an integration constant. The total flux through all such planes will be related to the expectation value of an operator, and the time dependence of this operator will be studied using Ehrenfest's theorem.

Fig. 4.21 shows a sketch of a cylinder. This cylinder shall extend in both the radial direction r and in the height z to infinity (in practice it has to be large enough to contain all non-negligible parts of the electron density). The center of the cylinder at $r = 0, z = 0$ represents the nuclear center of mass. At some angle φ_1 there is a half plane consisting of the points $\{r \in (0, \infty), z \in (-\infty, \infty), \varphi = \varphi_1\}$, and the flux through this plane is $F(\varphi_1)$.

The flux through any surface S is given by

$$\int_S \mathbf{j} \cdot \mathbf{n} dS, \quad (4.64)$$

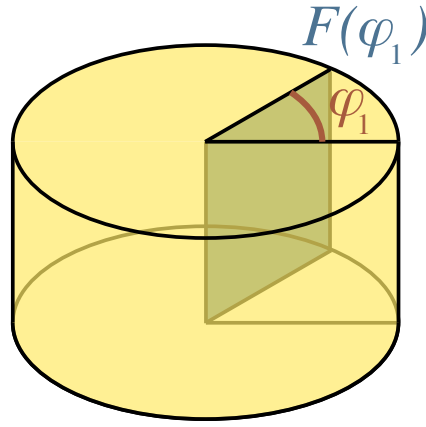


Figure 4.21: This cylinder shall contain the electron density. At angle φ_1 , there is a half plane. The flux through this half plane is $F(\varphi_1)$

where dS denotes the surface element and \mathbf{n} is the unit normal vector of the surface. For the half plane above, $\mathbf{n} = e_\varphi$, the unit vector in φ -direction. The surface at φ_1 is just a flat Cartesian surface with surface element $dS = drdz$, such that

$$F(\varphi_1) = \int j_\varphi(r, \varphi_1, z) drdz. \quad (4.65)$$

Thus, to determine the flux $F(\varphi)$ the component of the flux density in φ -direction is needed. Note that in contrast to the angular momentum expectation value given in eqn. 4.61, the integration of j_φ over r to determine the flux through such a surface is not weighted by a factor r^2 .

The sum of the fluxes through all the half planes in some sector with boundaries φ_1, φ_2 , weighted by the size of the sector, is

$$\begin{aligned} G(\varphi_1, \varphi_2) &= \frac{1}{\varphi_2 - \varphi_1} \int_{\varphi_1}^{\varphi_2} F(\varphi) d\varphi \\ &= \frac{1}{\varphi_2 - \varphi_1} \int_{\varphi_1}^{\varphi_2} \int_{-\infty}^{\infty} \int_0^{\infty} j_\varphi(r, \varphi, z) drdz d\varphi \\ &= \frac{1}{\varphi_2 - \varphi_1} \int_{\varphi_1}^{\varphi_2} \int_{-\infty}^{\infty} \int_0^{\infty} \frac{j_\varphi(r, \varphi, z)}{r} r drdz d\varphi. \end{aligned} \quad (4.66)$$

This integral is not a volume integral over j_φ but over j_φ/r , as the volume element in cylindrical coordinates is $rdrdzd\varphi$. However, regarding the flux density j_φ the volume element in eqn. 4.66 is a Cartesian volume element, although with periodic boundary condition for φ . The volume for $G(\varphi_1, \varphi_2)$ defined by the boundaries at φ_1, φ_2 may be thought of as a box, as shown in Fig. 4.22. From the six faces of the box four are closed, because the integration is performed over all r and z (the face at $r = 0$ may be thought of as a face at $r = \epsilon$, with $\epsilon > 0$ small). Thus, there can only be a flow into or out of the box through two opposite faces.

The left-hand side of Fig. 4.22 shows a situation where density inside the box decreases, and there is flow out of the box through both surfaces. The total outflow is given by the sum of the flows through the two surfaces. However, the orientation along φ is such that the flux at φ_2 is positive, while the flux at φ_1 is negative, and the total outflow is $F(\varphi_2) - F(\varphi_1)$. This is just the respective continuity equation,

$$\int_{\varphi_1}^{\varphi_2} \partial_t \rho(\varphi) d\varphi + F(\varphi_2) - F(\varphi_1) = 0. \quad (4.67)$$

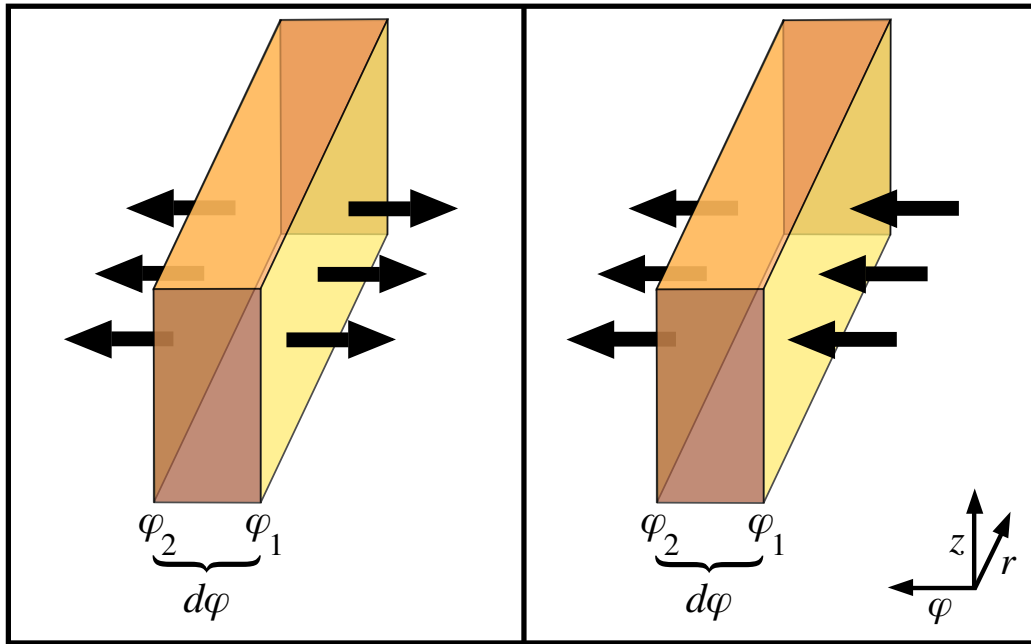


Figure 4.22: Illustration of the angular flux through a box. The surfaces $\varphi = \varphi_1$, $r \in (0, \infty)$, $z \in (-\infty, \infty)$ and $\varphi = \varphi_2$, $r \in (0, \infty)$, $z \in (-\infty, \infty)$ are open, while all other surfaces are closed. Arrows indicate the flux direction relative to the open surfaces.

In contrast, $G(\varphi_1, \varphi_2)$ is related to the difference between the flux through the surfaces out of the box, because the integral of eqn. 4.66 may be approximated for small $\varphi_2 - \varphi_1$ by the product of average flux and box width,

$$G(\varphi_1, \varphi_2) \approx \frac{1}{\varphi_2 - \varphi_1} \frac{1}{2} (F(\varphi_1) + F(\varphi_2)) (\varphi_2 - \varphi_1) \quad (4.68)$$

$$= \frac{1}{2} (F(\varphi_1) + F(\varphi_2)). \quad (4.69)$$

Again, note that due to the induced directionality the sum of $F(\varphi_1)$ and $F(\varphi_2)$ is just the difference of the fluxes out of the volume. For the case shown in the left-hand side of Fig. 4.22, $G(\varphi_1, \varphi_2)$ tells how much more (or less) is flowing through the plane at φ_2 than is flowing through the plane at φ_1 .

If the volume becomes smaller, the left-hand side of Fig. 4.22 represents a very special case: it may only happen that density flows out of a volume through both sides for situations where there is a plane of zero flux between φ_2 and φ_1 . Thus, in the limit $d\varphi = \varphi_2 - \varphi_1 \rightarrow 0$, this may only happen at single points and does not contribute to the integral.

The right-hand side of Fig. 4.22 shows one of the two generic cases for small volumes, where there is some flow into the volume at φ_1 and some flow out of the volume at φ_2 . The second possible case is when the flow is in the reverse direction, and one of the two situations is present whenever the volume is in between two zero net flux surfaces. Consequently, $G(\varphi_1, \varphi_2)$ is the average flux through the box. The sum of all those fluxes,

$$G = G(-\pi, \pi) = \frac{1}{2\pi} \int j_\varphi(r, \varphi, z) dr d\varphi dz, \quad (4.70)$$

can be seen as the sum of infinitely many $G(\varphi_i, \varphi_{i+1})$ for neighboring boxes,

$$G \approx \sum_i G(\varphi_i, \varphi_{i+1}) \quad (4.71)$$

4.3. Proton tunneling in the formic acid dimer and in malonaldehyde

with $-\pi \leq \varphi_i < \varphi_{i+1} \leq \pi$. These fluxes may either be in positive or negative φ -direction (or zero). Consequently, G represents the average flux along φ .

If φ was not an angular variable but a Cartesian variable x and if the density becomes zero for $|x| \rightarrow \infty$ (i.e., if the density is confined within some finite box), a $G > 0$ represents a net flux of the system towards positive x -direction, together with a net motion of the system, and a shift of the center of mass as well as a net linear momentum in positive x -direction. By the requirement of conservation of linear momentum, and for a system of zero initial linear momentum along x , $G = 0$ for all times. Similarly, for the angular variable φ a $G > 0$ represents a net flux of the system along positive φ -direction. However, this net flux is not necessarily connected with an angular momentum expectation value different from zero: Eqn. 4.61 and eqn. 4.70 differ by a factor of r^2 , and thus the integral over r in general gives different results for G than for $\langle \hat{l}_z \rangle$.

A comparison of eqn. 4.61 (and its derivation in section 2.3.4) with eqn. 4.70 shows that the average angular flux G is essentially the expectation value of an operator $\hat{\omega}_z$,

$$2\pi G = \langle \hat{\omega}_z \rangle = \frac{1}{m} \left\langle \frac{\hat{l}_z}{r^2} \right\rangle = \left\langle \frac{\hat{l}_z}{x_1^2 + x_2^2} \right\rangle. \quad (4.72)$$

The operator $\hat{\omega}_z$ is the angular momentum operator divided by the operator for the moment of inertia around the z -axis, mr^2 . Thus, it is the quantum mechanical analogue of the z -component of the classical angular velocity vector

$$\boldsymbol{\omega} = \frac{\mathbf{x} \times \mathbf{v}}{|\mathbf{x}|^2} = \frac{\mathbf{x} \times \mathbf{p}}{m|\mathbf{x}|^2}. \quad (4.73)$$

The eigenfunctions of $\hat{\omega}_z$ are similar to the known eigenfunctions of \hat{l}_z , and are given by

$$\Gamma_n(r, \varphi, z) = f(r, z) r^2 \exp\left(\frac{inr^2}{a_0^2} \varphi\right) \quad (4.74)$$

with some undetermined function $f(r, z)$ and with the Bohr radius a_0 . The Bohr radius is used here only for convenience: More appropriately, the fundamental constants \hbar , m_e (the electron mass), ϵ_0 (the permittivity of vacuum) and e (the elementary charge) could be used via [94]

$$a_0 = \frac{4\pi\epsilon_0\hbar^2}{m_e e^2}. \quad (4.75)$$

The quantum number n is an integer, $n = 0, \pm 1, \pm 2, \dots$, and the eigenvalues of $\hat{\omega}_z$ are determined by operation of $\hat{\omega}_z$ on Γ_n as

$$\hat{\omega}_z \Gamma_n = \frac{n\hbar}{ma_0^2} \Gamma_n. \quad (4.76)$$

Although $\hat{\omega}_z$ is Hermitian and commutes with \hat{l}_z , it does neither commute with the square of the total angular momentum operator nor with the Hamiltonian (see below). Thus, its observable is not a constant of motion, and there is no apparent reason why the expectation value of $\hat{\omega}_z$ should have any particular value for pericyclic reactions in the electronic ground state, even though it might be tempting to assume it to be zero. In the following, it shall be investigated how $\langle \omega_z \rangle$ changes with time and what the dynamics of this expectation value depends on.

The time dependence of $\langle \omega_z \rangle$ can be calculated using Ehrenfest's theorem [146],

$$\partial_t \langle \hat{\omega}_z \rangle = \frac{1}{i\hbar} \langle [\hat{\omega}_z, H] \rangle. \quad (4.77)$$

To evaluate the commutator, the one-particle Hamiltonian

$$H = -\frac{\hbar^2}{2m}\partial_{\mathbf{x}}^2 + V(\mathbf{x}) \quad (4.78)$$

in cylindrical coordinates will be used. The Laplacian $\partial_{\mathbf{x}}^2$ is then

$$\partial_{\mathbf{x}}^2 = \frac{1}{r}\partial_r r \partial_r + \frac{1}{r^2}\partial_\varphi^2 + \partial_z^2, \quad (4.79)$$

and thus

$$H = -\frac{\hbar^2}{2m}\partial_z^2 - \frac{\hbar^2}{2mr}\partial_r r \partial_r + \frac{\hat{l}_z^2}{2mr^2} + V. \quad (4.80)$$

Because $\hat{\omega}_z$ commutes with \hat{l}_z and ∂_z^2 , the commutator of eqn. 4.77 reduces to

$$[\hat{\omega}_z, H] = \frac{\hat{l}_z \hbar^2}{2m^2 r} \left(\partial_r r \partial_r \frac{1}{r^2} - \frac{1}{r^2} \partial_r r \partial_r \right) + \frac{\hbar \partial_\varphi V}{imr^2}. \quad (4.81)$$

The potential term $\hbar \partial_\varphi V / (imr^2)$ is entirely complex for real potentials and will not contribute to the time dependence of G , as shown below. Straightforward calculations for the other terms of eqn. 4.81 give

$$\partial_r r \partial_r \frac{1}{r^2} = \partial_r \left(\frac{\partial_r}{r} - \frac{2}{r^2} \right) = \frac{1}{r^2} \left(r \partial_r^2 - 3\partial_r + \frac{4}{r} \right) \quad (4.82)$$

for the first term in the brackets and

$$\frac{1}{r^2} \partial_r r \partial_r = \frac{1}{r^2} (\partial_r + r \partial_r^2) \quad (4.83)$$

for the second one. The second derivatives cancel and the commutator between the angular velocity operator and the Hamiltonian is

$$[\hat{\omega}_z, H] = \frac{2\hat{l}_z \hbar^2}{m^2 r^3} \left(\frac{1}{r} - \partial_r \right) + \frac{\hbar \partial_\varphi V}{imr^2}. \quad (4.84)$$

Next, this expression is inserted in eqn. 4.77 and $\hat{l}_z = -i\hbar \partial_\varphi$ is used. The expectation value is taken with respect to an arbitrary wave function ϕ ,

$$\begin{aligned} \partial_t \langle \hat{\omega}_z \rangle &= \frac{1}{i\hbar} \int \phi^* [\hat{\omega}_z, H] \phi r dr d\varphi dz \\ &= \frac{2\hbar^2}{m^2} \int \left(\phi^* \frac{1}{r^2} \partial_\varphi \partial_r \phi - \frac{\phi^* \partial_\varphi \phi}{r^3} \right) dr d\varphi dz. \end{aligned} \quad (4.85)$$

In the second line it was already used that

$$\int \frac{\hbar \partial_\varphi V}{imr^2} d\varphi = \frac{\hbar}{imr^2} (V(\pi) - V(-\pi)) = 0 \quad (4.86)$$

by the periodic boundary conditions. The potential does not influence $\partial_t G$ directly, but via the wave functions which are used to compute the expectation value at a given time.

A number of partial integrations will now be applied to eqn. 4.85 in order to investigate the meaning of this equation. The first term in the brackets is split in two equal parts which

4.3. Proton tunneling in the formic acid dimer and in malonaldehyde

may be written as

$$\begin{aligned}
\int \phi^* \frac{1}{r^2} \partial_\varphi \partial_r \phi dr &= \frac{1}{2} \int \left(\phi^* \frac{1}{r^2} \partial_\varphi \partial_r \phi + \phi^* \frac{1}{r^2} \partial_\varphi \partial_r \phi \right) dr \\
&= \frac{1}{2} \int \phi^* \frac{1}{r^2} \partial_\varphi \partial_r \phi dr - \frac{1}{2} \int (\partial_\varphi \phi) \partial_r \frac{\phi^*}{r^2} dr \\
&= \frac{1}{2} \int \phi^* \frac{1}{r^2} \partial_\varphi \partial_r \phi dr - \frac{1}{2} \int (\partial_\varphi \phi) \frac{1}{r^2} \partial_r \phi^* dr + \int \frac{\phi^* \partial_\varphi \phi}{r^3} dr. \quad (4.87)
\end{aligned}$$

From the first to the second line, a partial integration was performed for r and the result was evaluated in the third line. Using eqn. 4.87 with eqn. 4.85 will remove the second term in the brackets of eqn. 4.85, giving

$$\partial_t \langle \hat{\omega}_z \rangle = \frac{\hbar^2}{m^2} \int \frac{1}{r^2} (\phi^* \partial_\varphi \partial_r \phi - (\partial_\varphi \phi) (\partial_r \phi^*)) dr d\varphi dz. \quad (4.88)$$

The integration over φ can be used to identify

$$\int \frac{1}{r^2} (\partial_\varphi \phi) (\partial_r \phi^*) d\varphi = - \int \frac{1}{r^2} \phi \partial_\varphi \partial_r \phi^* d\varphi, \quad (4.89)$$

so that

$$\begin{aligned}
\partial_t \langle \hat{\omega}_z \rangle &= - \frac{\hbar^2}{m^2} \int \frac{1}{r^2} ((\partial_\varphi \phi) (\partial_r \phi^*) + (\partial_\varphi \phi^*) (\partial_r \phi)) dr d\varphi dz \\
&= \frac{\hbar^2}{m^2} \int \frac{1}{r^2} (\phi \partial_\varphi \partial_r \phi^* + \phi^* \partial_\varphi \partial_r \phi) dr d\varphi dz \\
&= - \frac{2}{m} \text{Re} \langle \hat{\omega}_z \hat{p}_r \rangle \quad (4.90)
\end{aligned}$$

with the linear momentum operator in r -direction,

$$\hat{p}_r = \frac{\hbar}{i} \frac{1}{r} \partial_r. \quad (4.91)$$

The factor $1/r$ was included in the definition of \hat{p}_r to make the operator hermitian. Note, however, that although both $\hat{\omega}_z$ and \hat{p}_r are hermitian, their product is not, and taking the real part of $\langle \hat{\omega}_z \hat{p}_r \rangle$ in eqn. 4.90 is necessary.

Eqn. 4.90 shows that the time dependence of the average angular velocity, and thus of the average angular flux G , depends on both the change of the wave function along r and along φ . To proceed a bit further, in analogy to the discussion of section 2.3.3 the polar representation $\phi = A \exp(iS/\hbar)$ with $A, S \in \mathbb{R}$ will be used together with the first line of eqn. 4.90. Then

$$(\partial_\varphi \phi^*) (\partial_r \phi) = \left(\partial_r A + \frac{i}{\hbar} A \partial_r S \right) \left(\partial_\varphi A - \frac{i}{\hbar} A \partial_\varphi S \right) \quad (4.92)$$

and

$$(\partial_\varphi \phi^*) (\partial_r \phi) + (\partial_\varphi \phi) (\partial_r \phi^*) = 2(\partial_r A) (\partial_\varphi A) + \frac{2}{\hbar^2} A^2 (\partial_r S) (\partial_\varphi S). \quad (4.93)$$

Inserting this result into eqn. 4.90, it follows that

$$\partial_t \langle \hat{\omega}_z \rangle = - \frac{2\hbar^2}{m^2} \int \frac{(\partial_r A) (\partial_\varphi A)}{r^2} dr d\varphi dz - 2 \int \frac{A^2}{r^2} (\partial_r S) (\partial_\varphi S) dr d\varphi dz. \quad (4.94)$$

In cylindrical coordinates, the components of the velocity field $\mathbf{v} = \partial_{\mathbf{q}} S/m$ of 2.3.3 are

$$v_r = \frac{1}{m} \partial_r S \quad (4.95)$$

in r -direction and

$$v_\varphi = \frac{1}{m} \frac{1}{r} \partial_\varphi S \quad (4.96)$$

in φ -direction. Also, $A^2 = \phi\phi^*$, and thus the second term of eqn. 4.94 can be written as

$$\begin{aligned} \int \frac{A^2}{r^2} (\partial_r S) (\partial_\varphi S) dr d\varphi dz &= \int \frac{A^2}{r^2} v_r v_\varphi dr d\varphi dz \\ &= \int \frac{1}{r^2} j_r v_\varphi dr d\varphi dz = \int \frac{1}{r^2} v_r j_\varphi dr d\varphi dz. \end{aligned} \quad (4.97)$$

While the first term of eqn. 4.94 represents the product of the changes of the length of ϕ with respect to both φ and r , the second term shows that the change in $\langle \hat{\omega}_z \rangle$ with time depends on the flux density in both φ - and r -direction. Note that the flux density in z -direction (which has to conserve linear momentum in this direction) does not play a role.

To summarize, the preceding calculations showed that $G = \langle \hat{\omega}_z \rangle / (2\pi)$, the average flux in φ -direction, is neither directly related to the expectation value of the angular momentum in φ -direction nor does it have a simple time dependence. Although this average flux depends only on the flux density in φ -direction, its time dependence is both related to the dynamics in φ - and r -direction. Nevertheless, there has to be a change of the flux direction along φ , and in the following it will be investigated how much the reaction mechanism depends on the exact location of the change of direction.

4.3.4 Model systems formic acid dimer and malonaldehyde

The systems to be investigated are proton transfer in malonaldehyde and double proton transfer in the formic acid dimer, in the coherent tunneling regime. In both systems there is a mirror symmetry for the nuclei at certain times, but not during the whole reaction. In consequence, there are no symmetry-enforced zero-flux surfaces, and the fluxes are not completely known for both reactions.

Fig. 4.23 shows Lewis structures of the reactions as well as some possible reaction mechanisms. As in the previous cases, for both of these reactions at least three mechanisms can be drawn, as indicated in the figure. These mechanisms may be called hydride transfer (M1/F1), hydrogen atom transfer (M2/F2) and proton transfer (M3/F3), depending on the direction of motion of the electron density close to the transferred proton: In the case of hydride transfer, both the proton and the electron density in the vicinity of the proton move in the same direction. For atom transfer, electron density moves only partly in the direction of the proton motion, while for proton transfer, the electron density and the proton move into opposite directions. For the discussion both processes will be called proton transfer, but after investigation of the reaction mechanism the terminology (hydride transfer vs. hydrogen atom transfer vs. proton transfer) will be reconsidered.

Due to the missing mirror symmetry compared to the previous processes in benzene and cyclooctatetraene, the unidirectional processes M1/F1 and M3/F3 may not be excluded: Although a process that is only unidirectional must be excluded due to the constraint of zero electronic angular momentum, it is still possible that the process is mainly unidirectional and thus well represented by the first and third mechanism.

The time-dependent electron densities for these model systems were obtained by using the coherent tunneling theory for a double well as explained in section 4.1.3. Tunneling times and tunneling splittings were not calculated, because they are not necessary in this model: For the analysis the time-dependent electron density is needed. The tunneling period only changes the time scale on which the tunneling happens, but not the time-evolution of the electron density relative to the tunneling period. Specifically, the time-dependent electron

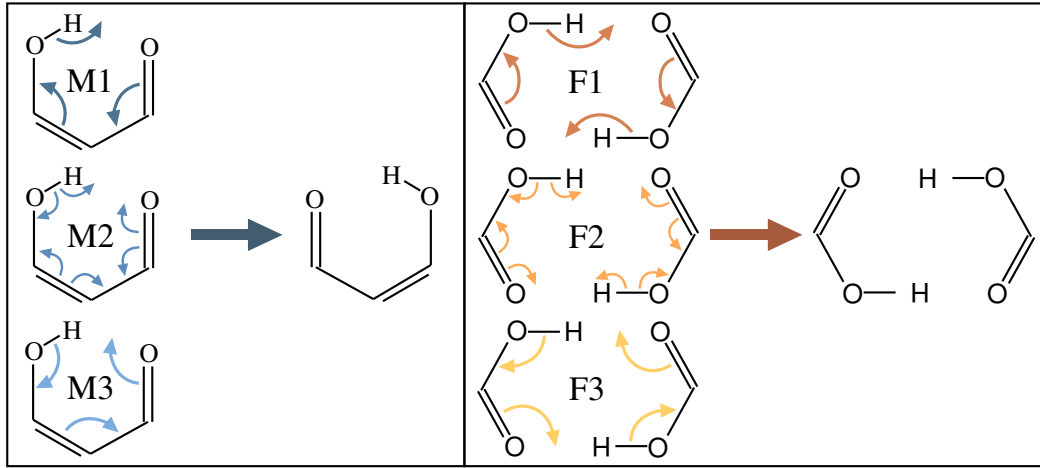


Figure 4.23: Lewis structures for the proton transfer in malonaldehyde (left) and the double proton transfer in the formic acid dimer (right). Different possible reaction mechanisms (M1, M2, M3 and F1, F2, F3) are indicated by arrows.

density is given by

$$n(t, \varphi) = n_{\text{R}}(\varphi) \cos^2(\Delta Et/(2\hbar)) + n_{\text{P}}(\varphi) \sin^2(\Delta Et/(2\hbar)) \quad (4.98)$$

for the one-electron density of the reactant configuration n_{R} and that of the product configuration n_{P} . The tunneling time is $\tau = \hbar/(2\pi\Delta E)$. Below, all times in units of the tunneling time, and thus the graph of n is the same for all tunneling times.

The initial one-electron densities $\rho_{\text{R}}(\mathbf{x}, \mathbf{Q})$ for construction of $n_{\text{R}}(\varphi)$ were obtained with a Hartree-Fock structure optimization employing a cc-pVTZ basis set [70], using the program MOLPRO [225]. Note that accurate energies of the structures were not needed. Also, previous experience showed that the electronic fluxes as well as the electron densities are rather robust with respect to the details of the nuclear structure. The equilibrium structure of the two molecules is already well enough described with the Hartree-Fock calculation for the purposes here, see Appendix E.

The product structure was determined from the reactant structure by the constraint of zero nuclear angular momentum during the reaction. To find the product structure, the nuclei were first reflected at some plane perpendicular to the molecular plane. Thereafter, the nuclei of the reflected molecule were assigned to the nuclei of the reactant molecule by minimizing the distance between each pair of nuclei of the same type. Finally, the reflected structure was obtained from momentum conservation by assuming a linear reaction path from reactants to products. The classical angular momenta along the axis perpendicular to the molecular plane are

$$L_Z = \sum_i M_i (X_i \partial_t Y_i - Y_i \partial_t X_i), \quad (4.99)$$

with the masses M_i and coordinates in the molecular plane, $X_i(t)$ and $Y_i(t)$, of the nuclei i . Initially, at $t = 0$, the reactant structure $X_i^{\text{R}}, Y_i^{\text{R}}$ is present, while after quarter of the tunneling time, $t = \tau/4$, the product structure $X_i^{\text{P}}, Y_i^{\text{P}}$ is present. For intermediate times, $t \in [0, \tau/4]$, the nuclear coordinates are approximated as

$$\begin{aligned} X_i(t) &= \frac{4}{\tau} \left(t X_i^{\text{P}} + \left(\frac{\tau}{4} - t \right) X_i^{\text{R}} \right) \\ Y_i(t) &= \frac{4}{\tau} \left(t Y_i^{\text{P}} + \left(\frac{\tau}{4} - t \right) Y_i^{\text{R}} \right). \end{aligned} \quad (4.100)$$

The sum of the classical angular momenta along the path from reactants to products shall be zero,

$$\int L_Z dt \stackrel{!}{=} 0. \quad (4.101)$$

Consequently, by inserting $\partial_t X_i$ and $\partial_t Y_i$ from eqn. 4.100,

$$\begin{aligned} 0 &= \int_0^{\tau/4} \sum_i M_i (X_i \partial_t Y_i - Y_i \partial_t X_i) dt \\ &= \int_0^{\tau/4} \sum_i \frac{4M_i}{\tau} (X_i (Y_i^P - Y_i^R) - Y_i (X_i^P - X_i^R)) dt \end{aligned} \quad (4.102)$$

follows. Next, X_i and Y_i from eqn. 4.100 are inserted. The individual contributions to eqn. 4.102 are

$$\begin{aligned} X_i (Y_i^P - Y_i^R) &= \frac{4}{\tau} \left(t X_i^P + \left(\frac{\tau}{4} - t \right) X_i^R \right) (Y_i^P - Y_i^R) \\ &= X_i^R Y_i^P - X_i^R Y_i^R + \frac{4t}{\tau} (X_i^P Y_i^P - X_i^P Y_i^R - X_i^R Y_i^P + X_i^R Y_i^R) \end{aligned} \quad (4.103)$$

and

$$\begin{aligned} Y_i (X_i^P - X_i^R) &= \frac{4}{\tau} \left(t Y_i^P + \left(\frac{\tau}{4} - t \right) Y_i^R \right) (X_i^P - X_i^R) \\ &= X_i^P Y_i^R - X_i^R Y_i^R + \frac{4t}{\tau} (X_i^P Y_i^P - X_i^P Y_i^R - X_i^R Y_i^P + X_i^R Y_i^R), \end{aligned} \quad (4.104)$$

which differ only in the first terms, $X_i^R Y_i^P$ and $X_i^P Y_i^R$, respectively. Thus, eqn. 4.102 becomes

$$\begin{aligned} 0 &= \int_0^{\tau/4} \sum_i M_i \frac{4}{\tau} (X_i^R Y_i^P - X_i^P Y_i^R) dt \\ &= \sum_i M_i (X_i^R Y_i^P - Y_i^R X_i^P) \end{aligned} \quad (4.105)$$

is obtained from which the product structure can be determined.

Fig. 4.24 illustrates the change of the nuclear positions from reactants to products. It is found that for malonaldehyde there is very little change from reactants to products for all nuclei but the tunneling proton. In the case of the formic acid dimer, next to the motion of the tunneling protons also the oxygen nuclei move, but directed radially out- or inwards. This motion is not expected to affect the angular electron density much, because the angles at which the oxygen nuclei are located do almost not change.

Proton tunneling in malonaldehyde and in the formic acid dimer have been investigated a number of times, see e.g. [22, 32, 59, 130, 137, 190, 209, 218, 222, 232]. These studies show that in order to describe tunneling in both molecules correctly, several nuclear coordinates need to be taken into account. This is because the process described is a transfer of a light nucleus between two heavies nuclei, and for such systems the intrinsic reaction path (path of steepest descent between reactant and product) is strongly curved [100, 232]. For malonaldehyde, in [232] a full-dimensional potential energy surface was constructed. During this construction it was found that to describe tunneling correctly, a three-dimensional space around the intrinsic reaction path, spanned by a ring deformation coordinate, an OH-stretching coordinate and a bond alternation coordinates, needs to be used. For the formic acid dimer, in [137] it was found that again the space around the intrinsic reaction path is three-dimensional, spanned by an asymmetric hydrogen-transfer mode as well as a symmetric and an anti-symmetric ring deformation mode. Also, it was found that inclusion of

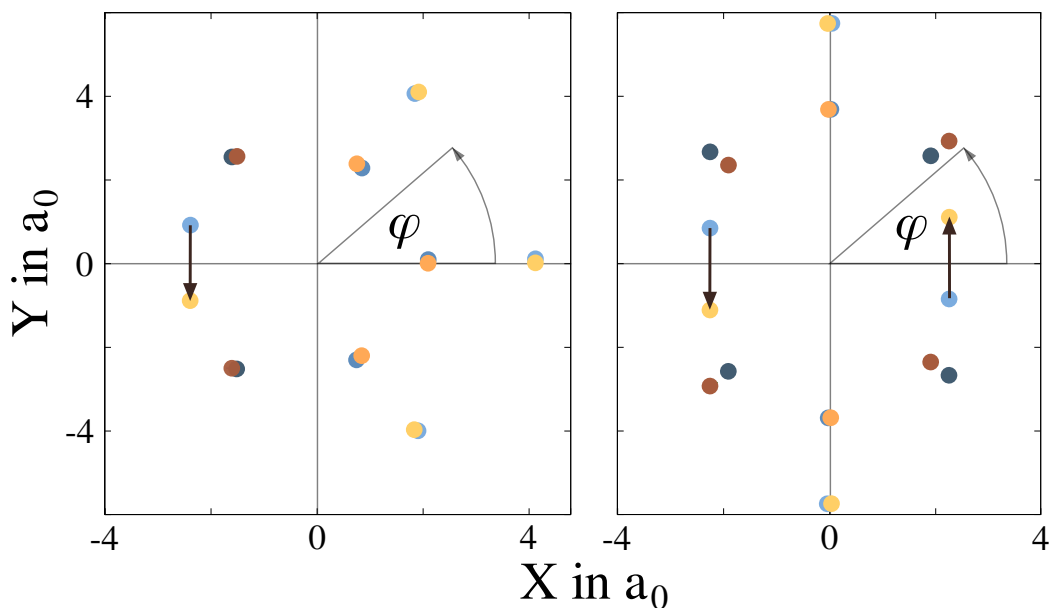


Figure 4.24: Position of the nuclei for the reactants (blue dots) and products (yellow/orange/brown dots) for proton tunneling in malonaldehyde (left) and double proton tunneling in the formic acid dimer (right). The motion of the tunneling protons is indicated by arrows. The angle $\varphi \in (-\pi, \pi]$ of the cylindrical coordinates for the electrons is also shown, counted positive in the indicated direction.

another two modes describing the dissociative motion of the dimer did influence the tunneling dynamics. However, in the current work only the circular electron dynamics along an angle is of importance. Thus, to investigate the reaction mechanism the proposed coherent tunneling model should suffice to capture the effective dynamics. It would nevertheless be interesting to compare with a dynamics simulation using the spaces spanning the intrinsic reaction path.

The static one-dimensional electron density $n_R(\varphi)$ is obtained from $\rho_R(\mathbf{x})$ with cylindrical coordinates $\mathbf{x} = (r, \varphi, z)$, with $z = 0$ being the molecular plane and φ as indicated in Fig. 4.24, as

$$n_R(\varphi) = \iint \rho_R(\mathbf{x}) r dr dz. \quad (4.106)$$

$n_P(\varphi)$ is determined analogously. For this integration, the density ρ_R was not calculated using cylindrical coordinates $\mathbf{x} = (r, \varphi, z)$, but represented on Cartesian grids $\mathbf{x} = (x_1, x_2, x_3)$, as explained in section 3.4. For both molecules, $600 \times 600 \times 300$ points were used. Only half of these points were calculated because the mirror symmetry in x_3 -direction could be exploited. The space covered is $x_1, x_2 \in [-11, 11]a_0$ and $x_3 \in [-5.5, 5.5]a_0$. However, although the grid spacing was as small as $0.037 a_0$, spherical averaging as explained in section 3.4 was needed to obtain data smooth enough for computation of the fluxes. Thus, the molecule was rotated in 20 steps from 0 to π around the z -axis and the electron density obtained from these calculation was averaged. Last, fitting of the density using a Fourier series was performed as explained in section 3.4.

Time-dependent one-dimensional electron densities $n(t, \varphi)$ were calculated for valence and π -electrons, for both molecules. Fig. 4.25 and Fig. 4.26 show the molecular orbitals included in the π -electron densities.

For the formic acid dimer, there are four π -molecular orbitals. Two of them extend from one oxygen of a formic acid molecule to the other oxygen of the molecule, but with larger electron density at the position of the carbon-oxygen double bond. The other two are localized at the two carbon atoms of each formic acid dimer and have a nodal plane which passes close to the position of the carbon atom.

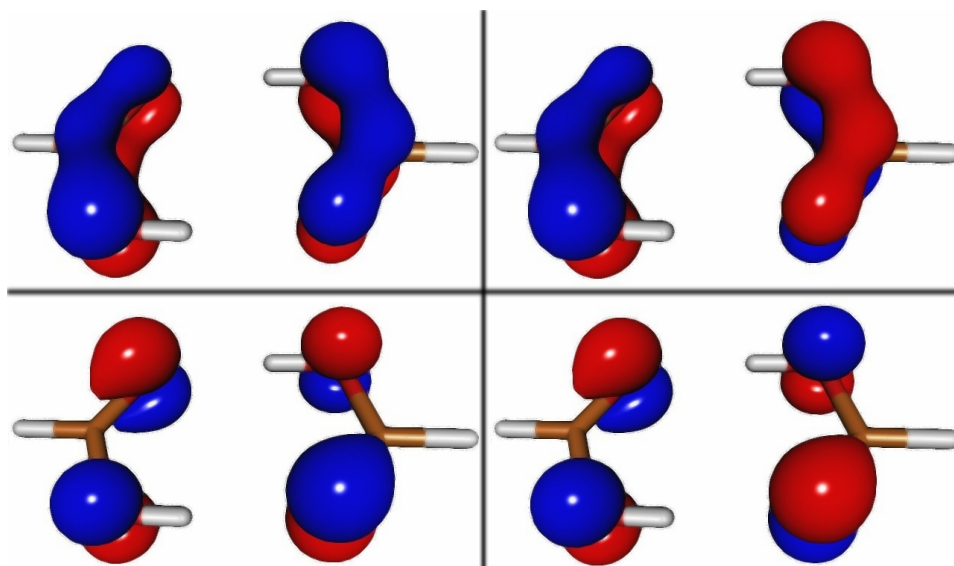


Figure 4.25: Orbitals included in the π -electron density for the formic acid dimer, obtained from a Hartree-Fock calculation with cc-pVTZ basis set, using the program Molpro [225].

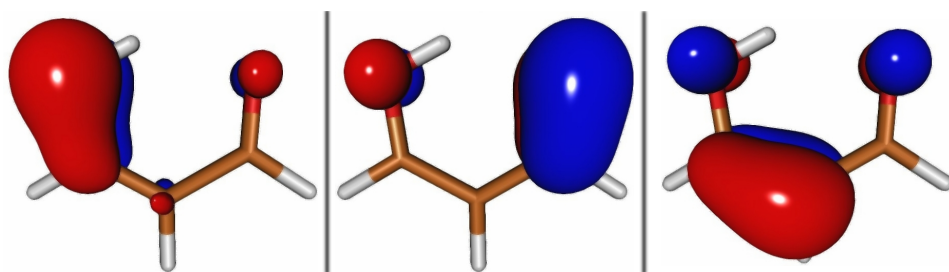


Figure 4.26: Orbitals included in the π -electron density for malonaldehyde, obtained from a Hartree-Fock calculation with cc-pVTZ basis set, using the program Molpro [225].

For malonaldehyde, there are three π -molecular orbitals. Two of them (the central and right part of Fig. 4.26) are located at the position of the two double bonds, but with some density also at the position of the oxygen(s). The third one is mainly located at the position of the oxygen of the hydroxyl group, but with some density also at the nearby carbon as well as at the other oxygen.

Consequently, the π -orbitals included in the π -density consist of the double bonds of the molecules as well as of the π -orbitals at the oxygen nuclei. If only the time dependence of the double bonds is of interest, one might apply an orbital localization scheme like that of Boys [38] or Pipek-Mezey [175]. However, also after such a localization it might be questionable to look at only part of the π -orbitals and draw conclusions. Hence, in the following only the well-defined π -density including all the π -orbitals will be discussed.

The final one-dimensional electron densities $n(t, \varphi)$ are each represented on a grid with 200 points for the time from zero to one tunneling period, and with 2000 point for the angular variable from $-\pi$ to π .

4.3.5 Results I: Fluxes from the density and the resulting mechanisms

The time-dependent electron densities and the fluxes obtained from the continuity equation will be discussed. For analysis of the reaction mechanism, the electron density is partitioned into core and valence electrons. As seen in the previous examples, the core electrons can be

4.3. Proton tunneling in the formic acid dimer and in malonaldehyde

expected to stay at the positions of the nuclei and their motions are not of interest for the reaction mechanism. For the valence electrons, especially the behavior of the π -electrons is of interest, and thus the valence electrons are separated into π - and other valence electrons. This decomposition gives rise to separate fluxes for each of those sets of electrons. Thus, there are also separate time-dependent flux parameters. For the discussion, a flux parameter $c^\pi(t)$ for the π -electrons and a flux parameter $c^{\text{oval}}(t)$ for the other valence electrons is used. The flux parameter for the valence electrons is $c^{\text{val}}(t) = c^\pi(t) + c^{\text{oval}}(t)$.

For analysis of the reaction mechanisms with respect to the behavior of the flux parameter, the following steps are taken:

- At first, the parameters are chosen such that the average flux along φ is zero. In this reference situation there is no net flux in one direction. The initial value of the integration of the continuity equation is chosen such that in this case $c^{\text{oval}}(t) = c^\pi(t) = c^{\text{val}}(t) = 0$ for all times. The resulting mechanisms are discussed for both molecules.
- Next, it is discussed how stable the qualitative mechanism is with respect to the specific choice of the flux parameters and to what degree the position of the zero-flux surfaces may vary.
- Finally, the quantitative mechanism is determined for the reference case, i.e. bond sectors are defined and fluxes into or out of the bond sectors are calculated.

General statements about the densities and fluxes for both molecules

Snapshots of the time-dependent one-electron densities n^π , n^{oval} and n^{val} as well as of the corresponding π -, other valence and valence electron fluxes F^π , F^{oval} and F^{val} for the proton tunneling are shown for the formic acid dimer in Fig. 4.27 and for malonaldehyde in Fig. 4.28. The fluxes were calculated as

$$F^\pi(t, \varphi) = - \int_{\varphi_0}^{\varphi} \partial_t n^\pi(t, \varphi') d\varphi' + c^\pi(t), \quad (4.107)$$

and

$$F^{\text{val}}(t, \varphi) = - \int_{\varphi_0}^{\varphi} \partial_t n^{\text{val}}(t, \varphi') d\varphi' + c^{\text{val}}(t), \quad (4.108)$$

respectively. Note that the integration starts from $\varphi_0 \neq -\pi$, and that for $\varphi < \varphi_0$ the cyclic boundary conditions are used. The parameters c^π and c^{val} depend on φ_0 , and thus φ_0 is chosen such that $c^\pi = 0$ and $c^{\text{val}} = 0$ have a convenient meaning. Specifically, these situations mean that the respective average flux along φ is zero, see below.

Although there are labels at the tick marks in the plot of the fluxes in Fig. 4.27 and Fig. 4.28, these labels are for now only meant to indicate the magnitude of flux differences. The absolute value of the fluxes is in general unknown, because the flux parameters $c^\pi(t)$ and $c^{\text{val}}(t)$ are unknown. Especially the position of the zero of the fluxes is unknown, and thus the angle at which zero-flux surfaces occur and where the direction of the flux is reversed are unknown.

Both Fig. 4.27 and Fig. 4.28 show the density and fluxes at 0, quarter of the tunneling time, half of the tunneling time, and three-quarters of the tunneling time. After one tunneling time, the dynamics repeats as if it was $t = 0$. Note that all densities are normalized to the number of the respective electrons.

Initially as well as after half the tunneling time, there is constant flux independent of the angle. Because there shall be no unidirectional flux, at these times the flux has to be zero and the tick marks in the figures indeed represent the values of the fluxes. The flux parameters

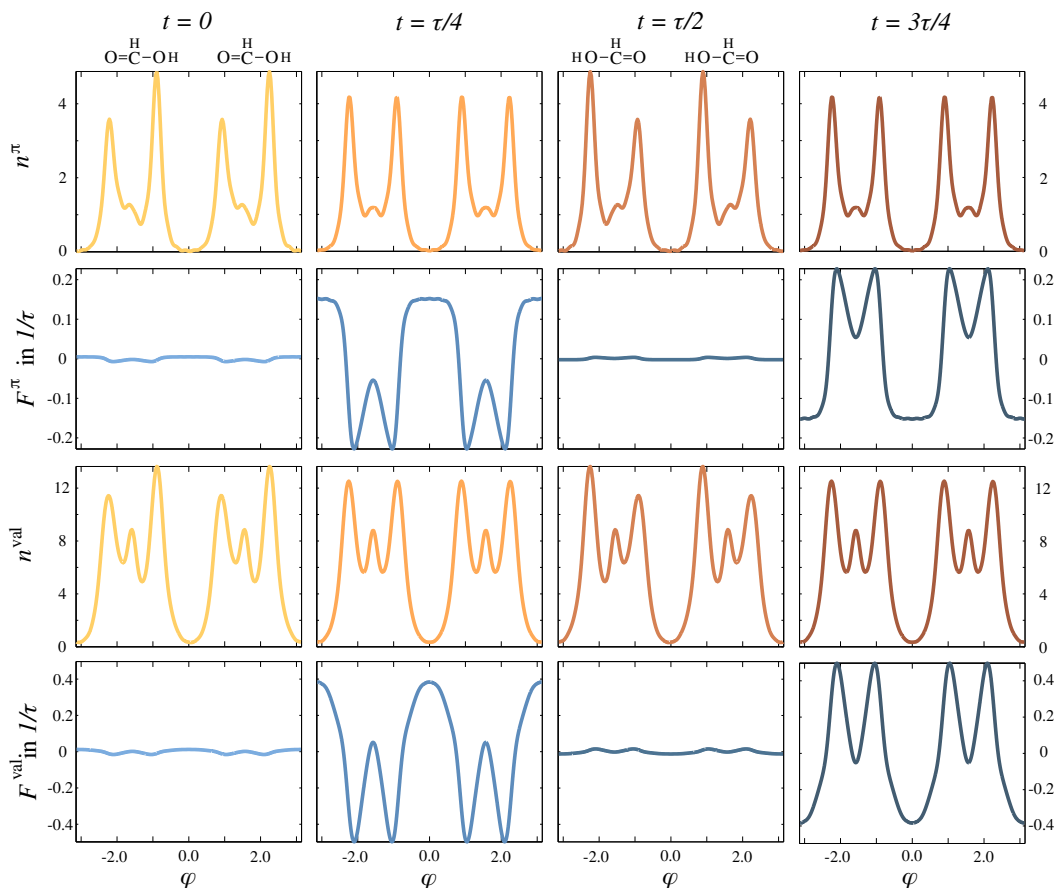


Figure 4.27: Angular densities $n(t, \varphi)$ and fluxes $F(t, \varphi)$ for π -electrons (top half) and valence electrons (bottom half) at times $t = 0, \tau/4, \tau/2$ and $3\tau/4$, for double proton transfer in the formic acid dimer. At $t = 0$ and $t = \tau/2$ the nuclei corresponding to the peaks in the density are shown above the graphs. The labels at the ticks for the graphs of the fluxes are determined only up to a constant in φ , which may be different for each time (see text for explanation). Here, the constant is determined such that $\int F d\varphi = 0$, or that the average angular flux is zero.

have to be zero, $c^\pi(k\tau/2) = 0$ and $c^{\text{val}}(k\tau/2) = 0$ for $k = 0, 1, 2, \dots$. Note that in the figures the flux is not exactly zero. This is because the fluxes were calculated numerically from the time-derivative of the densities using finite differences. The time step used was $\Delta t = \tau/200$. Thus, to be precise, the fluxes shown in the figures do not correspond to $t = 0, \tau/4, \dots$, but to these times shifted by half the time step, $t = \Delta t/2, \tau/4 + \Delta t/2, \dots$.

After one quarter and three-quarters of the tunneling time the nuclear structure is quite symmetric: In case of malonaldehyde there is one mirror plane perpendicular to the nuclear plane at $\varphi = 0$, and in case of the formic acid dimer there are two such mirror planes, at $\varphi = 0$ and $\varphi = \pi/2$. However, in contrast to the mirror planes present in the models of benzene and cyclooctatetraene, the mirror planes found here are not persistent in time. Consequently, no statement about the zero-flux surfaces and the flux parameters can be made from these mirror planes. Thus, in Fig. 4.27 and Fig. 4.28 the fluxes at $t = \tau/4$ and $t = 3\tau/4$ are indeed only determined up to a constant in the angle.

In the formic acid dimer there are eight π -electrons and 36 valence electrons. In Fig. 4.27 the highest peaks of the density correspond to the position of the oxygen nuclei, while the smaller peaks in between the two pairs of large peaks corresponds to the carbon nuclei (or the CH-groups between the pairs of oxygen nuclei). Also, at times $t = 0$ and $t = \tau/2$ the position of the CO-double bond can be easily identified, because at the corresponding angles the density is larger compared to angles corresponding to a single bond. For example, at

4.3. Proton tunneling in the formic acid dimer and in malonaldehyde

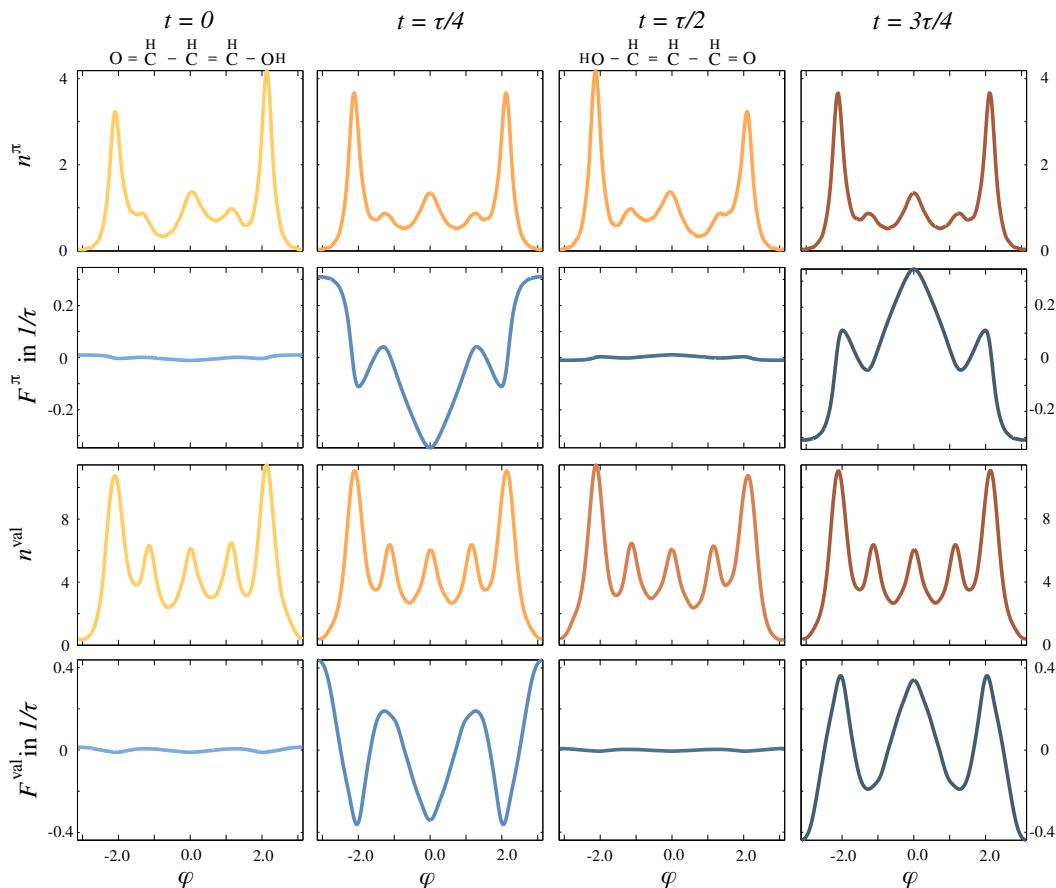


Figure 4.28: Angular densities $n(t, \varphi)$ and fluxes $F(t, \varphi)$ for π -electrons (top half) and valence electrons (bottom half) at times $t = 0, \tau/4, \tau/2$ and $3\tau/4$, for proton tunneling in malonaldehyde. At $t = 0$ and $t = \tau/2$ the nuclei corresponding to the peaks in the density are shown above the graphs. The labels at the ticks for the graphs of the fluxes are determined only up to a constant in φ , which may be different for each time (see text for explanation). Here, the constant is determined such that $\int F d\varphi = 0$, or that the average angular flux is zero.

$t = 0$ the density n^π shows a local minimum between the (from left to right) first large and second small local maximum. The value of this local minimum is larger than that of the next minimum. The first local minimum corresponds to the location of the CO-double bond, while the second corresponds to the single bond connecting a carbon nucleus with the OH-group.

This feature can also be seen in the valence electron density, albeit less pronounced due to the larger number of other electrons. Although the locations of the maxima close to the oxygen nuclei are similar for the π - and the valence electron density, the locations of the maxima close to the carbon nuclei change a bit: For the π -electrons, the maximum at the carbon position is slightly closer to oxygen of the CO-double bond as compared to the respective maximum for the valence electrons.

At $t = \tau/4$ the density is completely symmetric and the amplitudes of the fluxes are maximal, while at $t = \tau/2$ the initial situation is reversed. Note that there is both more π - and valence electron density at the position of the oxygen nucleus of the hydroxyl group than there is at the position of the oxygen nucleus of the aldehyde group. The approximate position of the hydrogen nucleus cannot be inferred from the density because of the absence of a corresponding peak. It is buried in the shoulders of the oxygen peak. Due to the hydrogen nucleus there is some small density at $\varphi = 0, \pi$ in case of the valence electrons, while there is none in case of the π -electrons.

For malonaldehyde, there are six π -electrons and 28 valence electrons. In Fig. 4.28 the

positions of the oxygen and carbon nuclei are apparent by peaks in the electron density, like for the formic acid dimer. Double bonds are distinguishable from single bonds by higher values of the local minima. As in the case of the formic acid dimer, the position of the peaks in the π - and valence electron density does almost not change, except for the carbon peak of the CO-double bond. The peak is slightly closer to the corresponding oxygen peak for the π -electron density than it is for the valence electron density. As for the formic acid dimer, the position of the tunneling proton cannot be directly seen. It manifests itself only in the small but non-zero density at $\varphi = \pi$ in the valence electron density as compared to the zero π -electron density at this position.

To characterize the complete tunneling process it is enough to consider the fluxes until $t = \tau/4$: From the flux $F(t, \varphi)$ in the interval $t \in [0, \tau/4]$, the flux in the interval $t \in [\tau/4, \tau/2]$ can be obtained as

$$F(t, \varphi) = F(\tau/2 - t, \varphi) \quad \text{for } t \in [0, \tau/2]. \quad (4.109)$$

Similarly, the flux up to $t = \tau$ can be obtained as

$$F(t, \varphi) = -F(\tau - t, \varphi) \quad \text{for } t \in [0, \tau]. \quad (4.110)$$

In the following only the fluxes until $t = \tau/4$ are discussed.

The reference case $c(t) = 0$

The position of the zero for the fluxes in Fig. 4.27 and Fig. 4.28 was chosen deliberately: The fluxes were shifted such that the sum of the fluxes, $\int F(\varphi)d\varphi$, is zero, which is equivalent to zero average angular flux. This situation is called the reference situation, and for this choice $c(t)$ is defined to be zero for all times. For the time being, the dependence of the flux parameter c on the start of the integration in eqn. 4.58 is made explicit again. By eqn. 4.58 (or eqn. 4.107 and eqn. 4.108),

$$\begin{aligned} 0 &\stackrel{!}{=} \int F(t, \varphi)d\varphi \\ &= - \int_0^{2\pi} \int_{\varphi_0}^{\varphi} \partial_t n(t, \tilde{\varphi})d\tilde{\varphi}d\varphi + 2\pi c(t, \varphi_0) \end{aligned} \quad (4.111)$$

and thus

$$c(t, \varphi_0) = \frac{1}{2\pi} \int_0^{2\pi} \int_{\varphi_0}^{\varphi} \partial_t n(t, \tilde{\varphi})d\tilde{\varphi}d\varphi. \quad (4.112)$$

The value of φ_0 is chosen such that the first line of eqn. 4.111 is fulfilled if $c(t, \varphi_0) = 0$.

The expectation value of the angular velocity operator $\hat{\omega}_z$ and the average angular flux G are related by

$$\langle \hat{\omega}_z \rangle = \int F(t, \varphi)d\varphi = 2\pi G. \quad (4.113)$$

Thus, for the just defined reference situation, $c(t) = 0$ is equivalent to $\langle \hat{\omega}_z \rangle = 0$ and $G = 0$, i.e. to zero average angular flux. Also, if $c(t) > 0$, the sum of all angular fluxes becomes positive, and thus there is an average angular flux in the direction of positive φ . If $c(t) < 0$, the sum of all angular fluxes is negative, and there is an average angular flux in the direction of negative φ .

The value of $c(t)$ depends on φ_0 , the start of the integration over $\partial_t n$. Consequently, by choosing the definition of $c = 0$ by a global property, namely, the result of an integral, φ_0 becomes a function of time: The integration has to start at an angle where $F = 0$, and this angle may change with time. However, in practice for this definition of $c = 0$ the position of φ_0 does not change with time within an accuracy of $\pi/1000$.

4.3. Proton tunneling in the formic acid dimer and in malonaldehyde

Fig. 4.29 and Fig. 4.32 show the densities and fluxes for the π -, other valence and all valence electrons at $t = \tau/4$ for the formic acid dimer and for malonaldehyde, respectively. These pictures are for the reference case, $c^\pi = c^{\text{oval}} = c^{\text{val}} = 0$. In the figures, the locations of the zero-flux surfaces are shown by vertical lines. As just mentioned, they do not change with time within an accuracy of $\pi/1000$. Also, the fluxes from $t = 0$ up to $t = \tau/4$ rise almost linearly, and fluxes between $t = 0$ and $t = \tau/4$ would just show the same qualitative behavior as shown in Fig. 4.29 and Fig. 4.32, but with smaller amplitude, cf. eqn. 4.98. Consequently, depiction of these intermediate fluxes is omitted.

The reference case $c(t) = 0$ is expected to be already a good approximation to the true dynamics. This is because of the shape and dynamics of the electron density. The expectation value of the angular momentum around the z -axis,

$$\langle l_z \rangle = \iiint j_\varphi r^2 dr d\varphi dz, \quad (4.114)$$

and the average angular flux G with

$$2\pi G = \iiint j_\varphi dr d\varphi dz \quad (4.115)$$

differ by the weighting of the angular flux density j_φ (which, in the cases discussed here is equivalent to the angular flux $F(t, \varphi)$) with respect to the radial distance.

During dynamics in the electronic ground state, the electrons in proximity of the nuclei move in the direction of the nuclei. This was shown for the examples of tunneling in cyclooctatetraene and nuclear dynamics of benzene along the Kekulé mode, and it holds also for proton tunneling in malonaldehyde and in the formic acid dimer. The electron density is distributed mainly torus- or doughnut-like around the approximate circle on which the nuclei are located. The nuclear motion conserves the expectation value of the angular momentum, which is zero for all processes discussed here. Then, for each radial distance r the contributions of the angular flux density at this distance can be expected to cancel approximately,

$$f(r) = \iint j_\varphi d\varphi dz \approx 0. \quad (4.116)$$

While eqn. 4.114 is zero by electronic angular momentum conservation, eqn. 4.115 is also approximately zero, and thus also

$$c(t) \approx 0. \quad (4.117)$$

Moreover, as the electron density is (to a very good approximation) confined to a cylinder with some radius r_{max} , the generalized mean value theorem for integrals can be used. Because r^2 does not change sign for $r \in [0, r_{\text{max}}]$, it holds that [47]

$$\langle l_z \rangle = \int f(r) r^2 dr = f(\tilde{r}) \int_0^{r_{\text{max}}} r^2 dr = \frac{r_{\text{max}}^3}{3} f(\tilde{r}) \quad (4.118)$$

for some $0 < \tilde{r} < r_{\text{max}}$. Zero expectation value of the electronic angular momentum for ground state reactions, $\langle l_z \rangle = 0$, means that for \tilde{r} the integral of j_φ over the φ and z is zero, $f(\tilde{r}) = 0$. The function $f(r)$ does not vary much for the electron densities of interest, as explained above. Thus, eqn. 4.117 should, in the cases to be discussed, be a good approximation.

That the average angular flux should not be too different from zero should be a very good approximation for the core electrons, which are distributed almost spherically around the nuclei. Thus, these are excluded from the following discussion, and only the valence electrons are investigated. However, partitioning of the valence electrons into π - and other

valence electrons does partition the flux parameter $c^{\text{val}}(t)$ in an arbitrary way. Nevertheless, because also π - and other valence electron density move together with the nuclei (albeit with different speed), and because their densities are also mainly torus- or doughnut-like distributed, their individual flux parameters should also be close to zero. However, the approximation that $c^\pi(t) \approx 0$ and $c^{\text{oval}}(t) \approx 0$ is certainly worse than the approximation that $c^{\text{val}}(t) = c^\pi(t) + c^{\text{oval}}(t) \approx 0$, which should be kept in mind during the following discussion. Also, for different, more complicated systems (when the electron density is not mainly centered around one ring, e.g. when there are larger substituents than just hydrogens at the carbon nuclei of the ring) this approximation may not hold.

Reaction mechanism for double proton tunneling in the formic acid dimer

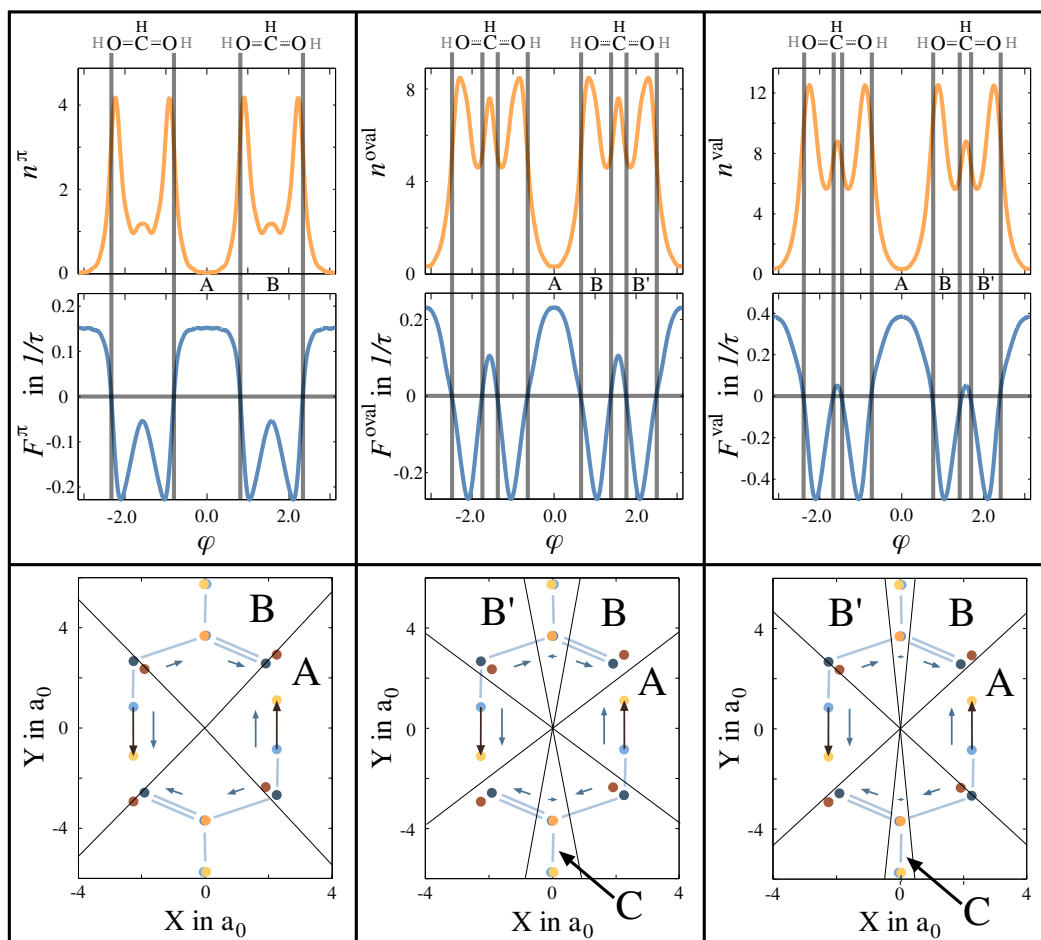


Figure 4.29: Angular densities $n(t, \varphi)$ and fluxes $F(t, \varphi)$ for π -electrons (top left), the other valence electrons (top center) and all valence electrons (top right) at $t = \tau/4$, for double proton tunneling in the formic acid dimer. Horizontal lines in the flux plots indicate $F = 0$ (the flux parameters c^π , c^{oval} and c^{val} , and thus the respective average angular fluxes were chosen to be zero) and vertical lines indicate the position of the zero-flux surfaces. Below, the initial and final nuclear positions are shown as in Fig. 4.24, with initial Lewis structure (light blue), zero-flux surfaces (black lines, left for π -electrons, middle for the other valence electrons, and right for all valence electrons) and flux directions (blue arrows). Dark arrows indicate motion of the tunneling protons. Sectors A, B, B' are bound by zero-flux surfaces, sector C is between B and B'.

For the formic acid dimer, Fig. 4.29 shows that the choice $c^\pi = 0$ leads to four zero-flux surfaces for the π -electron density, but $c^{\text{oval}} = 0$ leads to eight zero-flux surfaces for the other valence electron density. The valence electron density is just the sum of the two densities as are the fluxes, and there are also eight zero-flux surfaces at positions between those of the

4.3. Proton tunneling in the formic acid dimer and in malonaldehyde

π - and other valence electron density. The location of the zero-flux surfaces relative to the initial and final nuclear configuration is also shown in the figure as well as the flux direction in terms of arrows.

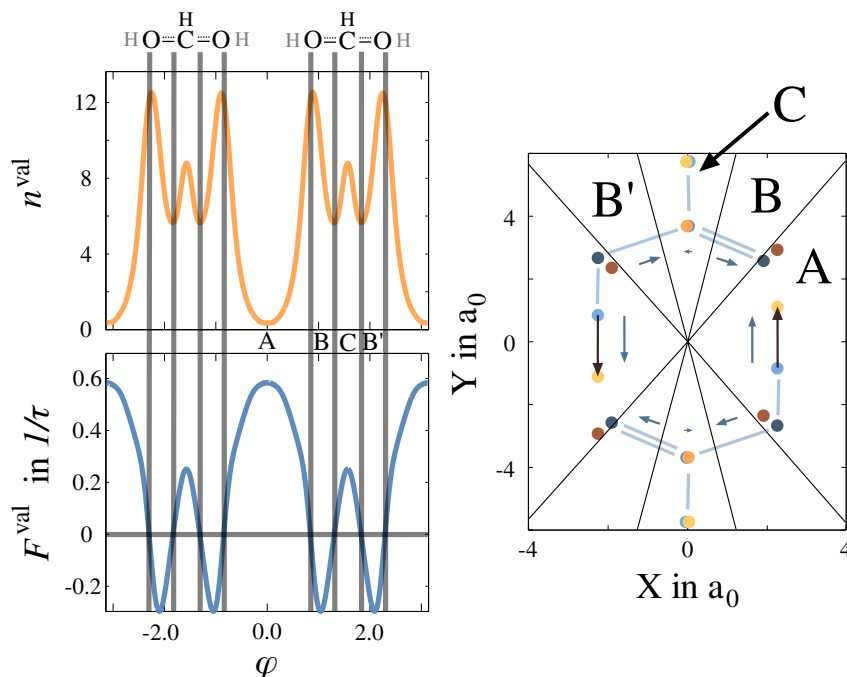


Figure 4.30: Left: Angular density $n(t, \varphi)$ and flux $F(t, \varphi)$ for valence electrons at $t = \tau/4$, for double proton transfer in the formic acid dimer. The horizontal line in the flux plots indicates $F = 0$ (the flux parameter is $c^{\text{val}} = 0.2$, and thus there is an average angular flux in direction of positive φ) and vertical lines indicate the zero-flux surfaces. Right: The initial and final nuclear positions are shown as in Fig. 4.24, with initial Lewis structure (light blue), zero flux surfaces (black lines, left for π -electrons, right for valence electrons) and flux directions (blue arrows). Dark arrows indicate motion of the tunneling protons. Sectors A, B, B' are bound by zero-flux surfaces, sector C is between B and B'.

Bound by the zero-flux surfaces, there are four regions for the π -electron flux and eight regions for the other valence and all valence electron flux. However, only two (A and B in the figure) and four (A, B and B' in the figure, and C between B and B') regions are not symmetry equivalent for the π - and (other) valence electrons, respectively.

For the π -electrons, the zero-flux surfaces pass very close to the position of the oxygen nuclei. Region A contains the tunneling proton, and the π -electron flux is in the direction of motion of the tunneling proton. The flux first rises strongly, then reaches a plateau, and finally drops strongly again. However, this region also contains hardly any π -electron density at all. Region B contains the CH-group. The π -electron flux is directed, surprisingly, from the initial carbon-oxygen single bond towards the initial carbon-oxygen double bond, which will become the single bond. The flux in this region has two local minima located at the center of the carbon-oxygen bonds, and a local maximum at the position of the CH-group. In the left bottom part of Fig. 4.29, the behavior in region B is indicated schematically using two arrows, as compared to the one arrow used to denote the flux for region A.

The local maximum in region B is smaller than zero for the π -electrons. However, for the other valence electrons it is larger than zero, and for all valence electrons it is larger than, but close to zero. Thus, compared to the π -electron fluxes a new region occurs in the center of region B. Thus, for the other valence electrons the sector B is split into two parts, B and B', and there is a sector C around the CH-group with opposite flux direction relative to B and B'. For all valence electrons, this sector does also exist, but it is very small.

The fluxes of the π -, other valence and all valence electrons are qualitatively similar, but the value of the flux parameter determines if the flux close to the CH-group is either just weaker than the flux between the CO-bonds, but with the same direction, or if there is a change of flux direction and the appearance of further zero-flux surfaces. In principle both cases are possible for π -, other valence and all valence electrons, depending on the actual value of the respective flux parameter. How different can the mechanism become?

The effect of a change of the flux parameter $c(t)$, and thus of the position of the zero of the fluxes, depends on the slope of the flux. For the zero-flux surfaces close to the position of the oxygen nuclei, the effect is rather small: The (absolute value of the) slope of the flux for a choice $c > 0$ (that means some average angular flux in direction of positive φ , or a shift of the zero line downwards relative to the graph of the fluxes) is large, and thus the zero-flux surface will always be close to the position of the oxygen nuclei. Changing $c = 0$ to its largest possible value, $c = 0.5$, will change the position of these surfaces by ca. 17° . However, such an extreme value of c is very unlikely in the electronic ground state and without interaction with external field, see the explanation above. A more realistic case, $c^{\text{val}} = 0.2$, is shown in Fig. 4.30. As can be seen from the figure, the respective zero-flux surfaces are still close to the oxygen nuclei. This statements hold also for $c^\pi < 0$. However, for $c^{\text{val}} < 0$ the (absolute value of the) slope of the flux is comparably small. If this is the case, region A may indeed become significantly smaller.

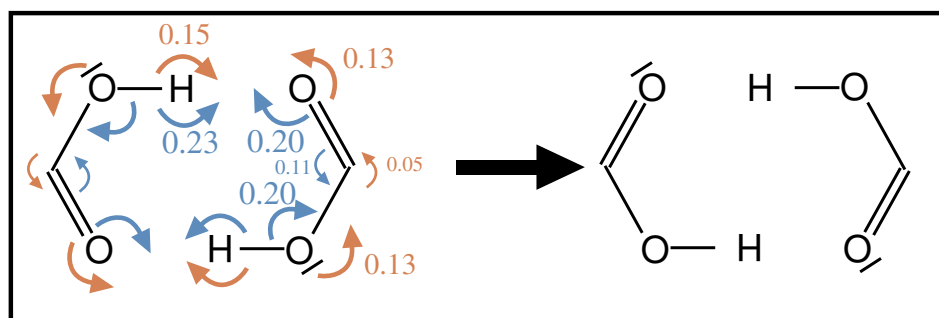


Figure 4.31: Mechanism of double proton tunneling in the formic acid dimer for the reference case of zero average angular flux and the flux parameter $c = 0$ at all times. Numbers and arrows (brown) outside the ring of the nuclei correspond to transferred π -electrons, while numbers and arrows (blue) inside the ring correspond to transferred other valence electrons from one bond sector to another. Boundaries of the bond sectors are defined by the mean values of initial and final position of the respective nuclei. The numbers of transferred electrons are shown for only half of the arrows, as the other equivalent arrows represent the same numbers. The sizes of the numbers and of the arrows indicate approximately the relative amount of electrons which are transferred.

In contrast to the relative stability of region A, region C and thus also region B and B' may vary strongly. The (absolute value of the) slope from a minimum of the flux to the local maximum at the position of the CH-group is comparably small: In this region, depending on the value of $c(t)$ the position of the zero flux surfaces may vary up to 32° . The two extreme cases are when either only region B exists but not region C, or when regions B and B' vanish almost completely, leaving a large region C. For $c^{\text{val}} = 0.2$, Fig. 4.30 shows that region C extends up to about one third of the carbon-oxygen single and double bond.

To analyze the reaction mechanism, fluxes into or out of bond sectors shall be used to represent the meaning of the arrows in Lewis structures. For the present tunneling processes, the definition of the bond sectors is slightly different from the previous definitions: For motion of benzene along the Kekulé mode, smooth bond sector boundaries were used defined by the nuclear wave function, while for tunneling in cyclooctatetraene a superposition of the

bond sectors of the initial and final structure were employed. In the two processes discussed here, the model does not yield a nuclear wave function, and the superposition of initial and final bond sectors is also not possible, because the individual bounding surfaces have to be used. Thus, a simple definition of the boundaries of the bond sectors is chosen: They correspond to the mean value of the angle of the nuclei of the ring at their initial and final position. As can be seen from Fig. 4.24, for all but the tunneling protons, the mean angle between initial and final position of the nuclei does almost coincide with the positions of the nuclei themselves, because they hardly move along φ .

For the reference case of zero average angular flux, the number of π - and other valence electrons moving from one bond sector to another one are shown in Fig. 4.31. As could already be inferred from the position of the zero flux surface and the shape of the flux, almost no π -electrons (0.05) and a small number of other valence electrons (0.11) move from the bond sector containing the initial carbon-oxygen double bond to the sector of the nascent carbon oxygen double bond, and the motion of the other valence electrons can be attributed to the motion of the proton of the CH-group into the nascent sector. There is a gain of both π -electrons and other valence electrons, of 0.13 and 0.20 electrons, respectively, coming from the bond of the initial hydroxyl group. The gain of π -electrons may be interpreted as coming from the lone pair at the oxygen nucleus of the hydroxyl group, while the other valence electrons come from the oxygen-hydrogen bond. The same number of π - and other valence electrons is also transferred from the double bond of the aldehyde group into the sector of the nascent hydrogen-carbon bond. The π -electrons are accumulated as the oxygen lone pair, while the other valence electrons are part of the nascent hydrogen-carbon bond. Finally, for the reference case 0.38 valence electrons accompany each tunneling proton. Compared to the total number of moving electrons, this is a significant amount. Thus, the process may be called double proton tunneling, but it may also be called double hydrogen atom tunneling because part of the electrons forming the nascent hydrogen-oxygen bond come from the initial hydrogen-oxygen bond. Interestingly, these electrons tunneling with the proton consist of 0.15 π -electrons and 0.23 other valence electrons. Thus, there is even some π -electron density moving together with the tunneling proton.

It shall be remarked that, to some extent, the static definition of the bond sectors precludes such effects as the compensation of flux of π -electrons out of a bond sector by flux of other valence electrons into the sector, and vice versa, as found in the previous examples. This is because the electrons close to a nucleus move in general in the direction of the nucleus, but with different speed. As the boundaries of the bond sector do not move or change with time, π - and other valence electrons should move in the same direction. The only exception is the bond sector boundary at the location of the CH-group, as the proton moves faster than the carbon nucleus relative to the sector boundary.

The mechanism of Fig. 4.31 is a reasonable guess of the mechanism without knowledge of the exact behavior of the average angular flux with time, as explained above. It is even better to look at all the valence electrons together, thus avoiding the somewhat arbitrary division of the flux parameter into two parts. It is worth to compare the present result of the overall valence electron flux with a study of Okuyama and Takatsuka on the mechanism of double proton transfer in the formic acid dimer [168]. This study is quite different from the case discussed here, because it is a dynamics study including electronically excited states, in contrast to the coherent tunneling model in the electronic ground state discussed here. In Okuyama's and Takatsuka's study, it was found that the net flow of electrons during proton transfer resembles the mechanism shown in Fig. 4.29 for the π -electrons or the qualitative mechanism shown in Fig. 4.31 (counting together the π - and other valence electrons): Electron density moves together with the proton, as well as from the oxygen

of the initial hydroxyl group to the oxygen of the initial aldehyde group. The study of Okuyama and Takatsuka is a dynamics study which uses semiclassical Ehrenfest dynamics to calculate first the dimerization and then the proton transfer. Although different from the study presented here, the similarity of the mechanisms found in the coherent tunneling limit and in the finite-temperature simulation is remarkable.

Reaction mechanism for proton tunneling in malonaldehyde

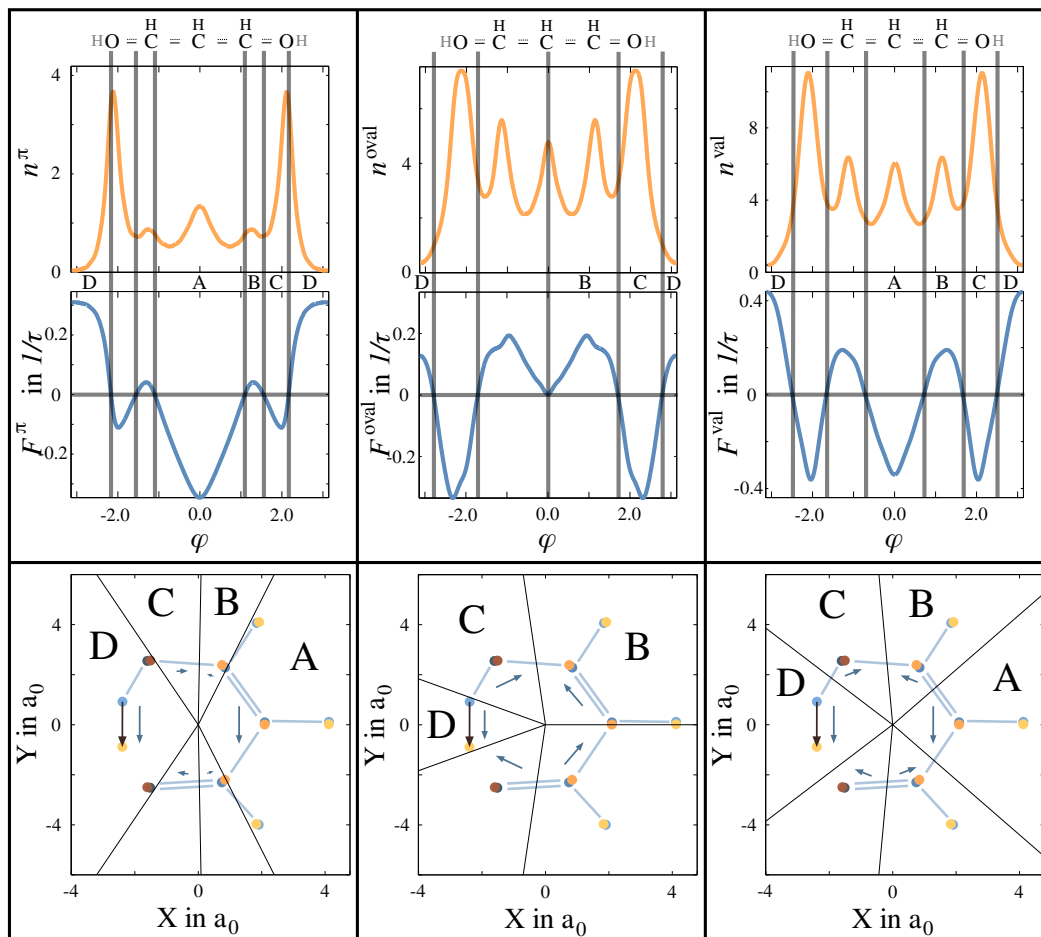


Figure 4.32: Angular densities $n(t, \varphi)$ and fluxes $F(t, \varphi)$ for π -electrons (top left), valence electrons (middle) and valence electrons except the π -electrons (top right) at $t = \tau/4$, for proton tunneling in malonaldehyde. Horizontal line in the flux plots indicates $F = 0$ (the average angular flux as well as the flux parameter c are zero) and vertical lines indicate the position of the zero-flux surfaces. Below, the initial and final nuclear positions are shown as in Fig. 4.24, with initial Lewis structure (light blue), position of the zero flux surfaces (black lines, left for π -electrons, middle for valence electrons, right for all valence electrons but the π -electrons) and flux directions (blue arrows). Dark arrow indicates motion of the tunneling proton. Sectors A, B, C, D are bound by zero-flux surfaces.

For malonaldehyde, in Fig. 4.32 the fluxes of π -electrons, valence electrons and the other valence electrons except the π -electrons are shown for zero average angular flux, $c^\pi = c^{\text{val}} = c^{\text{oval}} = 0$ (see eqn. 4.107, eqn. 4.108 and eqn. 4.111). For π - and valence electrons there are six zero-flux surfaces, and bound by these surfaces there are six regions. Four of them, labeled A, B, C and D in Fig. 4.32, are not symmetry-related. For the other valence electrons there are four normal zero-flux surfaces and one almost-zero-flux surface. Consequently, there are three different regions, labeled B, C and D. As in the case of the formic acid dimer, the location of the zero-flux surfaces for $c(t) = 0$ does not change with

time within an accuracy of $\pi/1000$.

Two of the zero-flux surfaces for the π -electrons pass close to both oxygen nuclei, while two pass close to the position of the nearby carbon nuclei. The last two pass through the carbon-hydrogen bond. In contrast, the zero-flux surfaces for all the valence electrons are different: They pass close to the center of the connections between neighboring nuclei of the ring. Thus, they pass through all bonds along the ring, but are not in close proximity of any nucleus. The zero-flux surfaces for the other valence electrons are located at the initial and final position of the tunneling proton, in the middle of the carbon-oxygen bonds, and at the position of the central CH-group.

The difference between the location of the zero-flux surfaces is explained by the shape of the fluxes. For all valence electrons, there are minima in regions A and C of approximately the same magnitude, and there is some significant flux in region B. For the π -electrons, the flux in region A is much stronger than the flux in region C. Also, the flux in region B is very small. As can be seen from the flux of the other valence electrons, the flux in region A in clockwise direction is due to the π -electrons.

In region D, which contains the tunneling proton, the electronic flux is always in the same direction as the tunneling proton, albeit there is some mechanistic difference between the π - and the other valence electrons, explained below. From the location of the zero-flux surfaces alone it follows that the π - and the total valence electron fluxes follow qualitatively the mechanism M2 of Fig. 4.23.

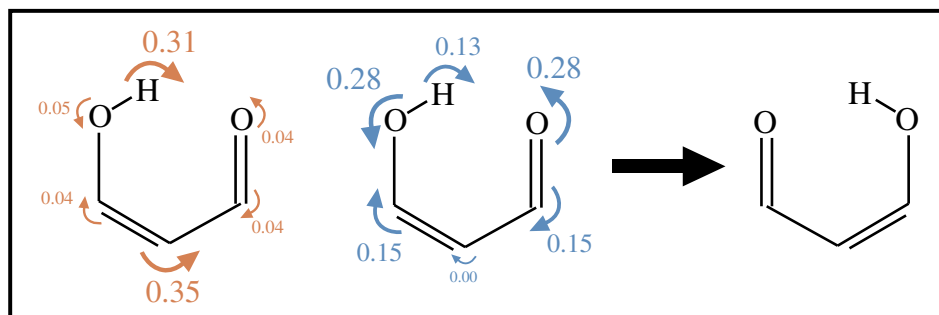


Figure 4.33: Mechanism of proton tunneling in malonaldehyde for the reference case of zero average angular flux and the flux parameter $c = 0$ at all times. Brown numbers and arrows in the left structure correspond to transferred π -electrons, while blue numbers and arrows in the central structure correspond to transferred other valence electrons from one bond sector to another. Boundaries of the bond sectors are defined by the mean values of initial and final position of the respective nuclei.

The effect of values of $c^\pi \neq 0$ and $c^{\text{oval}} \neq 0$ are very different, because the shape of the π -electron flux and the full valence electron flux is different. Note that a positive/negative value of c^π , c^{oval} and c^{val} means an average angular flux in direction of positive/negative φ , or a shift of the zero line downwards/upwards relative to the graph of the fluxes. For the π -electrons, already $c^\pi < -0.04$ would make region B disappear and regions A and C merge, while $c^\pi > 0.11$ would make region C disappear and regions B and D merge. These values of c^π have to be contrasted to the range of possible values, $-0.31 < c^\pi < 0.35$. This means that the qualitative reaction mechanism for the π -electrons is rather instable with respect to the value of c^π . Specifically, regions B and C contain initially the carbon-oxygen single bond that will become a double bond. Thus, for $c^\pi = 0$ the π -electrons forming the nascent double bond come from both the oxygen and the carbon nucleus (which is part of the carbon-carbon bond initially). For $c^\pi < -0.04$, the π -electrons come essentially from the oxygen only, while for $c^\pi > 0.11$ the π -electrons come from the initial carbon-carbon double bond.

In contrast, for the other valence electrons a $c^{\text{oval}} < 0$ would make region A appear,

while a $c^{\text{oval}} > 0$ would make the almost-zero-flux surface at the central CH-group disappear, but would otherwise not change the mechanism. For all valence electrons, the dependency on the flux parameter of π -electrons and other valence electrons cancel each other to some extent. The fluxes in regions B and C are stronger as they are for the π -electrons. With $c^{\text{val}} > 0$ regions A and C become smaller. The larger the value of c^{val} , the smaller these regions become, and for almost unidirectional fluxes (in direction of positive φ) region A vanishes. Region C cannot vanish unless the flux is unidirectional. Region B would vanish for $c^{\text{val}} < -0.19$, which is almost half of the minimal possible value $c^{\text{val}} < -0.44$. Thus, the qualitative mechanism for the valence electrons is rather stable with respect to the value of c^{val} .

For the reference case $c = 0$ (see eqn. 4.111), the numbers of electrons moving from one bond sector to another are determined as shown in Fig. 4.33. Again, the boundaries of the bond sectors are defined by the mean value of the angles of initial and final positions of the nuclei along the ring. From the reference case, one can deduce a number of interesting features of the reaction.

From the position of the zero-flux surfaces for the valence electrons it is apparent that the overall mechanism can be described as the mechanism M2 of Fig. 4.23, a mechanism similar to the motion of the electrons in the examples of the Kekulé mode of benzene and tunneling in cyclooctatetraene. However, the individual contributions of π - and other valence electrons are different. For the π -electrons, the only notable contributions are a flux from the region of the initial carbon-carbon double bond into the region of the nascent carbon-carbon double bond (0.35 electrons) and a flux together with the tunneling proton (0.31) electrons. Interestingly, there is little flux out of the sector belonging to the initial carbon-oxygen double bond towards the sectors of the nascent carbon-carbon double bond (0.04 electrons) and towards the nascent hydrogen oxygen bond (also 0.04 electrons). Consequently, there is little difference between the numbers of π -electrons in the sector for the lone pair at the hydroxyl group and for the double bond of the aldehyde group.

In contrast, the number of the other valence electrons moving from the initial carbon-carbon single bond towards the nascent carbon-carbon single bond is close to zero (0.003 electrons), and also the other valence electrons accompanying the tunneling proton is small (0.13 electrons) compared to the number of π -electrons. The flux of other valence electrons from the initial double bonds towards the sectors of the nascent double bonds is both 0.15 electrons. The strongest flux is away from the initial hydrogen-oxygen bond to the nascent carbon-oxygen double bond and vice versa, each accumulating to 0.28 electrons.

In summary, for proton tunneling in malonaldehyde a mechanism was found that could have been anticipated in advance, except for the interesting detail that there is significant π -electron motion accompanying the tunneling proton. This flux exists independent of the choice of the flux parameter (excluding the pathological case of making the flux of π -electrons unidirectional). It is found that for the reference case 0.44 valence electrons move together with the tunneling proton, which is a significant amount. Thus, the process may be called hydrogen atom transfer.

4.3.6 Cluster analysis of the electron density

A second approach to circumvent the lack of knowledge of the flux parameter is to make reasonable assumptions about the behavior of the angular fluxes. One possibility, inspired by applications in the field of classical molecular dynamics simulations of molecules, is to assume that the flux at some point is determined by the difference of the density at that point and the neighboring points. If such a behavior was assumed for the time-evolution of

the system, an incoherent equilibration would happen which at zero temperature (i.e. for the cases discussed in this work) would lead to no flux at all. However, the densities at different times are taken as given, and fluxes are determined such that the density at one time step is converted to the density at the next time step. The time-dependence of these densities fulfills the requirement of local conservation, and for the approach presented here the continuity equation is fulfilled. The fluxes are determined according to the average of the densities of neighboring points.

In the following, the assumptions to be made are explained in detail. The angular electron density is used as input, and in the end angular regions with large flux inside but little flux between them will be obtained. These regions, called clusters, can be used to find the location of minimal flux surfaces in this model. In the next section, the results of the method are compared for proton tunneling in malonaldehyde and for double proton tunneling in the formic acid dimer with the fluxes determined from the electron density and the continuity equation.

Roadmap

The time of conversion from reactants to products, here $t = [0, \tau/4]$, is partitioned into M intervals $[t_\alpha, t_{\alpha+1}]$ with $\tau/4 = t_M > \dots > t_1 = 0$. The number of time intervals is small, e.g. for the applications in the next section $M = 6$. The angular electron density $n(t, \varphi)$ is given at the times $t = t_\alpha$ and at N points φ_i , with $-\pi = \varphi_1 < \dots < \varphi_N = \pi$. Each of these points represents an interval in the angular space, which will in the following be called a sector. The column vector containing the N entries $n(t, \varphi_i) = n_i(t)$, i.e. the amount of density in the sectors, is denoted by $n(t)$.

The first step of the model is to construct a matrix $\tilde{P}(t_{\alpha+1}, t_\alpha)$ which transforms the density at time step t_α to the density at time step $t_{\alpha+1}$. It is constructed from the assumption that much density difference between two sectors leads to much flux, which is made precise below. The entry \tilde{P}_{ji} with $i \neq j$ tells how much density is moving from sector i to sector j from one time step to the next, and thus the entry \tilde{P}_{ij} tells how much density is moving from sector j to sector i in this time interval. Because there are fluxes to and out of the sector, \tilde{P} is called a gross transition matrix.

The density is interpreted as a classical probability density, and the gross transition matrix shall satisfy microscopic reversibility. The second step of the model is to construct a net transition matrix $P(t_{\alpha+1}, t_\alpha)$ from the gross transition matrix \tilde{P} . Elements P_{ji} of this matrix with $i \neq j$ contain the difference of the conditional probability of the electrons, relative to sector i , to move from sector i to sector j from t_α to $t_{\alpha+1}$ (i.e. \tilde{P}_{ji}) and the probability of the electrons to move from sector j to sector i in this time interval (obtained from \tilde{P}_{ji} and the densities in the sectors). By calculating this difference, it would hold that $P_{ji} = -P_{ij}$. The matrix shall, however, only contain information which represents from which place to which place the electron density moves. It thus shall have only positive entries, and negative entries are set to zero. The matrix P is approximately block diagonal or can be made approximately block diagonal by exchanging rows and columns in an appropriate way, and each block represents a range of sectors. Within this range of sectors, called clusters, there is a lot of flux, while between those sectors there is little flux.

In the third step, all those matrices $P(t_{\alpha+1}, t_\alpha)$ for the different times steps are used to construct a matrix T that represents the whole tunneling process as a reversible process. This matrix is analyzed by using its eigenvectors and a method called the robust Perron cluster analysis, which yields the clusters that tell at which angles there is a lot of flux, and where there is little flux.

Construction of the gross transition matrix

The gross transition matrix $\tilde{P}(t_{\alpha+1}, t_\alpha)$ shall transform the density at t_α to the density at $t_{\alpha+1}$,

$$n(t_{\alpha+1}) = \tilde{P}(t_{\alpha+1}, t_\alpha)n(t_\alpha). \quad (4.119)$$

The process of moving from one time step to the next is described by classical probability theory [46], and is assumed to be a homogeneous Markov process. For such a process, there exists in infinitesimal, time-independent generator matrix Q which is related to P by the Chapman-Kolmogorov equation [46, 109, 113]

$$\partial_t \tilde{P} = Q \tilde{P}(t). \quad (4.120)$$

Thus, \tilde{P} is obtained by Q as

$$\tilde{P}(t_{\alpha+1}, t_\alpha) = \exp((t_{\alpha+1} - t_\alpha)Q). \quad (4.121)$$

For the elements of Q it holds that

$$\begin{aligned} -Q_{ii} &< \infty \\ -Q_{ii} &= \sum_{j \neq i} Q_{ji}. \end{aligned} \quad (4.122)$$

Note that the off-diagonal elements are all positive, while the diagonal elements are all negative. The quantity $-Q_{ji}/Q_{ii}$ is the conditional probability of moving from sector i to sector j in an infinitesimally small time step, given the particle was initially in sector i [113]. Also, $-Q_{ii}$ is the rate of particles leaving sector i [113]. Hence, Q is called the instantaneous transition rate matrix, and by eqn. 4.121 it generates the transition matrix for the finite time interval from t_α to $t_{\alpha+1}$.

In principle, for small enough time steps the matrix \tilde{P} may always be written as eqn. 4.121, with the correct choice of Q . In practice, Q is unknown and may also not easily be derived from the Schrödinger equation in the Born-Oppenheimer approximation. Consequently, an assumption is made for the entries of Q .

A possibility to construct a Q such that the entries of \tilde{P} obtained from eqn. 4.121 meet the condition of microscopic reversibility, $n_i \tilde{P}_{ji} = n_j \tilde{P}_{ij}$, is to choose

$$Q_{ji} = \frac{1}{n_i} S_{ji}, \quad (4.123)$$

where S_{ji} is symmetric with respect to i and j [113]. In the following, the rates Q_{ji} from sector i to sector j are zero for non-neighboring sectors, and S is an average of the density of the sectors for neighboring sectors. The choice made here is that the rates are

$$Q_{ji} = \gamma \sqrt{n_j/n_i}, \quad j = i \pm 1. \quad (4.124)$$

This is the geometric mean of the densities in neighboring sectors, $\sqrt{n_j n_i}$, weighted by the amount of density in the starting sector i . Other averages, like the arithmetic or harmonic mean, were also tested but did not alter the results presented in the next section. Thus, they are not further discussed. Note that in a quantum mechanical system, eqn. 4.121 can only be approximately valid, and $Q_{ji} = 0$ for non-neighboring sectors does not follow automatically by continuity. Note also that Q depends on time, as the densities n_i depend on time. Thus, the condition of microscopic reversibility is fulfilled for each Q only at that given time step.

4.3. Proton tunneling in the formic acid dimer and in malonaldehyde

The constant γ with dimensions of inverse time is an unknown parameter. It is determined indirectly by ensuring that the second largest eigenvalue of Q has a certain value (the largest eigenvalue is zero). If the angular space is divided into two regions such that the flux between the two regions is as small as possible, the second largest eigenvalue of Q is the negative value of this flux [57]. It is not zero in the approach presented here, but small, and it has to be guessed. However, in practice, the algorithm used works only for some range of values for γ , and within this range the results are robust with respect to the specific γ .

By assumption, the instantaneous rate matrix Q may be different for each time interval $[t_\alpha, t_{\alpha+1}]$, but shall not change within the time interval. This condition is not met by a Q defined by eqn. 4.124, as the densities $n(t)$ depend on time. Thus, an average between Q at t_α and Q at $t_{\alpha+1}$ is used, and eqn. 4.121 is replaced by

$$\tilde{P}(t_{\alpha+1}, t_\alpha) \approx \exp\left((t_{\alpha+1} - t_\alpha) \frac{Q(t_\alpha) + Q(t_{\alpha+1})}{2}\right). \quad (4.125)$$

Using this \tilde{P} , eqn. 4.119 is not fulfilled exactly anymore. However, it is important that the continuity equation is fulfilled, and thus row and column rescaling by the method of Sinkhorn [193] is used to correct for this small error. As $\tilde{P}(t_{\alpha+1}, t_\alpha)$ is constructed by using the transition rate matrix at two different time steps, $Q(t_\alpha)$ and $Q(t_{\alpha+1})$, it does not fulfill the condition of microscopic reversibility anymore, although the individual rate matrices do with respect to the densities n_i at the respective time steps.

Construction of the net transition matrix

After obtaining the gross transition matrix \tilde{P} , the net transition matrix P can be constructed as the difference between forward and backward flux with respect to a given sector. The conditional probability of transition from sector i at time t_α to sector j at time $t_{\alpha+1}$, relative to sector i , is \tilde{P}_{ji} . (because the instantaneous rates Q_{ji} were always referred to the given sector, cf. eqn. 4.123). The conditional probability of transition from sector j at t_α to sector i at time $t_{\alpha+1}$, relative to sector i , can be obtained from \tilde{P}_{ij} as [46]

$$\tilde{P}'_{ji}(t_{\alpha+1}, t_\alpha) = \frac{n_j(t_\alpha)}{n_i(t_\alpha)} \tilde{P}_{ij}(t_{\alpha+1}, t_\alpha). \quad (4.126)$$

While \tilde{P}_{ji} may be called the yield of the forward flux, \tilde{P}'_{ji} may be called the yield of the backward flux. The net transition matrix is constructed from the difference between forward and backward flux, and it shall only contain the information from which place to which place the density moves. Thus, it is set to zero if the backward flux is larger than the forward flux. The off-diagonal elements of P are then given by

$$P_{ji}(t_{\alpha+1}, t_\alpha) = \max\left(\tilde{P}_{ji}(t_{\alpha+1}, t_\alpha) - \frac{n_j(t_\alpha)}{n_i(t_\alpha)} \tilde{P}_{ij}(t_{\alpha+1}, t_\alpha), 0\right). \quad (4.127)$$

The diagonal elements $P_{ii}(t_{\alpha+1}, t_\alpha)$ are determined by conservation of the density, i.e. such that the column sums of the matrix are equal to 1.

Off-diagonal entries of P tell how density is moving from one sector to another, and thus P can be used to find regions of large flux. But before this can be done, the matrix describing the overall process has to be made time-reversible, as there are different matrices P for transition from each time step to the next. This requirement is accomplished by construction

of a matrix T from $P(t_{\alpha+1}, t_\alpha)$ such that

$$T = \frac{1}{2} \begin{pmatrix} 0 & P(t_2, t_1) & 0 & \cdots \\ P(t_1, t_2) & 0 & P(t_3, t_2) & \cdots \\ 0 & P(t_2, t_3) & 0 & \cdots \\ \vdots & \vdots & \vdots & \ddots \end{pmatrix} \quad (4.128)$$

The factor $1/2$ is introduced because T shall also have the column sum 1. The matrix describing the process backward in time, $P(t_\alpha, t_{\alpha+1})$, is just the transpose of $P(t_{\alpha+1}, t_\alpha)$. It should be remembered that each $P_{ji}(t_{\alpha+1}, t_\alpha)$ represents the net probability of going from sector i at time t_α to sector j at time $t_{\alpha+1}$. The diagonal blocks of T are empty, as there is no transition if there is no change in the time step. Also, blocks of T corresponding to time steps which do not follow each other are also zero, as there shall be only transitions from the current time step to the next, or to the previous one.

Robust Perron Cluster Analysis PCCA+

The matrix P was designed such as to be used with the Robust Perron Cluster Analysis, called PCCA+ (Perron Cluster Cluster Analysis, the + stands for improvements regarding the original method) [63, 64]. This method is now described.

Along the angle φ , there are regions bounded with zero-flux surfaces, and there is flux inside this regions, but not between those regions. These regions will be called clusters in the following. The matrix T describing the complete process can, by appropriate row and column reordering under the condition of the cyclic boundary conditions, be made approximately block diagonal.

It is assumed for the time being that this matrix is exactly block diagonal. For example, there may be three different blocks \odot , \ominus and \otimes of sizes $m \times m$, $n \times n$ and $l \times l$, respectively, each representing one of the clusters. T has three eigenvectors with eigenvalue 1 (in this context, the eigenvalue 1 is called the Perron eigenvalue), because its column sum is 1 by construction. They are given by

$$\begin{pmatrix} \odot & 0 & 0 \\ 0 & \ominus & 0 \\ 0 & 0 & \otimes \end{pmatrix} \kappa = \kappa \quad (4.129)$$

as $\kappa_1 = (1_m, 0_n, 0_l)^T$, $\kappa_2 = (0_m, 1_n, 0_l)^T$ and $\kappa_3 = (1_m, 0_n, 0_l)^T$. Symbols like 1_m and 0_n represent vectors with m entries 1 or n entries 0, respectively, and each entry of the eigenvectors κ_i corresponds to one sector centered around an angles φ . Thus, if an entry of κ_i is equal to 1, the corresponding sector belongs to region i , and if it is equal to 0, it does not belong to this region. In case of infinitesimally small sectors along the angular coordinates φ , the matrix T becomes an operator, and the κ_i are eigenfunctions of this operator. These depend on time and angle, $\kappa_i(t, \varphi)$, and they are called membership functions, because they tell if a certain angle belongs to a given cluster i . In practice, the angular region is always partitioned into finite sectors, T is a matrix and the κ_i are vectors. Nevertheless, from now on they will be called membership functions.

All those membership functions are eigenvectors of T to the same eigenvalue, and other linear combinations of the membership functions are also eigenvectors. However, such a linear combination cannot be interpreted as a membership function anymore. Thus, to be a membership function, not only does κ_i need to be an eigenfunction of T , but it has also to consist only of ones and zeros.

4.3. Proton tunneling in the formic acid dimer and in malonaldehyde

The ones and zeros of κ_i are actually vectors. However, if the entries of all the κ_i are taken together, they may be considered as the corners of a so-called simplex. In the case of three blocks, above,

$$(\kappa_1 \kappa_2 \kappa_3) = \begin{pmatrix} 1 & 0 & 0 \\ 1 & 0 & 0 \\ \vdots & \vdots & \vdots \\ 0 & 1 & 0 \\ 0 & 1 & 0 \\ \vdots & \vdots & \vdots \\ 0 & 0 & 1 \\ 0 & 0 & 1 \\ \vdots & \vdots & \vdots \end{pmatrix} \quad (4.130)$$

and each row of this matrix defines the corner of a triangle. For four blocks, the rows of such a matrix would be the corners of a tetrahedron, which has triangles as its faces. For five blocks, the lines of this matrix would correspond to the four-dimensional simplex, which has tetrahedrons as its faces, and so forth. In general, for L eigenvectors to the eigenvalue one, the lines of this matrix correspond to the L corners of the respective simplex. An algorithm that searches for the eigenvalues of T with eigenvalue one will in general find linear combinations of the membership functions κ_i . Geometrically, such a linear combination represents a rotated and stretched simplex, and this can be exploited to find the membership functions.

The matrix in eqn. 4.130 is redundant, as the corners of the simplex are already given by the rows of the matrix

$$\begin{pmatrix} 1 & 0 & 0 \\ 0 & 1 & 0 \\ 0 & 0 & 1 \end{pmatrix}.$$

This matrix contains all points given by the rows of eqn. 4.130. It is quadratic, as there are as many corners of the considered simplex as there are entries in a row. Below, the eigenvectors will be determined from a matrix that is only approximately block diagonal. However, such a quadratic matrix can also be obtained by selecting some of the rows of the matrix constructed of its eigenvectors. The other rows of this matrix will not coincide with the selected rows, but if the selection is done as explained below, the points represented by these rows will be (almost) within the simplex.

By construction of T according to the recipe given above, the matrix T cannot be made exactly block diagonal, and the eigenvalues will only be approximately 1. Thus, a method is needed which, given some eigenvectors of T to an eigenvalue close to one, creates approximate membership functions which represent the probability of an angle to belong to a given cluster. The method used here is the Robust Perron Cluster Algorithm, called PCCA+ [63, 64]. This method uses the eigenvectors of P and the number of clusters to determine membership functions κ_i with entries between zero and one.

The number of clusters is simply the number of eigenvalues close to 1. Then, in order to find the membership functions κ_i , the geometrical picture sketched above is used in order to determine the corners of the rotated and stretched simplex. The individual set of points obtained from the L eigenvectors with eigenvalue close to 1 are not exactly on this deformed simplex, but close by. To find the L corners of the rotated and deformed simplex, the following steps are taken:

- For eigenvectors e_1, e_2, \dots, e_L , each being a column vector, the rows of the matrix

(e_1, e_2, \dots, e_L) are interpreted as data points.

- The data point farthest away from the origin is the first corner of the rotated and stretched simplex.
- The data point farthest away from the first corner is the second corner.
- The data point farthest away from the line connecting the first and second corner is the third corner.
- This procedure is repeated, always searching the data point farthest away in the space orthogonal to the existing shape, until there are L corners, i.e. there are as many corners as there are eigenvectors.
- Application of the inverse of the (quadratic $L \times L$) matrix containing all corners transforms the corners of the stretched and rotated simplex to the simplex itself. As by construction of the corners, these form an approximate convex hull for the other points (i.e. the other points are approximately within the shape generated by the corners), application of this inverse matrix to all data points yields points which are approximately within the simplex. These are the approximate membership functions $\kappa_1, \kappa_2, \kappa_3, \dots$.

The described steps are only a sketch of the method. For details, please refer to [63, 64].

4.3.7 Results II: Cluster analysis and the resulting mechanisms

The valence electron densities $n^{\text{val}}(t, \varphi)$ for the proton tunneling in malonaldehyde and in the formic acid dimer were used to calculate the rate matrix Q and the transition matrix P described in the previous section. These densities were obtained as described in section 4.3.4, with angular step size $\Delta\varphi = 0.025$. The results from section 4.3.5 will be compared with the present model, but only the valence electrons will be considered: Partitioning the electron density into contributions of core and valence electrons is not problematic for the unknown flux parameter. Further partitioning, however, introduces further arbitrariness, see definition of the reference case above.

The time of conversion from reactant to product was divided into six steps. For these steps, the instantaneous rate matrices Q and net transition matrices P were constructed, and the PCCA+ algorithm was applied to find a number of clusters along the angle φ . Within each cluster, electron flux is large, whereas flux between the clusters is small. The membership functions $\kappa_i(t, \varphi)$ giving the probability of an angle φ to belong to cluster i were determined for a parameter γ such that the smallest flux between two optimally chosen clusters is 0.04 per tunneling period, cf. the explanation after eqn. 4.124.

In Fig. 4.34, the membership functions $\kappa_i(t, \varphi)$ of the clusters are shown for both processes, for the six analyzed time steps from reactants to products. Note that by the method described above, a matrix T for all time steps is constructed, and the membership functions are calculated for all time steps simultaneously and thereafter divided into the six parts, each representing one time step. For proton tunneling in malonaldehyde five clusters were determined, while for double proton tunneling in the formic acid dimer four clusters were found. Except for the region of the tunneling proton, the membership functions at different time steps do almost not differ from each other.

For malonaldehyde, three clusters encompass a CH-group, while the other two are centered around the oxygen nuclei. As explained above, the angles corresponding to the transition region between two clusters are regions of minimal flux. Thus, close to where

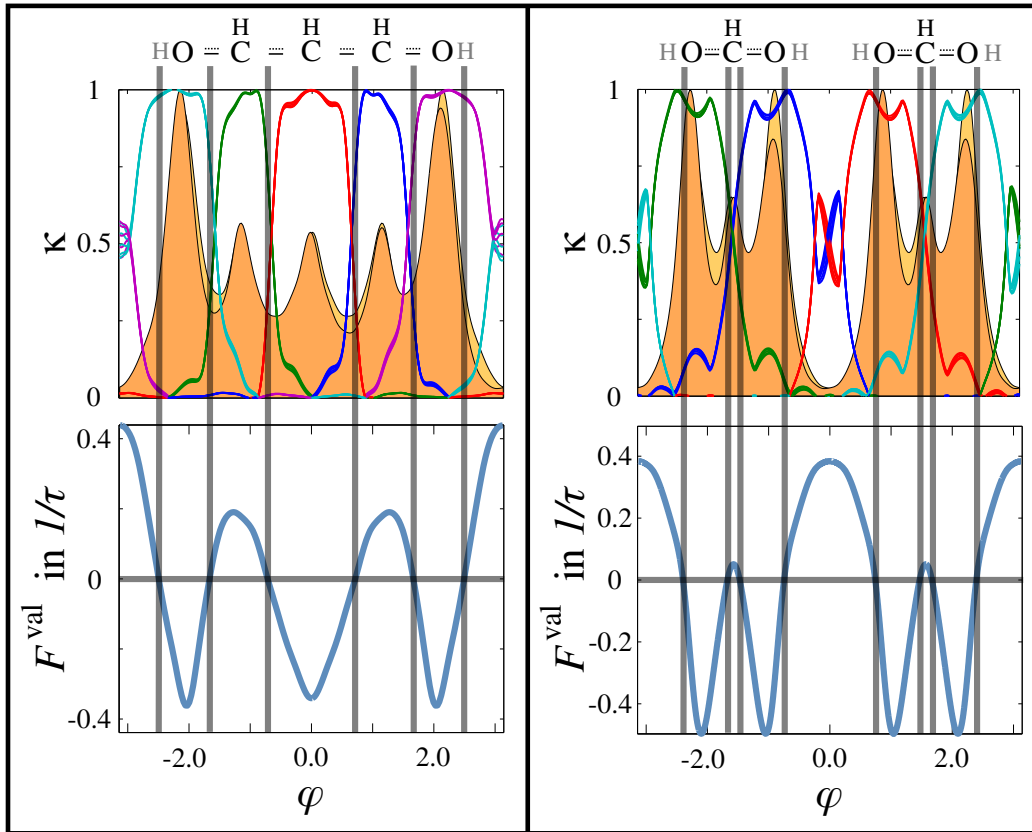


Figure 4.34: Top: Membership functions $\kappa_i(t, \varphi)$ representing the probability of an angle to belong to one of the sectors for proton tunneling in malonaldehyde (top left) and in the formic acid dimer (top right). For malonaldehyde, there are five membership functions (cyan, green, red, blue, violet), while for the formic acid dimer there are four (green, blue, red, cyan). Each of those functions is shown at six different time steps, thus there are six lines of each color present (which are almost distinguishable on the graphical scale). In the background, the initial electron density and the electron density after half the tunneling time are shown. Bottom: Fluxes for the respective processes at quarter a tunneling time, for the case of zero average angular flux. Angles with zero flux are indicated by vertical lines through bottom and top pictures.

two neighboring membership functions cross (at a value of ca. 0.5) zero flux surfaces can be expected. Comparison of the cluster transition regions with the zero-flux surfaces of the reference case (with zero average angular flux), depicted in Fig. 4.34, show interesting similarities: The zero-flux surfaces between two carbon nuclei or between a carbon and an oxygen nucleus are within the region of transition between two clusters. However, the zero-flux surfaces between the oxygen nucleus and the proton, bounding the region of the tunneling proton, are not reproduced. These zero-flux surfaces, at $\varphi \approx \pm 2.5$, are still within the cyan and violet clusters. Instead, the region of cluster transition from the violet to the cyan cluster, around $\varphi = \pm\pi$, is located at the angles where the flux has its maximum. This region corresponds to the tunneling proton. Because this is the global maximum of the flux, a zero flux surface at this place would imply that all fluxes are negative, corresponding to an entirely unidirectional flux. Thus, a zero flux surface at this position is forbidden due to conservation of electronic angular momentum, see [134].

For the formic acid dimer, the situation is similar. All four clusters are centered around the position of an oxygen nucleus, and transition from the two clusters within a molecule (from green to blue, and from red to cyan) happens at the position of the carbon nucleus of the molecule. This region is also the region of the zero-flux surfaces in the reference

case of zero average angular flux. Depending on the choice of the free parameter γ in the determination of the rate matrix eqn. 4.124, even the two zero-flux surfaces in close proximity to each other at this region may be seen as a deformation of the membership function. The zero-flux surfaces between the oxygen nuclei and the tunneling protons, bounding the two proton tunneling regions at angles $\varphi \approx \pm 0.6$ and $\varphi \approx \pm 2.4$, are not found, as in the case of malonaldehyde. These lines are within the region of the green, blue, red and cyan cluster. Instead, the respective transition regions between the cyan and green, as well as blue and red clusters around the angles $\varphi = \pm\pi$ and $\varphi = 0$, respectively, are again at positions where the electron flux has its global maxima. Thus, if the zero-flux surfaces were at these positions, the electron flux would be unidirectional, and the selection rules for electronic fluxes in the ground state would be violated, cf. [134]. Thus, these locations are forbidden for zero-flux surfaces.

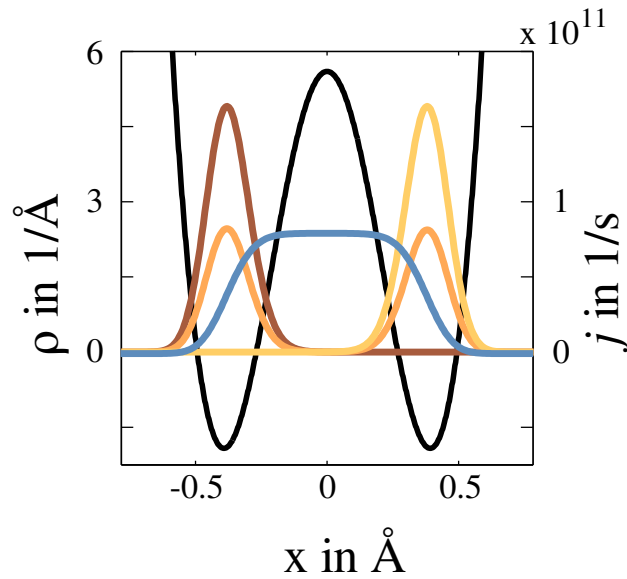


Figure 4.35: Nuclear probability density ρ at time zero (brown), a quarter of the tunneling time (orange) and half the tunneling time (yellow), and flux density j at quarter a tunneling time (blue) for tunneling in ammonia, from [86].

The reason why the assumption that the fluxes are determined by the density difference between neighboring points in space lead to reasonable zero-flux surfaces between the heavy nuclei, but fails to describe proton tunneling, can easily be understood. The assumption is based on classical probability theory. If the density represents classical particles, and if these are located at time t_0 around \mathbf{x}_0 and at a later time t_1 around \mathbf{x}_1 , at some intermediate times the particles have to be found in between \mathbf{x}_0 and \mathbf{x}_1 . If the particles move essentially on a straight line from \mathbf{x}_0 to \mathbf{x}_1 , there will be a large flux between the two places in space. Translated to the density, this means that in order to have a lot of flux between two places in space during some time interval, the time-dependence of the density needs to be such that the density is peaked at one place, and this peak moves to the final place. The shape of the peak may change, but it has to be found at intermediate places for intermediate times. In contrast, the present scenario of tunneling is a quantum effect, where density at a certain location may be transferred to a location further away, without ever being found in between the initial and final location. Already by the approximation that the electron density at a given time is the sum of initial and final densities weighted by the respective probabilities to find initial and final configuration at that time (see eqn. 4.98), the quantum nature of the process is apparent.

What happens in the case of tunneling can further be investigated by considering another model system, from which the behavior of the nuclear density and flux density are known. In Fig. 4.35, the density and flux density for ground-state nuclear tunneling of ammonia are presented. The model is taken from [120], and the densities and fluxes are discussed in [86]. The figure shows an initial localization of the nuclear wave packet at the left potential well, corresponding to one of the two equilibrium structures of ammonia. At a quarter of the tunneling time, the wave packet is split in two parts, each localized in one of the wells. Finally, after half the tunneling time, the wave packet is completely localized in the second well, corresponding to the other, inverted equilibrium structure of ammonia. As can clearly be seen, the density is never significant in between the two wells, e.g. at $x = 0$, representing planar ammonia. Classical particles would have to travel continuously from one well into another, and if these probability distributions were interpreted classically, (almost) zero flux would be expected at $x = 0$. However, the quantum mechanical flux density is also shown in the figure. It is clearly at a maximum at $x = 0$, and thus there can be no almost-zero-flux surface there. Although this model is for the nuclear density and flux density, a similar behavior can be expected for the electron density in proximity to the tunneling hydrogens: While the electron density disappears together with the nuclear density of the proton at one location and appears at another, the flux density in between the two locations should be significant.

In the case of tunneling in malonaldehyde and the formic acid dimer, the assumption that the density behaves classically, moving continuously from one place to another instead of disappearing at one place and appearing at another, is not applicable for the tunneling protons, but applicable to the heavier nuclei. The tunneling of the proton happens such that electron density disappears at one position and appears at another position far away. Thus, it is not possible for the PCCA+ algorithm to find the path from one position to the other. For heavy nuclei, the density tunnels, but only a very short distance. As can be seen from Fig. 4.27 and Fig. 4.28, the maxima of the electron density at the nuclei shift, effectively, from initial to final position, while visiting the intermediate region. Thus, the density behaves similar to a classical density, and the PCCA+ algorithm can find sensible clusters. This difference between the light and heavy nuclei can also be compared with the 2nd Born-Oppenheimer approximation [133], for which not only the dynamics of the light electrons and heavy nuclei, but also the dynamics of the light nuclei and heavy nuclei can be approximately separated. Heavy nuclei exhibit approximately classical behavior, while light nuclei often do not.

The assumption that only the density differences between neighboring points determines the fluxes can nevertheless also give reasonable results for the tunneling protons, if one is aware of the applicability of the assumption. The problematic regions can be identified from the membership functions: From Fig. 4.34 it can be seen that the membership functions in the regions of the tunneling proton stay close to a value of 0.5 for a rather wide range of angles, so that an assignment of the angles to one of the clusters is impossible. Reasonable zero-flux surfaces for such regions can be found by using the other minimal-flux surfaces together with the fluxes from the continuity equation. If, for example, for malonaldehyde the minimal-flux surfaces between two carbon nuclei or a carbon and an oxygen nucleus were used as zero-flux surfaces for the fluxes, the zero-flux surfaces for the tunneling protons would automatically follow, see section 4.3.3.

The systems studied here exhibit clearly quantum mechanical behavior, as they describe large-distance tunneling. Thus, the assumptions made in this section seem to be problematic at first glance, but nevertheless the results are very encouraging. How would the method perform for a quantum dynamics study above the barrier? This question may be answered

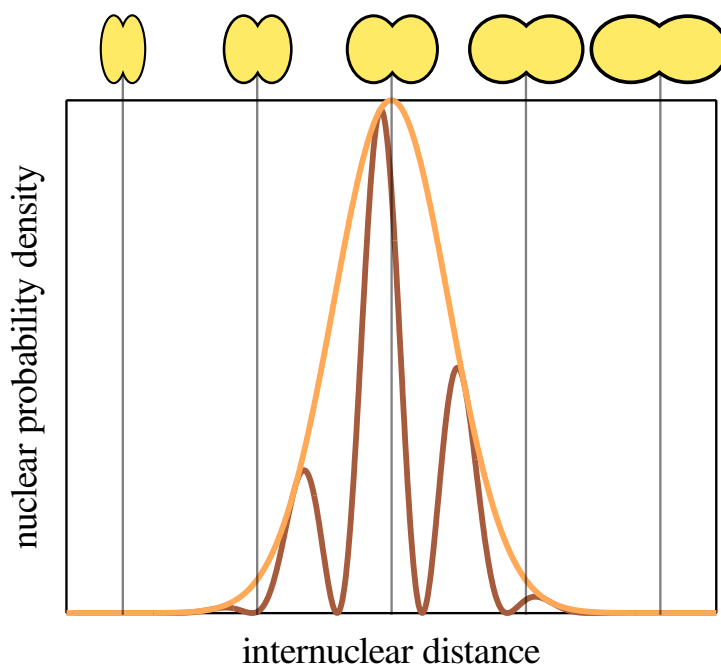


Figure 4.36: Sketch of two possible (not normalized) nuclear probability densities (orange and brown) for a diatomic molecule along the internuclear distance. The brown curve shows interference effects, while the orange curve does not. Above, there is a sketch of a cut of the electron density for the individual internuclear distances. If the total electron density is built as a superposition of the individual electron densities weighted by the respective nuclear probability density, the resulting electron densities will look qualitatively similar, and interference effects will not be seen.

by asking how “quantum” the electron density becomes. In Fig. 4.36, for some diatomic molecule a sketch of a nuclear density along the internuclear distance as well as a cut of the electron density along this coordinate and a coordinate perpendicular is shown. Although the nuclear density may show quantum effects like interference patterns, the electron density in the Born-Oppenheimer approximation is a superposition of the ground-state electron densities for all internuclear distances, weighted by the nuclear density for this distance. Consequently, it will exhibit hardly any quantum effects or interference patterns. An example is simulation of the electronic flux density of vibrating H_2^+ in [69]: There, the nuclear wave packet at the turning point of the potential clearly shows interference effects, and these are also apparent in the nuclear flux density. However, these effects do not translate to the electron density or the electronic flux density.

It may thus be possible to use the assumptions made here also for determination of fluxes from a density obtained by a quantum dynamics simulation. However, further work regarding the validity of the assumptions is necessary, as these have not yet been justified. A detailed analysis of the relation between quantum mechanical probability theory and classical probability theory for electron dynamics in the Born-Oppenheimer approximation would be necessary, and this still has to be done. Also, the method is based on the density only, and fluxes that are not apparent in the density, but only encoded in the wave function, can also not be described.

Chapter 5

Conclusion

In the Introduction, the goal was set to make the arrows in Lewis structures describing the reaction mechanism of an electron rearrangement time dependent, focusing on reactions in the electronic ground state. How well has this goal been achieved?

The electronic flux density would be the tool of choice to achieve this goal. Analysis of the concept of a flux density and the fate of the electronic flux density in the Born-Oppenheimer approximation in Chapter 2 showed a major problem: There exists an electronic flux density for reactions, for which the approximation that they happen in the electronic ground state is applicable. However, the Born-Oppenheimer approximation precludes straightforward calculation of the electronic flux density. Few approaches to remedy this problem are known in the literature, and these were reviewed in Chapter 2. These approaches are promising, but they also show that a fully quantum mechanical determination of electronic flux densities is very difficult. On one hand, such a quantum mechanical electronic flux density would be very important to learn about the details of the reaction mechanism, and to analyze situations where the quantum mechanical nature of the particles becomes important. On the other hand, chemists use a mixture of quantum mechanical and classical concepts to describe chemical reactions, and often the nuclear motion can be considered approximately classical. Thus, the methods to calculate electronic flux densities to analyze chemical reactions should incorporate this knowledge. An important step forward would be, for example, to be able to calculate an electronic flux density from the data of an ab-initio molecular dynamics simulation, i.e. from positions and velocities of the nuclei in combination with the electron density. Developments in this direction were made by Diestler [67] and Patchkovskii [172], and further development would help a lot for the understanding of chemical reactions.

In contrast to the electronic flux density, the time-dependent electron density is readily available, also for the case of a chemical reaction in the electronic ground state. From the electron density, electron fluxes into or out of regions of space can be calculated. These represent less information than the flux density, but also the arrows in Lewis structures represent much less information than the flux density. It was shown by Barth, Hege, Ikeda, Kenfack, Koppitz, Manz, Marquardt and Paramonov in [25] that electron fluxes from the time-dependent electron density in the Born-Oppenheimer approximation agree very well with the exact fluxes. Thus, these can be used to analyze time-dependent reaction mechanisms for model systems.

However, to obtain the electron fluxes in sectors is also far from trivial. Some of the problems were explained in Chapter 3. The development of a program (the Magic Density Creator, developed with the help of Gunter Hermann and Vincent Pohl from Freie Universität Berlin) to calculate the electron density from the basis set coefficients of a quantum chemical calculation efficiently was already an important step. There are still a number of technical

problems to be solved, like stable integration of the electron density in arbitrary regions of space, until electronic fluxes can be used to analyze simulations of chemical reactions in a simple manner.

The model systems investigated in this work are the double bond shift of cyclooctatetraene in the tunneling limit, motion of benzene along the Kekulé vibrational mode, and proton tunneling in malonaldehyde as well as double proton tunneling in the formic acid dimer. All these processes are mainly circular electron rearrangements, and in a first approximation only the circular mechanism is of interest. Thus, the applications focused on the circular mechanisms.

For cyclooctatetraene, presented in section 4.1, first a model for coherent tunneling was developed, and the electronic fluxes were calculated within this model. To obtain a reaction mechanism, the electronic space was divided into bond sectors that should represent a bond along the ring structure of the molecule. Electron fluxes into and out of the bond sector were calculated, and interesting results were found: While the core electrons are uninteresting for the mechanism and the π -electrons move as can be expected from conservation of electronic angular momentum, the other valence electrons move into the direction opposite to the π -electrons. This flux is strong enough so that the net flux of electrons is opposite to the expected reaction mechanism. However, this effect is to some extent due to the definition of the bond sectors, and only the following investigation of benzene could show that this effect is not only an artifact of the model but a feature of the reaction. Also, it could be seen that the net flux of electrons is very small, and that there are much less electrons moving as suggested by the arrows in Lewis structures.

Motion of benzene along the Kekulé mode is another example, presented in section 4.2. The molecule was prepared in one of the Kekulé structures, an effectively one-dimensional model for the nuclear motion was set up, and a quantum dynamics calculation for the nuclei was performed. The resulting time-dependent electron density was again used to calculate fluxes into or out of bond sectors representing the bonds along the nuclear ring. It was found that again comparably little electron density moves, and that π - and other valence electrons move into opposite directions. However, all valence electrons taken together move into the direction of the π -electrons, and thus into the direction implied by the expected reaction mechanism based on the Lewis structures. By the setup of the model it could be concluded that this effect is indeed present. Further analysis showed that in principle all electrons move into the direction of the nuclear motion of the nearby nucleus. The effect of an effective motion of π - and other valence electrons into different directions relative to the bond sector could be explained by the different speed of the electrons: The π -electrons are faster than the nuclei, while the other electrons are slower.

The examples of cyclooctatetraene and benzene had the advantage that possible reaction mechanisms were already known from the beginning by conservation of electronic angular momentum for reactions in the electronic ground state, and by symmetry of the process. For general circular electron rearrangements that do not exhibit the appropriate symmetries the possible reactions mechanisms are constrained much less. Examples of such processes are proton tunneling in malonaldehyde and double proton tunneling in the formic acid dimer. For both processes, already the circular flux is only determined up to a time-dependent, but angle-independent flux parameter.

In Chapter 4.3, it is found that this angular flux parameter is related to the expectation value of a new operator, the angular velocity operator. However, the time-dependence of this expectation value, and thus also of the flux parameter is difficult to obtain without knowledge of the flux density. For the considered tunneling dynamics of malonaldehyde and the formic acid dimer the value of the flux parameter can nevertheless be estimated via the

known shape of the electron density and the connection between the angular flux and the electronic angular momentum.

The reaction mechanisms of proton tunneling in malonaldehyde and in the formic acid dimer were determined, depending on the value of the flux parameter. For the dynamics, the coherent tunneling model that was previously used for cyclooctatetraene could be employed again. The electron fluxes were determined by the continuity equation, up to the unknown flux parameter. It was found that independent of the exact value of the flux parameter, the qualitative reaction mechanisms could be reliably determined. For proton tunneling in malonaldehyde, the mechanism is similar to the previous mechanisms found for double bond shift in cyclooctatetraene or motion of benzene along the Kekulé mode. For double proton tunneling in the formic acid dimer, it was found that an important ingredient of the mechanism is the π -electron density at the oxygen of the hydroxyl group, and that the mechanism is counterintuitive. It is also found that compared to the number of electrons that move in total, the number of electrons accompanying the tunneling proton is significant. Thus, it is concluded that instead of proton tunneling, one may also speak of hydrogen atom tunneling. Finally, it was also found that some π -electron density tunnels together with the proton, which is also unexpected.

Last, the time-dependent densities of malonaldehyde and the formic acid dimer were used to test a model based on classical probability theory. This model has a number of ad-hoc assumptions, that still need to be justified. Interestingly, the results obtained with this model are, for the electron density close to the heavy nuclei, in very good agreement with the reference results based on the continuity equation for the electron density. For the electron density in proximity to the tunneling proton(s) the model fails, but behavior of these electrons can be recovered from the results obtained for the electron density close to the heavy nuclei. Still, a derivation of this model starting from quantum probability theory has to be performed, in order to assess the applicability of the assumptions.

In summary, a number of new insights could be gained, but there are also a number of open questions and problems. One immediately apparent problem that was already mentioned in the introduction is the question of how to define a chemical bond. Moreover, not only bonds need to be defined, but also regions of the electronic configuration space have to be assigned to a bond. In the analysis presented here, geometrically simple bond sectors were defined, and these are to some extent interpreted as representing bonds in Lewis structures. However, the definition used here is in fact just a partitioning of the angular space which parametrizes the molecular ring structure. It thus cannot be used for other systems, and it would be already difficult to use for ring structures with large substituents. Do these substituents count to a bond sector, or should they be removed? And if so, how could they be removed? For example, one may consider to replace the quantum chemical ansatz of molecular orbitals as linear combination of atomic orbitals by valence bond theory [188], which naturally yields localized bonds. However, although in both cases chemical bonds are well-defined, the respective definitions are nevertheless arbitrary. The only way to determine reaction mechanisms without the problem of first defining bonds is to look at the electronic flux density, the quantity that is so difficult to obtain.

But this brings up a second issue, which is also a problem for the interpretation of electronic flux densities as chemical reaction mechanisms: The partition of electrons into classes, like core and valence electrons or σ - and π -electrons. This division of the electron density is important, as the different chemical kinds of electrons play different roles in the theory of chemistry as well as in general chemical thinking. However, this division is also arbitrary, and the dynamics analyzed here and the conclusions drawn for the reaction mechanisms are very much depending on this partitioning. The different behavior between

π -electrons and other valence electrons, for example, is a dynamics that arises from the quantum chemical calculation itself, and from the way of how the partitioning arises there. In this work, partitioning was simple as only Hartree-Fock calculations or suitable complete-active space self-consistent field calculations were performed, and the molecular orbitals can be easily separated. For other quantum chemical methods this may not be the case. Also, while π -electrons are a well-defined concept and double bonds in Lewis structures like that of benzene have a clear meaning, this is already different for non-planar systems like cyclooctatetraene in its electronic ground state. There, molecular orbitals that represent the double bond are only π -like orbitals, and these are not well-defined anymore.

At this point, the question of how much work should be invested to continue interpreting Lewis structures shall not be further discussed. The idea of reaction mechanisms and shifting electron bonds in Lewis structures is very useful. However, supplementing these ideas with knowledge of how the electronic flux density behaves during a reaction will definitively widen the horizon of the theory of chemical reactions in the future, and there will be many new effects that are still waiting to be discovered.

The final conclusion is the same as of any scientific work: A lot has been tried, a few problems have been solved, and many new problems have been discovered. Thus, the scientific journey continues.

Appendix A

Notational conventions

The notation is different for electrons, nuclei, and for general relations. The rules are:

- There are n electrons with position (operator) $\mathbf{q} = (\mathbf{x}_1, \dots, \mathbf{x}_n) \in \mathbb{R}^{3n}$, with $\mathbf{x}_i \in \mathbb{R}^3$. Lowercase letters are always used to denote electronic coordinates. Every other lowercase bold-face roman letter referring to electronic properties, like \mathbf{j} , has always dimension $\dim \mathbf{j} = \dim \mathbf{q} = 3n$ or $\dim \mathbf{j} = \dim \mathbf{x} = 3$. The electronic wave functions are ϕ or ϕ_i , the electronic probability density is ρ , and the electronic flux densities are \mathbf{j} or \mathbf{j}_{ij} . The electronic mass is m_e .
- There are N nuclei with position (operator) $\mathbf{Q} = (\mathbf{X}_1, \dots, \mathbf{X}_N) \in \mathbb{R}^{3N}$, with $\mathbf{X}_i \in \mathbb{R}^3$. Uppercase letters are always used to denote nuclear coordinates. Every other uppercase bold-face roman letter referring to nuclear properties, like \mathbf{J} , has always dimension $\dim \mathbf{J} = \dim \mathbf{Q} = 3N$ or $\dim \mathbf{J} = \dim \mathbf{X} = 3$. The nuclear wave functions are χ or χ_i , the nuclear probability density is ϱ , and the nuclear flux densities are \mathbf{J} or \mathbf{J}_{ij} . Nuclear masses are M or M_i , respectively.
- In case the discussion does not refer to electronic or nuclear properties explicitly, the notation for electrons is used as generic notation. The generic mass is m .

Special notations for an operator and its expectation value are not used, except where it is necessary to distinguish both. In this cases, the operator gets a hat, like $\hat{\mathbf{j}}$.

Derivative operators are written e.g. as ∂_t or $\partial_{\mathbf{q}}$, where the latter is short for the vector of the derivatives with respect to all components of \mathbf{q} . Specifically, the gradient of a scalar field $\rho(\mathbf{q})$ is $\text{grad } \rho = \partial_{\mathbf{q}}\rho$, and the divergence and curl of a vector field $\mathbf{j}(\mathbf{q})$ are $\text{div } \mathbf{j} = \partial_{\mathbf{q}} \cdot \mathbf{j}$ and $\text{curl } \mathbf{j} = \partial_{\mathbf{q}} \times \mathbf{j}$, respectively. If derivative operators have to be applied several times, exponents are used for the operators. For example, the Laplacian is $\partial_{\mathbf{q}}^2$. Also, operators always act on everything to the right, unless their action is limited by the usage of brackets.

Similar notation is used for elementary differential forms. For example, $d\mathbf{x} = dx_1 dx_2 dx_3$, and

$$\int f(\mathbf{x})d\mathbf{x} = \iiint f(\mathbf{x})dx_1 dx_2 dx_3.$$

The notation \iint and \iiint for double and triple integrals is only used for emphasis, and it is always understood that an integral is performed over all coordinates indicated by the differential form. If the bra-ket notation is used for scalar products, like

$$\int \phi^* \hat{O} \phi d\mathbf{q} = \langle \phi | \hat{O} | \phi \rangle,$$

the integral is always performed with respect to the electronic coordinates \mathbf{q} only. Differential forms, which are not (necessarily) the elementary forms of the vector space, get a check, like

the form \check{j} .

Electron fluxes are denoted by F , electron yields (time-integrated electron fluxes) by Y , and electron numbers (electron density integrated in some sector) by N . A one-dimensional electron density obtained from the electron density ρ by integration over all but one coordinate is denoted by n . The electron density ρ is split into the density of core electrons ρ^{core} and the density of valence electrons ρ^{val} . The latter is split again into the density of pericyclic electrons or π -electrons, ρ^{per} or ρ^{π} , and the density of the other valence electrons ρ^{oval} . This decomposition carries over to the fluxes, yields, electron numbers, and one-dimensional densities. Accordingly, these obtain similar superscripts “core”, “val”, “per”/“ π ”, and “oval” as the densities. Note that there will be no ambiguity in the text whether N and n have the meaning of an electron number or a one-dimensional electron density, respectively, or whether the symbols denote the total number of nuclei and electrons.

Cyclic electron rearrangements are discussed throughout the text, hence often the coordinates for one electron \mathbf{x} are expressed in cylindrical coordinates. The cartesian coordinates are $\mathbf{x} = (x_1, x_2, x_3)$, and the cylindrical coordinates are $\mathbf{x} = (r, \varphi, z)$, with $x_1 = r \cos \varphi$, $x_2 = r \sin \varphi$, and $x_3 = z$.

Appendix B

A brief introduction to differential forms

This section will cover parts of the calculus of differential forms in a rather casual way, as a formalism used interchangeably with standard vector calculus. There is more to differential forms, but the modest aim of this appendix is to present the basic concepts which will be of use in the main text. After introduction of the algebra of differential forms two very important results are presented: Poincaré's Lemma and Stoke's Theorem. Both are given without proof. Details on differential forms and the proofs can be found in [73, 161]. In extension to the usual vector calculus, the usage of differential forms will allow to write equations in a concise and dimension-independent way (e.g. there is no need to bother about how the generalization of a cross product looks like). Additionally, it will provide information by only the algebra of differential forms instead of tedious vector calculations and it simplifies the notation sometimes significantly. In this section a notation for the forms is used which is similar to their appearance in the main text.

Differential forms are what is left from an integral over a k -dimensional surface after removing the integral symbol. As Flanders says: "These are the things which occur under integral signs" [73]. They combine and generalize line integrals, surface integrals and volume integrals. Consider a linear vector space of dimension K with coordinates q_1, \dots, q_K , and let \bigwedge^k denote the space of k -forms. A symbol for the linear vector space is omitted, as in general it will not be dealt with multiple vector spaces at once. Then,

- $c = c(t)$ is a constant with respect to q_1, \dots, q_K , but possibly a function of other variables denoted by t .
- $f \in \bigwedge^0$, called a 0-form, is a function of q_1, \dots, q_K and possibly also of other variables t , i.e. $f = f(q_1, \dots, q_K, t)$.
- $\check{j} \in \bigwedge^1$, a 1-form, is the equivalent of a vector field in K dimensions, i.e.

$$\check{j} = j_1 dq_1 + \dots + j_K dq_K, \quad (\text{B.1})$$

with the j_k being understood as functions of q_1, \dots, q_K, t .

- $\check{A} \in \bigwedge^2$, a 2-form, is e.g. in three dimensions

$$\check{A} = A_1 dq_1 \wedge dq_2 + A_2 dq_2 \wedge dq_3 + A_3 dq_3 \wedge dq_1, \quad (\text{B.2})$$

with A_k being understood as functions of q_1, \dots, q_K, t . The exterior product of two

basis 1-forms dq_i and dq_j is skew-symmetric, that is,

$$dq_i \wedge dq_j = -dq_j \wedge dq_i. \quad (\text{B.3})$$

For 2-forms, this is equivalent to having oriented surface elements, and the property of orientation generalizes naturally to higher dimensions. It follows immediately that $dq_i \wedge dq_i = 0$. In the following, as customary in the literature, the explicit use of the \wedge -symbol for basis forms is omitted.

- $\check{\beta} \in \wedge^k$ is a k -form and has $\binom{K}{K-k} = \binom{K}{k}$ basis k -forms like $dq_1 dq_2 \dots dq_k$, $dq_2 dq_3 \dots dq_{k+1}$, etc. Consequently, the space of k -forms and the space of $(K - k)$ -forms have the same dimensionality. This property will be useful for the definition of the scalar product.
- $\check{\rho} \in \wedge^K$, a K -form, is the volume element

$$\check{\rho} = \rho(q_1, \dots, q_K) dq_1 \dots dq_K. \quad (\text{B.4})$$

The scalar product is defined as a map of two k -forms to \wedge^K via the Hodge dual $*$. This operator maps a k -form to its dual, a $K - k$ -form. For this mapping it is important that both spaces \wedge^k and \wedge^{K-k} have the same dimensionality, as just explained. The action of the Hodge dual depends in general on the metric of the space. We will be working here with the simple flat Euclidean metric only, for which $*$ is defined via the basis forms as

$$*dq_{i_1} \dots dq_{i_k} = \epsilon_{j_1 \dots j_k j_{k+1}} dq_{j_{k+1}} \dots dq_{j_K}, \quad (\text{B.5})$$

with $\epsilon_{j_1 \dots j_k j_{k+1}}$ being the Levi-Civita symbol. This symbol is defined as

$$\epsilon_{j_1 \dots j_k} = \begin{cases} 1 & \text{for } (j_1 \dots j_k) \text{ even permutations of } (1, 2, \dots, k), \\ -1 & \text{for } (j_1 \dots j_k) \text{ odd permutations of } (1, 2, \dots, k), \text{ and} \\ 0 & \text{else.} \end{cases} \quad (\text{B.6})$$

For example, for a one-form $\check{\alpha} = \sum_{i=1}^K a_i dq_i$ in \wedge^1 , application of the Hodge dual gives

$$*\check{\alpha} = a_1 dq_2 dq_3 dq_4 - a_2 dq_1 dq_3 dq_4 + a_3 dq_1 dq_2 dq_4 - a_4 dq_1 dq_2 dq_3. \quad (\text{B.7})$$

With the Hodge dual, a scalar product of two forms $\check{\alpha}, \check{\beta} \in \wedge^k$ can be defined as

$$\check{\alpha} \wedge (*\check{\beta}) = (*\check{\alpha}) \wedge \check{\beta} = \langle \alpha, \beta \rangle dq_1 \dots dq_K. \quad (\text{B.8})$$

For example, consider the scalar product between two vectors $\mathbf{a} = (a_1, a_2)$, $\mathbf{b} = (b_1, b_2)$ in two-dimensional space. In the language of differential forms, the two differential forms $\check{\alpha}, \check{\beta} \in \wedge^1$,

$$\check{\alpha} = a_1 dq_1 + a_2 dq_2 \quad (\text{B.9})$$

$$\check{\beta} = b_1 dq_1 + b_2 dq_2 \quad (\text{B.10})$$

would be used. The scalar product $\mathbf{a} \cdot \mathbf{b}$ is given by

$$\begin{aligned} \check{\alpha} \wedge (*\check{\beta}) &= (a_1 dq_1 + a_2 dq_2) \wedge *(b_1 dq_1 + b_2 dq_2) \\ &= (a_1 dq_1 + a_2 dq_2) \wedge (b_1 dq_2 - b_2 dq_1) \\ &= (a_1 b_1 + a_2 b_2) dq_1 dq_2. \end{aligned} \quad (\text{B.11})$$

The previous example is repeated for three-dimensional space, for the vectors $\mathbf{a} = (a_1, a_2, a_3)$, $\mathbf{b} = (b_1, b_2, b_3)$. The respective differential forms $\check{\alpha}, \check{\beta} \in \bigwedge^3$ give

$$\begin{aligned}\check{\alpha} \wedge (*\check{\beta}) &= (a_1 dq_1 + a_2 dq_2 + a_3 dq_3) \wedge *(b_1 dq_1 + b_2 dq_2 + b_3 dq_3) \\ &= (a_1 dq_1 + a_2 dq_2 + a_3 dq_3) \wedge (b_1 dq_2 dq_3 - b_2 dq_1 dq_3 + b_3 dq_1 dq_2) \\ &= (a_1 b_1 + a_2 b_2 + a_3 b_3) dq_1 dq_2 dq_3.\end{aligned}\tag{B.12}$$

Note that this is a 3-form, and thus stands for a volume. Usually, the scalar product is considered to give a number. We can force this by application of the Hodge dual:

$$*(\check{\alpha} \wedge (*\check{\beta})) = a_1 b_1 + a_2 b_2 + a_3 b_3.\tag{B.13}$$

However, such a transformation is practice usually not necessary, as the spaces \bigwedge^k and \bigwedge^{K-k} are equivalent.

The cross product $\mathbf{a} \times \mathbf{b}$ for $\mathbf{a} = (a_1, a_2, a_3)$, $\mathbf{b} = (b_1, b_2, b_3)$ can also be easily represented. All that needs to be done is to act with the Wedge product, to obtain

$$\begin{aligned}\check{\alpha} \wedge \check{\beta} &= (a_1 dq_1 + a_2 dq_2 + a_3 dq_3) \wedge (b_1 dq_1 + b_2 dq_2 + b_3 dq_3) \\ &= (a_2 b_3 - a_3 b_2) dq_2 dq_3 + (a_3 b_1 - a_1 b_3) dq_3 dq_1 + (a_1 b_2 - a_2 b_1) dq_1 dq_2.\end{aligned}\tag{B.14}$$

The result may look unfamiliar: In traditional vector calculus, the result of a cross product is again a vector. Vectors are identified with one-forms, but the result of eqn. B.14 is a two-form. However, this is in complete accord with the meaning of the cross product: The length of the vector $\mathbf{c} = \mathbf{a} \times \mathbf{b}$ is the area of the parallelogram spanned by the vectors \mathbf{a} and \mathbf{b} , and the direction of \mathbf{c} gives the orientation of the normal to the surface containing the parallelogram. The form $\check{\alpha} \wedge \check{\beta}$ is automatically describing this surface, with the orientation encoded in the order of the basis forms $dq_i dq_j$. The Hodge dual may be applied to eqn. B.14 to obtain a one-form (and thus to resemble the cross product completely):

$$*(\check{\alpha} \wedge \check{\beta}) = (a_2 b_3 - a_3 b_2) dq_1 + (a_3 b_1 - a_1 b_3) dq_2 + (a_1 b_2 - a_2 b_1) dq_3.\tag{B.15}$$

The product $\check{\alpha} \wedge \check{\beta}$ for arbitrary k -forms $\check{\alpha}, \check{\beta}$ generalizes the cross product to arbitrary dimensions.

The last important operation for differential forms that is considered is the action of the d -operator, which maps from \bigwedge^k to \bigwedge^{k+1} . For definition of this differential operator, a slight change is made in the notation, following [73]: A general k -form $\check{\beta}$ is written as

$$\check{\beta} = \sum_L \beta_L dq_L,\tag{B.16}$$

where dq_L denotes a basis k -form, i.e. L stands for the set of all indices of the 1-forms used to construct a given basis k -form. Then,

$$d\check{\beta} = \sum_{i=1}^K \sum_L \frac{\partial \beta_L}{\partial q_i} dq_i dq_L.\tag{B.17}$$

This definition is in the following applied to a few examples, to see how the d -operation works. Usually, when working with differential forms, the definitions look much more complicated than the application of the operators in practice, as will be seen below.

For a 0-form f in the K -dimensional linear vector space the d -operator acts as

$$df = \sum_{k=1}^K \frac{\partial f}{\partial q_k} dq_k. \quad (\text{B.18})$$

This is the gradient of the function f .

For a 1-form $\check{j} = \sum_{k=1}^3 j_k dq_k$ in 3-space,

$$\begin{aligned} d\check{j} &= d(j_1 dq_1) + d(j_2 dq_2) + d(j_3 dq_3) \\ &= \left(\frac{\partial j_1}{\partial q_2} dq_2 dq_1 + \frac{\partial j_1}{\partial q_3} dq_3 dq_1 \right) + \left(\frac{\partial j_2}{\partial q_1} dq_1 dq_2 + \frac{\partial j_2}{\partial q_3} dq_3 dq_2 \right) + \left(\frac{\partial j_3}{\partial q_1} dq_1 dq_3 + \frac{\partial j_3}{\partial q_2} dq_2 dq_3 \right) \\ &= \left(\frac{\partial j_3}{\partial q_2} - \frac{\partial j_2}{\partial q_3} \right) dq_2 dq_3 + \left(\frac{\partial j_1}{\partial q_3} - \frac{\partial j_3}{\partial q_1} \right) dq_3 dq_1 + \left(\frac{\partial j_2}{\partial q_1} - \frac{\partial j_1}{\partial q_2} \right) dq_1 dq_2. \end{aligned} \quad (\text{B.19})$$

This is the curl of the corresponding vector \mathbf{j} . Again, this is not a 1-form but a 2-form and represents a surface, like the equivalent of the cross product, eqn. B.14.

Finally, for the same 1-form $\check{j} = \sum_{k=1}^3 j_k dq_k$ in 3-space,

$$\begin{aligned} d(*\check{j}) &= d(j_1 dq_2 dq_3) - d(j_2 dq_1 dq_3) + d(j_3 dq_1 dq_2) \\ &= \left(\frac{\partial j_1}{\partial q_1} dq_1 dq_2 dq_3 \right) - \left(\frac{\partial j_2}{\partial q_2} dq_2 dq_1 dq_3 \right) + \left(\frac{\partial j_3}{\partial q_3} dq_3 dq_1 dq_2 \right) \\ &= \left(\frac{\partial j_1}{\partial q_1} + \frac{\partial j_2}{\partial q_2} + \frac{\partial j_3}{\partial q_3} \right) dq_1 dq_2 dq_3. \end{aligned} \quad (\text{B.20})$$

This is the divergence of the corresponding vector \mathbf{j} . It is a 3-form, similarly to the definition of the scalar product, cf. eqn. B.12.

With these definitions, it is possible to state the two most important results of the calculus of differential forms:

- **Poincaré's Lemma:** For any differential form $\check{\beta}$,

$$d\check{\beta} = 0. \quad (\text{B.21})$$

Also, if $d\check{\gamma} = 0$ for any $(k+1)$ -form $\check{\gamma}$, it follows that there is a k -form $\check{\beta}$ such that $\check{\gamma} = d\check{\beta}$.

- **Stoke's Theorem** For any k -form $\check{\beta}$ and any region Ω with boundary $\partial\Omega$,

$$\int_{\Omega} d\check{\beta} = \int_{\partial\Omega} \check{\beta}. \quad (\text{B.22})$$

These two identities unify many formulas used in traditional vector calculus. For example, for a 0-form in 3-space it follows from Poincaré's Lemma that

$$\text{curl grad } f = 0 \quad (\text{B.23})$$

for a function f , whereas for a 1-form it follows that

$$\text{div curl } \mathbf{a} = 0 \quad (\text{B.24})$$

for a vector \mathbf{a} . Stoke's theorem is the generalization of what is known as Green's theorem as well as the Divergence/Gauss's/Ostrogradsky's theorem. There will be the opportunity to apply both when the solution of the continuity equation is discussed, see section 2.2.

As a final application, consider the solution of the integral of eqn. 2.30. Specifically,

$$I = \int_B \partial_{\mathbf{q}} \cdot \frac{\mathbf{q}}{|\mathbf{q}|^K} d\mathbf{q} \quad (\text{B.25})$$

is to be solved for integration over a small ball B centered around the origin. The integral I resembles the integral of eqn. 2.30, if the problem is centered around zero, $\mathbf{q} = 0$, and if the substitution $\mathbf{q}' \rightarrow \mathbf{q}$ is made. The problem at hand is similar to the calculation for gravitational flux given in [16].

The one-form

$$\check{\alpha} = \frac{1}{|\mathbf{q}|^K} \sum_{i=1}^K q_i dq_i \quad (\text{B.26})$$

is introduced, so that eqn. B.25 becomes

$$I = \int_B d * \alpha. \quad (\text{B.27})$$

For example, for three dimensions

$$* \alpha = \frac{1}{|\mathbf{q}|^K} (dq_2 dq_3 - q_2 dq_1 dq_3 + q_3 dq_1 dq_2) \quad (\text{B.28})$$

and it is to be integrated over

$$d * \alpha = \left(\partial_{q_1} \frac{q_1}{|\mathbf{q}|^K} + \partial_{q_2} \frac{q_2}{|\mathbf{q}|^K} + \partial_{q_3} \frac{q_3}{|\mathbf{q}|^K} \right) dq_1 dq_2 dq_3. \quad (\text{B.29})$$

Using Stoke's Theorem, the volume integral can be replaced by the surface integral

$$I = \int_B d * \alpha = \int_{\partial B} * \alpha. \quad (\text{B.30})$$

As a next step, spherical coordinates in K dimensions are introduced, defined by

$$\begin{aligned} q_1 &= r \cos \varphi_1 \\ q_2 &= r \sin \varphi_1 \cos \varphi_2 \\ q_i &= r \sin \varphi_1 \sin \varphi_2 \dots \sin \varphi_{i-1} \cos \varphi_i \\ q_K &= r \sin \varphi_1 \sin \varphi_2 \dots \sin \varphi_{i-1} \sin \varphi_{K-1}. \end{aligned} \quad (\text{B.31})$$

The radius is defined in $r \in [0, \infty]$, and all the angles are defined in $\varphi_i \in [0, \pi]$ except φ_{K-1} , for which $\varphi_{K-1} \in [0, 2\pi]$. The basis forms transform as

$$dq_i = \frac{\partial q_i}{\partial r} dr + \sum_{j=1}^{K-1} \frac{\partial q_i}{\partial \varphi_j} d\varphi_j. \quad (\text{B.32})$$

Now $*\alpha$ can be calculated in this basis to solve eqn. B.30. For the calculation, a computer algebra system is strongly recommended due to the large number of terms. Using Sage [7], the simple result

$$* \alpha = \frac{r^K}{|\mathbf{q}|^K} (\sin \varphi_1)^{K-2} (\sin \varphi_2)^{K-3} \dots \sin \varphi_{K-2} d\varphi_1 d\varphi_2 \dots d\varphi_{K-2} d\varphi_{K-1} \quad (\text{B.33})$$

was obtained. It is evident that all other basis forms except $d\varphi_1 d\varphi_2 \dots d\varphi_{K-2} d\varphi_{K-1}$ vanish.

For the integration over the boundary ∂B of the ball $r = |\mathbf{q}|$, so that

$$\int_{\partial B} * \alpha = \int_0^\pi \cdots \int_0^\pi \int_0^{2\pi} (\sin \varphi_1)^{K-2} (\sin \varphi_2)^{K-3} \cdots \sin \varphi_{K-2} d\varphi_1 d\varphi_2 \cdots d\varphi_{K-2} d\varphi_{K-1}. \quad (\text{B.34})$$

Specific solutions to this integral for a given dimensionality are straightforward. The general solution, which will not be discussed further here, is the surface of the unit K -sphere

$$A_K = \frac{2\pi^{K/2}}{\Gamma(K/2)}. \quad (\text{B.35})$$

Appendix C

Kinetic energy operators from symmetry-adapted curvilinear coordinates

For an accurate quantum dynamics simulation of the nuclear wave function during a process there is a computational problem: The dimensionality even for rather small systems, like the molecules considered in this text, is already far too large to be able to calculate the nuclear wave function completely. For cyclooctatetraene, for example, there are 48 nuclear coordinates, and already the storage of the wave function on a computer becomes a challenge. Even with today's most successful quantum dynamics methods which use efficient basis sets to represent the wave function, like the MCTDH method [31, 147] or the coupled coherent states approach [189], only a dozen degrees of freedom may be calculated completely (although, under certain circumstances more dimensions may be treated approximately by a multilayer approach, see [144]).

Additionally, for the calculation of the nuclear quantum dynamics a potential energy surface is needed, and this has to be calculated by quantum chemical means. Depending on the region of the configuration space which the molecule visits, expensive quantum chemical methods may be necessary. For some problems this calculation becomes unfeasible, and even though the nuclear dynamics might be determined in principle, in practice it cannot due to the lack of an accurate potential.

Thus, it is almost always necessary to set up a model system with a reduced number of degrees of freedom. Fortunately, the processes of interest do often happen in a small subspace of the nuclear configuration space. In consequence, a transformation (the model) from Cartesian coordinates of the nuclei to more appropriate coordinates is sought, which divides the set of coordinates into two parts: A (hopefully small) relevant part, and an irrelevant part, which may be neglected. Two aspects are important for such a transformation: On one hand, the set up of the model is influenced by assumptions about how the process happens. Consequently, if results of the model do not agree with reference data, the original assumptions need to be modified. On the other hand, a well-designed model can be systematically improved by inclusion of more and more degrees of freedom. Thus, even if it was possible to calculate the whole dynamics in a brute-force approach, from construction and investigation of a model of reduced dimensionality a lot can be learned.

Notwithstanding, setting up such an appropriate transformation for the process is in general necessary anyway, and a lot of effort has already been undertaken by scientists in this matter. These approaches shall be reviewed in the following.

One way to find coordinates which achieve the goal of separating coordinates into relevant and irrelevant parts is the transformation to Jacobi coordinates [101, 119] (also called mobile coordinates), which are defined as coordinates that separate the center of mass motion and leave the kinetic energy operator of the internal motions diagonal. There are also generalized Jacobi coordinates, which only separate the center of mass motion [74]. This separation is always desirable for quantum dynamics simulations, except if one needs the reference to an external frame (e.g. if an external field is included in the simulation). Jacobi coordinates are also used below, and will be further discussed. For now, it should be noted that usually Jacobi coordinates are used as rectilinear coordinates, but they may also be expressed as curvilinear coordinates, e.g. in terms of spherical coordinates. While rectilinear Jacobi coordinates are suitable both for small amplitude motions (often, normal coordinates are almost Jacobi coordinates) as well as the large amplitude motions, curvilinear Jacobi coordinates may be used for large amplitude motions to keep the dimensionality of the problem as small as possible.

There has been much interest in curvilinear coordinates: Already in 1928, Podolsky [176] derived a form of the kinetic energy operator for general coordinates. The book of Wilson, Decius and Cross [226] discusses several types of coordinate systems for the ro-vibrational problem, which is extended in the book of Bunker and Jensen [48]. Other examples for curvilinear coordinates usable to describe the dynamics of molecules can e.g. be found in the work of Handy [92] on internal coordinates, in the work of Bramley et al. [40] on the separation of rotation and vibration, in the work of Mladenović [151–153] on spherical polar parametrization and in the work of Okuno [166] on quasi-rectilinear coordinates. Also, interesting work on general curvilinear coordinates including numerical solutions was done by Chapuisat, Nauts and Durand [53], Nauts and Chapuisat [162] and Lauvergnat and Nauts [117], as well as on the polyspherical coordinates by Gatti, Muñoz and Iung [83], Gatti and Iung [82], Sadri et al. [181] and Joubert-Doriol et al. [105]. Another approach is to use hyperspherical coordinates, see e.g. the work of Hauke, Manz and Römelt [95].

If the nuclear configurations retains symmetry elements during the dynamical process, these symmetries are very handy and should be exploited as much as possible. Thus, the coordinate transformation should be adapted to the symmetry, i.e. the relevant coordinate subspace shall exhibit the symmetries of the process. Examples for such situations are the processes discussed in the text, i.e. the motion of benzene along the Kekulé mode as well as ring inversion and double bond shift in cyclooctatetraene. In this section, a way to perform a coordinate transformation is introduced that is simple, symmetry-adapted, and easily improvable. The route map of this transformation is the following: First, Jacobi coordinates are set up to separate the center of mass motion by keeping the kinetic energy operator diagonal. Next, some of those Jacobi coordinates are expressed in terms of polar or spherical coordinates. The symmetry elements are introduced by combination of radii and angles, to yield symmetry-adapted curvilinear coordinates. Finally, the coordinates which represent the process are selected.

The method is first illustrated for a diatomic molecule, for which the calculation of the coordinates can be performed on the back of an envelope. Then, the method is applied for four nuclei, to construct a model for double bond shift in cyclobutadiene. Thereafter, six nuclei are considered, and the kinetic energy operator for benzene of section 4.2.3 is derived in a more general way, which allows systematic improvements. Finally, the procedure is used for eight nuclei, to construct a two-dimensional model for double bond shift in cyclooctatetraene, and a possible extension to build a four-dimensional model including ring inversion is discussed. While the method itself is very simple, the detailed calculations are cumbersome. This is a good application for a computer algebra system. For the calculations

presented below, the Symbolic Toolbox [8] for Matlab [4] was used.

C.1 The kinetic energy operator in general coordinates

To transform a general kinetic energy operator (KEO) from Cartesian coordinates to an arbitrary coordinate system,

1. the motion of the center of mass is separated,
2. the equations for the transformation to the new coordinates are set up,
3. the metric tensor is constructed, and
4. the volume element as well as the integration limits for normalization of the wave function are determined.

To accomplish item 1 on the list, Jacobi coordinates are a natural choice. Jacobi coordinates are constructed by introduction of linearly independent quasi-particles with coordinates that are the difference between the center of mass of subsets of the particles. These subsets may also contain one particle only. Such constructions are exemplified below, and they always yield one coordinate which corresponds to the center of mass of the whole system. In the following it is at some point of the discussion always assumed that all particles have the same mass. Extension to particles with different masses is straightforward, and may always be accomplished by scaling of the original Cartesian coordinates. In the cases discussed below, coordinates which include rotation of the whole molecule are automatically apparent. In general, however, rotational invariance may have to be enforced. Also, although the rotation group has three parameters, it is in principle not possible to separate three rotational coordinates for any (even infinitesimally small) displacement (a prove for this statement is given by Littlejohn and Reinsch [125]).

Item 2 is tailored to the problem at hand. The metric, item 3, is needed to know how the second derivative with respect to the Cartesian coordinates in the KEO transforms, and thus to set up the KEO in the new coordinates. To keep the correct normalization, item 4 is needed, i.e. the scalar product in terms of the new coordinates needs to be found.

It will be handy to introduce a few notations. These notations differ from the rest of the work, but will be applied throughout this appendix. The original Cartesian coordinates of the particles are \mathbf{r} with elements r^i , the Jacobi coordinates are \mathbf{u} with elements u^i , and the arbitrary final coordinates that are to be transformed to are \mathbf{q} with q^i . There are, of course, the same number of elements for each of those sets. After transformation from \mathbf{r} to \mathbf{u} the kinetic energy operator is still diagonal in the coordinates (i.e. it contains no mixed monomials of the components of \mathbf{u}). This is a special and convenient property of the Jacobi coordinates. Next, \mathbf{r} needs to be expressed as a function of \mathbf{u} , which might already be a task for a computer algebra system. Given the transformation from \mathbf{u} to \mathbf{q} , the coordinates \mathbf{u} are needed as a function of \mathbf{q} . Then, the Jacobian matrix J can be calculated and from that the components of the metric tensor g_{ij} . The inverse g^{ij} of the metric is used to calculate the Laplacian.

In the following, summation over repeated indices (the Einstein summation convention) is implied, unless specified otherwise. Then,

$$\begin{aligned}
 \partial_i &:= \frac{\partial}{\partial q^i} && \text{is the covariant derivative,} \\
 g_{ij} &:= \frac{\partial r^k}{\partial q^i} \frac{\partial r^k}{\partial q^j} \equiv (\partial_i r^k)(\partial_j r^k) && \text{is the metric or first fundamental form,} \\
 g^{ij} &:= \frac{\partial q^i}{\partial r^k} \frac{\partial q^j}{\partial r^k} = g_{ij}^{-1} && \text{is the inverse metric, for which } g^{ij} g_{jk} = g_{ij} g^{jk} = \delta_k^i, \\
 J &:= \det \left(\frac{\partial r^i}{\partial q^j} \right) && \text{is the Jacobian determinant,} \\
 g &:= \det(g_{ij}) = J^2 && \text{is the determinant of the metric, and} \\
 d\tau &:= \prod_i dr^i = J \prod_i dq^i && \text{is the Cartesian volume element.}
 \end{aligned}$$

Using this notations, the Laplacian becomes

$$L = \sum_i \left(\frac{\partial}{\partial r^i} \right)^2 = g^{-1/2} \partial_j \left(g^{1/2} g^{ij} \partial_i \right) \equiv J^{-1} \partial_j \left(J g^{ij} \partial_i \right). \quad (\text{C.1})$$

For the evaluation of these expressions a large number of terms have to be kept track of. This can be conveniently accomplished by a computer algebra system.

C.2 Vibration of a diatomic molecule

The procedure of the coordinate transformations is first illustrated for two particles in a plane. This problem is very simple, as it is known in advance that only the inter-particle distance is of importance, if no external potentials (like electromagnetic fields) are present. Thus, in view of the later treatment of more complicated systems, the two-particle system is treated in a seemingly too intricate way.

The particles have masses m_1 and m_2 and are located at (x^1, x^2) and (x^3, x^4) , respectively. The total mass of the system is denoted by $M = m_1 + m_2$. There is only one possible choice for the Jacobi coordinates, i.e.

$$\begin{aligned}
 u^1 &= x^1 - x^3 & u^3 &= \frac{1}{M}(m_1 x^1 + m_2 x^3) \\
 u^2 &= x^2 - x^4 & u^4 &= \frac{1}{M}(m_1 x^2 + m_2 x^4).
 \end{aligned} \quad (\text{C.2})$$

Two fictive particles are defined by these coordinates, one of which, (u^3, u^4) , describes the motion of the center of mass of the system. This particle is of little interest, because it is assumed that the problem is invariant with respect to translation of the whole system. For the other fictive particle at (u^1, u^2) , the rectilinear Cartesian coordinates are replaced by polar coordinates as

$$u^1 = r \cos(\varphi) \quad u^2 = r \sin(\varphi). \quad (\text{C.3})$$

A change in the angle φ corresponds to rotation of the whole system, and this coordinate is also of no interest. Thus, there is only one relevant coordinate, the inter-particle distance r . In analogy to the treatments in the next section, the final coordinates are defined as $q^1 := r, q^2 := \varphi, q^3 := u^3, q^4 := u^4$. At the moment this seems like a trivial change of notation, but below the symmetry constraints will be introduced with this last transformation. In

C.3. Double bond shift of cyclobutadiene

total, the transformation thus reads

$$x^1 = q^3 + \frac{m_2}{M}q^1 \cos(q^2) \quad x^3 = q^3 - \frac{m_1}{M}q^1 \cos(q^2) \quad (\text{C.4})$$

$$x^2 = q^4 + \frac{m_2}{M}q^1 \sin(q^2) \quad x^4 = q^4 - \frac{m_1}{M}q^1 \sin(q^2). \quad (\text{C.5})$$

As a next step, all masses are set equal, $m_1 = m_2 = m$. For the final coordinates the Jacobian is $J = q^1$. Now, again in view of the treatment of the other systems below, $q^1 =: 2R$ is defined such that R denotes distance of both of the particles from the center of mass.

All coordinates except q^1 (i.e. the position of the center of mass and the rotation of the molecule relative to a space-fixed frame) are set to zero. The Laplacian is then obtained by calculation of the metric g^{ij} and application of eqn. C.1 as

$$L = \frac{1}{2}(\partial_R)^2 + \frac{1}{R}\partial_R. \quad (\text{C.6})$$

There is one last point that has to be taken care of: By constraining coordinates to zero, the form of the wave function Ψ is assumed to be a product of the system part and a constrained part. Specifically, δ -functions have to appear in the density $|\Psi|^2$ for all constrained coordinates [24]

$$|\Psi(q^1, q^2, q^3, q^4)|^2 = \chi(q^1)\delta(q^2)\delta(q^3)\delta(q^4). \quad (\text{C.7})$$

The normalization of the wave function and the corresponding limits of integration have to be adjusted. Note that the δ -functions can also be replaced by wave functions of Gaussian shape, which makes the wave function in momentum space also well-behaved.

In the case of only two particles the integration limits are simple, because the final coordinates are simple spherical coordinates. For the choice of normalization $\int |\Psi|^2 d\mathbf{x} = 1$ it follows that

$$1 = \int_{-\infty}^{\infty} \int_{-\infty}^{\infty} \int_0^{2\pi} \int_0^{\infty} |\Psi|^2 q^1 dq^1 dq^2 dq^3 dq^4. \quad (\text{C.8})$$

Note that $J = q^1 = 2R$. The constant is best included in the Laplacian, such that

$$L = (\partial_R)^2 + \frac{2}{R}\partial_R, \quad (\text{C.9})$$

and $J = R$ with normalization of the model wave function $\tilde{\chi}(R) = \chi(q^1)$ as

$$1 = \int_0^{\infty} |\tilde{\chi}|^2 R dR. \quad (\text{C.10})$$

C.3 Double bond shift of cyclobutadiene

The procedure is used now to obtain a model for cyclobutadiene which is capable of describing double bond shift dynamics in the molecule. In its equilibrium configuration, cyclobutadiene has point group symmetry D_{2h} and a rectangular shape. Thus, the transformation shown in Fig. C.1 is to be described, where the oblong structure distorts to a square (point group D_{4h}) and then to the other oblong structure. Each point corresponds to a particle and symbolizes a CH-group. It would probably be no good to represent the motion of Fig. C.1 by rectilinear coordinates: In the D_{4h} -structure, the square would be rather small, and this configuration would be energetically unfavorable. Thus, the atoms shall move on a circle as indicated in the figure. If this effectively one-dimensional motion along a circle with fixed radius turns out to be not accurate enough, the radius (a breathing motion) may also be included as a

variable, and the model becomes two-dimensional.

It is assumed that the hydrogen nuclei are rigidly attached to the corresponding carbon nuclei, and that they move along the circle with the same angular velocity as the carbon nuclei. All particles of the model therefore have the same mass m (the mass of the CH-group) and are located at the center of mass of the CH-group. The radius of the circle is ξ , and the angle describing the motion of all the particles simultaneously is φ , to be defined below. For a more accurate model, motion of the carbon and hydrogen nuclei may also be considered separately, such that the model discussed below is applied for both types of atoms (i.e. there is one ξ and φ for carbon nuclei, and one for hydrogen nuclei).

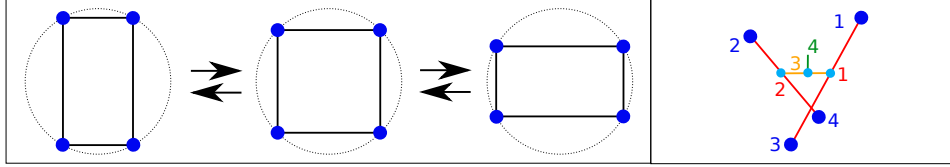


Figure C.1: Left: Relevant motion for the four particle system. The circle may also change size (breathing motion). Right: Particle numbering (blue) and Jacobi coordinates (orange and red; green is the center of mass), shown for a distorted configuration, to be able to see all coordinates.

For the masses, the notations $m_{ij} = m_i + m_j$ and $M = \sum_i m_i$ is used. The Cartesian coordinates are again denoted by $r^i = (x^i, y^i)$. The Jacobi coordinates are chosen to be

$$\begin{aligned} u^1 &= r^1 - r^3 & u^3 &= \frac{1}{m_{13}}(m_1 r^1 + m_3 r^3) - \frac{1}{m_{24}}(m_2 r^2 + m_4 r^3) \\ u^2 &= r^2 - r^4 & u^4 &= \frac{1}{M} m_i r^i \end{aligned} \quad (\text{C.11})$$

with the inverse transformation

$$\begin{aligned} r^1 &= \frac{m_3}{m_{13}} u^1 + \frac{m_{24}}{M} u^3 + u^4 & r^3 &= r^1 - u^1 \\ r^2 &= \frac{m_4}{m_{24}} u^2 + \frac{m_{13}}{M} u^3 + u^4 & r^4 &= r^2 - u^2. \end{aligned} \quad (\text{C.12})$$

The Jacobi coordinates are shown in figure C.1, for an asymmetrical configuration, as some of these would otherwise not be visible. Two of the Jacobi coordinates, u^1 and u^2 , are expressed in terms of polar coordinates with the center of mass as origin and the angles measured from, say, the (particle 3)-(particle 1) connection. Specifically,

$$\begin{aligned} u^1 &=: \left(\xi^1 \cos\left(\frac{\varphi^1}{2}\right), \xi^1 \sin\left(\frac{\varphi^1}{2}\right) \right) \\ u^2 &=: \left(\xi^2 \cos\left(\frac{\pi}{2} - \varphi^2\right), \xi^2 \sin\left(\frac{\pi}{2} - \varphi^2\right) \right). \end{aligned} \quad (\text{C.13})$$

The angles φ^1 and φ^2 thus reflect the angular displacement from the square configuration. Note the minus sign for φ^2 , which is introduced to adopt to the symmetry. Later, the two angles are set equal to describe the process at hand.

The final coordinates to be considered are combinations of the radii and angles, i.e.

$$\begin{aligned} q^1 &:= \frac{1}{2}(\xi^1 + \xi^2) & q^2 &:= \xi^1 - \xi^2 \\ q^3 &:= \frac{1}{2}(\varphi^1 + \varphi^2) & q^4 &:= \varphi^1 - \varphi^2 \\ u^3 &=: (q^5, q^6) & u^4 &=: (q^7, q^8). \end{aligned} \quad (\text{C.14})$$

C.3. Double bond shift of cyclobutadiene

The Jacobi coordinates u^3 and u^4 are not transformed, as these are the coordinates of the center of mass and thus of no interest. The coordinate q^1 is the sum of the radii and thus corresponds to the breathing coordinate. In contrast, q^2 corresponds to a motion where two diagonally opposite particles of the rectangle move away from each other, while the other two come closer together. For the definition eqn. C.13 and for $\varphi^1 = \varphi^2$, it follows that q^3 is the motion depicted in the left panel of fig. C.1, while q^4 corresponds to a rotation, where all particles move along the circle in the same direction.

It is straightforward to express the ξ^i in terms of the q^i :

$$\begin{aligned}\xi^1 &= q^1 + \frac{1}{2}q^2 & \varphi^1 &= q^3 + \frac{1}{2}q^4 \\ \xi^2 &= q^1 - \frac{1}{2}q^2 & \varphi^2 &= q^3 - \frac{1}{2}q^4.\end{aligned}\quad (\text{C.15})$$

With the masses of all four particles set equal, the Jacobian is $J = \frac{1}{4}(q^2)^2 - (q^1)^2$ or $J = -\xi^1\xi^2$, the product of the two inter particle distances.

Next, the distance of the particles from the center of mass is defined $q^1 = \xi$, as well as the change of the opening angle between neighboring particles from the equilibrium value $\pi/2$, $q^3 = \varphi$. The other coordinates are set to zero, $q^i = 0$ for $i = 1, 2, 4, \dots, 8$ for the whole process. With this constraints, the Laplacian for this model is given by

$$L = \frac{1}{\xi^2} \frac{\partial^2}{\partial \varphi^2} + \frac{2}{\xi} \frac{\partial}{\partial \xi} + \frac{\partial^2}{\partial \xi^2}.\quad (\text{C.16})$$

with $J = -\xi^2$. The sign reflects the choice of orientation for the Jacobi coordinates and may be easily changed by a redefinition of the coordinates. From the Laplacian, the kinetic energy operator can be determined. For example, if ξ is kept fixed, the kinetic energy operator is given by

$$KEO = -\frac{\hbar^2}{2\mu\xi^2} \frac{\partial^2}{\partial \varphi^2},\quad (\text{C.17})$$

where μ is twice the reduced mass of two CH-groups moving against each other, i.e. $\mu = 2\frac{m}{2} = m$.

Finally, care has to be taken for the normalization of the wave function. If $\int |\Psi|^2 d\mathbf{x} = 1$, then

$$1 = \int_{-\infty}^{\infty} \dots \int_{-\infty}^{\infty} \int_0^{\infty} \int_0^{\infty} \int_0^{2\pi} \int_0^{2\pi} |J| |\Psi|^2 d\varphi^2 d\varphi^1 d\xi^2 d\xi^1 dq^8 \dots dq^5.\quad (\text{C.18})$$

The integral boundaries change due to the change from rectilinear coordinates to polar coordinates. For the radii,

$$\int_0^{\infty} d\xi^1 \int_0^{\infty} d\xi^2 = \int_0^{\infty} dq^1 \int_{-2q^1}^{2q^1} dq^2\quad (\text{C.19})$$

and for the angles

$$\int_0^{2\pi} d\varphi^1 \int_0^{2\pi} d\varphi^2 = \int_0^{\pi} dq^3 \int_{-2q^3}^{2q^3} dq^4 + \int_{\pi}^{2\pi} dq^3 \int_{-2(q^3-\pi)}^{2(q^3-\pi)} dq^4.\quad (\text{C.20})$$

The constraint of normalization thus reads

$$1 = \int_{-\infty}^{\infty} \dots \int_{-\infty}^{\infty} dq^5 \dots dq^8 \int_0^{\infty} dq^1 \int_{-2q^1}^{2q^1} dq^2 \left(\int_0^{\pi} dq^3 \int_{-2q^3}^{2q^3} dq^4 + \int_{\pi}^{2\pi} dq^3 \int_{-2(q^3-\pi)}^{2(q^3-\pi)} dq^4 \right) |J| |\Psi|^2. \quad (\text{C.21})$$

C.4 The Kekulé vibrational mode of benzene

The procedure will be used to derive again the kinetic energy operator of section 4.2.3 in another way. To this end, the same assumptions as for the cyclobutadiene molecule are made, i.e. only motion in a plane is considered, each point of the hexagon is considered to be a CH-group and the same angles are used for the carbon nuclei and the attached hydrogen nuclei. Additionally, the distance between the carbon nuclei and the attached hydrogen nuclei are again kept fixed.

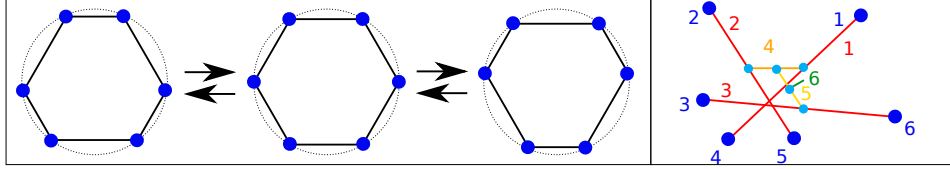


Figure C.2: Left: Relevant coordinate for the six particle system. Right: Particle numbering (blue) and Jacobi coordinates (yellow, orange and red; green is the center of mass), shown for an arbitrary configuration.

First, the Jacobi coordinates shown in figure C.2 are set up as

$$\begin{aligned} u^1 &= r^1 - r^4 \\ u^2 &= r^2 - r^5 \\ u^3 &= r^3 - r^6 \\ u^4 &= \frac{1}{m_{14}}(m_1 r^1 + m_4 r^4) - \frac{1}{m_{25}}(m_2 r^2 + m_5 r^5) \\ u^5 &= \frac{1}{m_{1245}}(m_1 r^1 + m_2 r^2 + m_4 r^4 + m_5 r^5) - \frac{1}{m_{63}}(m_3 r^3 + m_6 r^6) \\ u^6 &= \frac{1}{M} \sum_i m_i r^i. \end{aligned} \quad (\text{C.22})$$

The notation of the masses is similar as before, i.e. $m_{ij} = m_i + m_j$ and $m_{ijkl} = m_{ij} + m_{kl}$. The coordinates of interest are u^1, u^2, u^3 , as keeping their length fixed but rotating them appropriately will result in the motion that is to be described. Thus, these shall be expressed in terms of polar coordinates

$$\begin{aligned} u^1 &=: (\xi^1 \cos(\varphi^1), \xi^1 \sin(\varphi^1)) \\ u^2 &=: \left(\xi^2 \cos\left(\frac{\pi}{3} - \varphi^2\right), \xi^2 \sin\left(\frac{\pi}{3} - \varphi^2\right) \right) \\ u^3 &=: \left(\xi^3 \cos\left(\frac{2\pi}{3} + \varphi^3\right), \xi^3 \sin\left(\frac{2\pi}{3} + \varphi^3\right) \right). \end{aligned} \quad (\text{C.23})$$

The angles are chosen again such that their meaning is the displacement from the regular hexagon, which for benzene is the equilibrium configuration. The radii and angles are

combined via the orthogonal transformations

$$\begin{aligned} q^1 &= \frac{1}{3} (\xi^1 + \xi^2 + \xi^3) & q^4 &= \frac{1}{3} (\varphi^1 + \varphi^2 + \varphi^3) \\ q^2 &= \xi^1 - \xi^2 & q^5 &= \varphi^1 - \varphi^2 \\ q^3 &= \xi^2 - \xi^3 & q^6 &= \varphi^2 - \varphi^3 \end{aligned} \quad (\text{C.24})$$

with the inverse transformation

$$\begin{aligned} \xi^1 &= q^1 + \frac{2}{3}q^2 + \frac{1}{3}q^3 & \varphi^1 &= q^4 + \frac{2}{3}q^5 - \frac{1}{3}q^6 \\ \xi^2 &= q^1 - \frac{1}{3}q^2 + \frac{1}{3}q^3 & \varphi^2 &= q^4 - \frac{1}{3}q^5 - \frac{1}{3}q^6 \\ \xi^3 &= q^1 - \frac{1}{3}q^2 - \frac{2}{3}q^3 & \varphi^3 &= q^4 - \frac{1}{3}q^5 + \frac{2}{3}q^6. \end{aligned} \quad (\text{C.25})$$

By the choice made of measuring the angles, q^4 will correspond to the Kekulé mode motion. The masses of the particles are set equal again. With this coordinates, the Jacobian is a rather complicated expression, given by

$$J = \frac{1}{27}((3q^1 - q^2 + q^3)(q^2 - 3q^2 + 2q^3)(3q^1 + 2q^2 + q^3)). \quad (\text{C.26})$$

To reproduce the kinetic energy operator eqn. 4.44, the constraints $\varphi^1 = \varphi^2 = \varphi^3 =: \varphi$ (i.e. $q^5 = q^6 = 0$) and $\xi^1 = \xi^2 = \xi^3 =: \xi$ (i.e. $q^2 = q^3 = 0$) are used. Then, the Jacobian is obtained as $J = -\xi^3$ and the Laplacian is given by

$$L = \frac{2}{3\xi^2} \frac{\partial^2}{\partial \varphi^2} + \frac{2}{\xi} \frac{\partial}{\partial \xi} + \frac{2}{3} \frac{\partial^2}{\partial \xi^2}. \quad (\text{C.27})$$

For the kinetic energy, ξ is kept fixed to its equilibrium value. Then the kinetic energy operator is given by

$$KEO = -\frac{\hbar^2}{2\mu\xi^2} \frac{\partial^2}{\partial \varphi^2}, \quad (\text{C.28})$$

where the mass μ corresponds to three times the reduced mass of two particles moving against each other, $\mu = 3\frac{m}{2} = \frac{3}{2}m$. This is the same kinetic energy operator as was obtained in section 4.2.3. It can easily be extended, for example by not keeping ξ fixed and thus including a breathing motion of the ring.

C.5 Double bond shift and ring inversion of cyclooctatetraene

The final example is a model for the double bond shift in cyclooctatetraene with possible extension to include ring inversion. The process of changing from one D_{4h} configuration of cyclooctatetraene to the other via a D_{8h} configuration, cf. fig. C.3, is to be described. Then, it is shown how appropriate three-dimensional coordinates can be set up to include the two orthogonal ring inversion coordinates.

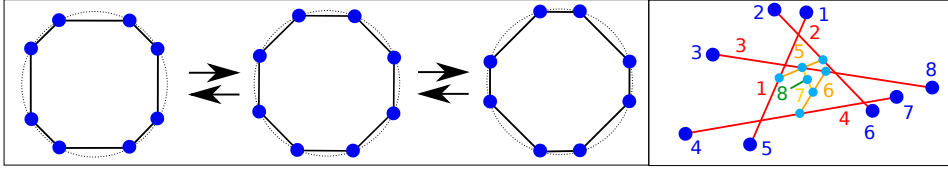


Figure C.3: Left: Relevant coordinate for the eight particle system, next to a breathing motion. Right: Particle numbering (blue) and jacobi coordinates (yellow, orange and red; green is the center of mass), shown for an arbitrary configuration.

The Jacobi coordinates of choice are

$$\begin{aligned}
 u^1 &= r^1 - r^5 \\
 u^2 &= r^2 - r^6 \\
 u^3 &= r^3 - r^7 \\
 u^4 &= r^4 - r^8 \\
 u^5 &= \frac{1}{m_{15}}(m_1 r^1 + m_5 r^5) - \frac{1}{m_{26}}(m_2 r^2 + m_6 r^6) \\
 u^6 &= \frac{1}{m_{37}}(m_3 r^3 + m_7 r^7) - \frac{1}{m_{48}}(m_4 r^4 + m_8 r^8) \\
 u^7 &= \frac{1}{m_{1256}}(m_1 r^1 + m_2 r^2 + m_5 r^5 + m_6 r^6) \\
 &\quad - \frac{1}{m_{3478}}(m_3 r^3 + m_4 r^4 + m_7 r^7 + m_8 r^8) \\
 u^8 &= \frac{1}{M} \sum_i m_i r^i.
 \end{aligned} \tag{C.29}$$

shown in figure C.3. The coordinates of interest are expressed in terms of polar coordinates as

$$\begin{aligned}
 u^1 &=: (\xi^1 \cos(\varphi^1), \xi^1 \sin(\varphi^1)) \\
 u^2 &=: \left(\xi^2 \cos\left(\frac{\pi}{4} - \varphi^2\right), \xi^2 \sin\left(\frac{\pi}{4} - \varphi^2\right) \right) \\
 u^3 &=: \left(\xi^3 \cos\left(\frac{\pi}{2} + \varphi^3\right), \xi^3 \sin\left(\frac{\pi}{2} + \varphi^3\right) \right) \\
 u^4 &=: \left(\xi^4 \cos\left(\frac{3\pi}{4} - \varphi^4\right), \xi^4 \sin\left(\frac{3\pi}{4} - \varphi^4\right) \right).
 \end{aligned} \tag{C.30}$$

These are combined to the final coordinates

$$\begin{aligned}
 q^1 &= \frac{1}{4} (\xi^1 + \xi^2 + \xi^3 + \xi^4) & q^5 &= \frac{1}{4} (\varphi^1 + \varphi^2 + \varphi^3 + \varphi^4) \\
 q^2 &= \xi^1 - \xi^2 & q^6 &= \varphi^1 - \varphi^2 \\
 q^3 &= \xi^2 - \xi^3 & q^7 &= \varphi^2 - \varphi^3 \\
 q^4 &= \xi^3 - \xi^4 & q^8 &= \varphi^3 - \varphi^4
 \end{aligned}$$

with the inverse transformation

$$\begin{aligned}
 \xi^1 &= q^1 + \frac{3}{4}q^2 + \frac{1}{2}q^3 + \frac{1}{4}q^4 & \varphi^1 &= q^5 + \frac{3}{4}q^6 + \frac{1}{2}q^7 + \frac{1}{4}q^8 \\
 \xi^2 &= q^1 - \frac{1}{4}q^2 + \frac{1}{2}q^3 + \frac{1}{4}q^4 & \varphi^2 &= q^5 - \frac{1}{4}q^6 + \frac{1}{2}q^7 + \frac{1}{4}q^8 \\
 \xi^3 &= q^1 - \frac{1}{4}q^2 - \frac{1}{2}q^3 + \frac{1}{4}q^4 & \varphi^3 &= q^5 - \frac{1}{4}q^6 - \frac{1}{2}q^7 + \frac{1}{4}q^8 \\
 \xi^4 &= q^1 - \frac{1}{4}q^2 - \frac{1}{2}q^3 - \frac{3}{4}q^4 & \varphi^4 &= q^5 - \frac{1}{4}q^6 - \frac{1}{2}q^7 - \frac{3}{4}q^8.
 \end{aligned}$$

The Jacobian is given by

$$J = \frac{-1}{256}((4q^1 - q^2 - 2q^3 + q^4)(4q^1 - q^2 + 2q^3 + q^4)(q^2 - 4q^1 + 2q^3 + 3q^4)(4q^1 + 3q^2 + 2q^3 + q^4)). \quad (\text{C.31})$$

Once more, all angles are set equal, $\varphi^1 = \varphi^2 = \varphi^3 = \varphi^4 =: \varphi$, so that q^6, q^7 and q^8 are zero and q^5 corresponds to the double bond shift. Also, all radial distances are set equal, $\xi^1 = \xi^2 = \xi^3 = \xi^4 =: \xi$. With this definitions, the Jacobian is $J = \xi^4$ and the Laplacian is

$$L = \frac{1}{2\xi^2} \frac{\partial^2}{\partial \varphi^2} + \frac{2}{\xi} \frac{\partial}{\partial \xi} + \frac{1}{2} \frac{\partial^2}{\partial \xi^2}. \quad (\text{C.32})$$

For a model of the double bond shift, the radial distance ξ can be kept fixed, as it does almost not change during the process [183]. However, if ring inversion is to be included, this degree of freedom may have to be taken into account: During ring inversion, the centers of mass of the CH-groups do not move on a sphere, but the radial distance is smaller for the equilibrium D_{2d} structure of cyclooctatetraene than it is for the planar D_{4h} transition state structure [183].

There are two orthogonal ring inversion coordinates, as explained in Appendix D. These can be incorporated by using spherical coordinates instead of the polar coordinates of eqn. C.30,

$$\begin{aligned} u^1 &=: \left(\xi^1 \cos(\varphi^1) \cos(\theta^1) \quad , \quad \xi^1 \sin(\varphi^1) \cos(\theta^1) \quad , \quad \xi^1 \sin(\theta^1) \right) \\ u^2 &=: \left(\xi^2 \cos\left(\frac{\pi}{4} - \varphi^2\right) \cos(\theta^2) \quad , \quad \xi^2 \sin\left(\frac{\pi}{4} - \varphi^2\right) \cos(\theta^2) \quad , \quad \xi^2 \sin(\theta^2) \right) \\ u^3 &=: \left(\xi^3 \cos\left(\frac{\pi}{2} + \varphi^3\right) \cos(\theta^3) \quad , \quad \xi^3 \sin\left(\frac{\pi}{2} + \varphi^3\right) \cos(\theta^3) \quad , \quad \xi^3 \sin(\theta^3) \right) \\ u^4 &=: \left(\xi^4 \cos\left(\frac{3\pi}{4} - \varphi^4\right) \cos(\theta^4) \quad , \quad \xi^4 \sin\left(\frac{3\pi}{4} - \varphi^4\right) \cos(\theta^4) \quad , \quad \xi^4 \sin(\theta^4) \right). \end{aligned}$$

While the equations for the radii ξ^i and in-plane angles φ^i stay the same, there are additional collective coordinates describing the out-of plane motion, given by

$$\begin{aligned} q^9 &= \frac{1}{4} (\theta^1 + \theta^2 + \theta^3 + \theta^4) \\ q^{10} &= \frac{1}{4} (\theta^1 + \theta^2 - \theta^3 - \theta^4) \\ q^{11} &= \frac{1}{4} (\theta^1 - \theta^2 - \theta^3 + \theta^4) \\ q^{12} &= \frac{1}{4} (\theta^1 - \theta^2 + \theta^3 - \theta^4) \end{aligned}$$

with back-transformation

$$\begin{aligned} \theta^1 &= q^9 + q^{10} + q^{11} + q^{12} \\ \theta^2 &= q^9 + q^{10} - q^{11} - q^{12} \\ \theta^3 &= q^9 - q^{10} - q^{11} + q^{12} \\ \theta^4 &= q^9 - q^{10} + q^{11} - q^{12}. \end{aligned}$$

The two ring inversion coordinates are q^{10} and q^{11} . By repetition of the procedure explained above, the Jacobian and the Laplacian for a four-dimensional model describing double bond shift (bond-alternation coordinate and a ring-breathing coordinate) as well as ring inversion

(two ring inversion coordinates) can be obtained.

Appendix D

Quantum chemistry of cyclooctatetraene

In chapter 4.1, coherent nuclear tunneling in cyclooctatetraene at zero temperature was discussed. Tunneling happens in a symmetric quadruple-well potential. Each minimum corresponds to a D_{2d} equilibrium structure of cyclooctatetraene. The minimum energy path for the interconversion of one of these structures into another passes either through a transition state of D_{4h} point group symmetry, or through a transition state of D_{8h} point group symmetry. The former path is called ring inversion, and the latter double bond shift. Fig. 4.2 in section 4.1.2 shows the potential energy surface schematically.

In order to estimate the tunneling times for the interconversion of the equilibrium structures as described in section 4.1.3, accurate values for the barrier heights of ring inversion and double bond shift were needed. Literature values for these barriers were either estimated by experiment [14, 15, 169, 171] or computed using at best the CASPT2 method [13, 30, 33, 79–81, 174, 237]. However, test calculations showed that CASPT2 is not suited to describe the double bond shift. Consequently, a quantum chemical study of the system was performed. Part of the results are presented here, and further information can be found in [183].

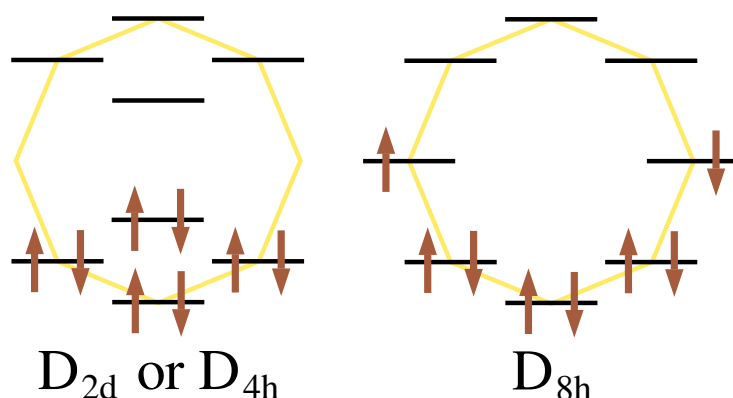


Figure D.1: Energetical ordering and occupation of the π -electrons or π -like electrons for the transition state of ring inversion and the equilibrium structure (left), as well as for the π -electrons of the transition state of double bond shift (right). Black bars represent location of orbital energies (with lowest energy at the bottom and highest energy at the top; not to scale) and brown arrows represent occupation of the orbitals with electrons, in a Hückel picture.

In the following, the D_{2d} ground state equilibrium structure will be denoted GS, the D_{4h}

	ΔE_{RI}	$\Delta E_{\text{RI}}(\text{MRCI})$	ΔE_{DBS}	$\Delta E_{\text{DBS}}(\text{MRCI})$
HF	13.46	-	24.16	-
CCSD(T)	12.62	-	13.30	-
CAS(8,8)	10.61	10.44	7.38	7.37
CASPT2*	14.06	-	3.67	-
CASPT2	11.68	-	0.17	-
CASPT3*	13.00	13.00	7.31	7.31
CASPT3	10.50	11.14	6.69	6.68
MRCI(Dav.)*	13.29	13.29	7.40	7.40
MRCI(Dav.)	-	11.73	-	6.55
MR-ACPF*	12.99	13.00	7.36	7.36
MR-ACPF	-	11.19	-	6.65

Table D.1: Energy differences in kcal/mol between the equilibrium structure and the transition state for ring inversion (ΔE_{RI}) as well as between the transition state for ring inversion and the transition state for double bond shift (ΔE_{DBS}) obtained with different methods (first column), with a cc-pVTZ basis set. The second and fourth column represent the values obtained with structures optimized with the given method, while the third and fifth column represent the values obtained with structures optimized with the MRCI(Dav.)* method. Red values show problematic energy differences. Blue values show the energy decrease from inclusion of only a limited number of valence orbitals (the methods with an asterisk) to inclusion of all valence orbitals in the calculations. Green values show the recommended barrier heights for the respective processes.

transition state structure for ring inversion TS-RI, and the D_{8h} transition state structure for double bond shift by TS-DBS. The energetic situation of the π -orbitals for the three structures is shown in Fig. D.1. Note that in case of the GS, the respective orbitals are not π -orbitals but only π -like orbitals, as the molecule is not planar. However, this distinction is of minor importance for now and will thus be ignored.

In case of the GS and the TS-RI there is a gap between the highest occupied and the lowest unoccupied molecular orbital. In both cases it can be expected that already a single reference quantum chemical method will give a reasonable energy for the structures, and thus a reasonable value for the barrier of ring inversion. However, for TS-DBS there are two degenerate highest occupied orbitals. Consequently, it can be expected that any method which uses only a single Hartree-Fock reference determinant will not capture this so-called static electron correlation.

A multi-reference method needs to be used to describe the three structures on equal footing, and to give reliable barriers for both ring inversion and double bond shift. Thus, at least a CASSCF(8,8) calculation including eight electrons in eight π -orbitals should be used. Such a calculation alone would prefer the contribution of the π -orbitals over the other orbitals. In order to get a more balanced description (to capture the dynamic electron correlation), subsequently either multi-reference perturbation theory or multi-reference configuration interaction calculations have to be performed.

GS, TS-RI and TS-DBS were calculated using the program package Molpro [225] with a cc-pVTZ basis set. Table D.1 shows the results for the barrier heights of ring inversion and double bond shift using a variety of methods. The energy difference ΔE_{RI} is the difference between the energy of GS and the energy of TS-RI, and ΔE_{DBS} is the difference between the energy of TS-RI and the energy of TS-DBS. Thus, the barrier for ring inversion is ΔE_{RI} , while the barrier for double bond shift is $\Delta E_{\text{RI}} + \Delta E_{\text{DBS}}$.

From experiment it is known that $\Delta E_{\text{RI}}^0 \approx 10$ kcal/mol [15, 169, 171] and $\Delta E_{\text{DBS}}^0 \approx 4$ kcal/mol [14, 169]. These values have to be compared with the energy differences of the structures, but including the zero point vibration. The effect of zero point vibration was not calculated here but can be estimated using the values of [80]: In order to compare with the experimental values, for the ΔE_{RI} and ΔE_{DBS} calculated here ca. 0.5 kcal/mol and

-2.7 kcal/mol have to be added, respectively.

From the table, it is immediately apparent that single reference methods already give reasonable values for ΔE_{RI} but are completely off for ΔE_{DBS} : While e.g. CCSD(T) gives $\Delta E_{\text{RI}} = 12.6$ kcal/mol which compares well with experiment, $\Delta E_{\text{DBS}} = 13.3$ kcal/mol is more than twice as large as the experimental estimation. A CAS(8,8) calculation lowers ΔE_{RI} to 10.6 kcal/mol and ΔE_{DBS} to 7.4 kcal/mol, which, including the zero point energy, is already in very good agreement with the experiment.

To describe the electron correlation in a balanced way, subsequent multi-reference perturbation theory to second order (CASPT2) and to third order (CASPT3), as well as multi-reference configuration interaction with Davidson correction (MRCI) and the multi-reference averaged coupled pair functional method (MR-ACPF) were used. While CASPT2 is still a comparably cheap method, already CASPT3 is computationally expensive, and the other methods are even more so. Consequently, for some calculations of the dynamical correlation, only a subset of orbitals was included. All methods marked with an asterisk have been calculated treating the eight valence (natural) orbitals with mainly CH-bond character as core orbitals, thus correlation only the "CC-bonds". Although structure optimizations with the demanding methods were not possible, single point calculations with the nuclear structure optimized at MRCI(Dav.)* level were performed. The results of these calculations are given in the table as $\Delta E_{\text{RI}}(\text{MRCI})$ and $\Delta E_{\text{DBS}}(\text{MRCI})$. Note that the nuclear structure agrees very well with the experiment for all methods, as discussed in detail in [183].

Inclusion of dynamic correlation of the CC-bonds increases the barriers for ring inversion compared to the CAS(8,8) value to ca. 13 kcal/mol. However, inclusion of all valence orbitals for calculation of the dynamic correlation reduces the barrier again. This effect can be seen with all methods, and the resulting numbers are all very similar. The best method for which structure optimization was still possible is CASPT3. Consequently, the best estimate for ΔE_{RI} is 10.5 kcal/mol (or 11.0 kcal/mol with inclusion of the zero point vibrational energy).

For double bond shift, the best method found in the literature so far, CASPT2, seems to completely fail: The barrier is far too low and almost vanishes when all valence orbitals are included for determination of the dynamic correlation. However, CASPT3 gives values for ΔE_{DBS} that compare favorably with MRCI and MR-ACPF. Again, all valence orbitals have to be included for determination of the dynamic correlation. The best estimate for ΔE_{DBS} is the CASPT3 value of 6.7 kcal/mol (or 4.0 kcal/mol with inclusion of the zero point vibrational energy).

Finally, it should be noted that CAS(8,8) already gives surprisingly good values for both ΔE_{RI} and ΔE_{DBS} . It thus seems like dynamic correlation is similar in the three structures, and CAS(8,8) might be a computationally cheap method for a dynamics simulation of the system.

Appendix E

Structure of malonaldehyde and the formic acid dimer

For the calculations in chapter 4.3 the electron density of the equilibrium structure of malonaldehyde and the formic acid dimer was used. The equilibrium structure was determined by a Hartree-Fock calculation with a cc-pVTZ basis set (HF/cc-pVTZ), using the program Molpro [225].

In table E.1 the structure parameters of the molecules are compared with experimental reference values. The reference values are found in [21] for the formic acid dimer and in [212] for malonaldehyde. In both articles, the experimental values are compiled from different sources in order to compare with MP2 and B3LYP calculations, using a comparable basis set.

The aim in chapter 4.3 is to analyze the reaction mechanism of coherent proton tunneling in both molecules by using the electron density and electron fluxes due to the change of the electron density in time. In the HF/cc-pVTZ calculations for both molecules, all nuclei were constrained to be in a plane. This assumption reduced the number of parameters to be optimized but does not influence the reaction mechanism significantly, as both molecules are almost planar in their equilibrium structure.

Table E.1 shows that the structure parameters of the HF/cc-pVTZ calculations are already in reasonable agreement with the experimental structure. Although in [21] it was shown that a B3LYP/6-311++G(3df,2p) calculation gives better structure parameters for the formic acid dimer, and in [212] it was shown that a MP2/6-31G** calculation gives better structure parameters for malonaldehyde, the deviation of the HF/cc-pVTZ values from the experiment will not affect the angular reaction mechanism significantly. Only the electron density, a rather robust quantity, was needed for the analysis, and thus calculations with methods improving the Hartree-Fock result were not performed.

formic acid dimer	HF/cc-pVTZ	experiment	malonaldehyde	HF/cc-pVTZ	experiment
C–H	108.4	107.9	C–C	145.2	145.4
C=O	119.0	121.7	C=C	133.9	134.8
C–O	129.6	132.0	C=O	120.0	123.4
O–H	96.1	103.3	C–O	130.8	132.0
O⋯H	182.7	-	C–H(1)	107.0	109.1
O⋯O	278.4	270.3	C–H(2)	109.2	109.4
			C–H(3)	107.4	108.9
			O–H	95.4	96.9
			O⋯H	188.1	168.0
			O⋯O	268.1	255.3
H–C=O	122.3	115.4	C–C=C	121.0	119.4
O=C–O	125.9	126.2	C=C–O	126.1	124.5
C–O–H	111.3	108.5	C–O–H	109.3	106.3
O⋯H–O	174.1	180	O⋯H–O	139.8	147.6
			H⋯O=C	99.5	-
			O=C–C	124.3	123.0
			O=C–H	119.5	-
			H–C–C	116.2	117.6
			C–C–H	119.5	-
			H–C=C	119.5	-
			C=C–H	121.2	122.3
			H–C–O	112.7	-

Table E.1: Equilibrium structure parameters of the formic acid dimer and of malonaldehyde calculated with the Hartree-Fock method and a cc-pVTZ basis set (HF/cc-pVTZ), and experimental values from [21] (formic acid dimer) and [212] (malonaldehyde). All distances are in pm, all angles are in degrees. For malonaldehyde, C–H(1) is the C–CH=C hydrogen nucleus, C–H(2) is the O=CH–C hydrogen nucleus, and C–H(3) is the C=CH–O hydrogen nucleus.

Bibliography

- [1] Gnu octave. See <http://www.gnu.org/software/octave>.
- [2] Gnuplot 4.4. See <http://www.gnuplot.info/>.
- [3] Inkscape 0.47. See <http://www.inkscape.org>.
- [4] Matlab r2011a. See <http://www.mathworks.com>.
- [5] Molden 5.0. See <http://www.cmbi.ru.nl/molden/molden.html>.
- [6] Python programming language 2.7. See <http://www.python.org>.
- [7] Sage open source mathematics software. See <http://www.sagemath.org>.
- [8] Symbolic math toolbox for matlab r2011a. See <http://www.mathworks.com/help/symbolic/index.html>.
- [9] Ali Abedi, Neepa T. Maitra, and Eberhard K.U. Gross. Exact Factorization of the Time-Dependent Electron-Nuclear Wave Function. *Physical Review Letters*, 105:123002(4), 2010.
- [10] Antonio Accardi, Ingo Barth, Oliver Kühn, and Jörn Manz. From Synchronous to Sequential Double Proton Transfer: Quantum Dynamics Simulations for the Model Porphine. *The Journal of Physical Chemistry A*, 114:11252–11262, 2010.
- [11] Santiago Alvarez. Chemistry: A Panoply of Arrows. *Angewandte Chemie International Edition*, 51:590–600, 2012.
- [12] Dirk Andrae, Ingo Barth, Timm Bredtmann, Hans-Christian Hege, Jörn Manz, Falko Marquardt, and Beate Paulus. Electronic Quantum Fluxes during Pericyclic Reactions Exemplified for the Cope Rearrangement of Semibullvalene. *The Journal of Physical Chemistry B*, 115:5476–5483, 2011.
- [13] José Andrés, Obis Castaño, Antonio Morreale, Raul Palmeiro, and Roberto Gomperts. Potential energy surface of cyclooctatetraene. *The Journal of Chemical Physics*, 108:203–207, 1998.
- [14] F. A. L. Anet. The Rate of Bond Change in Cycloöctatetraene. *Journal of the American Chemical Society*, 84:671–672, 1962.
- [15] F. A. L. Anet, A. J. R. Bournand, and Y. S. Lin. Ring inversion and bond shift in cyclooctatetraene derivatives. *Journal of the American Chemical Society*, 86:3576–3577, 1964.
- [16] Donu Arapura. Introduction to differential forms, 2012. See <http://www.math.purdue.edu/~dvb/>.

- [17] Rutherford Aris. *Vectors, Tensors, and the Basic Equations of Fluid Mechanics*. Dover Publications, New York, 1989.
- [18] Jochen Autschbach and Tom Ziegler. Double perturbation theory: A powerful tool in computational coordination chemistry. *Coordination Chemistry Reviews*, 238/239:83–126, 2003.
- [19] Richard F. W. Bader, Jesus Hernández-Trujillo, and Fernando Cortés-Guzmán. Chemical bonding: From Lewis to atoms in molecules. *Journal of Computational Chemistry*, 28:4–14, 2007.
- [20] Michael Baer. *Beyond Born-Oppenheimer: Conical Intersections and Electronic Nonadiabatic Coupling Terms*. John Wiley & Sons, Hoboken, New Jersey, 2006.
- [21] Roman M. Balabin. Polar (Acyclic) Isomer of Formic Acid Dimer: Gas-Phase Raman Spectroscopy Study and Thermodynamic Parameters. *The Journal of Physical Chemistry A*, 113:4910–4918, 2009.
- [22] George L. Barnes, Shane M. Squires, and Edwin L. Silbert III. Symmetric Double Proton Tunneling in Formic Acid Dimer: A Diabatic Basis Approach. *The Journal of Physical Chemistry B*, 112:595–603, 2008.
- [23] Ingo Barth. Translational Effects on Electronic and Nuclear Ring Currents. *The Journal of Physical Chemistry A*, 116:11283–11303, 2012.
- [24] Ingo Barth, Christian Bressler, Shiro Koseki, and Jörn Manz. Strong Nuclear Ring Currents and Magnetic Fields in Pseudorotating OsH₄ Molecules Induced by Circularly Polarized Laser Pulses. *Chemistry – An Asian Journal*, 7:1261–1295, 2012.
- [25] Ingo Barth, Hans-Christian Hege, Hiroshi Ikeda, Anatole Kenfack, Michael Koppitz, Jörn Manz, Falko Marquardt, and Guennaddi K. Paramonov. Concerted quantum effects of electronic and nuclear fluxes in molecules. *Chemical Physics Letters*, 481:118–123, 2009.
- [26] Ingo Barth and Jörn Manz. Periodic Electron Circulation Induced by Circularly Polarized Laser Pulses: Quantum Model Simulations for Mg-Porphyrin. *Angewandte Chemie International Edition*, 45:2962–2965, 2006.
- [27] Ingo Barth and Jörn Manz. Electric ring currents in atomic orbitals and magnetic fields induced by short intense circularly polarized π laser pulses. *Physical Review A*, 75:012510, 2007.
- [28] Ingo Barth, Jörn Manz, Yasuteru Shigeta, and Kiyoshi Yagi. Unidirectional Electronic Ring Current Driven by a Few Cycle Circularly Polarized Laser Pulse: Quantum Model Simulations for Mg-Porphyrin. *Journal of the American Chemical Society*, 128:7043–7049, 2006.
- [29] David E. Bean and Patrick W. Fowler. Effect on Ring Current of the Kekulé Vibration in Aromatic and Antiaromatic Rings. *The Journal of Physical Chemistry A*, 115:13649–13656, 2011.
- [30] Michael J. Bearpark, Luis Blancafort, and Michael A. Robb. The pseudo-Jahn-Teller effect: a CASSCF diagnostic. *Molecular Physics*, 100:1735–1739, 2002.

- [31] Michale H. Beck, Andreas Jäckle, Graham A. Worth, and Hans-Dieter Meyer. The multiconfiguration time-dependent Hartree method: A highly efficient algorithm for propagating wavepackets. *Physics Reports*, 324:1–105, 2000.
- [32] Jozef Bicerano, Henry F. Schäfer III, and William H. Miller. Structure and Tunneling Dynamics of Malonaldehyde. A Theoretical Study. *Journal of the American Chemical Society*, 105:2550–2553, 1983.
- [33] Luis Blancafort, Michael J. Bearpark, and Michael A. Robb. Ring puckering of cyclooctatetraene and cyclohexane is induced by pseudo-Jahn-Teller coupling. *Molecular Physics*, 104:2007–2010, 2006.
- [34] Katharina Boguslawski, Konrad H. Marti, Örs Legeza, and Markus Reiher. Accurate ab Initio Spin Densities. *Journal of Chemical Theory and Computation*, 8:1970–1982, 2012.
- [35] Arno Bohm, Brian Kendrick, Mark E. Loewe, and Luis J. Boya. The Berry connection and Born-Oppenheimer method. *Journal of Mathematical Physics*, 33:977–989, 1992.
- [36] Max Born and Robert J. Oppenheimer. Zur Quantentheorie der Molekeln. *Annalen der Physik*, 84:457–474, 1927.
- [37] Timothy B. Boykin. An alternative view of the continuity equation in quantum mechanics. *American Journal of Physics*, 68:665–667, 1999.
- [38] S. Francis Boys. Construction of Some Molecular Orbitals to Be Approximately Invariant for Changes from One Molecule to Another. *Reviews of Modern Physics*, 32:296–299, 1960.
- [39] Olaf Brackhagen, Oliver Kühn, Jörn Manz, Volkhard May, and Rolf Meyer. Coherent and dissipative wave packet dynamics in cyclic model systems with four equivalent potential minima. *The Journal of Chemical Physics*, 100:9007, 1994.
- [40] Matthew J. Bramley, William H. Green, and Nicholas C. Handy. Vibration-rotation coordinates and kinetic energy operators for polyatomic molecules. *Molecular Physics*, 73:1183–1208, 1991.
- [41] Fabian Brau, Francis Michel, and Guy Reidemeister. Barrier and internal wave contributions to the quantum probability density and flux in light heavy-ion elastic scattering. *Physical Review C*, 57:1386–1397, 1998.
- [42] Timm Bredtmann, Emanuel Hupf, and Beate Paulus. Electronic fluxes during large amplitude vibrations of single, double and triple bonds. *Physical Chemistry and Chemical Physics*, 14:15494–15501, 2012.
- [43] Timm Bredtmann, Hiroyuki Katsuki, Jörn Manz, Kosuke Nakamura, and Christian Stemmlé. Nuclear Flux Densities during a Model Pericyclic Reaction with Energies Well Above and Below the Potential Barrier. *ChemPhysChem*, 14:1397–1404, 2013.
- [44] Timm Bredtmann, Hiroyuki Katsuki, Jörn Manz, Kenji Ohmori, and Christian Stemmlé. Wavepacket interferometry for nuclear densities and flux densities. *Molecular Physics*, 2013.
- [45] Timm Bredtmann and Jörn Manz. Electronic Bond-to-Bond Fluxes in Pericyclic Reactions: Synchronous or Asynchronous? *Angewandte Chemie International Edition*, 50:12652–12654, 2011.

- [46] Heinz-Peter Breuer and Francesco Petruccione. *The Theory of Open Quantum Systems*. Oxford University Press, New York, 2002.
- [47] Ilja N. Bronstein and Konstantin A. Semendjajew. *Taschenbuch der Mathematik*. B.G. Teubner, Leipzig, 1958.
- [48] Philip R. Bunker and Per Jensen. *Molecular Symmetry and Spectroscopy*. NRC Research Press, Ottawa, 2006.
- [49] Mauricio Cafiero and Ludwik Adamowicz. Molecular structure in non-Born-Oppenheimer quantum mechanics. *Chemical Physics Letters*, 387:136–141, 2004.
- [50] Obis Castaño, Raúl Palmeiro, Luis Manuel Frutos, and José Luis Andrés. Role of bifurcation in the bond shifting of cyclooctatetraene. *Journal of Computational Chemistry*, 23:732–736, 2002.
- [51] Lorenz S. Cederbaum. *Born-Oppenheimer approximation and beyond*. Advanced Series in Physical Chemistry 15, World Scientific, Singapore, 2004.
- [52] Lorenz S. Cederbaum. Born-Oppenheimer approximation and beyond for time-dependent electronic processes. *The Journal of Chemical Physics*, 128:124101(8), 2008.
- [53] Xavier Chapuisat and André Nauts. A Method to obtain the Eckart Hamiltonian and the equations of motion of a highly deformable polyatomic system in terms of generalized coordinates. *Chemical Physics*, 56:91–105, 1981.
- [54] Mark S. Child. *Molecular Collision Theory*. Dover, New York, 1996.
- [55] Claude Cohen-Tannoudji, Bernard Diu, and Frank Laloë. *Quantum Mechanics*. Hermann, Paris, 1977.
- [56] Claude Cohen-Tannoudji, Jacques Dupont-Roc, and Gilbert Grynberg. *Photons & Atoms*. John Wiley & Sons, New York, 1989.
- [57] Frank Cordes, Marcus Weber, and Johannes Schmidt-Ehrenberg. Metastable Conformations via successive Perron-Cluster Cluster Analysis of dihedrals. Technical report, Konrad-Zuse-Zentrum für Informationstechnik Berlin, 2002.
- [58] Maurício D. Coutinho-Neto, Alexandra Viel, and Uwe Manthe. The ground state tunneling splitting of malonaldehyde: Accurate full dimensional quantum dynamics calculations. *Journal of Chemical Physics*, 121:9207–9210, 2004.
- [59] Maurício D. Coutinho-Neto, Alexandra Viel, and Uwe Manthe. The ground state tunneling splitting of malonaldehyde: Accurate full dimensional quantum dynamics simulations. *The Journal of Chemical Physics*, 121:9207–9210, 2004.
- [60] David P. Craig and Thiru Thirunamachandran. *Molecular Quantum Electrodynamics*. Dover, New York, 1998.
- [61] Ernest R. Davidson. Properties and Uses of Natural Orbitals. *Reviews of Modern Physics*, 44:451–463, 1972.
- [62] Philippe Dennery and André Krzywicki. *Mathematics for Physicists*. Dover, New York, 1996.

- [63] Peter Deuffhard and Marcus Weber. Robust Perron Cluster Analysis in Conformational Dynamics. Technical report, Konrad-Zuse-Zentrum für Informationstechnik Berlin, 2003.
- [64] Peter Deuffhard and Marcus Weber. Robust Perron cluster analysis in conformation dynamics. *Linear Algebra and its Applications*, 398:161–184, 2005.
- [65] Otto Diels and Kurt Alder. Synthesen in der hydroaromatischen Reihe. *Justus Liebig's Annalen der Chemie*, 460:98–122, 1928.
- [66] Dennis J. Diestler. Coupled-Channels Quantum Theory of Electronic Flux Density in Electronically Adiabatic Processes: Fundamentals. *The Journal of Physical Chemistry A*, 116:2728–2735, 2012.
- [67] Dennis J. Diestler. Quasi-Classical Theory of Electronic Flux Density in Electronically Adiabatic Molecular Processes. *The Journal of Physical Chemistry A*, 116:11161–11166, 2012.
- [68] Dennis J. Diestler, Anatole Kenfack, Jörn Manz, and Beate Paulus. Coupled-Channels Quantum Theory of Electronic Flux Density in Electronically Adiabatic Processes: Application to the Hydrogen Molecule Ion. *The Journal of Physical Chemistry A*, 116:2736–2742, 2012.
- [69] Dennis J. Diestler, Anatole Kenfack, Jörn Manz, Beate Paulus, Jhon Fredy Pérez-Torres, and Vincent Pohl. Computation of the Electronic Flux Density in the Born-Oppenheimer Approximation. *The Journal of Physical Chemistry A*, 2013. doi:10.1021/jp4002302.
- [70] Thom H. Dunning. Gaussian basis sets for use in correlated molecular calculations. I. The atoms boron through neon and hydrogen. *The Journal of Chemical Physics*, 90:1007–1023, 1989.
- [71] Marta B. Ferraro, Francesco Faglioni, Andrea Ligabue, Stefano Pelloni, and Paolo Lazzeretti. Ring current effects on nuclear magnetic shielding of carbon in the benzene molecule. *Magnetic Resonance in Chemistry*, 43:316–320, 2005.
- [72] Alexander L. Fetter and John Dirk Walecka. *Quantum Theory of Many-Particle Systems*. Dover, New York, 2003.
- [73] Harley Flanders. *Differential Forms with Applications to the Physical Sciences*. Dover, New York, 1989.
- [74] L. Fortunato. All transformations of coordinates that separate the center of mass kinetic energy, their group structure and geometry. *Journal of Physics A: Mathematical and Theoretical*, 43:065301(9), 2010.
- [75] Teresa B. Freedman, Xuling Gao, Mei-Ling Shih, and Laurence A. Nafie. Electron Transition Current Density in Molecules. 2. Ab Initio Calculations for Electronic Transitions in Ethylene and Formaldehyde. *The Journal of Physical Chemistry A*, 102:3352–3357, 1998.
- [76] Teresa B. Freedman, Mei-Ling Shih, Eunah Lee, and Laurence A. Nafie. Electron Transition Current Density in Molecules. 3. Ab Initio Calculations for Vibrational Transitions in Ethylene and Formaldehyde. *Journal of the American Chemical Society*, 119:10620–10626, 1997.

- [77] Gernot Frenking and Sason Shaik (editors). Special Issue: “90 Years of Chemical Bonding”. *Journal of Computational Chemistry*, 28:1–466, 2007.
- [78] Gernot Frenking and Andreas Krapp. Unicorns in the world of chemical bonding models. *Journal of Computational Chemistry*, 28:15–24, 2007.
- [79] Luis-Manuel Frutos, Obis Castaño, and Manuela Merchán. Theoretical determination of the singlet \rightarrow singlet and singlet \rightarrow triplet electronic spectra, lowest ionization potentials, and electron affinity of cyclooctatetraene. *The Journal of Physical Chemistry A*, 107:5472–5478, 2003.
- [80] Marco Garavelli, Fernando Bernardi, Alessandro Cembran, Obis Castaño, Luis Manuel Frutos, Manuela Merchán, and Massimo Olivucci. Cyclooctatetraene computational photo- and thermal chemistry: A reactivity model for conjugated hydrocarbons. *Journal of the American Chemical Society*, 124:13770–13789, 2002.
- [81] Marco Garavelli, Fernando Bernardi, Vincente Moliner, and Massimo Olivucci. Intrinsically competitive photoinduced polycyclization and double-bond shift through a boatlike conical intersection. *Angewandte Chemie International Edition*, 40:1466–1468, 2001.
- [82] Fabien Gatti and Christophe Iung. Exact and constrained kinetic energy operators for polyatomic molecules: The polyspherical approach. *Physics Reports*, 484:1–69, 2009.
- [83] Fabien Gatti, Claudio Muñoz, and Christophe Iung. A general expression of the exact kinetic energy operator in polyspherical coordinates. *Journal of Chemical Physics*, 114:8275–8281, 2001.
- [84] Ronald J. Gillespie and Edward A. Robinson. Gilbert N. Lewis and the chemical bond: The electron pair and the octet rule from 1916 to the present day. *Journal of Computational Chemistry*, 28:87–97, 2007.
- [85] Jan Govaerts. A Pedestrian Introduction to the Mathematical Concepts of Quantum Physics. *arXiv:0812.0721*, 2008.
- [86] Thomas Grohmann, Jörn Manz, and Axel Schild. Effects of molecular symmetry on the directions of nuclear flux densities during tunneling in double well potentials. *Molecular Physics*, 2013. doi:10.1080/00268976.2013.800599.
- [87] George A. Hagedorn. A Time Dependent Born-Oppenheimer Approximation. *Communications of Mathematical Physics*, 77:1–19, 1980.
- [88] George A. Hagedorn. High order corrections to the time-dependent Born-Oppenheimer approximation I: Smooth potentials. *Communications of Mathematical Physics*, 124:571–590, 1986.
- [89] George A. Hagedorn and Alain Joye. Mathematical Analysis of Born-Oppenheimer Approximations. In *Proceedings of Symposia in Pure Mathematics 76*, volume 76, pages 203–226, 2007. Online at <http://www-fourier.ujf-grenoble.fr/>
- [90] Richard Wesley Hamming. *Numerical Methods for Scientists and Engineers*. Dover, New York, 1986.
- [91] Claudia Hampel, Kirk A. Peterson, and Hans-Joachim Werner. A comparison of the efficiency and accuracy of the quadratic configuration interaction (QCISD), coupled cluster (CCSD), and Brueckner coupled cluster (BCCD) methods. *Chemical Physics Letters*, 190:1–12, 1992.

- [92] Nicolas C. Handy. The derivation of vibration-rotation kinetic energy operators, in internal coordinates. *Molecular Physics*, 61:201–223, 1987.
- [93] Bernd Hartke and Jörn Manz. Do Chemical Reactions React along the Reaction Path? *Journal of the American Chemical Society*, 110:3063–3068, 1988.
- [94] Douglas R. Hartree. The Wave Mechanics of an Atom with a Non-Coulomb Central Field. Part I. Theory and Methods. *Mathematical Proceedings of the Cambridge Philosophical Society*, 24:89–110, 1928.
- [95] Gernot Hauke, Jörn Manz, and Joachim Röhmelt. Collinear Triatomic Reactions Described by Polar Delves Coordinates. *The Journal of Chemical Physics*, 73:5040–5044, 1980.
- [96] Remco W. A. Havenith, Partick W. Fowler, and Leonardus W. Jenneskens. Persistence of Paratropic Ring Currents in Nonplanar, Tub-Shaped Geometries of 1,3,5,7-Cyclooctatetraene. *Organic Letters*, 8:1255–1258, 2006.
- [97] Daniel J. Haxton, Keith V. Lawler, and C. William McCurdy. Multiconfiguration time-dependent Hartree-Fock treatment of electronic and nuclear dynamics in diatomic molecules. *Physical Review A*, 83:063416(16), 2011.
- [98] Hans-Christian Hege, Jörn Manz, Falko Marquardt, Beate Paulus, and Axel Schild. Electron flux during pericyclic reactions in the tunneling limit: Quantum simulation for cyclooctatetraene. *Chemical Physics*, 376:46–55, 2010.
- [99] Walter Heitler and Fritz London. Wechselwirkung neutraler Atome und homöopolare Bindung nach der Quantenmechanik. *Zeitschrift für Physik*, 44:455–472, 1927.
- [100] Niels Engholm Henriksen and Flemming Yssing Hansen. *Theories of Molecular Reaction Dynamics: The Microscopic Foundation of Chemical Kinetics*. Oxford University Press, New York, 2008.
- [101] Joseph O. Hirschfelder. Coordinates which Diagonalize the Kinetic Energy of Relative Motion. *International Journal of Quantum Chemistry*, IIIS:17–31, 1969.
- [102] Joseph O. Hirschfelder, W. Byers Brown, and Saul T. Epstein. Recent Developments in Perturbation Theory. *Advances in Quantum Chemistry*, 1:255–374, 1964. partially online at <http://ntrs.nasa.gov/search.jsp?R=19650016348>.
- [103] Sigeru Huzinaga. *Gaussian basis sets for molecular calculations*. Elsevier, Amsterdam, 1984.
- [104] Mikael P. Johansson, Jonas Jusélius, and Dage Sundholm. Sphere Currents of Buckminsterfullerene. *Angewandte Chemie International Edition*, 44:1843–1846, 2005.
- [105] Loïc Joubert-Doriol, Benjamin Lasorne, Fabien Gatti, Markus Schröder, and Oriol Vendrell. Suitable coordinates for quantum dynamics: Applications using the multiconfiguration time-dependent Hartree (MCTDH) algorithm. *Computational and Theoretical Chemistry*, 990:75–89, 2012.
- [106] Manabu Kanno, Kunihito Hoki, Hirohiko Kono, and Yuichi Fujimura. Quantum optimal control of electron ring currents in chiral aromatic molecules. *The Journal of Chemical Physics*, 127:204314, 2007.

- [107] Manabu Kanno, Hirohiko Kono, and Yuichi Fujimura. Control of π -Electron Rotation in Chiral Aromatic Molecules by Nonhelical Laser Pulses. *Angewandte Chemie International Edition*, 45:7995–7998, 2006.
- [108] Tosio Kato. On the Adiabatic Theorem in Quantum Mechanics. *Journal of the Physical Society of Japan*, 5:435–439, 1950.
- [109] Masaaki Kijima. *Markov Processes for Stochastic Modeling*. The University Press, Cambridge, 1997.
- [110] Matthias F. Kling and Marc J.J. Vrakking. Attosecond electron dynamics. *Annual Reviews of Physical Chemistry*, 59:463–492, 2007.
- [111] Peter Knowles, Martin Schütz, and Hans-Joachim Werner. Ab initio methods for electron correlation in molecules. In Johannes Grotendorst, editor, *Modern Methods and Algorithms of Quantum Chemistry*, pages 79–179, Jülich, 2000. John von Neumann Institute for Computing. Online at <http://www-fourier.ujf-grenoble.fr/>
- [112] Wolfram Koch and Max C. Holthausen. *A Chemist's Guide to Density Functional Theory*. Wiley-VCH, Weinheim, 2001.
- [113] Susanna Kube and Marcus Weber. Conformation Kinetics as a Reduced Model for Transition Pathways. Technical report, Konrad-Zuse-Zentrum für Informationstechnik Berlin, 2005.
- [114] Werner Kutzelnigg. What I like about Hückel theory. *Journal of Computational Chemistry*, 28:25–34, 2007.
- [115] Cornelius Lanczos. *The Variational Principles of Mechanics*. Dover, New York, 1970.
- [116] Stephen R. Langhoff and Ernest R. Davidson. Configuration interaction calculations on the nitrogen molecule. *International Journal of Quantum Chemistry*, 8:61–72, 1974.
- [117] David Lauvergnat and André Nauts. Exact numerical computation of a kinetic energy operator in curvilinear coordinates. *Journal of Chemical Physics*, 116:8560–8570, 2002.
- [118] Andrew R. Leach. *Molecular Modeling: Principles and Applications*. Pearson Education Limited, Essex, 2001.
- [119] J. P. Leroy and R. Wallace. Procedures Leading to a Variety of Orthonormal Jacobi-Type Coordinates of Relevance to Large-Amplitude Vibration and Scattering Problems. *Chemical Physics*, 111:11–16, 1987.
- [120] Jorge Ricardo Letelier and Constantino A. Utreras-Días. A numerical molecular potential for the umbrella inversion in ammonia. *Spectrochimica Acta Part A*, 53:247, 1997.
- [121] Benjamin G. Levine and Todd J. Martínez. Isomerization Through Conical Intersections. *Annual Reviews of Physical Chemistry*, 58:613–634, 2007.
- [122] Gilbert N. Lewis. The Atom and the Molecule. *Journal of the American Chemical Society*, 38:762–785, 1916.
- [123] David Ley, Dennis Gerbig, and Peter R. Schreiner. Tunneling control of chemical reactions – the organic chemist's perspective. *Organic & Biomolecular Chemistry*, 10:3781, 2012.

- [124] Robert G. Littlejohn. Adiabatic Invariance, the Geometric Phase, and the Born-Oppenheimer Approximation, 2011. Quantum Mechanics lecture notes 36, see <http://bohr.physics.berkeley.edu/classes/221/1011/221.html>.
- [125] Robert G. Littlejohn and Matthias Reinsch. Gauge fields in the separation of rotations and internal motions in the n -body problem. *Reviews of Modern Physics*, 69:213–275, 1997.
- [126] Fritz London. *Über den Mechanismus der Homöopolaren Bindung*. Herzel, Leipzig, 1928.
- [127] Rodney Loudon. *The Quantum Theory of Light*. Oxford Science Publications, Oxford, 2000.
- [128] Per-Olov Löwdin. Quantum Theory of Many-Particle Systems. I. Physical Interpretations by Means of Density Matrices, Natural Spin-Orbitals, and Convergence Problems in the Method of Configurational Interaction. *Physical Review*, 97:1474–1489, 1955.
- [129] Per-Olov Löwdin. On the long way from the Coulombic Hamiltonian to the electronic structure of molecules. *Pure and Applied Chemistry*, 61:2065–2074, 1989.
- [130] David Luckhaus. Hydrogen exchange in formic acid dimer: tunneling above the barrier. *Physical Chemistry Chemical Physics*, 12:8357–8361, 2010.
- [131] Erwin Madelung. Quantentheorie in hydrodynamischer Form. *Zeitschrift für Physik*, 40:322–326, 1926.
- [132] Jean-Paul Malrieu, Nathalie Guihéry, Carmen Jiménez Calzado, and Celestino Angeli. Bond electron pair: Its relevance and analysis from the quantum chemistry point of view. *Journal of Computational Chemistry*, 28:35–50, 2007.
- [133] Jörn Manz, Rolf Meyer, and Joachim Röhmelt. On vibrational bonding of IHI. *Chemical Physics Letters*, 96:607–612, 1983.
- [134] Jörn Manz and Kentaro Yamamoto. A selection rule for the directions of electronic fluxes during unimolecular pericyclic reactions in the electronic ground state. *Molecular Physics*, 110:517–530, 2012.
- [135] Dominik Marx. *An Introduction to Ab Initio Molecular Dynamics Simulations*. John von Neumann Institute for Computing, Jülich, 2006.
- [136] Dominik Marx and Jürg Hutter. *Ab Initio Molecular Dynamics*. Cambridge University Press, Cambridge, 2009.
- [137] Ivana Matanović, Nadja Došlić, and Bruce Johnson. Generalized approximation to the reaction path: The formic acid dimer case. *The Journal of Chemical Physics*, 128:084103(10), 2008.
- [138] Richard D. Mattuck. *A Guide to Feynman Diagrams in the Many-Body Problem*. Dover Publications, New York, 1992.
- [139] Edit Mátyus, Jürg Hutter, Ulrich Müller-Herold, and Markus Reiher. Extracting elements of molecular structure from the all-particle wave function. *The Journal of Chemical Physics*, 135:204302(12), 2011.
- [140] Edit Mátyus, Jürg Hutter, Ulrich Müller-Herold, and Markus Reiher. On the emergence of molecular structure. *Physical Review A*, 83:052512(5), 2011.

- [141] Edit Mátyus and Markus Reiher. Molecular structure calculations: A unified quantum mechanical description of electrons and nuclei using explicitly correlated Gaussian functions and the global vector representation. *The Journal of Chemical Physics*, 137:024104(17), 2012.
- [142] Volkhard May and Oliver Kühn. *Charge and Energy Transfer Dynamics in Molecular Systems*. WILEY-VCH, Berlin, 2011.
- [143] Edward A. McCullough and Robert E. Wyatt. Dynamics of the Collinear H+H₂ Reaction. I. Probability Density and Flux. *The Journal of Chemical Physics*, 54:3578–3591, 1971.
- [144] Qingyong Meng and Hans-Dieter Meyer. A multilayer MCTDH study on the full dimensional vibronic dynamics of naphthalene and anthracene cations. *The Journal of Chemical Physics*, 138:014313(12), 2013.
- [145] Gabriel Merino, Thomas Heine, and Gotthard Seifert. The Induced Magnetic Field in Cyclic Molecules. *Chemistry – A European Journal*, 10:4367–4371, 2004.
- [146] Albert Messiah. *Quantum Mechanics*. Dover Publications, New York, 1999.
- [147] Hans-Dieter Meyer, Uwe Manthe, and Lorenz S. Cederbaum. The multi-configurational time-dependent Hartree approach. *Chemical Physics Letters*, 165:73–78, 1990.
- [148] Thomas M. Miller, Albert A. Viggiano, and Amy E. Stevens Miller. Electron attachment and detachment: Cyclooctatetraene. *The Journal of Physical Chemistry A*, 106:10200–10204, 2002.
- [149] William H. Miller. Periodic orbit description of tunneling in symmetric and asymmetric double-well potentials. *The Journal of Physical Chemistry*, 83:960–963, 1979.
- [150] Katsunori Mita. Fluid-like properties of the probability densities in quantum mechanics. *American Journal of Physics*, 69:470–475, 2001.
- [151] Mirjana Mladenović. Rovibrational Hamiltonians for general polyatomic molecules in spherical polar parametrization. I. Orthogonal representations. *The Journal of Chemical Physics*, 112:1070–1081, 2000.
- [152] Mirjana Mladenović. Rovibrational Hamiltonians for general polyatomic molecules in spherical polar parametrization. II. Nonorthogonal descriptions of internal molecular geometry. *The Journal of Chemical Physics*, 112:1082–1095, 2000.
- [153] Mirjana Mladenović. Rovibrational Hamiltonians for general polyatomic molecules in spherical polar parametrization. III. Global vs local axis system and angular coordinates. *The Journal of Chemical Physics*, 113:10524–10534, 2000.
- [154] Wolfgang H. Müller. *Streifzüge durch die Kontinuumstheorie*. Springer, Heidelberg, 2011.
- [155] Laurence A. Nafie. Adiabatic molecular properties beyond the Born-Oppenheimer approximation. Complete adiabatic wavefunctions and vibrationally induced electronic current density. *The Journal of Chemical Physics*, 79:4950–4957, 1983.
- [156] Laurence A. Nafie. Velocity-gauge formalism in the theory of vibrational circular dichroism and infrared absorption. *The Journal of Chemical Physics*, 96:5687–5702, 1992.

- [157] Laurence A. Nafie. Electron Transition Current Density in Molecules. 1. Non-Born-Oppenheimer Theory of Vibronic and Vibrational Transitions. *The Journal of Physical Chemistry A*, 101:7826–7833, 1997.
- [158] Laurence A. Nafie and Teresa B. Freedman. Vibronic coupling theory of infrared vibrational transitions. *The Journal of Chemical Physics*, 78:7108–7118, 1983.
- [159] Kengo Nagashima and Kazuo Takatsuka. Electron-Wavepacket Reaction Dynamics in Proton Transfer of Formamide. *The Journal of Physical Chemistry A*, 113:15240–15249, 2009.
- [160] Kengo Nagashima and Kazuo Takatsuka. Early Stage Dynamics in Coupled Proton-Electron Transfer from π - π^* State of Phenol to Solvent Ammonia Clusters: A Nonadiabatic Electron Dynamics Study. *The Journal of Physical Chemistry A*, 116:11167–11179, 2012.
- [161] Charles Nash and Siddhartha Sen. *Topology and Geometry for Physicists*. Dover, New York, 2011.
- [162] André Nauts and Xavier Chapuisat. Momentum, quasi-momentum and hamiltonian operators in terms of arbitrary curvilinear coordinates, with special emphasis on molecular hamiltonians. *Molecular Physics*, 55:1287–1318, 1985.
- [163] Mathias Nest. The multi-configuration electron-nuclear dynamics method. *Chemical Physics Letters*, 472:171–174, 2009.
- [164] Kyriacos Costa Nicolaou, Scott A. Snyder, Tamsyn Montagnon, and Georgios Vasilikogiannakis. The Diels-Alder Reaction in Total Synthesis. *Angewandte Chemie International Edition*, 41:1668–1698, 2002.
- [165] Mary Jo Nye. Working tools for theoretical chemistry: Polanyi, Eyring, and debates over the semiempirical method. *Journal of Computational Chemistry*, 28:98–108, 2007.
- [166] Yoshishige Okuno. A reaction-path Hamiltonian described with quasirectilinear vibrational coordinates constructed from a nonlinear combination of curvilinear internal coordinates: Formulation. *The Journal of Chemical Physics*, 113:3130–3135, 2000.
- [167] Michihiro Okuyama and Kazuo Takatsuka. Electron flux in molecules induced by nuclear motion. *Chemical Physics Letters*, 476:109–115, 2009.
- [168] Michihiro Okuyama and Kazuo Takatsuka. Dynamical Electron Mechanism of Double Proton Transfer in Formic Acid Dimer. *Bulletin of the Chemical Society Japan*, 85:217–227, 2012.
- [169] Jean F. M. Oth. Conformational mobility and fast bond shift in annulenes. *Pure and Applied Chemistry*, 25:537–622, 1971.
- [170] Gianluca Panati, Herbert Spohn, and Stefan Teufel. The time-dependent Born-Oppenheimer approximation. *Mathematical Modeling and Numerical Analysis*, 41:297–314, 2007.
- [171] Leo A. Paquette. Ring inversion and bond shifting energetics in substituted chiral cyclooctatetraenes. *Pure and Applied Chemistry*, 54:987–1004, 1982.
- [172] Serguei Patchkovskii. Electronic currents and Born-Oppenheimer molecular dynamics. *The Journal of Chemical Physics*, 137:084109, 2012.

- [173] Ángel Martín Pendás, Miguel A. Blanco, and Evelio Francisco. Chemical Fragments in Real Space: Definitions, Properties, and Energetic Decompositions. *Journal of Computational Chemistry*, 28:161–184, 2007.
- [174] Michael W. P. Petryk and Bryan R. Henry. CH stretching vibrational overtone spectra of 1,3,5,7-cyclooctatetraene and 1,1,1-trichloroethane. *The Journal of Physical Chemistry A*, 109:7113–7120, 2005.
- [175] János Pipek and Paul G. Mezey. A fast intrinsic localization procedure applicable for ab initio and semiempirical linear combination of atomic orbital wave functions. *The Journal of Chemical Physics*, 90:4916–4926, 1989.
- [176] Boris Podolsky. Quantum-mechanically correct form of the Hamiltonian function for conservative systems. *Physical Review*, 32:812–816, 1928.
- [177] Pekka Pyykkö and John F. Stanton (editors). Quantum Chemistry 2012. *Chemical Reviews*, 112:1–672, 2012.
- [178] Pekka Pyykkö and John F. Stanton. Introduction to the Quantum Chemistry 2012 Issue. *Chemical Reviews*, 112:1–3, 2012.
- [179] Markus Reiher and Alexander Wolf. *Relativistic Quantum Chemistry: The Fundamental Theory of Molecular Science*. Wiley-VCH, Weinheim, 2009.
- [180] Joachim Reinhold. *Quantentheorie der Moleküle*. Springer, Wiesbaden, 2013.
- [181] Keyvan Sadri, David Lauvergnat, Fabien Gatti, and Hand-Dieter Meyer. Numerical kinetic energy operators for molecules in polyspherical coordinates. *The Journal of Chemical Physics*, 136:234112(10), 2012.
- [182] Axel Schild, Deepanshu Choudhary, Vaibhav D. Sambre, and Beate Paulus. Electron Density Dynamics in the Electronic Ground State: Motion Along the Kekulé Mode of Benzene. *The Journal of Physical Chemistry A*, 116:11355–11360, 2012.
- [183] Axel Schild and Beate Paulus. Multireference calculations for ring inversion and double bond shifting in cyclooctatetraene. *Journal of Computational Chemistry*, 34:1393–1397, 2013.
- [184] Burkhard Schmidt and Ulf Lorenz. Wavepacket 4.7: A program package for quantum-mechanical wavepacket propagation and time-dependent spectroscopy, 2009. Available via <http://wavepacket.sourceforge.net>.
- [185] Erwin Schrödinger. Quantisierung als Eigenwertproblem. *Annalen der Physik*, 384:361–376, 1926.
- [186] Melvin Schwartz. *Principles of Electrodynamics*. Dover Publications, New York, 1987.
- [187] Sason Shaik. The Lewis legacy: The chemical bond – A territory and heartland of chemistry. *Journal of Computational Chemistry*, 28:51–61, 2007.
- [188] Sason S. Shaik and Philippe C. Hiberty. *A Chemist's Guide to Valence Bond Theory*. John Wiley & Sons, Hoboken, New Jersey, 2008.
- [189] Dmitrii V. Shalashilin and Mark S. Child. The phase space CCS approach to quantum and semiclassical molecular dynamics for high-dimensional systems. *Chemical Physics*, 304:103–120, 2004.

- [190] Norihiro Shida, Paul F. Barbara, and Jan E. Almlöf. A theoretical study of multi-dimensional nuclear tunneling in malonaldehyde. *The Journal of Chemical Physics*, 91:4061–4072, 1989.
- [191] Alan J. Shusterman and Gwendolyn P. Shusterman. Teaching Chemistry with Electron Density Models. *Journal of Chemical Education*, 74:771, 1997.
- [192] Ana Simões. In between worlds: G.N. Lewis, the shared pair bond and its multifarious contexts. *Journal of Computational Chemistry*, 28:62–72, 2007.
- [193] Richard Sinkhorn. A Relationship Between Arbitrary Positive Matrices and Doubly Stochastic Matrices. *Annals of Mathematical Statistics*, 35:876–879, 1964.
- [194] Lubomir Skála and Vojtěch Kapsa. From probabilities to quantum and classical mechanics. *Physica E*, 29:119–128, 2005.
- [195] Alessandro Soncini and Patrick W. Fowler. Ipsocentric and allocentric methods of mapping induced current density. *Chemical Physics Letters*, 396:174–181, 2004.
- [196] Detlev Stalling, Malte Westerhoff, and Hans-Christian Hege. *amira: A Highly Interactive System for Visual Data Analysis*, chapter 38, page 749. Elsevier, Amsterdam, 2005.
- [197] Erich Steiner and Patrick W. Fowler. Ring Currents in Aromatic Hydrocarbons. *International Journal of Quantum Chemistry*, 60:609–616, 1996.
- [198] Erich Steiner and Patrick W. Fowler. Four- and two-electron rules for diatropic and paratropic ring currents in monocyclic π systems. *Chemical Communications*, 0:2220–2221, 2001.
- [199] Erich Steiner and Patrick W. Fowler. Patterns of Ring Currents in Conjugated Molecules: A Few-Electron Model Based on Orbital Contributions. *Journal of Physical Chemistry A*, 105:9553–9562, 2001.
- [200] Brian T. Sutcliffe. What mathematicians know about the solutions of Schrodinger's Coulomb Hamiltonian. Should chemists care? *Journal of Mathematical Chemistry*, 44:988–1008, 2008.
- [201] Brian T. Sutcliffe. To what questions is the clamped-nuclei electronic potential the answer. *Theoretical Chemistry Accounts*, 127:121–131, 2010.
- [202] Brian T. Sutcliffe and R. Guy Woolley. Comment on ‘Molecular structure in non-Born-Oppenheimer quantum mechanics’. *Chemical Physics Letters*, 408:445–447, 2005.
- [203] Brian T. Sutcliffe and R. Guy Woolley. Molecular structure calculations without clamping the nuclei. *Physical Chemistry Chemical Physics*, 7:3664–3676, 2005.
- [204] Attila Szabo and Neil S. Ostlund. *Modern Quantum Chemistry - Introduction to Advanced Electronic Structure Theory*. Dover Publications, New York, 1996.
- [205] Péter G. Szalay, Thomas Müller, Gergely Gidofalvi, Hans Lischka, and Ron Shepard. Multiconfiguration Self-Consistent Field and Multireference Configuration Interaction Methods and Applications. *Chemical Reviews*, 112:108–181, 2012.
- [206] Kazuo Takatsuka. Toward Non-Born-Oppenheimer Quantum Chemistry. *International Journal of Quantum Chemistry*, 109:2131–2142, 2009.

- [207] Kazuo Takatsuka and Takehiro Yonehara. Exploring dynamical electron theory beyond the Born-Oppenheimer framework: from chemical reactivity to non-adiabatically coupled electronic and nuclear wavepackets on-the-fly under laser field. *Physical Chemistry Chemical Physics*, 13:4987–5016, 2011.
- [208] David J. Tannor. *Introduction to Quantum Mechanics, A time-dependent perspective*. University Science Books, Sausalito, California, 2005.
- [209] Christofer S. Tautermann, Andreas F. Voegelé, and Klaus R. Liedl. The ground-state tunneling splitting of various carboxylic acid dimers. *The Journal of Chemical Physics*, 120:631–637, 2004.
- [210] Matt Tearle. Simple real fourier series approximation. See <http://www.mathworks.com/matlabcentral/fileexchange/31013-simple-real-fourier-series-approximation>.
- [211] Seiichiro Ten-no and Jozef Noga. Explicitly correlated electronic structure theory from R12/F12 ansätze. *WIREs Computational Molecular Science*, 2:114–125, 2012.
- [212] David P. Tew, Nicholas C. Handy, and Stuart Carter. A reaction surface Hamiltonian study of malonaldehyde. *The Journal of Chemical Physics*, 125:084313(16), 2006.
- [213] Donald G. Truhlar. Valence bond theory for chemical dynamics. *Journal of Computational Chemistry*, 28:73–86, 2007.
- [214] Inga S. Ulusoy and Mathias Nest. Correlated Electron Dynamics: How Aromaticity Can Be Controlled. *Journal of the American Chemical Society*, 133:20230–20236, 2011.
- [215] Inga S. Ulusoy and Mathias Nest. Remarks on the Validity of the Fixed Nuclei Approximation in Quantum Electron Dynamics. *The Journal of Physical Chemistry A*, 116:11107–11110, 2012.
- [216] Inga S. Ulusoy and Mathias Nest. The multi-configuration electron-nuclear dynamics method applied to LiH. *The Journal of Chemical Physics*, 136:054112(6), 2012.
- [217] Brigita Urbanc, Jose M. Borreguero, Luis Cruz, and H. Eugene Stanley. Ab initio discrete molecular dynamics approach to protein folding and aggregation. *Methods in Enzymology*, 412:314–338, 2006.
- [218] Alexandra Viel, Maurício D. Coutinho-Neto, and Uwe Manthe. The ground state tunneling splitting and the zero point energy of malonaldehyde: A quantum Monte Carlo determination. *The Journal of Chemical Physics*, 126:024308(9), 2007.
- [219] Giovanni Vignale. Current Density Functional Theory. *Lecture Notes in Physics*, 706:75–91, 2006.
- [220] David J. Wales. *Energy Landscapes*. Cambridge University Press, Cambridge, 2003.
- [221] Philip R. Wallace. *Mathematical Analysis of Physical Problems*. Dover Publications, New York, 1984.
- [222] Yimin Wang, Bastiaan J. Braams, Joel M. Bowman, Stuart Carter, and David P. Tew. Full-dimensional quantum calculations of ground-state tunneling splitting of malonaldehyde using an accurate ab initio potential energy surface. *The Journal of Chemical Physics*, 128:224314(9), 2008.
- [223] Mitchel Weissbluth. *Atoms and Molecules*. Academic Press, New York, 1978.

- [224] Paul G. Wenthold, David A. Hrovat, Weston Thatcher Borden, and W. Carl Lineberger. Transition-state spectroscopy of cyclooctatetraene. *Science*, 272:1456–1459, 1996.
- [225] H.-J. Werner, P. J. Knowles, G. Knizia, F. R. Manby, M. Schütz, P. Celani, T. Korona, R. Lindh, A. Mitrushenkov, G. Rauhut, K. R. Shamasundar, T. B. Adler, R. D. Amos, A. Bernhardsson, A. Berning, D. L. Cooper, M. J. O. Deegan, A. J. Dobbyn, F. Eckert, E. Goll, C. Hampel, A. Hesselmann, G. Hetzer, T. Hrenar, G. Jansen, C. Köppl, Y. Liu, A. W. Lloyd, R. A. Mata, A. J. May, S. J. McNicholas, W. Meyer, M. E. Mura, A. Nicklass, D. P. O’Neill, P. Palmieri, K. Pflüger, R. Pitzer, M. Reiher, T. Shiozaki, H. Stoll, A. J. Stone, R. Tarroni, T. Thorsteinsson, M. Wang, and A. Wolf. Molpro, version 2012.1, a package of ab initio programs, 2010. see <http://www.molpro.net>.
- [226] Edgar Bright Wilson, J. C. Decius, and Paul C. Cross. *Molecular Vibrations: The Theory of Infrared and Raman Vibrational Spectra*. Dover, New York, 1980.
- [227] R. Guy Woolley. Quantum Theory and molecular structure. *Advances in Physics*, 25:27–52, 1976.
- [228] R. Guy Woolley. Molecular Shapes and Molecular Structures. *Chemical Physics Letters*, 125:200–205, 1986.
- [229] R. Guy Woolley. Quantum Chemistry Beyond the Born-Oppenheimer Approximation. *Journal of Molecular Structure (Theochem)*, 230:17–46, 1991.
- [230] R. Guy Woolley. Is there a quantum definition of a molecule? *Journal of Mathematical Chemistry*, 23:3–12, 1998.
- [231] Robert E. Wyatt. *Quantum Dynamics with Trajectories, Introduction to Quantum Hydrodynamics*. Springer, New York, 2005.
- [232] Kiyoshi Yagi, Tetsuya Taketsugu, and Kimihiko Hirao. Generation of full-dimensional potential energy surface of intramolecular hydrogen atom transfer in malonaldehyde and tunneling dynamics. *The Journal of Chemical Physics*, 115:10647–10655, 2001.
- [233] David R. Yarkony. Nonadiabatic Quantum Chemistry – Past, Present and Future. *Chemical Reviews*, 112:481–498, 2012.
- [234] Takehiro Yonehara, Kota Hanasaki, and Kazuo Takatsuka. Fundamental Approaches to Nonadiabaticity: Toward a Chemical Theory beyond the Born-Oppenheimer Paradigm. *Chemical Reviews*, 112:499–542, 2012.
- [235] Takehiro Yonehara and Kazuo Takatsuka. Characterization of electron-deficient chemical bonding of diborane with attosecond electron wavepacket dynamics and laser response. *Chemical Physics*, 366:115–128, 2009.
- [236] Takehiro Yonehara and Kazuo Takatsuka. Non Born-Oppenheimer electronic and nuclear wavepacket dynamics. *The Journal of Chemical Physics*, 130:214113(14), 2009.
- [237] Xuefeng Zhou, Ruifeng Liu, and Peter Pulay. Theoretical study on the structures, force field, and vibrational spectra of cyclooctatetraene and cyclooctatetraene-d8. *Spectrochimica Acta*, 49A:953–964, 1993.

Curriculum vitæ

Der Lebenslauf ist in der Online-Version aus
Gründen des Datenschutzes nicht enthalten.

For reasons of information privacy, the curriculum vitae
is not included in the online version of this document.

